922

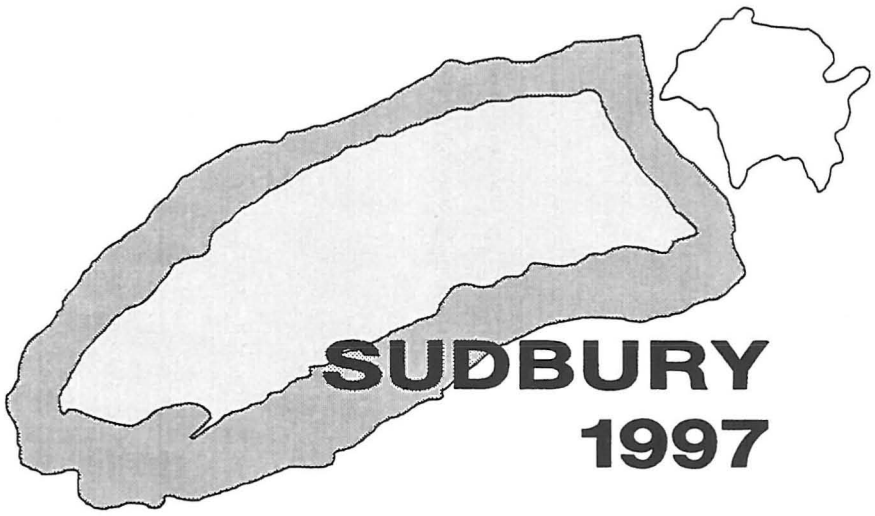

LARGE METEORITE IMPACTS AND PLANETARY EVOLUTION

September 1–3, 1997
Sudbury, Ontario

CONFERENCE ON

LARGE METEORITE IMPACTS AND PLANETARY EVOLUTION

(SUDBURY 1997)

Hosted by

Ontario Geological Survey

Sponsored by

Inco Limited
Falconbridge Limited
The Barringer Crater Company
Geological Survey of Canada
Ontario Ministry of Northern Development and Mines
Quebec Ministère des Ressources naturelles
Lunar and Planetary Institute

Scientific Organizing Committee

A. Deutsch
University of Münster, Germany
B. O. Dressler, Chair
Lunar and Planetary Institute, Houston, Texas
B. M. French
Smithsonian Institution, Washington, DC
R. A. F. Grieve
Geological Survey of Canada, Ottawa, Ontario
G. W. Johns
Ontario Geological Survey, Sudbury, Ontario
V. L. Sharpton
Lunar and Planetary Institute, Houston, Texas

LPI Contribution No. 922

Compiled in 1997 by
LUNAR AND PLANETARY INSTITUTE

The Institute is operated by the Universities Space Research Association under Contract No. NASW-4574 with the National Aeronautics and Space Administration.

Abstracts in this volume may be cited as

Author A. B. (1997) Title of abstract. In *Conference on Large Meteorite Impacts and Planetary Evolution (Sudbury 1997)*, p. XX, LPI Contribution No. 922, Lunar and Planetary Institute, Houston.

This volume is distributed by

ORDER DEPARTMENT
Lunar and Planetary Institute
3600 Bay Area Boulevard
Houston TX 77058-1113, USA

Mail order requestors will be invoiced for the cost of shipping and handling.

Contents

BP and Oasis Impact Structures, Libya, and Their Relation to Libyan Desert Glass: Petrography, Geochemistry, and Geochronology
B. Abate, C. Koeberl, J. R. Underwood Jr., E. P. Fisk, and R. F. Giegengack 1

Overview of Bosumtwi Crater, Ghana
S. T. Ahulu 1

Crater-fill Sequence, Onaping Formation: Petrographic and Geochemical Signature of Regional Hydrothermal Alteration
D. E. Ames and H. L. Gibson 1

Impact-induced Hydrothermal Base Metal Mineralization, Whitewater Group, Sudbury Structure
D. E. Ames, H. L. Gibson, and I. R. Jonasson 2

Nickel- and Platinum-Group-Element-Enriched Quartz Norite in the Latest Jurassic Morokweng Impact Structure, South Africa
M. A. G. Andreoli, R. J. Hart, L. D. Ashwal, and M. Tredoux 3

Simulating Phase Equilibria and *In Situ* Differentiation for the Proposed Parental Sudbury Magmas
A. A. Ariskin 3

Investigations on the Green Member of the Onaping Formation, Sudbury Structure, Ontario, Canada
M. E. Avermann 4

Extraterrestrial Helium ($He@C_{60}$) Trapped in Fullerenes in the Sudbury Impact Structure
L. Becker, J. L. Bada, R. J. Poreda, and T. E. Bunch 5

Summary of Work in Manicouagan Impact Structure
L. Boivin 5

Composition and Structure of the Chicxulub Crater Using Wide-Angle Seismic Velocities
J. Brittan, H. Macintyre, and the Chicxulub Working Group 6

Synthetic Aperture Radar Characteristics of a Glacially Modified Meltsheet, Manicouagan, Quebec
P. Budkewitsch and R. Grieve 6

New Potential Sources for Black Onaping Carbon
T. E. Bunch, L. Becker, P. H. Schultz, and W. S. Wolbach 7

Ecosystem-Structure Analysis Applied to Indication and Study of Earth Astroblemes
G. G. Burba Jr. 7

Sedimentary Interbeds of the Rooiberg Group at the Loskop Dam Section, Bushveld Complex, South Africa
M. E. Caress and W. E. Elston 8

The Chicxulub Seismic Experiment
Chicxulub Working Group: J. Morgan, M. Warner, J. Brittan, H. Macintyre, D. Snyder, R. Hobbs, G. Suarez, L. Marin, A. Trejo, R. Buffler, G. Christeson, Y. Nakamura, A. Hildebrand, M. Pilkington, V. Sharpton, P. Maguire, P. Denton, G. Mackenzie, and A. Camargo 9

Structure of the Chicxulub Impact Crater from Wide-Angle Ocean-Bottom Seismograph Data
G. L. Christeson, Y. Nakamura, R. T. Buffler, and the Chicxulub Working Group 9

The Chicxulub Impact Structure and Its Proximal Ejecta
P. Claeys, A. Deutsch, F. Langenhorst, S. Heuschkel, B. Dissman, and D. Stöffler 9

Chemical Compositions of Chicxulub Impact Breccias
C. M. Corrigan, V. L. Sharpton, T. A. Vogel, and L. E. Marín 10

Funnel-shaped Emplacement Geometry of the Sudbury Igneous Complex: A Structural Perspective
E. J. Cowan and W. M. Schwerdtner 11

Sudbury: Geochemical Evidence for a Single-Impact Melting Event
A. P. Dickin and J. H. Crocket 11

The Separation of Platinum and Palladium During High-Temperature Vaporization of Sulfide-rich Picrite
Yu. P Dikov, V. V. Distler, M. V. Gerasimov, and O. I. Yakovlev 12

The Sudbury Structure, Ontario, Canada: A Persistent Enigma
B. O. Dressler and V. L. Sharpton 12

Review of the Geophysical Signature of the Vredefort Structure and Its Interpretations
R. J. Durrheim and W. U. Reimold 13

Base of the Rooiberg Group: Evidence for an Initial Bushveld Catastrophe
W. E. Elston and M. E. Caress 14

Classification and Distribution of Sudbury Breccia
J. S. Fedorowich, D. H. Rousell, and W. V. Peredery 14

Impact Materials with Mixed Compositions of Iron-Silicon-Nickel-Sulfur System
S. Fukuyama, Y. Miura, and H. Kobayashi 15

Experimental Investigation of the Chemistry of Vaporization of Targets in Relation to the Chicxulub Impact
M. V. Gerasimov, Yu. P. Dikov, O. I. Yakovlev, and F. Wlotzka 15

The Onaping Formation: Stratigraphy, Fragmentation, and Mechanisms of Emplacement
S. F. M. Gibbins, H. L. Gibson, D. E. Ames, and I. R. Jonasson 16

Diagnostic Criteria for the Recognition of Shatter Cones
H. M. Gibson and J. G. Spray 16

Multiple Origins for Impact-produced Diamonds
I. Gilmour, R. M. Hough, and C. T. Pillinger 17

Asteroid/Comet Mega-Impacts and Mantle Melting Episodes: Consequences for Precambrian Crustal Evolution
A. Y. Glikson 17

Large-Scale Impact of Cratering and Early Earth Evolution
R. A. F. Grieve and M. J. Cintala 18

Geophysical Modeling of the Mjølnir Impact Structure, Barents Sea
S. T. Gudlaugsson, F. Tsikalas, O. Eldholm, and J. I. Faleide 19

Magnetic Anomalies of the Vredefort Central Rise Structure
H. Henkel 19

NBCS: The Baltic-Nordic Network for Impact Crater Studies
H. Henkel 20

Combined Geophysical Modeling of the Vredefort Structure
H. Henkel and W. U. Reimold 20

Reconstruction of the Vredefort Impact Crater
H. Henkel and W. U. Reimold 20

Origin of Carbonaceous Matter in Rocks from the Whitewater Group of the Sudbury Structure
D. Heymann and B. O. Dressler 21

Carbon Isotopic Composition of Carbonaceous Matter in Rocks from the Whitewater Group of the Sudbury Structure
D. Heymann, B. O. Dressler, R. B. Dunbar, and D. A. Mucciarone 22

Origin of Native Sulfur in Rocks from the Sudbury Structure, Ontario, Canada
D. Heymann, B. O. Dressler, and M. H. Thiemens 22

The Search for Fullerenes in Rocks from the Whitewater Group of the Sudbury Structure, Ontario, Canada
D. Heymann, P. R. Buseck, J. Knell, and B. O. Dressler 23

The Steen River Impact Structure, Alberta, Canada
A. R. Hildebrand, M. Pilkington, R. A. F. Grieve, R. R. Stewart, M. J. Mazur, D. W. Hladiuk, and D. Sinnott 23

Mapping Chicxulub Crater Structure with Gravity and Seismic Reflection Data
A. R. Hildebrand, M. Pilkington, J. F. Halpenny, R. V. Cooper, M. Connors, C. Ortiz-Aleman, R. E. Chavez, J. Urrutia-Fucugauchi, E. Graniel-Castro, A. Camara-Zi, and R. T. Buffler 24

Geochemical Characteristics of Impactites from the Popigai Impact Structure, Russia
Th. Hölker, A. Deutsch, and V. L. Masaitis 25

Diamonds in the Ejecta and Fireball Layers of the Cretaceous-Tertiary Boundary in the U.S. and Mexico
R. M. Hough, I. Gilmour, and C. T. Pillinger 26

Sudbury Impact Event: Cratering Mechanics and Thermal History
B. A. Ivanov and A. Deutsch 26

Artificial Ozone Hole Generation Following a Large Meteoroid Impact into an Oceanic Site
B. A. Klumov and I. I. Korobov 27

Large Chemical Vapor Deposition Diamond-like Carbon Formed by Multi-Impact Reactions
H. Kobayashi, Y. Miura, and S. Fukuyama 27

The Jurassic-Cretaceous Boundary Impact Event: The Morokweng Impact Structure, South Africa
C. Koeberl, W. U. Reimold, and R. A. Armstrong 28

Deep Anatomy, Composition, and Evolution of Large Meteorite Impacts: Scientific Drilling Data on the Puchezh-Katunki Astrobleme, Russia
A. A. Kremenetskiy and N. A. Yushko 29

Structure and Kinematics of a Complex Crater, Upheaval Dome, Southeast Utah
B. J. Kriens, K. E. Herkenhoff, and E. M. Shoemaker 29

Can Impact-generated Melts Have Mantle Contributions?: Geochemical Evidence from the Sudbury Igneous Complex
P. C. Lightfoot, R. R. Keays, and W. Doherty 30

Geological and Geochemical Relationships Between the Contact Sublayer, Offsets, and Main Mass of the Sudbury Igneous Complex
P. C. Lightfoot, R. R. Keays, G. G. Morrison, and A. Bite 30

Cratering on Titan: A Pre-Cassini Perspective
R. D. Lorenz 31

Original Size and Shape of the Sudbury Structure
P. D. Lowman Jr. 31

The Mystery of the 536 A.D. Dust Veil Event: Was It A Cometary or Meteoritic Impact?
A. A. Mardon 32

Three-Dimensional Modeling of Impactite Bodies of Popigai Impact Crater, Russia
V. L. Masaitis, M. V. Naumov, and M. S. Mashchak 32

Discovery of Impact Diamonds at the Sudbury Structure
V. L. Masaitis, G. I. Shafranovsky, R. A. F. Grieve, F. Langenhorst, W. V. Peredery, E. L. Balmasov, I. G. Fedorova, and A. Therriault 33

Diamonds Originated by Meteorite Impact: Magnetic and Other Properties
V. L. Masaitis, G. I. Shafranovsky, L. J. Pesonen, and K. A. Kinnunen 33

A Study of Mineral and Rock Fragments and Shock Features in the Late Granite Breccia at the Fraser Mine, North Range, Sudbury Structure
K. A. McCormick, R. S. James, J. S. Fedorowich, D. H. Rousell, A. M. McDonald, and H. L. Gibson 34

Slow Impact Vapor Plume Expansion with Realistic Equations of State
H. J. Melosh and E. Pierazzo 35

Integrated Geophysical Study of the Sudbury Structure
B. Milkereit and D. E. Boerner 35

The Chicxulub Seismic Experiment: Crater Morphology
J. Morgan and the Chicxulub Working Group 35

The Circular Structure at Ramgarh, India: An Astrobleme(?)
V. K. Nayak 36

The Lycksele Structure, A Huge Ring Formation in Northern Sweden: Result of an Impact?
D. H. Nisca, H. Thunehed, L. J. Pesonen, and S-Å. Elming 36

Chicxulub Impact Ejecta in Belize
A. Ocampo, K. Pope, A. Fischer, W. Alvarez, B. Fouke, F. Asaro, C. Webster Jr., F. Vega, J. Smit, A. E. Fritsche, P. Claeys, M. Rampino, and D. King Jr. 37

Geological Setting of the Manchester Offset Dike Within the South Range of the Sudbury Impact Structure
J. P. O'Connor and J. G. Spray 38

The Middle Ordovician Lockne Crater as a Small-scale Model for Impacts at Sea
J. Ormo, M. Lindstrom, E. Sturkell, and R. Tornberg 38

The Sudbury Igneous Complex (SIC) as Impact Melt Layer: Geochemical Evidence for *In Situ* Differentiation
M. Ostermann and A. Deutsch 38

The Karikkoselkä Impact Structure, Central Finland: New Geophysical and Petrographic Results
L. J. Pesonen, S. Elo, R. Puranen, T. Jokinen, M. Lehtinen, L. Kivekäs, and I. Suppala 39

Hydrocode Simulations of Chicxulub as an Oblique Impact Event
E. Pierazzo and D. A. Crawford 40

Estimates of Climatically Important Gases Released in the Chicxulub Impact Event
E. Pierazzo, H. J. Melosh, and D. A. Kring 40

Geophysical Signatures of Large Impact Structures
M. Pilkington, R. A. F. Grieve, and A. R. Hildebrand 41

Gravity and Magnetic Modeling of a Complex Impact Structure: Effect of Deformation and Erosion
J. Plado, L. J. Pesonen, and V. Puura 42

The Chesapeake Bay Structure: Earth's Largest Submarine Peak-Ring Impact Crater
C. W. Poag 42

The Public Interest in Impact Cratering: The Ries Crater Museum, Nördlingen, Germany
G. Poesges and M. Schieber 43

Morphology of Diamonds from Impactites and Metamorphic Rocks
T. V. Posukhova and E. D. Nadezhdina 43

Postmagmatic Zircon Growth or Exotic Early Magmatic Phases Associated with the Emplacement of the Sudbury Igneous Complex: Samarium-Neodymium Isotopic, Geochemical, and Petrographic Evidence
S. A. Prevec, F. Corfu, M. L. Moore, P. C. Lightfoot, and R. R. Keays 44

Origin of the Sublayer of the Sudbury Igneous Complex: Samarium-Neodymium Isotopic, Geochemical, and Petrographic Evidence for Incomplete Crustal Homogenization
S. A. Prevec, R. R. Keays, P. C. Lightfoot, and Q. Xie 44

Geochemical and Samarium-Neodymium Isotopic Evidence Regarding the Origin of Offset Dikes of the Sudbury Igneous Complex, Ontario
S. A. Prevec, Q. Xie, R. R. Keays, and P. C. Lightfoot 45

Postimpact Impactite Phase
J. Raitala 45

Impact Crises, Mass Extinctions, and Galactic Dynamics: A Unified Theory
M. R. Rampino 46

Striations, Polish, and Related Features from Clasts in Impact-Ejecta Deposits and the "Tillite Problem"
M. R. Rampino, K. Ernstson, F. Anguita, and F. Claudin 47

Vredefort 1997: A Controversy Resolved—Still a Challenge for the Future
W. U. Reimold 47

Paleoproterozoic Tectonism in the Eastern Penokean Orogen and Its Significance for the Origin of the Norite of the Sudbury Igneous Complex
U. Riller and W. M. Schwerdtner 48

Charlevoix and Sudbury as Simple Readjusted Craters
J. Rondot 48

Do Outliers of the Huronian Supergroup Mark the Downfaulted Rim of the Sudbury Crater?
D. H. Rousell and D. G. F. Long 49

Serenitatis: The Oldest, Largest Impact Basin Sampled in the Solar System
G. Ryder 49

Impact-induced Melting of Granitic Rock Samples in Shock Experiments
C. Schrand and A. Deutsch 49

Constraints on the Nature and Distribution of Iridium Host Phases at the Cretaceous-Tertiary Boundary: Implications for Projectile Identity and Dispersal on Impact
B. C. Schuraytz, D. J. Lindstrom, and V. L. Sharpton 50

Characteristics of the Frood-Stobie Pseudotachylyte Belt, Sudbury Impact Structure, Canada
R. G. Scott and J. G. Spray 51

Assessing Impact Trajectory in the Geologic Record
P. H. Schultz 51

Shock Attenuation and Breccia Formation at a Complex Impact Structure: Slate Islands, Northern Lake Superior, Canada
V. L. Sharpton and B. O. Dressler 52

Impact Deposits from the Southern Inner Flank of the Chicxulub Impact Basin
V. L. Sharpton, L. E. Marín, C. M. Corrigan, and B. O. Dressler 53

Distortion Indexes and Other Structural Parameters as a Measure of Degree of Shock Metamorphism in Quartz
R. Skála 54

X-Ray Diffraction Study of Three Calcite-Rich Samples from the Kara Structure
R. Skála 55

Shock-induced Effects in Malmian Limestones from the Steinheim Crater Revealed by X-Ray Powder Diffraction Study
R. Skála and P. Jakeš 56

Characterization of Terrestrial Impact Structures by RADARSAT
S. K. Smith, R. A. F. Grieve, J. Harris, and M. Lamontagne 56

Crustal-Scale Structural Geometries of the Chicxulub Impact from British Institutions Reflection Profiling Syndicate Seismic Reflection Profiles
D. B. Snyder, R. W. Hobbs, and the Chicxulub Working Group 57

New Types of Fault Behavior Associated with Hypervelocity Impact
J. G. Spray 57

Cretaceous-Tertiary Ejecta Layer: A Case Study for Locating Source Craters and Implications for Ejecta Scaling
J. A. Stansberry, A. R. Hildebrand, and P. A. Collins 58

Seismic Analysis of the Mjølnir Impact Structure, Barents Sea
F. Tsikalas, S. T. Gudlaugsson, and J. I. Faleide 59

On Formation Mechanism of Flattened Subsurface Fracture Zone in Meteorite Craters: Results of High-Explosive Laboratory Experiments
V. M. Tsvetkov and Y. V. Zenchenko 59

Numerical Modeling of the Formation of Multiring Basins
E. P. Turtle and H. J. Melosh 60

Mineralogical, Geochemical, and Geological Data for the Interpretation of the Crater Base Structure of the Complex Terny Astrobleme, Krivoy Rog, Ukraine
A. A. Valter 60

On the Water Regime of Impactites in Large Astroblemes
S. A. Vishnevsky 61

Chicxulub Seismic Experiment: Overview and Size of the Transient Cavity
M. Warner and the Chicxulub Working Group 61

Large Meteorite Impacts and Lunar Differentiation
P. H. Warren 62

Examination of the Effects of Fireball Radiation on Material of the Ejecta Curtain
T. J. Wdowiak, K. M. Arnoult, and B. G. R. Coltress 63

The Structure of Lunar Basins: Implications for the Basin-Forming Process
M. A. Wieczorek and R. J. Phillips 63

Cryptoblemes: A New Discovery with Major Economic Implications and Profound Changes to the Geologic Paradigm
J. Windolph Jr. and J. Sutton 64

Emplacement of the Hess Offset in the North Range of the Sudbury Impact Structure
C. R. Wood, J. G. Spray, and M. Napoli 65

Origin of the Sudbury Igneous Complex and Sulfide Mineralization: Evidence from Platinum Group Elements
Q. Xie, R. R. Keays, S. A. Prevec, and P. C. Lightfoot 65

Abstracts

BP AND OASIS IMPACT STRUCTURES, LIBYA, AND THEIR RELATION TO LIBYAN DESERT GLASS: PETROGRAPHY, GEOCHEMISTRY, AND GEOCHRONOLOGY. B. Abate[1], C. Koeberl[1], J. R. Underwood Jr.[2], E. P. Fisk[3], and R. F. Giegengack[4], [1]Institute of Geochemistry, University of Vienna, Althanstrasse 14, A-1090 Vienna, Austria (christian.koeberl@univie.ac.at), [2]Department of Geology, Kansas State University, Manhattan KS 66506-3201, USA, [3]1026 N. 600 E Street, Logan UT 84341, USA, [4]Department of Geology, University of Pennsylvania, Philadelphia PA 19104, USA.

The BP impact structure, in Libya at 25°19'N, 24°20'E, consists of two eroded and discontinuous rings of hills surrounding a central block, the southern half of which is deeply eroded [1]. The inner ring is about 2 km in diameter and has an average relief of 30 m, while the outer ring has a diameter of about 2.8 km and a maximum relief of about 20 m. Recent space-shuttle radar studies show that the structure probably is 3.2 km in diameter [2,3], with the outermost disturbed beds covered by a veneer of sand. Rocks exposed are of the Cretaceous(?) Nubia Group and include quartz sandstone, siltstone, and conglomerate, as well as some shocked minerals [4]. The Oasis impact structure, also in Libya (centered at 24°35'N, 24°24'E), has a diameter originally determined to be about 11.5 km. The most prominent part of the impact structure, however, is a central ring of hills about 5.1 km in diameter and 100 m high. The diameter of the Oasis, determined from radar images, is estimated to be ~18 km. As at BP, a thin cover of sand obscures the outermost disturbed beds. The structure exposes the same rocks as the BP structure (~85 km north-northwest of Oasis). As with the BP structure, its age is constrained as younger than the target rocks, which are sandstones of the Nubia Group.

Libyan Desert Glass (LDG) is an enigmatic natural glass found in an area of about 6500 km^2 between sand dunes of the southwestern corner of the Great Sand Sea in western Egypt (near the Libyan border). The glass has a fission track age of 29 Ma [5] and occurs as centimeter- to decimeter-sized irregular, strongly wind-eroded pieces. It seems likely that this glass formed by impact, but no source crater has been determined. Evidence for an impact origin includes the presence of schlieren and partly digested mineral phases, lechatelierite (a high-temperature mineral melt of quartz), baddeleyite, a high-temperature breakdown product of zircon, and the possible existence of a meteoritic component. However, the proximity of the BP and Oasis structures to the LDG site has led to speculation that one of them might be the LDG source. Our geochemical studies provide the first data for such a comparison. We have studied the petrographical characteristics and geochemical composition of 29 samples from the BP and Oasis sites. Petrographic studies of thin sections of the samples showed that they represent mostly submature, moderately to poorly sorted, medium- to fine-grained quartzite sandstone or quartzitic breccia. Most of the studied samples do not show evidence of shock, but in a few sections some quartz grains with up to three sets of shock-characteristic planar deformation features were found. Major-element compositions of the samples were determined by XRF, while trace-element compositions were determined by neutron-activation analysis. The results available so far indicate a limited range in composition of all analyzed samples. The average LDG composition is very similar to the composition of some of the BP and Oasis sample compositions, indicating a possible relation. We are currently working on Rb-Sr and Sm-Nd isotope studies that will provide additional constraints for or against such a relation.

Acknowledgments: This research is supported by the Austrian Academic Exchange Service (to B.A.) and the Austrian Fonds zur Förderung der wissenschaftlichen Forschung (to C.K.). We are grateful to H. C. Cloete, Council of Geoscience, Pretoria, for XRF analyses.

References: [1] Martin A. J. (1969) *Nature, 223,* 940. [2] McHone J. F. et al. (1995) *Meteoritics, 30,* 543. [3] McHone J. F. et al. (1995) *GSA Abstr. w. Progr., 27(6),* A-209. [4] French B. M. et al. (1974) *GSA Bull., 85,* 1425. [5] Storzer D. and Wagner G. A. (1977) *Meteoritics, 12,* 368. [6] Barnes V. E. and Underwood J. R. (1976) *EPSL, 30,* 117. [7] Rocchia R. et al. (1996) *Compt. Rend. Acad. Sci. Paris, 322, IIa,* 839. [8] Koeberl C. (1997) in preparation.

OVERVIEW OF BOSUMTWI CRATER, GHANA. S. T. Ahulu, Geological Survey of Ghana, Geological Survey Department, P.O. Box M 80, Accra, Ghana.

Lake Bosumtwi in Ghana occupies a deep circular depression with no outlet. The depression has a raised rim with a north-south diameter of 11 km and an east-west diameter of 10 km. The rim is 250–300 m above the surface of the lake, which has a depth of ~80 m.

Early studies of the lake, dating back to 1891, appear to have favored a volcanic origin. This view was supported by periodic emissions of sulfurous gas accompanied by the appearance of dead fish, as well as the interpretation of brecciated rocks in the area as volcanic in origin. More recent studies have confirmed that the lake is contained in an impact crater with all the features associated with a structure this size. The crater has steep inner walls, and the presence of a central uplift buried beneath the lake sediments is inferred.

Rocks of the impact area are Precambrian and consist of metamorphosed upper- and lower-Birimian sediments and volcanics. Strike is northwest-southeast, with steep to vertical dips. Small granite intrusions and a few dikes are also present.

The age of the structure has been placed at ~1 Ma. The impacting meteorite has been calculated to have had a diameter of ~300 m and a mass of ~10^8 tons. Evidence suggests that the meteorite had an Fe composition [1].

The Geological Survey of Ghana has instituted a program of studies that includes detailed geological mapping of selected areas of the Bosumtwi structure and ongoing seismic monitoring. The objective of this program is to gain a fuller understanding of the effects of the impact on the surrounding rocks and to explain the sulfurous emissions.

References: [1] Jones et al. (1981) *GSA Bull.*

CRATER-FILL SEQUENCE, ONAPING FORMATION: PETROGRAPHIC AND GEOCHEMICAL SIGNATURE

OF REGIONAL HYDROTHERMAL ALTERATION. D. E. Ames[1] and H. L. Gibson[2], [1]Geological Survey of Canada, 601 Booth Street, Ottawa, Ontario K1A 0E8, Canada, [2]Laurentian University, Ramsey Lake Road, Sudbury, Ontario P3E 2C6, Canada.

Comprehensive field and geochronologic evidence indicates that the 1400-m-thick Onaping Formation is a hydrothermally altered impact crater-fill sequence with characteristics similar to pyroclastic fall and flow, debris flow, and hydroclastic breccia deposits. A major hydrothermal circulation system in the Sudbury Structure altered the crater-fill deposits around the entire circumference of the exposed structure. Evidence for a regional subseafloor hydrothermal system in the Onaping Formation includes vertically stacked, basin-wide, semiconformable alteration zones in which the rocks have undergone, from base to top, silicification, albitization, chloritization, carbonatization, and, in the uppermost zone, complex feldspathization.

Discontinuous, semiconformable silicified zones up to 440 m thick have been traced for more than 30 km in the North Range at the exposed base of the Onaping Formation. Silicified fragments observed in overlying, relatively unaltered units 200 m above the semiconformable zone suggest at least a partial syndepositional timing. Mineralogically, this zone consists of albite, quartz, actinolite, chlorite, titanite, epidote and minor K-feldspar, calcite, pyroxene, muscovite with traces of chalcopyrite, pyrrhotite, covellite, sphalerite, and magnetite. An earlier phase of K-feldspar alteration is overprinted by albite, quartz, and epidote. Albitization of two types has affected the Sandcherry member (formerly Gray member) strata intensely. Whereas type 1 is a syndepositional pervasive phase, type 2 is fracture-controlled and postdates emplacement of discordant units of "basal intrusion." Type 1 albitization is spatially associated with flow-banded aphanitic sills, dikes, and breccia complexes. The least-altered units have actinolite and chlorite shards in a grayish-green matrix. Upon increasing alteration, the shards acquire variable proportions of actinolite/chlorite, albite, K-feldspar, and quartz. Fluidal fragments are preferentially and pervasively altered. Intense albitization has bleached the units; the matrix and most lithic fragments are partially replaced. Bleached fracture-controlled albitization has an actinolite core and/or an actinolite rim (alteration front). Uranium-lead dating of hydrothermal titanite within the bleached halos constrains the age of the Onaping Formation and defines the timing of the hydrothermal system to 1848 + 3.8/–1.8 Ma. Calcite is pervasive in the upper 1 km of the fragmental sequence except around base metal showings and local zones of lower temperature silicification. In detail, the upper and lower carbonate zone contacts are slightly discordant to stratigraphy. Calcite is ubiquitous in shards and matrix, as rims on lithic fragments, and as fragments with pyrrhotite, chalcopyrite, pyrite, and sphalerite. Calcite pseudomorphs after glass suggest that the calcite is due to syndepositional alteration and is not metamorphic. The upper zone of feldspathization contains low-temperature K-feldspar with minor albite overprinted by celsian, reflecting low-temperature seawater-rock reactions in the shallow sub-seafloor.

Emplacement of the Sudbury Igneous Complex and sublayer rocks provided the heat required to initiate fluid circulation in an upper crust that contained a permeable pile of clastic rocks and reactive glass and formed a low-temperature hydrothermal system that produced extensive alteration zones regionally and base-metal mineralization locally.

IMPACT-INDUCED HYDROTHERMAL BASE METAL MINERALIZATION, WHITEWATER GROUP, SUDBURY STRUCTURE. D. E. Ames[1], H. L. Gibson[2], and I. R. Jonasson[1], [1]Geological Survey of Canada, 601 Booth St. Ottawa, Ontario K1A 0E8, Canada, [2]Laurentian University, Ramsey Lake Road, Sudbury, Ontario P3E 2C6, Canada.

Mineralization within the basin fill of the Sudbury Structure is vastly overshadowed by the huge production and reserves of Cu-Ni-PGE along the outer rim of the Sudbury Igneous Complex. The Onaping Formation is the footwall to Errington and Vermilion massive sulfides that contain proven and probable reserves of 6.4 Mt grading 4.36% Zn, 1.37% Cu, 1.15% Pb, and 55 g/t Ag, as well as minor base metal and Au showings. The sulfide forms multiple lenses; the "basal pyrite zone" is a replacement of uppermost Onaping Formation, and the Zn-Cu ore bodies lie within a Ca-Mg carbonate exhalite sinter vent complex that grades laterally into Mn-Fe-rich siliceous carbonates of the Vermilion Formation. The hanging wall consists of carbonaceous shales of the Onwatin Formation that contain a 25-km^2 plumelike zone enriched in Zn, Cu, Fe, Ba, As, V, and S, reflecting prolonged but diffuse hydrothermal activity. Deposits are mineralogically simple, containing pyrite, chalcopyrite, low-Fe sphalerite (<15 mol% FeS), galena, marcasite, pyrrhotite, and arsenopyrite. Freibergite and argentite occur at Errington. Gangue is dominated by various generations of Fe-Mg-Mn-Ca carbonates, quartz, barian-feldspar, barian-muscovite, pyrobitumen, trace barian stilpnomelane, and rare Fe-chlorite. Minor Onaping Formation base-metal mineralization occurs as replacement of lapillistone beds and fragments, veins, stringer zones, disseminations, and sulfide fragments situated in silicified zones near the contact with the SIC, near the base of the regional calcite alteration zone (~1 km from the top), and near the top of the sequence in the upper units.

Mineral chemistry and assemblages show that the mineralizing fluids had low $a(O_2)$ and $a(S_2)$. Organic C ($\delta^{13}C_{PDB} = -30.2$) deposited in the ore bodies buffered the hydrothermal system to a low $a(O_2)$. Silicification produced a cherty carapace above the sulfides and locally at their base along with Ba-rich feldspars and micas. These, as well as distal-banded Fe-Mn-carbonate and quartz/albite, are interpreted to be the products of diffuse upflow of low-temperature fluids. The dominant lower-temperature pyrite-sphalerite assemblages, enriched in Zn, Cd, and Ag, are crosscut and replaced by pyrrhotite, chalcopyrite, and high Fe-chlorite, reflecting a later phase of higher temperature upflow. Abundant Ba throughout the deposit suggests that late hydrothermal reworking was relatively minor and low in temperature. Low-temperature minerals precipitated at an early stage were remobilized to the top of the deposit, and retrograde cooling facilitated low-temperature mineralization in the remaining void spaces. The morphology and composition of regional alteration is similar to that of volcanogenic massive sulfide districts, and the ore assemblages are similar to those of black smokers, except that these deposits formed at 200°C and not 350°C. Extensive (>1 km) hydrothermally altered peperite bodies occur near the top of the Onaping Formation and are restricted to the southwestern part of the basin below the deposits. This implies deep-seated, relatively long-lived fracture systems that focused melt and hydrothermal upflow to shallow-water, low-pressure conditions.

The complex evolutionary history for the Sudbury impact crater terminated with the major hydrothermal system at 1848 Ma. Low-temperature, low $a(O_2)/a(S_2)$, hydrothermal fluids rising through and

altering the "glassy" fragmental rocks deposited base-metal sulfides due to interaction with carbonates at the base of the regional calcite alteration zone and replacement of the Vermilion Formation. Hydrothermal fluids responsible for regional alteration and base metals consisted of mixtures of downwelling modified seawater, deep crustal brines, and magmatic fluids.

NICKEL- AND PLATINUM-GROUP-ELEMENT-ENRICHED QUARTZ NORITE IN THE LATEST JURASSIC MOROKWENG IMPACT STRUCTURE, SOUTH AFRICA. M. A. G. Andreoli[1,2], R. J. Hart[2], L. D. Ashwal[3], and M. Tredoux[4], [1]Atomic Energy Corp. of South Africa, P.O. Box 582, Pretoria 0001, South Africa (aec@cis.co.za), [2]Schonland Research Centre, University of Witwatersrand, P.O. Box 3, Wits 2050, South Africa (hart@schonlan.src.wits.ac.za), [3]Department of Geology, Rand Afrikaans University, P.O. Box 524, Auckland Park 2006, South Africa (lda@rau3.rau.ac.za), [4]Department of Geological Sciences, University of Cape Town, Rondebosch 7700, South Africa (mtd@geology.uct.ac.za).

The 145 ± 0.8-Ma Morokweng impact structure (diameter ~350 km) is among the largest on Earth [1–3]. Borehole data [3] show that the center of the structure is represented by a texturally complex, sheet-like igneous body (diameter ~30 km, thickness ≥170 m), interpreted as an impact melt [1,3]. These igneous rocks consist of a variety of pyroxene-bearing lithologies, the most predominant of which is a homogeneous, medium-grained quartz norite.

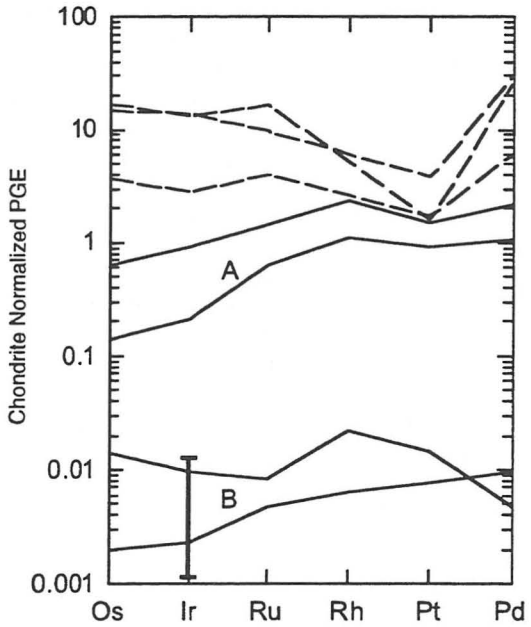

Fig. 1. Chondrite-normalized Ir concentrations of quartz norites (vertical bar) and PGE concentrations of millerite-trevorite veins (broken lines) from the Morokweng impact structure, compared to materials from the Barberton greenstone belt: trevorite-rich Ni ore (field A) and coarse-grained dunite and komatiite (field B). Data from [4] and [5].

The melt sheet has a chilled basal contact with underlying basement granitoids, which are intensely affected by shock and thermal metamorphism. In certain places, veins and dikes of heterogeneous and/or finer-grained quartz norite, pyroxene-bearing granitoids or pegmatoids, and granophyres crosscut the impact melt sheet.

Constituent minerals in the impact-melt rocks include plagioclase (An_{22-51}), orthopyroxene (En_{55}), minor subophitic augite (En_{38-42}, Wo_{40-46}), and granophyric quartz-K-feldspar intergrowths. The opaque minerals occur either as finely disseminated grains (mainly magnetite and ilmenite) or as occasional sulfide-rich blebs and tapering veinlets (up to 3 cm wide) in contact with pyroxenes and quartz. The mineralogy of these veins consists of Ni- and Cu-sulfides (Co-bearing millerite, bornite, chalcopyrite, chalcocite), Ni-rich oxides (bunsenite, Ni-rich ilmenite, trevorite), Ni-rich silicates (liebenbergite, willemseite), and traces of native Pt [3].

The quartz norites are marked by intermediate to acid bulk chemistry (SiO_2 = 59–66 wt%, MgO = 2.4–4.9 wt%). They show poorly fractionated REE and striking enrichments in siderophile elements (avg Ir = 3.8 ppb, Au = 9 ppb, Ni = 480 ppm, Cr = 360 ppm). These are equivalent to or above siderophile abundances in mantle-derived rocks from the Barberton greenstone belt (Fig. 1), possibly indicating an origin as impact-generated crustal melts with appreciable meteoritic contamination [3]. However, Morokweng differs from most other impacts, with the possible exception of Sudbury, in that its impact melts show some degree of differentiation between earlier, medium-grained quartz norite and the crosscutting, finer-grained varieties. There is also evidence of enrichment processes affecting the PGE and Au in the millerite-trevorite veins, which show non-chondritic PGE patterns (avg. Os = 9.5 ppm, Ir = 7.8 ppm, Ru = 9.9 ppm, Pt = 2.7 ppm, Pd = 23 ppm, Au = 0.9 ppm; Fig. 1). The Ni-rich mineral assemblages are unique, although reminiscent of an enigmatic 3.5-Ga Ni deposit from the Barberton greenstone belt [4].

References: [1] Andreoli M. A. G. et al. (1995) *Abstr. Centennial Congr. Geol. Soc. S. Afr., 1,* 541–544. [2] Corner B. et al. (1997) *EPSL, 146,* 351–364. [3] Hart R. J. et al. (1997) *EPSL, 147,* 25–35. [4] Tredoux M. et al. (1989) *JGR, 94,* 795–813. [5] Tredoux M. and McDonald I. (1996) *Geostandards Newsletter, 20,* 267–276.

SIMULATING PHASE EQUILIBRIA AND *IN SITU* DIFFERENTIATION FOR THE PROPOSED PARENTAL SUDBURY MAGMAS. A. A. Ariskin, Vernadsky Institute, 19 Kosygin Street, Moscow 117975, Russia (ariskin@glas.apc.org).

Summary: Phase equilibria calculations were performed on the equilibrium crystallization and *in situ* differentiation for two magma compositions assumed to be parental for the Sudbury Igneous Complex. Preliminary results of the simulations indicate that the observed SIC suite could not be formed during a closed-system fractionation of a single magma body.

One of the main problems with petrological interpretation of the Main Mass of the Complex concerns the probable genetic link between, as well as the volumetric relations of, granophyres and norites [1]. To address this problem, we used the COMAGMAT model designed for the calculation of melting-crystallization relationships in basaltic to dacitic systems [2]. This program calculates mineral temperatures and compositions step by step as the total amount of melt is decreased.

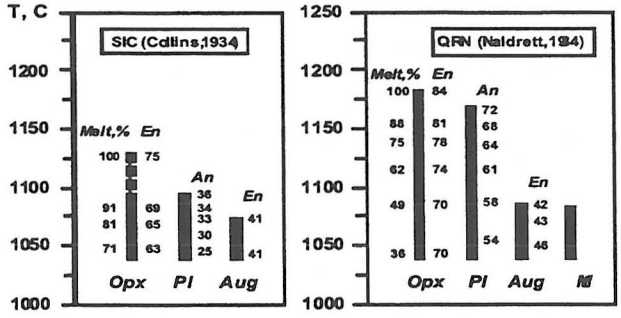

Fig. 1. Modeled crystallization sequences and mineral compositions.

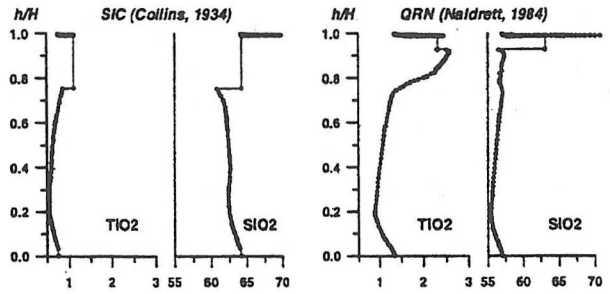

Fig. 2. Calculated structure of SIC "intrusion" for two parental magma compositions.

Modeling Phase Equilibria: Figure 1 compares results of 1-atm calculations conducted for QFM buffer conditions and two compositions proposed to be parental for SIC. SIC corresponds to the mix of granophyres and norites in the ratio 2:1 [3], and QRN represents the fine-grain, quartz-rich norites of the South Range [4]. Both compositions indicate Opx to be the first crystallizing phase, followed by plagioclase and Aug (+magnetite).

We draw attention to the fact that the bulk SIC composition can potentially produce about 70% of a residual melt that contains more than 67% SiO_2, whereas the QRN magma can produce only ~30% of such a "granophyre" liquid. This does not mean, however, that these volumetric proportions between differentiates could result from an *in situ* magma differentiation process.

Simulating *In Situ* Magma Differentiation: Due to a porosity of natural cumulates, a part of the silica-enriched liquid is known to be trapped as an intercumulus material. To study the effect numerically, we used the INTRUSION routine of COMAGMAT designed for the simulations of magma differentiation by the convective-cumulative model [5]. This model implies an efficient convective process that is assumed not to prevent eventual settling of crystals suspended in the magma and originated near the roof. COMAGMAT links the phase equilibria and heat-mass transfer calculations into a single algorithm, allowing one to analyze variations of modeled-rock compositions through the vertical section.

We performed a set of calculations to account for the settling of Opx, Pl, Cpx, and magnetite crystals in a magma body having an initial thickness of 2.5 km, followed by the formation of cumulates containing up to 50% of intercumulus liquid. Figure 2 demonstrates that, even in the case of highly silica enriched SIC composition, the total amount of modeled granophyres does not exceed 25% of the total thickness. In other words, *in situ* magma differentiation was not able to produce the observed volumetric relations, if the Main Mass indeed represents a complete section of the differentiated SIC magma body. Reasons for the misfit between the calculated succession of crystallizing phases and resulting rock compositions and the geochemical observations [6] are currently being explored.

Acknowledgments: This work is supported by a DFG grant (436 RUS 17/56/97) to A. Deutsch.

References: [1] Deutsch A. et al. (1995) *Geol. Rundsch., 84,* 697. [2] Ariskin A. A. et al. (1993) *Comp. Geosci., 19,* 1155. [3] Collins W. H. (1934) *Trans. R. Soc. Can., 28,* 123. [4] Naldrett A. J. (1984) *Ontario Geol. Surv. Spec. Vol., 1,* 533. [5] Frenkel M. Y. et al. (1989) In *Magma-Crust Interactions and Evolution,* pp. 3–88, Theophrastus Publ., Athens. [6] Ostermann M. and Deustch A., this volume.

INVESTIGATIONS ON THE GREEN MEMBER OF THE ONAPING FORMATION, SUDBURY STRUCTURE, ONTARIO, CANADA.

M. E. Avermann, Institut für Planetologie, Wilhelm-Klemm-Strasse 10, 48149 Münster, Germany (averman@uni-muenster.de).

The polymict, allochthonous breccias on the Onaping Formation occur in the central part of the Sudbury Structure, which is regarded as the possible remnant of a multiring basin [1]. The origin of these breccias has been debated for years [e.g., 2]. The Onaping breccias were mapped in the North and East Ranges and investigated in detail [3]. In this study an impact origin of the Sudbury Structure as presented by Stöffler et al. [4] is favored.

From bottom to top, the 1800-m-thick Onaping Formation is subdivided into Basal, Gray, and Black members. A fourth unit, the Green member (*sensu* Brockmeyer [5]), formerly known as the "chlorite shard horizon" [2], forms a relatively thin layer between the Gray and Black members [6]. It attains a maximum thickness of 70 m and is thought to be continuous around the structure [7].

The Green member appears as a layer of a rather uniform, strongly chloritized breccia. The contact with the Gray member varies from sharp to gradational. The Green member is characterized by a microcrystalline matrix of small, shocked country rock fragments, melt inclusions, and typical chloritized melt particles, all affected by high temperatures [6]. It is overlain by the clastic matrix breccias of the Black member, which is characterized by a carbonaceous matrix. In its lower unit it shows similarities to the Gray member. The upper Black member displays textural features of reworking and sedimentation under aquatic conditions.

The occurrence and texture of the Green member are unique with respect to other known impact structures. Melosh and Peirazzo [8] argue that, in large craters, plume dynamics may need to be considered as part of the late-stage impact processes. The Green member as a melt-rich fall-back layer overlies the suevitic breccias of the Gray member and is interpreted to represent the "collapsed fire ball horizon" of the Sudbury Structure. As such it originated from early excavation to high atmospheric regimes, condensation of a vapor phase [9], and deposition with the final fall-back material.

If this interpretation is correct, deposition of the Green member terminates the excavation phase. Rainout of melt particles continues into the Black members, but most of the lower Black member

represents redeposition and slumping of suevitic material into the central depression (modification process).

In summary, the breccias of the Onaping Formation are interpreted as follows: (1) Basal member, clast-rich melt breccia; (2) Gray member, ground surge and fall-back breccias; (3) Green member, melt-rich fall-back; (4) lower Black member, redeposited suevitic breccias; and (5) upper Black member, reworked impact breccias.

References: [1] Stöffler D. et al. (1989) *Meteoritics, 24,* 328. [2] Muir T. L. and Peredery W. V. (1984) *Ontario Geol. Surv. Spec. Vol. 1* (E. G. Pye et al., eds.). [3] Avermann M. (1992) Ph.D. thesis, Univ. Münster, 175. [4] Stöffler D. et al. (1994) *GSA Spec. Paper 293,* 303–318. [5] Brockmeyer P. (1990) Ph.D. thesis, Univ. Münster, 228. [6] Avermann M. (1994) *GSA Spec. Paper 293,* 264–274. [7] Dressler B. O. et al. (1987) *Research in Terrestrial Impact Structures* (J. Pohl, ed.), pp. 39–68. [8] Melosh H. J. and Pierazzo E. (1997) *LPS XXVIII,* 935–936. [9] Melosh H. J. (1989) *Impact Cratering: A Geologic Process,* Oxford, New York, 245 pp.

EXTRATERRESTRIAL HELIUM ($He@C_{60}$) TRAPPED IN FULLERENES IN THE SUDBURY IMPACT STRUCTURE.

L. Becker[1], J. L. Bada[1], R. J. Poreda[2], and T. E. Bunch[3], [1]Scripps Institution of Oceanography, University of California at San Diego, La Jolla CA 92093-0212B, USA, [2]Department of Earth and Environmental Sciences, University of Rochester, Rochester NY 14627, USA, [3]Space Science Division, NASA Ames Research Center, Moffett Field CA 94035, USA.

Introduction: Fullerenes (C_{60} and C_{70}) have recently been identified in a shock-produced breccia (Onaping Formation) associated with the 1.85-Ga Sudbury Impact Crater [1]. The presence of parts-per-million levels of fullerenes in this impact structure raises interesting questions about the processes that led to the formation of fullerenes and the potential for delivery of intact organic material to the Earth by a large bolide (e.g., asteroid or comet). Two possible scenarios for the presence of fullerenes in the Sudbury impact deposits are that (1) fullerenes are synthesized within the impact plume from the C contained in the bolide [1]; or (2) fullerenes are already present in the bolide and survived the impact event.

The correlation of C and trapped noble gas atoms in meteorites is well established [2]. Primitive meteorites contain several trapped noble gas components that have anomalous isotopic compositions [3], some of which may have a presolar origin [4]. Several C-bearing phases, including SiC, graphite, and diamond, have been recognized as carriers of trapped noble gases [5]. It has also been suggested that fullerenes (C_{60} and C_{70}) might be a carrier of noble gas components in carbonaceous chondrites [6]. Recently, fullerenes have been detected in separate samples in the Allende meteorite [7,8]. Carbon-60 is large enough to enclose the noble gases He, Ne, Ar, Kr, and Xe, but it is too small to contain diatomic gases such as N_2 or triatomic gases such as CO_2. Recent experimental work has demonstrated that noble gases of a specific isotopic composition can be introduced into synthetic fullerenes at high temperatures and pressures; these encapsulated gases can then be released by the breaking of one or more C bonds during step-heating under vacuum [9]. These thermal-release patterns for He encapsulated within the C_{60} molecule ($He@C_{60}$) are similar to the patterns for acid residues of carbonaceous chondrites [5], suggesting that fullerenes could be an additional carrier of trapped noble gases in acid residues of meteorites.

Analysis and Results: In order to characterize the noble gas compositions of the Sudbury fullerenes, we undertook a systematic study of acid-resistant residues throughout the C-rich layer (Black member) of the Onaping Formation. Samples were demineralized and extracted using standard techniques [1]. The Onaping extracts were analyzed using several techniques, including UV-Vis adsorption, electro spray mass spectrometry, and laser desorption (linear and reflectron) time-of-flight (TOF) mass spectrometry (LDMS). The Sudbury fullerenes were then separated and purified using HPLC coupled with a photo diode array detector [10]. The HPLC extracts containing the purified fullerenes were loaded into a metal tube furnace within a glove box under a N atmosphere in preparation for noble gas analyses. The ^3He and ^4He content of the fullerene extracts was measured using previously reported standard techniques [9].

Discussion: Fullerenes (C_{60} and C_{70}) in the Sudbury Impact Structure have been found to contain trapped He with a $^3He/^4He$ ratio greater than 5×10^{-4}. The $^3He/^4He$ ratio exceeds the accepted solar value by more than 30% and is more than 10× higher than the maximum reported mantle value. Terrestrial nuclear reactions or cosmic-ray bombardment are not sufficient to generate such a high ratio. The $^3He/^4He$ ratios in the Sudbury fullerenes are similar to those determined for interplanetary dust particles. The greater-than-solar ratios of $^3He/^4He$ in the Sudbury fullerenes may indicate a presolar origin, although alternative mechanisms occurring in the ISM to explain these high ratios (e.g., spallation reactions, selective He implantation, etc.) cannot be entirely ruled out. We are currently attempting to isolate enough fullerene material to measure anomalous Ne (or Kr or Xe) contained within the C_{60} (e.g., the "pure" ^{22}Ne component) [5] and thus determine whether the Sudbury fullerenes are indeed presolar in origin.

References: [1] Becker L. et al. (1994) *Science, 265,* 642. [2] Anders E. et al. (1975) *Science, 190,* 1262. [3] Black D. C. and Pepin R. O. (1969) *EPSL, 6, 395.* [4] Swart P. K. et al. (1983) *Nature, 220,* 406. [5] Zinner E. et al. (1995) *Meteoritics, 30,* 209. [6] Heymann D. (1986) *Proc. LPSC 17th,* in *JGR, 91,* E135. [7] Becker L. et al. (1994) *Nature, 372,* 507. [8] Becker L. and Bunch T. E. (1997) *Meteoritics & Planet. Sci.,* in press. [9] Saunders M. et al. (1993) *Science, 259,* 1428. [10] Heymann D. et al. (1994) *Science, 265,* 645.

SUMMARY OF WORK IN MANICOUAGAN IMPACT STRUCTURE.

L. Boivin, Minéraux Manic Inc., Montreal, Quebec, Canada.

The Manicouagan impact structure is located in the central part of Quebec at 51°25'N and 68°45'W. The 100-km circular structure is now unanimously considered to be the product of an hypervelocity-meteorite impact. This structure is located within Precambrian crystalline rocks metamorphosed during the Grenville orogeny at 1 Ga. On a regional scale the rocks are metamorphosed to upper amphibolite and locally granulite facies trending northeast-southwest. This structural fabric is interrupted by the Late Triassic impact structure that created a unique suite of rocks.

Physically, the impact structure is a complex crater with a central uplift of anorthositic composition. These anorthosites are sur-

rounded by melt rock rimmed by a margin of latite and suevite. Outcrops are controlled by topography. The main lithology of the Manicouagan structure is a flat-lying sheet with angular inclusions ~250 m thick and 55 km in diameter. This has been interpreted as impact melt rock [1]. The impact melt is intermediate in composition and shows no major vertical or lateral geochemical variation in the melt rock [2].

The presentation of field data collected by the company will reflect certain interesting observations, and current work should reveal the causes or sources of some of them in time for presentation at the conference. Data will include (1) the shock metamorphism and homogeneous magnetization of all mafic minerals within a certain radius of the impact; (2) the ubiquitous highly magnetic nature of the subaphanitic matrix of the suevite (fall-back breccia) and whether this is due to the Ni-Fe composition of the meteorite that fell there; (3) the condensation of gaseous silica within the suevite unit, producing what has erroneously been identified as amygdular tuff; (4) the presence of postimpact ultramafic magmatism; (5) the presence of sulfide mineralization in two distinct environments; and (6) drill results from a campaign to determine the cause of the 6000–8000 γ above background anomaly surrounding the point of impact (4 km × 6 km) in the center of the crater.

References: [1] Floran et al. (1978). [2] Grieve and Floran (1978).

COMPOSITION AND STRUCTURE OF THE CHICXULUB CRATER USING WIDE-ANGLE SEISMIC VELOCITIES.

J. Brittan[1], H. Macintyre[1], and the Chicxulub Working Group, [1]Department of Geology, Imperial College, London SW7 2BP, UK (j.brittan@ic.ac.uk).

The Chicxulub seismic experiment collected wide-angle seismic data using receivers on the seabed, on land, and on the sea surface. Seismic energy received at wide angles contains precise information about the seismic velocities of the material that the wave traversed and thus can be used to infer the composition of material to great depths within the subsurface.

We show seismic velocity images of the shallow (< 3 km deep) structure of the crater derived from marine seismic reflection data acquired across the structure. The P-wave velocity structure of the upper parts of the crater is derived from the inversion of wide-angle turning ray data acquired on the streamer during the experiment and during earlier seismic surveys for hydrocarbon exploration. The data show clear velocity images of the peak ring, crater rim, and crater fill. The velocity data allow for a differentiation between the Tertiary fill, the impact ejecta, and the preexisting Cretaceous stratigraphy. Radial asymmetry of the crater structure, which was suggested by gravity profiles in the area, is confirmed by the combined reflection/velocity analysis. The northeast-southwest radial line suggests that the thickened low velocity (and low density) Tertiary fill is responsible for the coincident low in the gravity profile of the crater. The northwest-southeast radial line shows high velocities relatively close to the surface, suggesting high-velocity (and high-density) Cretaceous sediments in this region. Comparisons with the coincident stacked seismic reflection data suggest that the peak ring of the crater is associated with low-velocity material. These low velocities and the position of the peak ring relative to the collapsed margins of the transient crater suggest that it is composed of brecciated material (which may include rocks from the deep basement). In this case the peak ring is thought to represent the outward collapse of a gravitationally unstable central structural uplift.

Seismic velocity images of the deeper parts of the crater, and, in particular, the deep central part of the impact structure, have been derived from wide-angle seismic energy collected on about 100 land stations on the Yucatán Peninsula. With further processing, these data will show the extent of the central uplift and the effect of the impact on the lower crust and Moho underneath the center of impact.

SYNTHETIC APERTURE RADAR CHARACTERISTICS OF A GLACIALLY MODIFIED MELTSHEET, MANICOUAGAN, QUEBEC.

P. Budkewitsch[1] and R. Grieve[2], [1]MIR Télédétection, under contract to Canada Centre for Remote Sensing, Ottawa, Canada, [2]Geological Survey of Canada, Ottawa, Canada.

Major features of large eroded terrestrial impact craters are often difficult to recognize in the field. Satellite images, however, provide synoptic views suitable for the examination of spatially large features such as impact structures. As part of a larger study, RADARSAT data are being utilized, with other SAR, LANDSAT, and other digital (e.g., DEM) data, to characterize large terrestrial impact structures. Here, we focus on the use of RADARSAT data to delineate some of the characteristics of the Manicouagan impact structure [1]. The RADARSAT data were acquired in wide mode beam 2 (W2) centered on the impact structure and covering an area approximately 150 km × 150 km, with a radar incidence angle of 31–39° and ground resolution of 27 m.

The pervasive tectonic fabric of the Grenvillian target rocks in the area is clearly outlined in the RADARSAT imagery. In addition, many lithotectonic units recognized from regional geological mapping are evident, due to differential erosion along zones of structural or lithological weakness. The preserved impact melt rocks at Manicouagan occur as a flat-lying, up to 250-m-thick, tabular unit on the ~50-km-diameter central island. The central uplifted block of the Grenvillian basement, which penetrates the impact melt sheet, is recognizable in the SAR imagery, contrasting sharply in radar texture with the impact melt rocks.

The SAR terrain features visible from the area of the melt-sheet are distinct and are similar to those typical of drumlin fields. To the north of the Manicouagan reservoir, a glacially fluted terrain is recognized with similar features. There are several differences, however, between the appearance of true drumlins and the radar texture of the melt-sheet area: (1) the "drumlin" features in the melt-sheet area have smaller length-to-width aspect ratios and are topographically higher than the true drumlins composed of drift found to the north; (2) whereas drumlins composed of drift are lenticular, many drumlin-like features on the melt sheet have two lateral terminations (swallow-tail appearance); (3) the north ends of melt-sheet "drumlins" are characterized by high radar backscatter, indicative of exposed bedrock and suggesting that they nucleated on a local erosionally resistant pocket of impact melt rock; and (4) the erosional pattern of the regional Grenville bedrock, as expressed in the RADARSAT data, is profoundly different in character from the erosion of the melt-sheet rocks.

While a north-northwest glacial fabric to the outcrop area of the impact melt rocks has been recognized before in optical imagery

[2], this drumlin-like texture is limited to SAR imagery and appears to varying degrees in ERS-1, Seasat and airborne SAR data over Manicouagan. It is not evident in LANDSAT data, and its distribution in SAR imagery corresponds with the geologic distribution of the melt rocks, suggesting that, at least in this case, RADARSAT data can be used as a lithological mapping tool. We interpret the drumlin-like landforms developed in the melt-sheet area to be the result of significant glacial scouring of relatively compliant, structurally isotropic impact melt rock. In contrast, in the outer zone of the impact structure, SAR data indicate that the glacial erosion preferentially enhances preexisting lithotectonic fabrics or brittle structures of the target bedrock. It is difficult, however, to recognize any radial density change in impact-related fractures in the RADARSAT imagery over the Manicouagan impact structure. The digital topographic data to the west of the central island, however, reveal a number of discontinuous concentric valleys, which are most likely related to structural features of the original impact crater.

References: [1] Grieve R. A. F. and Head J. W. (1983) *Proc. LPSC 13th*, in *JGR, 88*, A807–A818. [2] Dence M. R. (1978) *NASA SP-380*, 175–189.

NEW POTENTIAL SOURCES FOR BLACK ONAPING CARBON. T. E. Bunch[1], L. Becker[1], P. H. Schultz[2], and W. S. Wolbach[3], [1]Space Science Division, NASA Ames Research Center, Moffett Field CA 94035, USA, [2]Department of Geological Sciences, Brown University, Providence RI 02912, USA, [3]Department of Chemistry, Illinois Wesleyan University, Bloomington IL 61702, USA.

One intriguing and important issue of the Sudbury Structure concerns the source of the relatively large amount of C in the Onaping Formation Black member. This dilemma was recently addressed [1], and the conclusion was reached that an impactor could not have delivered all of the requisite C. Becker et al. have suggested that much of the C came from the impactor [2] and reported the presence of interstellar He "caged" inside some fullerenes that may have survived the impact [3]. So, conceivably, the C inventory in the Sudbury Structure comes from both target and impactor materials, although the known target rocks have little C. We discuss here the possibility of two terrestrial sources for at least some of the C: (1) impact evaporation/dissociation of C from carbonate target rocks and (2) the presence of heretofore-unrecognized C-rich (up to 26 wt%) siliceous "shale," fragments, which are found in the upper, reworked Black member.

Experimental: Hypervelocity impact of a 0.635-diameter Al projectile into dolomite at 5.03 km/s (performed at the Ames Research Center vertical gun range) produced a thin, black layer (≈0.05 mm thick) that partially lined the crater and coated impactor remnants. Scanning electronic microscope (SEM) imagery shows this layer to be spongelike on a submicron scale and Auger spectroscopic analyses yield: 33% C, 22% Mg, 19% O, and 9% Al (from the projectile). Elemental mapping shows that all of the available O is combined with Ca and Mg, Al is not oxidized, and C is in elemental form. Dissociation efficiency of C from CO_2 is estimated to be <10% of crater volume. Raman spectroscopy indicates that the C is highly disorganized graphite. Another impact experiment [4] also produced highly disorderd graphite from a limestone target (reducing collector), in addition to small amounts of diamond/lonsdaleite/chaoite (oxidizing collector). These experiments confirm the reduction of C from carbonates in impact vapor plumes.

Observational: SEM observations and microprobe analyses of small, black shalelike inclusions in the upper Black Onaping indicate high C contents (7–26 wt%; avg. = 16%). They contain mostly quartz and carbonaceous matter with small amounts of altered K-feldspar, clays, Fe oxide, and a sulfide. No evidence of shock is seen in quartz, and overall characteristics indicate a natural, lightly metamorphosed carbonaceous shale or mudstone that probably existed as a preimpact rock in the target region and distal fragments washed in during early crater filling. Fragments range in size from tens of microns to cm and increase in abundance in the upper Black toward the Onwatin contact, although their distribution is highly irregular. This increase corresponds to an increase in "organic" C with increasingly negative $\delta^{13}C$ values and S [5], together with a decrease in fullerene abundance. In addition, we have found soot in acid-demineralized residues of the Onwatin but not in the Onaping samples. These data could be consistent with impact plume and atmospheric chemical processes, with possible diagenetic overlays. We are analyzing carbonaceous fractions of the Onaping and Onwatin to determine diagnostic C isotopic signatures. Analyses by Whitehead et al. on bulk samples revealed no definitive source or processes [5], although $\delta^{13}C$ values for "organic" C overlapped those for some meteorites.

Discussion: If impact evaporation of Sudbury target carbonates did occur, then where are the carbonates? Distal carbonate (limestone/dolostone) exposures of the Espanola Formation (Huronian Supergroup) are generally thin-bedded, although remnants that partially encompass the Sudbury Crater are variable in thickness and may locally reach 250 m [6,7]. If a carbonate thickness of 100–200 m existed at the target site, then copious amounts of C could have been reduced by impact processing of carbonates and also C-shale, depending on the efficiency of the processing and the amount of postimpact oxidation.

Conclusion: The Sudbury crater offers a unique opportunity to study preserved characteristics of immediate carbonaceous fallback matter and particles of short-term residency in the impact plume as well as dust/aerosols from postimpact atmospheric processing.

References: [1] Heymann D. and Dressler B. (1997) *LPS XXVIII*, 563. [2] Becker L. et al. (1994) *Science, 265*, 642. [3] Becker L. et al. (1996) *Science, 272*, 249. [4] Miura Y. and Okamoto M. (1996) *Antarctic Meteorites XXI*, 107 (NIPR, Tokyo). [5] Whitehead R. E. S. et al. (1990) *Chem Geol., 86*, 9. [6] Dressler B. O. (1982) *Ont. Geol. Surv. Rpt.*, 2130. [7] Meyer W., personal communication.

ECOSYSTEM-STRUCTURE ANALYSIS APPLIED TO INDICATION AND STUDY OF EARTH ASTROBLEMES. G. G. Burba Jr., 236 L. W. Chase Hall, University of Nebraska, Lincoln NE 68583-0728, USA (agme026@unlvm.unl.edu; georgeburba@geocities.com).

Geological methods are usually used to locate and study astroblemes. These methods are less effective if the astroblemes are covered with glacial deposits, thick soil, or forest. For such astroblemes, it seems possible to use a method based on analysis of

the ecosystem structure. The rivers, geomorphology, soil, and canopy covers jointed into the ecosystem structure have a long memory for the catastrophic changes precipitated by impact explosion.

The ecosystem structure of the Zhamanshin astrobleme (Kazakhstan; 48°20'N, 60°58'E) was studied by this author during a field expedition [1]. The geomorphic data, soil profile, hydrologic pattern, and specie composition were studied at all structural parts of the crater (over 300 km^2). Data described 90 different types of ecosystems and included 250 individual ecosystems. Five maps were created in 1:200,000 scale (surface deposits, geomorphology, soils, vegetation, and drainage net). They were used together with LANDSAT images to produce a final ecosystem map of the astrobleme [2].

Based on the data and the experiences of the Zhamanshin expedition, cameral mapping was conducted on the ecosystem structures of three additional astroblemes. Features of the ecosystem structure of Zhamanshin (13 km in diameter, 0.75 m.y., Kazakhstan) were compared with those of the Popigay astrobleme (100 km diameter, 40 m.y., Siberia), the Araguinha astrobleme (40 km diameter, 250 m.y., Brazil), and the Gasses-Bluff astrobleme (22 km diameter, 143 m.y., Australia).

All compared astroblemes demonstrated very similar features of the ecosystem structure (in spite of considerable differences in age, climate, prevailing geomorphic processes, and display in relief): (1) The ecosystem structures inside the astroblemes had entirely different patterns compared to the area outside the ejecta blanket; (2) the landscape divisions had a concentric shape inside the astroblemes and an elongated-spotty shape outside the astroblemes; (3) the landscape subdivisions reflected the astroblemes' structures (i.e., central uplift, concentric ring uplifts, slopes, rim, and ejecta blanket); (4) the density of different ecosystems inside the astroblemes was higher than that of the outside areas; (5) in spite of drastic environmental changes during geological history, patterns of soil and vegetation types continued to keep position correspondingly to initial relief of the astroblemes; and (6) the ratio of circular-radial to chaotic patterns of the drainage net was 2.5–3× higher within the astroblemes as compared to the outside areas.

The above features demonstrate that the ecosystem structure of the astroblemes can exist much longer than relief or any particular natural component. It gives a strong indication that ecosystem-structure examination, along with geological and geophysical methods, can be used as a research tool for the study of astroblemes.

References: [1] Burba G. G. and Meshcherskaya V. A. (1993) *Ann. Geophys., III (11),* C-451. [2] Burba G. G. (1994) *Geography, 3,* Vestnik Mosc. Univ.

SEDIMENTARY INTERBEDS OF THE ROOIBERG GROUP AT THE LOSKOP DAM SECTION, BUSHVELD COMPLEX, SOUTH AFRICA. M. E. Caress and W. E. Elston, Department of Earth and Planetary Sciences, University of New Mexico, Albuquerque NM 87131-1116, USA.

The question of whether the Rooiberg Group, the basal unit of the Bushveld Complex, represents a catastrophic event or a gradual transition from normal Pretoria Group sedimentation to Bushveld magmatism [1] is central to identification of the Bushveld Complex as a multiple-impact site or the result of endogenic processes of an unprecedented scale. The Loskop Dam section is thought to represent ponding within an annular basin of initial ejecta and later outflow from the volcanic or psuedovolcanic system that resulted from a catastrophe. The Rooiberg Group in the Loskop Dam area consists of a 3.5-km-thick succession of nine "felsite" units [2]. In units 1–8 sedimentary interbeds are from a few to 60 m. A 250-m succession of pyroclastic and sedimentary beds occurs between units 8 and 9. The interbeds were traced along strike for 10 km [2]. While some interbeds separate felsite units, others occur within them [2,3].

Forty-six samples were collected from sedimentary interbeds from unit 1 through the transition from units 7 to 8. They record progressive changes that correlate with chemical and textural changes in associated felsites and indicate that emplacement of the Rooiberg Group can be divided into three stages:

1. An initial Bushveld catastrophe in a shallow subaqueous environment resulted in a multiring basin. The basal hot debris flow preserved in the Stavoren "fragment" and the Dullstroom paleochannel [4] are not exposed at Loskop Dam, but a 30-m section of quartzite with quartz paramorphs after tridymite is present near the middle of unit 1. Other sedimentary interbeds in units 1 and 2 (Upper Dullstroom and Lower Damwal Formation) [5] are interpreted as rapidly eroded material from uplifted rings of the pre-Bushveld Pretoria Group, resulting in sandstone and massive breccia. Few, if any, felsite components other than ashfall material are present in most beds. The sandstones are graywackes with subrounded to subangular quartz grains of silt to coarse sand, clay, sedimentary lithic clasts, and minor plagioclase and opaque minerals [3]. Derivation of quartz grains and lithics of the interbeds from the Pretoria Group is indicated by chemical similarities between the deposits and the scarcity of phenocrystic quartz in the felsite. Most breccias consist of matrix-supported sedimentary clasts of Pretoria Group rocks in a graywacke matrix. Two breccia zones, however—one within unit 1 and the other between units 2 and 3—consist mainly of felsite clasts in a graywacke matrix and are interpreted as locally derived. The 1400-m Loskop Dam section of units 1 and 2 seems to record repeated effusions of diverse superheated melts and hot-debris flows from a central basin into a ring syncline. Eruptions may have been triggered by influxes of resurgent waters carrying breccia of local derivation (felsite) and sand from more distant sources.

2. Units 3–6 (the upper part of the Damwal Formation) record further effusions of melts of more restricted composition during a period of magmatic equilibration and structural adjustment. The sedimentary interbeds are composed primarily of moderately well-sorted orthoquartzites, which change upward from a massive bed between units 3 and 4 to increasingly bedded sandstones with both planar and cross bedding, interbedded with minor breccia beds containing sedimentary clasts.

3. Units 7–9 reflect residual activity, as melts equilibrated with crustal rocks. Outflow deposits of meltrocks increasingly resemble conventional lavas and pyroclastic rocks in texture and chemical compositions and are interlayered with pyroclastic fall beds and sedimentary beds, which include erosional products of both felsites and the Pretoria Group [3]. These rocks constitute the Kwaggasnek and Schrikkloof Formations [5].

References: [1] Hall A. L. (1932) *S. Afr. Geol. Surv. Mem., 28,* 197–198. [2] Twist D. (1985) *Econ. Geol., 80,* 1153–1165. [3] Eriksson P. G. et al. (1994) *J. Sed. Petrol., A64,* 836–846. [4] Elston W. E. and Caress M. E., this volume. [5] Schweitzer J. K. et al. (1995) *S. Afr. J. Geol., 98,* 245–255.

THE CHICXULUB SEISMIC EXPERIMENT. Chicxulub Working Group: J. Morgan[1], M. Warner[1], J. Brittan[1], H. Macintyre[1], D. Snyder[2], R. Hobbs[2], G. Suarez[3], L. Marin[3], A. Trejo[3], R. Buffler[4], G. Christeson[4], Y. Nakamura[4], A. Hildebrand[5], M. Pilkington[5], V. Sharpton[6], P. Maguire[7], P. Denton[7], G. Mackenzie[7], and A. Camargo[8], [1]Department of Geology, Imperial College, London SW7 2BP, UK, [2]British Institutions Reflection Profiling Syndicate, University of Cambridge CB3 0EZ, UK, [3]Universidad Nacional Autonoma de Mexico, Mexico 04510, [4]University of Texas Institute for Geophysics, Austin TX 78757, USA, [5]Geological Survey of Canada, Ottawa K1A OY3, Canada, [6]Lunar and Planetary Institute, Houston TX 77058, USA, [7]University of Leicester, Leicester LE1 7RH, UK, [8]Petroleos Mexicanos, Villahermosa 86030, Mexico.

On the basis of an anomalous clay layer observed at Cretaceous-Tertiary boundary sites, Alvarez et al. (1980) proposed that there had been a large impact at the end of the Cretaceous 65 Ma. The Chicxulub crater in Mexico, which is the largest-known Phanerozoic impact structure, is now widely accepted as the site of this event.

The Chicxulub impact occurred on a gradually subsiding carbonate platform; the crater has been slowly buried beneath Tertiary sediments and remains relatively pristine and undeformed. Its location below the Earth's surface and partly onshore/offshore makes Chicxulub an ideal target for seismic investigation; many shots fired offshore were recorded on a dense array of offshore and onshore receivers, providing high density data coverage at relatively low cost. We acquired ~650 km of whole-crustal marine seismic reflection profile. The 13,000 airgun shots fired to generate these data were recorded simultaneously at wide angle on 91 land and 34 offshore stations (see Fig.1). In addition, we recorded local, regional, and teleseismic activity at 20 of the land stations for several months. These seismic data, together with existing gravity, magnetic and well control, provide a comprehensive image of the structure of the crater in three dimensions.

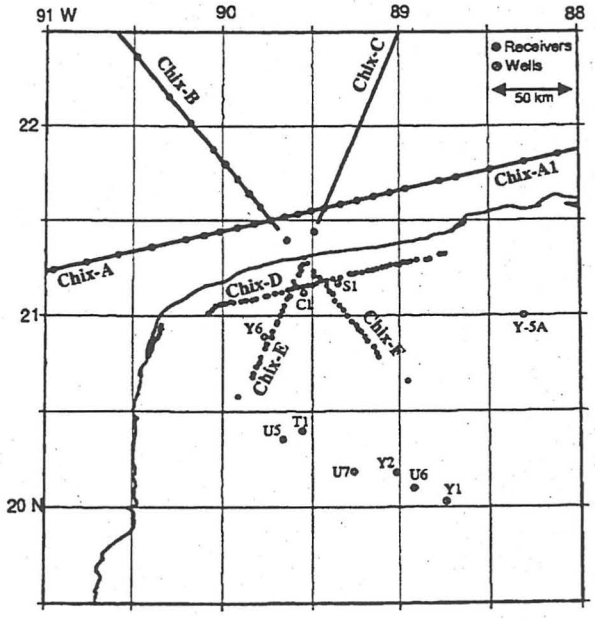

Fig. 1.

We present intermediate stacks of the new reflection data, which will be fully processed by fall 1997, and first results from the wide-angle and earthquake data, which will be fully processed by fall 1998.

STRUCTURE OF THE CHICXULUB IMPACT CRATER FROM WIDE-ANGLE OCEAN-BOTTOM SEISMOGRAPH DATA. G. L. Christeson[1], Y. Nakamura[1], R. T. Buffler[1], and the Chicxulub Working Group, [1]University of Texas Institute for Geophysics, 4412 Spicewood Springs Road, Building 600, Austin TX 78759-8500, USA.

During September–October 1996, BIRPS shot three seismic lines across the offshore portion of the Chicxulub impact crater. As part of a larger campaign with collaborators from the UK, Mexico, Canada, and the USA, the University of Texas Institute for Geophysics placed 34 ocean-bottom seismograph (OBS) receivers at 10–20 km spacing along two of the three lines (Lines A and B); 32 of the instruments recorded high-quality wide-angle seismic data. These data are being used to model the velocity structure and map deformation of the crust-mantle boundary beneath the Chicxulub impact crater. Seismic velocities can be used to infer compositions and structure of the crater, to properly position the seismic reflection data in depth, and to aid in the interpretation of gravity and magnetic modeling.

All receivers recorded a high-amplitude PmP arrival; the PmP event is formed from energy that reflects off the Moho at large angles of incidence. Normal-incidence Moho reflections are also of high amplitude locally. Along Line A, located close to and parallel to the coastline, the PmP event is delayed on receivers located within the crater and can be modeled by crustal thickening beneath the crater. This is in agreement with the seismic reflection data, which has the Moho at a later two-way travel time beneath the crater. Another major feature of the preliminary velocity model is a thickening by as much as 2 km of material with velocities less than 6 km/s beneath the crater. This correlates in the reflection data with the downdropping of Mesozoic blocks and a thickening of ejecta-breccia material toward the center of the crater. Preliminary modeling indicates asymmetry in the crater structure along Line A; this asymmetry will be refined with further analysis.

THE CHICXULUB IMPACT STRUCTURE AND ITS PROXIMAL EJECTA. P. Claeys[1], A. Deutsch[2], F. Langenhorst[3], S. Heuschkel[1], B. Dissman[2], and D. Stöffler[1], [1]Institut für Mineralogie, Museum für Naturkunde, D-10115 Berlin, Germany (philippe.claeys@rz.hu-berlin.de), [2]Institut für Planetologie, Universität Münster, D-48149 Münster, Germany (deutsca@uni-muenster.de), [3]Bayerisches Geoinstitut, D-Bayreuth, Germany.

The well-preserved Cretaceous-Tertiary (K/T) boundary Chicxulub crater, in Yucatán, Mexico, lies buried under approximately 1 km of Cenozoic sediments. The conflicting interpretations of size and morphology of the Chicxulub structure, ranging from an ≈180-km central peak crater [e.g., 1] up to a 310-km multiring impact basin [e.g., 2], demonstrate our limited knowledge of the original structural features of large (>100 km in diameter) terrestrial-impact structures. Only two other large structures are known

on Earth: the deeply eroded 2023-Ma Vredefort structure, South Africa [3], and the 1.85-Ga Sudbury structure [4]. The Sudbury, Canada, structure is highly tectonized, yet still contains a complete section in the central depression ranging from crater-floor lithologies up to the post-impact crater infill. Areas outside the inner ring, however, are eroded to the sub-crater floor level [4]. Analogies of Chicxulub to smaller, well-preserved craters such as the Ries are restricted, since the K/T impact occurred on the continental shelf in an area characterized by an ~3-km-thick sedimentary sequence topping Pan-African basement lithologies. Deciphering structural features of Chicxulub thus requires the combination of geophysical data with petrology and shock barometry of the impactites recovered by drilling. So far, relatively few studies have focused on impact lithologies in the crater or its vicinity. We are currently analyzing impactites from the Pemex wells Yucatan 6 and Chicxulub 1 with microscopic, microchemical, geochemical, and isotopic techniques. To detect a possible impactor contamination ("meteoritic component"), we have analyzed Chicxulub core samples for PGE abundance. The Ir content of the Chicxulub impactites appears elevated (15 ppb), but it is heterogeneously distributed in the melt-breccias, perhaps as small Ir nuggets a few μm long [5]. The proposed high meteoritic component of the Chicxulub impactite, combined with the almost uniform Ir-rich layer found at more than 112 K/T sites worldwide, advocates a much larger impactor than the 10-km object of the original hypothesis [6], and thus favors the larger crater estimates. Despite the large number of analyses, we could not reproduce the high Ir content given by Schuraytz et al. [5]. Iridium concentration was systematically below 0.1 ppb in all 50 samples, and extensive SEM/BSE searches of impact melt-breccia failed to reveal any Ir nuggets.

Due to the specific target situation, and the seemingly quick recovery of "normal" sedimentation in the Gulf of Mexico region, Chicxulub provides a unique opportunity to study the original distribution of ejecta in the near and far vicinity of a large impact crater. Recently, two ODP cruises (leg 165, Nicaragua rise; leg 171b, east of Florida) identified up to 20-cm-thick sequences of proximal ejecta. Analyses of the K/T sequence in Belize and the Gulf of Mexico region show that a large part of the ejecta is made of carbonate material originating from pre-impact platform sediments. In Belize, the K/T boundary is marked by a clastic-matrix breccia composed of huge dolomite blocks [7]. At more distal sites, the ejecta bed is composed of carbonate clasts associated with a few shocked minerals and many clay spherules, some with a preserved impact glass core. Thickness of the ejecta unit ranges from 0.5 to 1 m. It was highly reworked and probably transported by the tsunami waves triggered by the impact. The abundance of carbonate material in the ejecta clearly illustrates the special role played by the ~3-km-thick sedimentary layers of the Chicxulub target. The aerodynamically elongated shape of some of the clasts and its association with glass may indicate that it was transported as molten particles. Other, more angular fragments were clearly ejected as solid particles. For understanding long- and short-term atmospheric effects of the Chicxulub event, it is essential to better confine the phase under which this limestone ejecta was transported—specifically, whether it was transported as solid $CaCO_3$ (and evaporites), as molten or residual CaO, or in vaporized form. Sedimentological and petrographic observations may serve as a test for calculated reactions of $CaCO_3$ to shock loading [8].

Acknowledgments: Research is supported by DFG grants Cl 147/2-1 (P.C., F.L., D.S.) and De 401/13-1 (A.D.).

References: [1] Hildebrand A. R. et al. (1995) *Nature, 376,* 415. [2] Sharpton V. L. et al. (1993) *Science, 261,* 1564. [3] Therriault A. M. et al. (1997) *Meteoritics & Planet. Sci., 32,* 71. [4] Deutsch A. et al. (1995) *Geol. Rundsch., 84,* 687. [5] Schuraytz B. C. et al. (1996) *Science, 271,* 1573. [6] Alvarez L. W. et al. (1980) *Science, 208,* 1095. [7] Ocampo A. C. et al. (1996) *GSA Spec. Paper 307,* 75. [8] Martinez I. et al. (1995) *JGR, 100,* 15465.

CHEMICAL COMPOSITIONS OF CHICXULUB IMPACT BRECCIAS.

C. M. Corrigan[1], V. L. Sharpton[2], T. A. Vogel[1], and L. E. Marín[3], [1]Michigan State University, East Lansing MI, USA, [2]Lunar and Planetary Institute, Houston TX, USA, [3]Universidad Nacional Autónoma de Mexico, Mexico City, Mexico.

The excellent preservation state of the Chicxulub structure provides an unprecedented opportunity for studying the debris deposits generated in large-body impact events. The crater formed on a 2–3 km-thick Cretaceous platform underlain by a crystalline basement of Pan-African age [1]. We are examining breccia matrix materials from three holes (U5, U6, U7) drilled into the southern flank of the basin [1–3], as well as a selection of Pemex core samples of breccia (Y6-1196m) and basement rocks (Y2-3330m, Y1-3151m). Major- and trace-element analyses have been completed on these breccia samples using X-ray fluorescence (XRF) to determine the chemical compositions of matrix materials and the proportions of individual target lithologies that have been incorporated into these breccias.

The results shown in Table 1 indicate that the matrix of the U5 (~110 km) breccia samples contains more than two-thirds silicate material. This breccia is predominantly primary ejecta derived from deep crystalline target units. There is only a very small representation of material from the platform sequence in these breccias. This is consistent with previous interpretations of the U5 breccia as crater suevite [2,3]. In terms of major oxides, the U5 suevite is similar to the breccia from the Y6-N14 core interval collected from near the center of the basin.

The U7 (~125 km) well shows high SiO_2 compositions in samples from the upper portion of the breccia sequence. At greater depths,

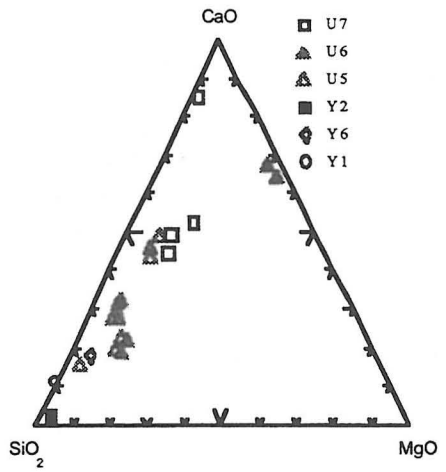

Fig. 1. Compositional plot of XRF data.

TABLE 1. XRF data normalized to 100%.

Sample	SiO_2	Al_2O_3	MgO	CaO
Y6-1196m	57.41	12.81	4.67	13.35
U5-360m	48.75	10.77	10.35	16.36
U5-362m-1	55.74	13.92	2.89	10.24
U5-362m-2	49.22	11.08	9.11	16.65
U5-365m	50.78	11.18	10.69	13.76
U5-389m	48.04	11.35	6.92	20.41
U5-390m	49.13	11.67	5.37	20.42
U5-397m	46.87	11.50	5.37	23.57
U5-400m	48.41	10.78	6.85	20.84
U5-420m	52.55	11.51	8.85	14.72
U5-450m	46.64	10.97	5.67	24.51
U5-480m	38.32	8.35	7.08	37.73
U5-483m	39.19	8.63	7.65	35.76
U5-489m	35.17	8.25	7.75	40.53
U7-244m	26.92	6.47	14.43	45.80
U7-318m	33.18	7.21	10.75	42.22
U7-335m	35.28	8.05	11.79	37.34
U7-699m	12.52	1.85	1.81	81.46
U6-302m	4.14	0.79	28.42	65.00
U6-508m	3.14	0.46	32.76	2.99
Y2-3330m	87.27	0.82	0.18	10.42
Y1-3151m	67.35	13.69	2.29	1.58

SiO_2 appears to be considerably lower, indicating a compositional boundary somewhere between ~350 and 675 m in depth. This is consistent with the inverted stratigraphy present in ejecta from the Ries Crater, Germany, where suevitic breccias lie above bunte breccias in the stratigraphic sequence [2,3]. These data also indicate that the SiO_2 decreases as a function of increasing radial distance, from 40–50% in the U5 samples to ~35% in U7 breccias and <5% in U6 (~150 km).

These observations support the basic stratigraphic interpretation that U5 sampled only suevitic breccias, U7 sampled suevites overlying bunte-breccia type deposits, and U6 sampled only bunte-breccia deposits.

References: [1] Sharpton et al., this volume. [2] Sharpton V. L. and Marín L. E., *Ann. N. Y. Acad. Sci.*, in press. [3] Marín L. E. and Sharpton V. L. (1996) *Meteoritics & Planet. Sci., 31,* A82.

FUNNEL-SHAPED EMPLACEMENT GEOMETRY OF THE SUDBURY IGNEOUS COMPLEX: A STRUCTURAL PERSPECTIVE. E. J. Cowan[1] and W. M. Schwerdtner[2], [1]Tectonics Special Research Centre, Department of Geology and Geophysics, University of Western Australia, Nedlands, Perth 6907 WA, Australia (jcowan@geol.uwa.edu.au), [2]Department of Geology, University of Toronto, Ontario M5S 3B1, Canada (fried@quartz.geology.utoronto.ca).

Published emplacement scenarios for the 1.85-Ga Sudbury Igneous Complex (SIC) based on geochemical studies suggest that the complex is either (1) a differentiated impact melt sheet [1,2], (2) an impact-induced magmatic intrusion [3], or (3) a combination of the two processes [4,5]. Geochemical data do not appear to provide a singular interpretation; therefore, an independent petrofabric study of the SIC phases was conducted to test these rival emplacement models and determine the original geometry of the complex [6]. The impact-melt model requires the melt-body to have been emplaced in a large flat-floored impact crater, with its subsequent differentiation into norite, gabbro, and granophyre phases of the SIC [1]. The folded Whitewater Group, which consists of the fall-back breccia (Onaping Formation) and turbidite deposits (Onwatin and Chelmsford Formations), overlies the SIC. While the folded nature of the Whitewater Group is well documented, the mechanism of how the SIC assumed its present funnel-shaped geometry has not been thoroughly examined.

Linear-planar (L-S) igneous mineral fabrics, initially identified with the aid of anisotropy of magnetic susceptibility (AMS), were confirmed by image analysis of unstrained gabbro and norite samples collected in the SIC. The igneous foliation (S) is subparallel to the inclined contacts of the SIC, while the mineral lineation (L) is parallel to the dip-direction at each site. This pattern is consistent with an apparent radial arrangement of L within the SIC, with the L trajectories converging in the center of the Sudbury Basin.

Qualitative models for several emplacement scenarios are compared with the regional igneous fabric pattern of the SIC gabbro-norite. Of these models, only intrusion scenarios dominated by frictional shearing between the wall and the magma and gravitationally driven reorientation of minerals within the magma chamber explain the radial pattern of L. The L pattern cannot be reconciled with crystal settling and convection in a horizontally ponded impact melt. The occurrence of similar L-S fabrics in the gabbro and norite phases implies that the processes responsible for the mineral fabric persisted during magmatic fractionation. This suggests that gravitationally driven magma readjustments are likely to be responsible for the L-S fabrics, which is consistent with a basin- or funnel-shaped geometry for the SIC at the time of its solidification. Similar radial arrangements of mineral lineation have been documented in other funnel-shaped mafic intrusions [7–9] but have not been identified in impact melt bodies.

In contrast to the contact-parallel orientation of the gabbro/norite mineral foliation, the granophyre is characterized by contact-orthogonal mineral lineation. The largely undeformed nature of this crescumulate fabric in the "north lobe" of the Sudbury Basin indicates that the SIC was not folded with the Whitewater Group. Instead, the low strain levels (<15% shortening strain as estimated from AMS numerical modeling) recorded by the granophyre in the north lobe is consistent with the SIC intruding along a curved interface between the Whitewater Group and the basement rocks. This pre-intrusive curvature, with dips of up to 70°, may have resulted from folding; however, it is more likely that it was a topographic feature created during the impact event.

References: [1] Grieve R. A. F. et al. (1991) *JGR, 96,* 22753–22764. [2] Deutsch A. et al. (1995) *Geol. Rundsch., 84,* 697–709. [3] Norman M. D. (1994) *GSA Spec. Paper, 293,* 331–341. [4] Chai G. and Eckstrand O. R. (1993) *Geol. Surv. Can. Paper, 93-1E,* 219–230. [5] Chai G. and Eckstrand R. (1993) *Chem. Geol., 112,* 221–244. [6] Cowan E. J. (1996) Ph.D. thesis, University of Toronto. [7] Brothers R. N. (1964) *J. Petrol., 5,* 255–274. [8] Nicolas A. et al. (1988) *Tectonophysics, 151,* 87–105. [9] Quadling K. and Cawthorn R. G. (1994) *S. Afr. J. Geol., 97,* 442–454.

SUDBURY: GEOCHEMICAL EVIDENCE FOR A SINGLE-IMPACT MELTING EVENT. A. P. Dickin and J. H. Crocket,

Department of Geology, McMaster University, Hamilton, Ontario L85 4M1, Canada.

Early geochemical investigations on the Sudbury Igneous Complex led to its interpretation as a single stratified body. The increasing weight of evidence favoring an impact origin for Sudbury has led to wide acceptance of the upper parts of the complex as crustal melts, but this has been accompanied by suggestions of a separate origin for the lower parts of the complex.

We have argued in the past for an impact-melting origin for the basal units of the complex, based on their Os-isotope signature and the similarity of their isotopic signatures to shock-melted Sudbury breccias. However, petrological and geochemical evidence must also be examined to understand the internal relationships between the lower and upper parts of the complex.

Petrologically, there is evidence for gradational contacts between the main units of the complex (norite, oxide-gabbro, and granophyre), and their major-element chemistry can be explained by crystal fractionation from a single parent magma. These relationships can be tested by ratios of incompatible trace elements and isotopes. For example, Ce/Yb ratios in the upper and lower parts of the complex show much greater similarity with each other than with most of the possible crustal sources of the complex, and these ratios also show a tendency toward reduced variability in the upper parts of the complex.

Isotopic evidence points to a similar process of homogenization in the upper part of the complex. Generally, Pb, Sr, and Nd isotopic variation decreases in the following sequence: Country rocks–Sudbury breccias–Sublayer inclusions and norites–Main Mass norite, gabbro, and granophyre. However, Pb, Nd, and Sr isotopic systems are partially decoupled from one another, so (1) Pb isotope ratios reflect the variable metamorphic grade of crustal target rocks (greenschist to granulite); (2) Nd isotope ratios reflect the variable petrology of target rocks (gabbro to granite and sediment); and (3) Sr isotope ratios reflect a combination of these controls. The detailed behavior of these isotopic systems will be examined at different locations around the margin of the complex.

THE SEPARATION OF PLATINUM AND PALLADIUM DURING HIGH-TEMPERATURE VAPORIZATION OF SULFIDE-RICH PICRITE.

Yu. P. Dikov[1], V. V. Distler[1], M. V. Gerasimov[2], and O. I. Yakovlev[3], [1]Institute of Ore Deposits, Petrography, Mineralogy and Geochemistry, Russian Academy of Sciences, Moscow, Russia, [2]Space Research Institute, Russian Academy of Sciences, Moscow, Russia, [3]Vernadsky Institute of Geochemistry and Analytical Chemistry, Russian Academy of Sciences, Moscow, Russia.

We have investigated experimentally the separation trends of Pt and Pd during high-temperature vaporization of ultramafic rocks. This experiment was aimed at the simulation of hypervelocity impact-induced vaporization of a hypothetical meteorite.

The samples for investigation were prepared as a 1:1 mixture of picrite from norilsk-differentiated intrusion and sulfide concentrate with a high concentration of Pt metals from the same intrusion. The composition of the picrite (in weight percent) was 39.5 SiO_2, 0.6 TiO_2, 6.5 Al_2O_3, 6.9 Fe_2O_3, 9.3 FeO, 26.5 MgO, 4.5 CaO, 0.4 Na_2O, 0.2 K_2O, 0.5 Cr_2O_3, 2.7 H_2O^-, and 2.5 H_2O^+. The composition of the sulfide concentrate was (in volume percent) ~ 62 hexagonal pyrrhotite, ~22 pentlandite, and ~16 chalcopyrite. The concentration of the sum of Pt + Pd in the sulfide concentrate was 5 wt %. The atomic ratio of Pt/S is 0.13; the atomic ratio of Pd/S is 0.48.

TABLE 1.

Levels	Si	Mg	Ca	Al	Pd	Pt	Fe	Ni	S
Surface	3.82	0.43	0.19	0.20	6.41	0.27	2.19	2.11	9.57
400 Å	3.04	0.62	0.35	0.42	2.91	0.84	1.35	1.17	3.14
800 Å	2.52	0.73	0.54	0.42	0.78	0.80	1.29	1.19	0.77

High-temperature vaporization was performed using a powerful pulse-laser installation. The parameters of the laser pulse were (1) pulse luminous energy ~ 600 J, (2) duration of pulse ~10^{-3} s, and (3) density of luminosity ~ 10^7 W/cm^2. The temperature of vaporization was 4000–5000 K. The condensate was collected on a Ni-foil placed ~7 cm from the sample on the path of spreading of the vapor cloud. The condensed film was analyzed using an X-ray photoelectron spectrometer (ES-2401). The XPS analysis of the internal chemical composition of the condensed film was provided layer by layer, with an argon-ion etching of 400 Å of the film per step.

Some results of the measurements of element concentration at different levels (at the surface of the condensed film and at depths 400 and 800 Å from the surface) inside the condensed film are presented in Table 1 (concentrations are in weight percent).

The results of analysis indicate a selectivity of vaporization. The vapor is enriched in Si and S. The ratio of Si to Mg in the surface layer is 8.9, compared to 1.4 in the initial sample. The condensate has a distinct zone separation of Pt and Pd. The concentration of Pd in the condensate correlates well with the concentration of S. The concentration of Pt has an anticorrelation with the concentration of S. The observation speaks for the chemically driven space separation of Pt and Pd during high-temperature vaporization of sulfide-silicate mixtures.

THE SUDBURY STRUCTURE, ONTARIO, CANADA: A PERSISTENT ENIGMA.

B. O. Dressler and V. L. Sharpton, Lunar and Planetary Institute, 3600 Bay Area Boulevard, Houston TX 77058 (dressler@lpi.jsc.nasa.gov; sharpton@lpi.jsc.nasa.gov).

The impact origin of the Sudbury Structure (SS) has gained wide acceptance over the last 15 years. Disagreement remains, however, concerning several aspects of the impact structure, including the origin of the Sudbury Igneous Complex (SIC). Likewise, important questions remain as to the predeformation size of the SS, the distribution and origin of pseudotachylites (Sudbury breccias) in the footwall rocks around the SIC, and, possibly, the significance of high-precision geochronological age determinations for various rock units associated with the SS.

In the past, the SIC has been interpreted as a strongly crustal-contaminated, differentiated magmatic body [1]. On the other hand, isotopic evidence has been used to argue for an impact-melt origin for all the SIC [2]. The ratios of incompatible trace elements of the granophyre are similar to those in the norites, supporting a one-magma (impact) origin for the SIC [3]. Yet other geochemical data have been interpreted as supporting a two-magma origin, in which an impact melt, the granophyre of the SIC, overlies an endogenic, noritic-quartz dioritic rock [4]. Structural observations and intru-

sive relationships between various units of the SIC also seem inconsistent with an impact origin for all or part of the SIC [5–7]. An open-minded reevaluation of geochemical and structural data is needed to advance our understanding of the SIC.

On the basis of the distribution of shatter cones, shock-metamorphic features, and pseudotachylites (Sudbury breccias) in the footwall rocks beneath the SIC, the SS is estimated to be 190–280 km in diameter [8,9]. Based on the interpretation of vibroseismic profiles across the SS, however, it can be surmised that the structure originally may have been considerably larger. Erosion, estimated to have amounted to 9.5 ± 2 km [10] since 1.25 Ga, complicates attempts to estimate the preerosion and predeformation size of the structure. Present estimates may be conservative.

There is no consensus on the origin of Sudbury breccia (pseudotachylites) or their orientation and distribution in the footwall rocks around the SIC [11,12]. Rock comminution, friction melting due to impact, or some combination of these two processes have all been suggested as possible explanations for the pseudotachylites (in contrast to a recent controversial interpretation that Sudbury breccia is related to basaltic magmatism [13]). It has been proposed that the distribution of the breccias is linked to the rings of a Sudbury multiring impact basin [12,14]. Further research is needed to substantiate the proposed continuity of breccia bodies around the SIC [11,12].

All units of the SIC, including ultramafic inclusions in the sublayer (the ore-bearing unit at the base of the SIC), have been dated radiometrically at ~1.85 Ga [15]. Recently, Early Proterozoic and Archean (preimpact) target rocks, located near the contacts with units of the SIC, have been dated at ~1.85 Ga; these results suggest that the U-Pb clock was reset at that time. These results may warrant a reevaluation of the significance of geochronological data, especially in view of results presented in two recent dissertations on the SIC and its footwall rocks [6, 7]. Is it conceivable that the 1.85-Ga age does not represent a melting/crystallization age for all components of the SIC?

References: [1] Naldrett A. J. and Hewins R. H. (1984) *Ont. Geol. Surv., Spec. Vol. 1,* 235–251. [2] Faggart et al. (1985) *Science, 230,* 436–439. [3] Lightfoot P. C. et al. (1997) *Ont. Geol. Survey,* 5959. [4] Chai G. and Eckstrand R. (1994) *Chem. Geol., 113,* 221–244. [5] Dressler et al. (1996) *GCA, 60,* 2019–2036. [6] Cowan E. J. (1996) Ph.D. thesis, Univ. Toronto. [7] Riller U. (1996) Ph.D. thesis, Univ. Toronto. [8] Dressler et al. (1987) *Research in Terrestrial Impact Structures,* pp. 39–68, Vieweg und Sohn. [9] Deutsch et al. (1995) *Geol. Rundsch., 84,* 697–709. [10] Schwarz E. J. and Buchan K. L. (1982) *EPSL, 58,* 65–74. [11] Dressler B. O. (1984) *Ont. Geol. Surv., Spec. Vol. 1,* 97–136. [12] Spray J. (1995) *Nature, 373,* 130–132. [13] Lowman P. D. Jr. (1996) *Geol. Assoc. Can. Annual Meeting,* abstract. [14] Brockmeyer P. (1990) Ph.D. thesis, Univ. Münster. [15] Lightfoot P. (1996) personal communication.

REVIEW OF THE GEOPHYSICAL SIGNATURE OF THE VREDEFORT STRUCTURE AND ITS INTERPRETATIONS.

R. J. Durrheim[1] and W. U. Reimold[2], [1]CSIR Division of Mining Technology, P.O. Box 91230, Auckland Park 2006, Johannesburg, South Africa, [2]Department of Geology, Witwatersrand University, Private Bag 3, P.O. Wits 2050, Johannesburg, South Africa.

The surface geology of the Kaapvaal Craton is characterized by the exposure of several basement granitoid domes. One such dome, located in the center of the Witwatersrand structural basin, differs from the others in that there is abundant evidence (including pseudotachylitic breccia, shatter cones, high-pressure polymorphs of quartz, and shock-metamorphic effects in quartz and zircon) that the structure was formed as the result of unusual dynamic processes. Many workers are satisfied that the Vredefort Structure is the result of a large meteorite or comet impact event; others still vigorously argue for an origin linked to internal agents. Comprehensive gravity, aeromagnetic, refraction, and reflection seismic data cover the entire Witwatersrand basin. While this contribution serves to review the entire database, the salient geophysical characteristics of the Vredefort Dome shall be highlighted.

The gravity signature of the Vredefort Dome differs from that of other granitoid domes, which are usually characterized by negative-gravity anomalies. This is because basement granite typically has a density of 2.65 g/cm^3—considerably less than the densities of the indurated shales, carbonates, and igneous rocks that make up the supracrustal strata. A 30-mGal positive Bouguer anomaly is centered on the approximately 40-km-diameter core of the Vredefort Dome. Stepto [1] modeled this anomaly using a vertical, 5-km-wide cylinder of 2.84 g/cm^3 density surrounded by an annulus of 18-km width and 2.73 g/cm^3 density. The interpretation of the gravity field is inherently ambiguous, and more recent models [e.g., 2] have been constrained by new seismic and geological data and have inclined rather than vertical boundaries between units. A 36-km seismic refraction profile was surveyed by Green and Chetty [3]. The Outer Granite Gneiss zone, forming an outer annulus in the core of the dome, yielded 5.9–6.1 km/s velocities, whereas velocities of 6.4 km/s were reliably defined in the center of the dome. A seismic-refraction profile was surveyed between Witbank and the Free State goldfields using mine tremors as the energy source [4]. Clear Pn arrivals were observed, corresponding to a 36-km Moho depth. There is no evidence of a significant deviation in Moho depth beneath the Vredefort Dome.

A remarkable feature of the magnetic field over the Vredefort Dome is a horseshoe-shaped negative-magnetic anomaly situated about 8 km from the perimeter of the granitoid core. A magnetite-rich zone has been inferred here by Corner et al. [5], which, according to Hart et al. [6], has distinct geochemical properties (a sharp increase in the ratio between light and heavy REE, anomalous U, and volatile element abundances). This magnetic zone has been correlated with magnetic anomalies found near the craton margin and proposed as a semicontinuous intracrustal zone. Prominent reflections observed on reflection-seismic sections [7] have been tentatively correlated with this inferred magnetite-rich layer. Such reflections are observed, for example, beneath the Westerdam Dome at the northwestern margin of the Witwatersrand structural basin and can be traced beneath the supracrustal strata to a point near Potchefstroom, some 40 km northwest of the collar of the Vredefort Dome. From this point onward onto the Dome, the basement becomes seismically transparent. This transparency has been linked to deformation caused by the catastrophic Vredefort event.

The gravity, magnetic, refraction, and reflection seismic data provide constraints on the geometry of the Vredefort Structure, but these data are equivocal with regard to its formation mechanism. Progress can only be made by integrating the geophysical data with other geological information.

References: [1] Stepto D. (1979) unpublished Ph.D. thesis, Univ. Witwatersrand, 378 pp. [2] Henkel H. and Reimold W. U. (1996) *EGRU Inf. Circ. 299,* Univ. Witwatersrand, 89 pp. [3] Green R. W. and Chetty P. (1990) *Tectonophysics, 171,* 105–113. [4] Durrheim R. J. and Green R. W. (1992) *Geophys. J. Inter., 108,* 812–832. [5] Corner B. et al. (1990) *Tectonophysics, 171,* 49–61. [6] Hart et al. (1990) *Chem. Geol., 82,* 21–50; *83,* 233–248. [7] Durrheim R. J. et al. (1991) *AGU Geodynamics Ser. 22,* 213–224.

BASE OF THE ROOIBERG GROUP: EVIDENCE FOR AN INITIAL BUSHVELD CATASTROPHE. W. E. Elston and M. E. Caress, Department of Earth and Planetary Sciences, University of New Mexico, Albuquerque NM 87131-116, USA.

Rocks at the basal contact of the Rooiberg "felsite" group, the earliest component of the Bushveld Complex, provide evidence for a high-temperature, high-energy catastrophe. These rocks differ, however, from all previously described volcanites and impactites and include (1) meltrocks with textural evidence for superliquidous heating followed by subsolidus undercooling; (2) high-temperature, high-energy debris flows (including pseudoignimbrites); and (3) underlying Pretoria Group arenite recrystallized to pseudofelsite by contact metamorphism.

The basal zone was studied in two locations where it rests on the Pretoria Group without intervening sills of bushveld-layered gabbro and granite: (1) proximal outflow in the Stavoren "fragment," interpreted as an allochthonous block that slumped into a transient cavity during enlargement, and (2) distal outflow in the type-Dullstroom Formation, a sliver of the lower Rooiberg preserved beneath layered gabbro [1].

In the Stavoren "fragment," the sharp contact between the Pretoria and Rooiberg groups recognized by previous workers has turned out to be a false contact between quartzite and pseudofelsite. Directly beneath the false contact, subgraywacke has recrystallized into quartzite with a coarse metamorphic fabric. The quartz grains are intensely strained and commonly divided into mosaics. Parallel and closely spaced fractures and twins with extinction angles to 4° are currently being investigated using optical microscopy and transmission electron microscopy (TEM). Within each mosaic domain, these fractures and twins have a single direction, but they may intersect near domain boundaries (cf. Brazil twins at Vredefort). In a ≥10-m zone of pseudofelsite above the false contact, quartz grains are replaced by a network of quartz needles and laths measuring up to ~0.5 cm, formerly interpreted as plagioclase or quartz pseudomorphs after plagioclase [2]. TEM studies have confirmed that these needles and laths are quartz paramorphs after high tridymite. In silica-brick furnace linings, quartz-high tridymite inversion occurs at ≥1200°C [3], while inversion back to quartz occurs at ~1125°C [4]. Contact metamorphism on this scale is unknown beneath siliceous volcanic rocks, but quartz needles have been found in siliceous meltrock at the base of the Onaping Formation at Sudbury [5]. Pseudofelsite is isochemical with underlying arenites; rare relict cross-beds confirm its sedimentary nature. Above a true contact, a basal-debris-avalanche deposit of the Rooiberg Group superficially resembles spherulitic rhyolite with a matrix of quartz needles and vague meter-sized pale patches. In "cool" spots, the patches resolve into angular quartzite clasts in a sandy matrix. In a paleochannel, a debris flow scoured a polished, striated, and mullioned pavement. True meltrock with skeletal quench textures, no longer isochemical with arenites, appears above the basal-debris flow.

Pseudoignimbrite, preserved at the base of the Dullstroom Formation in paleochannels (gouges?) radial to the Bushveld Complex, is interpreted as the distal facies of a hot debris flow. As in true ignimbrite, basal surge beds are overlain by a 25-m massive zone (cf. suevite) with abundant hornfels clasts. However, sand-sized quartz grains supported by chloritic matrix, rather than glass shards, make up the groundmass. Pumice fiamme is replaced by amphibolite lenses with pyrite cores and quartz coronas, evidently metamorphosed *in situ*. The overlying rhyolite-like unit has similar amphibolite lenses, but the quartzose matrix has a metamorphic fabric. Contorted flow bands show that the rock was hot and mobile (cf. rheoignimbrite).

The temperatures and energies required by these rocks are consistent with a megaimpact resulting in meltdown and obliteration of conventional shock criteria. Constraining the solid-liquid phase relations is more speculative.

References: [1] Schweitzer J. K. et al. (1995) *S. Afr. J. Geol., 98,* 245–255. [2] Lombaard B. V. (1932) *Geol. Soc. S. Afr. Trans., 35,* 125–190. [3] Schneider H. and Flörke O. W. (1982) *N. Jhb. Min. Abh., 145,* 280–290. [4] Hiroto K. and Ono A. (1977) *Naturwiss., 64,* 39–40. [5] Stevenson J. S. (1963) *Can. Mineral., 7,* 413–419.

CLASSIFICATION AND DISTRIBUTION OF SUDBURY BRECCIA. J. S. Fedorowich[1], D. H. Rousell[2], and W. V. Peredery[3], [1]Falconbridge Limited, P.O. Box 40, Falconbridge, Ontario P0M 1S0, Canada (jfedoro@falconbridge.com), [2]Department of Earth Sciences, Laurentian University, Sudbury, Ontario P3E 2C6, Canada, [3]1974 Armstrong, Sudbury, Ontario P3E 4V9, Canada.

In its occurrences circumferential to the Sudbury Basin, three principal types of breccia have been recognized within the rock unit known as Sudbury Breccia: (1) Flow-surface Sudbury breccia is characterized by well-developed surfaces indicative of laminar (originally turbulent?) flow; (2) chaotic Sudbury breccia is characterized by unoriented, subrounded to angular fragments supported in a cataclastic matrix derived by mechanical fragmentation of the host rock and subsequent sliding rotation and milling; and (3) igneous texture Sudbury breccia consists of a fine-grained primary intergrowth of felsic and mafic minerals.

In terms of distribution, type 1 is most abundant on the South Range, whereas type 2, intermixed with subsidiary type 1, dominates elsewhere along the basin margin. The overall abundance of igneous texture breccia is the most difficult to estimate, but this breccia type appears to be far less abundant. However, it is also the most difficult to recognize, and it is only unambiguous in a thin section.

Distribution patterns and brecciation intensity are generally not well constrained within the 5–15-km-wide collar containing minor to moderate amounts of Sudbury breccia. In an effort to quantify the percentage distribution of Sudbury breccia, measurements have been made from detailed outcrop mapping. For example, 1-km^2 areas are found to contain 2–5% Sudbury breccia within the total exposed area. At the scale of individual outcrops, this Sudbury breccia occurs both as discrete dikes (average outcrop area = 0.00025 km^2) and as ramifying vein networks. Detailed underground mapping re-

veals a similar overall distribution. In terms of orientation, there is a strong clustering subparallel to the basin margin and a decrease in dip angle with depth.

IMPACT MATERIALS WITH MIXED COMPOSITIONS OF IRON-SILICON-NICKEL-SULFUR SYSTEM.

S. Fukuyama, Y. Miura, and H. Kobayashi, Department of Chemistry and Earth Sciences, Faculty of Science, Yamaguchi University, Yoshida, Yamaguchi 753, Japan.

Introduction: There have been few systematic reports on the indicators of impact composition and structure. Impact craters on Earth are considered to have been formed by Fe-meteorite bombardments, since atmospheric effects can stop direct impacts of comets or stony meteorites [1]. The main purpose of this study is to elucidate the characteristic signatures of impact composition.

Composition of Iron-Nickel-Silicon-Magnesium-Sulfur: NASA's Johnson Space Center has conducted reports on the systematic composition of impact spherules and fragments [2]. Analytical electron microscopical (AEM) data of these particles on Earth are summarized as follows: (1) The meteoritic origin (shown as C) of the particles is 41% (from 403 analyses), with mixed composition of Fe-Ni-Si-Mg-S system; (2) terrestrial contamination from natural particles (shown as TCN) from volcanic ashes is 10% (from 403 analyses), with mixed composition of Si-Al-Na-K-Ca-Fe system and a few atoms of Ni, S, or Mg; and (3) mixed compositions from meteoritic and terrestrial sources, classified as unknown particles, are used for significant information on exposed terrestrial impact craters.

Meteoritic Impact Composition: Meteoritic compositions of Fe-Ni and Fe-Ni-S are melted from kamacite and troilite, respectively. Compositions of Si-Mg-Fe are believed to have originated from the olivine or pyroxene of a chondritic meteorite. With Mg and Fe elements, however, it is difficult to identify the sources on the terrestrial surface. Therefore, the characteristic compostion of an impact on the terrestrial surface is represented as Fe-Si-Ni-S system in this study. The particles formed by impacts are spherules, fragments, or micrometer-sized.

Spherules from the Cretaceous-Tertiary Geological Boundary: Spherules from the Cretaceous-Tertiary (KT) geological boundary, which was formed by impacts on Middle America, were distributed on a global scale and show a Fe-Si-Ni-S composition in Danish samples [3,4]. This indicates that the KT boundary is confirmed by the spherule composition of Fe-Si-Ni-S system (cf. Table 1).

TABLE 1. AEM analytical data of meteoritic impacts with Fe-Si-Ni-S [1,3].

Oxides*	Danish KT SK12 Crater	Barringer B8 Crater	Wolf Creek W20	Ries Crater R5-2	Takamatsu TK15	Anami-Oshima S7
SiO_2	13.5	44.2	2.5	8.7	8.2	8.6
FeO	80.4	46.5	89.9	82.9	63.2	90.4
MgO	0.0	0.0	0.0	0.0	0.0	0.0
CaO	1.2	1.3	0.0	0.0	0.0	0.0
NiO	2.3	8.0	7.7	1.5	5.0	1.0
SO_2	2.6	0.0	0.0	0.0	6.5	0.0
Total	100.0	100.0	100.1	93.1	82.9	100.0

*Weight percent calculated as oxides.

Impact Craters on the Earth: The Barringer (USA), Wolf Creek (Australia), and Ries (Germany) impact craters show mixed impact composition of Fe-Si-Ni-S system as listed in Table 1 [1,3,4]. The Takamatsu crater [3] shows anomalous grains of Fe-Si-Ni-S system, though there is some contamination of Cl, Ti, or Al. The Akaogi crater of Anami-Ohshima shows 26% grains from a meteoritic impact origin of the Fe-Si-Ni-S system and 74% grains from a terrestrial igneous origin as mixed compositions. Referenced data of Unzen volcanic ash show a Si-Fe-Ti-Al-Mg-K system from feldspar or mafic compositions in particle grains.

References: [1] Miura Y. et al. (1995) *Shock Waves Proc., 19,* 399–410. [2] Cosmic Dust Preliminary Examination Team (1982) *Cosmic Dust Catalog,* 129 pp., NASA Johnson Space Center. [3] Miura Y. et al. (1997) submitted. [4] Miura Y. (1991) *Shock Waves, 1,* 35–41.

EXPERIMENTAL INVESTIGATION OF THE CHEMISTRY OF VAPORIZATION OF TARGETS IN RELATION TO THE CHICXULUB IMPACT.

M. V. Gerasimov[1], Yu. P. Dikov[2], O. I. Yakovlev[3], and F. Wlotzka[4], [1]Space Research Institute, Russian Academy of Sciences, Moscow, Russia, [2]Institute of Ore Deposits, Petrography, Mineralogy and Geochemistry, Russian Academy of Sciences, Moscow, Russia, [3]Vernadsky Institute of Geochemistry and Analytical Chemistry, Russian Academy of Sciences, Moscow, Russia, [4]Max-Planck-Institut für Chemie, Mainz, Germany.

The Chicxulub impact is considered to be a possible cause for Cretaceous-Tertiary mass extinction. The presence of thick deposits of anhydrite and carbonates in the target rocks resulted in the evolution of enormous quantities of S- and C-containing gases. In addition, these deposits resulted in the synthesis in the ejecta of noticeable quantities of various species such as S acid aerosols that could strongly affect the biosphere.

The purpose of our experiment was to investigate the chemical products of high-temperature vaporization of target rocks of the Chicxulub impact structure. We have prepared different samples from mixtures that could qualitatively simulate the real target. We have used pure anhydrite and gypsum minerals, and some of the targets were prepared from a pressed powder mixture, such as $CaSO_4$/$CaSO_4 \Sigma 2H_2O + CaCO_3 + SiO_2$, $MgCO_3 + CaCO_3 + CaSO_4 \Sigma 2H_2O + SiO_2 + Al_2O_3$. For investigation of Ca-Si and C high-temperature chemistry, we used spurrite ($Ca_2SiO_4 \Sigma CaCO_3$) from South Yakutia and a compressed mixture of fine powders of $CaCO_3$ and SiO_2 with the same atomic Ca/Si ratio as in spurrite.

High-temperature vaporization was provided using a powerful neodymium glass pulse laser. Samples were vaporized in a cell filled with air at 1 atm room temperature. Condensate was collected on a Ni foil placed on the path of a spreading evaporated cloud at a distance of 6 cm. The analysis of condensed film was conducted using X-ray photoelectron spectroscopy (XPS). A film of condensate was etched layer by layer (with a step ranging from 100 to 400 Å) by Ar ions and for every step XPS analysis was performed, providing a cross-section of the film. XPS analysis provided information on both the elemental composition and charging state of elements.

A large portion of S is present in the condensed films in the form of adsorbed SO_3, proving the possible presence of S acid aerosols in

the expanding vapor plume. About 40% of S and from 40% to 60% of C from the vapor cloud is trapped as condensate. The main phase of S in the condensate is $CaSO_4$. Carbon is present in the condensate as carbonate, but in some cases the condensate contains about half of the C in reduced phases. Complex redox processes occur in the vapor cloud at dry conditions, providing some Si in metallic form and half of the C in graphite form. The reduction of Si was computed as up to 9% of total Si. Different forms of reduced C were identified, including C as graphite, Si carbide, and complex organic C agglomerates. Analyses indicate the presence of complex C aggregates such as C38 and C48. The presence of Si in a sample provides for more efficient volatilization of S, since a part of the Ca bonds with Si to produce Ca silicates. Analyses of the structural state of Si in condensates show the existence of mineral embryos of wollastonite and larnite groups. This could be the result of the production of a full range of Ca silicates. The presence in the vapor cloud of such volatiles as water, S, and C makes possible the origin in condensed phase of such rare minerals as ellestadite $Ca_5[OH|(SiO_4,SO_4)]$, spurrite $Ca_5[CO_3|(SiO_4)_2]$, and thaumasite $Ca_3H_2[CO_3|SO_4|SiO_4]\Sigma 13H_2O$. Experiments also prove the formation of sheet Mg-silicates and hydrous alumosilicates, which can be a good source for smectite clay formation.

THE ONAPING FORMATION: STRATIGRAPHY, FRAGMENTATION, AND MECHANISMS OF EMPLACEMENT. S. F. M. Gibbins[1], H. L. Gibson[2], D. E. Ames[3], and I. R. Jonasson[3], [1]Kidd Creek Mine, Falconbridge Limited, Timmins, Ontario P4N 7H9, Canada, [2]Department of Earth Sciences, Laurentian University, Sudbury, Ontario P3E 2C6, Canada, [3]Geological Survey of Canada, Ottawa, Ontario K1A 0E8, Canada.

The 1400-m-thick, Paleoproterozoic Onaping Formation is the lowermost formation of the Whitewater Group, the basin-fill succession of the Sudbury Structure. The Onaping Formation consists of "glass-rich" breccias and coeval hypabbysal intrusions that overlie the Sudbury Igneous Complex and are conformably overlain by the Vermilion, Onwatin, and Chelmsford Formations.

The Onaping Formation has been subdivided into upper Black and lower Gray members on the basis of C content (color). However, because the occurrence of C is not a reliable stratigraphic criterion and is often discordant, the Onaping Formation was informally subdivided, on the basis of shard morphology and the percentage of shards >1 mm, into a lower Sandcherry member and an upper Dowling member [1]. The Sandcherry member consists of peperite-like, massive and brecciated fluidal breccia complexes where a "melt" was emplaced into preexisting breccias and interacted with water, both passively and explosively, to form proximal "hyaloclastites." These hyaloclastites were redeposited by mass flows to form widespread, coarse, shard-rich, and matrix-poor units. Contacts between depositional units are not distinct, but are marked by a rapid variation in grain size and/or the occurrence of large blocks (>64 mm). The Dowling member is interpreted to be the product of a more explosive and renewed interaction of a "melt" with water and the explosive exsolution of volatiles (vesiculation), which resulted in the deposition of primary fall and finer, shard-poor, and matrix-rich, mass flow deposits. The contact between the Sandcherry and Dowling members marks a rapid stratigraphic change in the percentage of matrix, morphology and size of shards, percentage of lithic fragments, and depositional character of units. The lower or contact unit of the Dowling member is locally welded.

Thus, contrary to previous work, the Onaping Formation is not a succession of ash-flow tuffs and lavas as proposed by Thompson [2], Williams [3], and Stevenson [4], nor is it a fall-back breccia as proposed by French [5], Dence [6], Peredery [7], Morrison [8], and Averman [9]. The Onaping was emplaced by the continuous introduction of a "melt" of uniform composition, both passively and explosively, at surface level in a shallow subaqueous to locally subaerial setting. The melt may represent a contaminated magma or melt derived from an underlying impact melt sheet that consumed its fall-back breccia [10]. Regardless of the melt's origin—i.e., impact or contaminated magma—the Onaping was fragmented and emplaced by explosive and passive hydroclastic processes.

References: [1] Gibbins (1994). [2] Thompson (1957). [3] Williams (1957). [4] Stevenson (1972, 1990). [5] French (1967). [6] Dence (1972). [7] Peredery (1972). [8] Peredery and Morrison (1984). [9] Averman (1992). [10] Brockmeyer and Deutsch (1989); Grieve et al. (1991); Walker et al. (1991); Naldrett (1989); Dressler et al. (1991).

DIAGNOSTIC CRITERIA FOR THE RECOGNITION OF SHATTER CONES. H. M. Gibson and J. G. Spray, Department of Geology, University of New Brunswick, Fredericton, New Brunswick E3B 5A3, Canada.

Shatter cones are commonly described as being conical, striated fracture surfaces formed as a result of hypervelocity impact. Other structures having similar, but not identical, morphological elements include blast fractures, natural percussion marks, slickensides, wind-abrasion structures, and cone-in-cone structures. Precise identification of shatter cones is necessary to prevent confusion with these similar structures. Criteria for the identification of shatter cones are based on elements of their morphology combined with field habit.

Three basic criteria must be met for a structure to be considered a valid shatter cone: (1) The structure must be a conical, or part-conical, fracture surface; (2) ridge and groove striations diverging from an apex or central striae must be present; and (3) the structure must be pervasive and not surficial.

Blast fractures are true fracture surfaces but do not display a conical fracture surface. Most commonly, they consist of a radiating array of planar fractures. Percussion marks result from the impact of boulders in a rapid flow, fluvial setting. They have a conical fracture surface that may include crude striations, so their morphology is superficially similar to that of a shatter cone. However, their occurrence is restricted to the outcrop surface and, as such, they do not form a pervasive fracture system. Slickensides have ridge and groove striations similar to those of a shatter cone. However, the fracture surface is planar, or occasionally curviplanar, and lacks the conical shape and divergent striations of shatter cones. Cone-in-cone structures are not fracture surfaces, but are displacive growths of calcite within a carbonate-rich sediment. As such they possess a characteristic internal structure that is distinct from that found in shatter cones. Conical structures formed as a result of wind abrasion lack a fracture surface and are spatially restricted to outcrop surfaces and prevailing wind direction at the time of formation.

If care is taken, the above evidence can be used to distinguish true shatter cones formed by hypervelocity impact from other

conelike structures at the mesoscopic scale (i.e., in the field). At the microscopic scale, shatter cones may be further distinguished by the localization of planar deformation features (PDFs) in the vicinity of the cone surfaces, as well as by the presence of spherules (vapor condensates) and high-pressure polymorphs indicative of shock.

MULTIPLE ORIGINS FOR IMPACT-PRODUCED DIAMONDS. I. Gilmour, R. M. Hough, and C. T. Pillinger, Planetary Sciences Research Institute, The Open University, Walton Hall, Milton Keynes MK7 6AA, UK (I.Gilmour@open.ac.uk).

A genetic link between diamonds and terrestrial impact was initially proposed to explain the occurrence of diamonds in the Canyon Diablo meteorite [1] found at Meteor Crater in Arizona. It was suggested that the diamonds had been produced by the shock transformation of meteoritic graphite *in situ*. Direct evidence for the shock production of diamonds was first observed in experiments involving explosions [2]. Several classes of meteorites have since been identified that contain microcrystalline diamond aggregates thought to be produced by impacts with the Earth or in space [3,4]. Primitive chondrites also contain diamonds, but these nanometer cubic-form crystallites are circumstellar vapor phase condensates [5]. On Earth, some diamonds thought to have originated from giant impacts occur as placers. Diamonds directly related to craters, particularly the 100-km crater Popigai, are described in studies by Masaitis [6]. Other authors have proposed that giant Precambrian impacts in sedimentary structures produced the carbonado found as placers, which reach 300 g in size, in Brazil and the Central African Republic [7]. At the other end of the scale, nanometer-sized diamonds have been found at the Cretaceous-Tertiary boundary [8,9].

Evidence for Shock Formation: Koeberl et al. have reexamined diamonds from the Popigai impact structure [10]. Diamonds were found in impact melt and breccias, where they apparently preserve the crystallographic habit and twinning of graphites. From this it was concluded they had formed by shock transformation. Electron microscopy indicated that the samples were polycrystalline and contained very fine lamellae (or stacking faults), although the hexagonal polymorph of diamond, lonsdaleite, could not be unequivocally identified. Infrared spectroscopy of Popigai diamonds indicated the presence of solid CO_2 and water in microinclusions in the diamonds, with the CO_2 under a pressure of 5 Gpa (at room temperature). Similar C isotopic compositions for Popigai diamonds and graphite lend support to a shock origin for these particular diamonds.

Evidence for Vapor Phase Formation: Hough et al. undertook a detailed examination and search for diamonds in Suevites from the Ries Crater, Germany [11]. Acid dissolution techniques enabled diamond plates (up to 100 μm) and fine-grained diamond/Si carbide aggregates (up to 200 nm) of a never-previously-encountered morphology to be isolated. Individual SiC crystals up to 100 μm were also observed. Together these minerals constituted about 4–5 ppm by weight of the original impact-produced rock and were identified by chemical analysis, single-grain X-ray, and electron microscopy; diamond and SiC were verified by electron energy-loss spectroscopy. The C in the samples burned at temperatures below 700°C, suggesting that fine-grained composites contribute most of the mass. The close association between the diamond and Si carbide and the presence of SiC in the aggregates and as single grains had not previously been reported. SiC is not mentioned among the products of shock experiments performed under a variety of conditions to produce diamond [12]. However α-SiC can be produced from a vapor containing Si and C created by shaped-charge experiments to shock-powdered β-SiC. In chemical vapor deposition (CVD) type experiments, diamond grows on Si containing substrates and does so via an interfacial layer of 4H-SiC [13].

References: [1] Lipschutz M.E. and Anders E. (1961) *Science, 134,* 2095–2099. [2] DeCarli P. S. and Jamieson J. C. (1961) *Science, 133,* 1821–1822. [3] Lipschutz M. E. and Anders E. (1961) *GCA, 24,* 83–105. [4] Vydovykin G. P. (1970) *Space Sci. Rev., 10,* 483–510. [5] Anders E. and Zinner E. (1994) *Icarus, 112,* 303–309. [6] Masaitis V. L. et al. (1972) *Proc. All-Union Min. Soc., 1,* 108–112. [7] Smith J. V. and Dawson J. B. (1985) *Geology, 13,* 342–343. [8] Gilmour I. et al. (1992) *Science, 258,* 1624–1626. [9] Carlisle D. B. and Braman D. R. (1991) *Nature, 352,* 708–709. [10] Koeberl C. et al., in preparation. [11] Hough R. M. et al. (1995) *Nature, 378,* 41–44. [12] Heimann R. B. and Kleiman J. (1988) in *Crystals: Growth, Properties and Applications* (H.C. Freyhardt, ed.), pp. 1–75, Springer Verlag. [13] Yamada K. and Tobisawa S. (1990) *Phil. Mag., 89,* 2297–2304.

ASTEROID/COMET MEGA-IMPACTS AND MANTLE MELTING EPISODES: CONSEQUENCES FOR PRECAMBRIAN CRUSTAL EVOLUTION. A. Y. Glikson, Geospectral Research, P.O. Box 3698, Weston, Australian Capital Territory 2611, Australia.

The episodic short-lived nature of peak igneous and tectonic Precambrian events is difficult to reconcile with models of continental growth that hinge exclusively on the operation of continuous plate tectonics and arc-trench accretion or underplating processes. Some of these tectonic-thermal episodes potentially reflect the distal consequences of mega-impact by large-diameter (D_p>>5 km) projectiles on thin, tectonically mobile and geothermally active crustal domains—i.e., a Precambrian simatic crust overlying a relatively thin (<20 km) lithosphere. Large impacts (D_p>>10 km) can be expected to trigger global sublithospheric perturbations associated with local to extensive partial melting. Mega-impact effects can thus span a complete spectrum, from clearly recognizable proximal structural and shock metamorphic features (breccias, shatter cones, shock lamella, high-pressure polymorphs, pseudotachylite, and melt breccia) to distal impact-triggered formation of dike swarms related to deep lithosphere-penetrating faulting and asthenospheric melting. Such events may be difficult to recognize in view of (1) heat transfer from impact-rebounded adiabatically-melting mantle and related igneous activity, which is capable of overprinting proximal shock metamorphic effects through recrystallization and superposed deformation, and (2) widespread elimination of the proximal effects of mega-impacts by erosion of elevated terrains, burial, and subduction. For these reasons, distal impact deposits furnish the key for unraveling the Precambrian impact history. These deposits include olistostromes, diamictites, turbidity currents, microtektites, and microkrystites (spherulitic condensates of vaporized asteroid and target materials) accompanied by geochemical anomalies (Pt group elements). The release of energy on a scale $\geq 10^9$ Mt, triggering seismic activity orders of magnitude higher than purely endogenic per-

turbations, results in mega-earthquake-triggered slumps, turbidity currents, and mudflake conglomerates—the latter representing the seismic disturbance of sea-bottom sediments and concomitant deposition from quake-generated turbidity flows. The identification of the signatures of such events in the Precambrian crustal records requires a reexamination of the evidence. Further evidence may be provided by the reexamination of the parts of batholiths representing exhumed reactivated basement of major volcanic sequences. Clues for major impact events and bombardment periods are provided by comparisons between the isotopic ages of preserved impact signatures, dike swarms, volcanic sequences and alkaline intrusions, and thermal peaks on isotopic age distribution histograms. Tentative results of attempted correlations are encouraging, if inconclusive: (1) *ca. 3.45 Ga*: peak formation of greenstone-granite terrains; minor traces of possible impactite horizons in the Kaapvaal Craton (Zwartkopie Formation and Barberton Mountain Land) and the Pilbara Craton (Salgash Subgroup and North Pole dome). (2) *ca. 3.2 Ga*: rifting and clastic sedimentation, i.e., (a) Fig Tree Group, Kaapvaal Craton, South Africa, including a basal microkrystite unit, and (b) De Grey Group (Pilbara Block, Western Australia). (3) *ca. 3.0 Ga*: global greenstone-granite events; no impact correlation identified to date. (4) *ca. 2.7–2.67 Ga*: global greenstone-granite peak events; a possible clue for impacts from microkrystite horizons in the Jeerinah Formation (2.69–2.68 Ga), Hamersley Basin, Western Australia [1]; a search is continuing for buried impact structures underlying Late Archaean continental basalts in Western Australia. (5) *ca. 2.5–2.45 Ga*: emplacement of global mafic dike swarms; deposition of microkrystite beds, i.e., Wittenoom Formation, Carawine Dolomite (Hamersley Basin, Western Australia), Lokamonna Formation (west Transvaal). (6) *ca. 2.05–2.02 Ga*: initiation of global Proterozoic rift networks; Vredefort dome impact structure and emplacement of the Bushveld Complex of possible impact origin. (7) *ca. 1.85–1.80 Ga*: peak rifting and igneous activity in mobile belts; Sudbury Impact Structure (Ontario) and Uppland (Sweden) possible impact structure. (8) *ca. 1.4 ± 0.2 Ga*: the Morokweng impact structure (diameter = 340 km), southern Kalahari; a more precise age is needed for correlations. (9) *ca. 1.2–1.05 Ga (Grenvillean/Keweenawan)*: global rifting and magmatic activity; probable impact structures in Sweden. (10) *ca. 0.7–0.5 Ga (Vendian–Early Cambrian)*: global rifting, ocean-floor spreading (Iapetus Ocean), and igneous activity (Franklin Province, Canada); several impact structures, including the Beaverhead (Canada), Acraman (South Australia), and Janisjarvi (Karelia). Preliminary time-series analyses of Precambrian events yield values consistent with the Phanerozoic galactic rotation period (250 ± 50 Ma) and the solar system's cross-galactic oscillation period (33 ± 3 Ma). Further search for Precambrian impactite deposits and microkrystite horizons and correlations between isotopic ages of impact signatures and Precambrian igneous units will be required to test potential relationships.

References: [1] B. M. Simonson (1995) personal communication.

LARGE-SCALE IMPACT CRATERING AND EARLY EARTH EVOLUTION.

R. A. F. Grieve[1] and M. J. Cintala[2], [1]Geological Survey of Canada, Ottawa, Ontario, Canada, [2]NASA Johnson Space Center, Houston TX, USA.

The surface of the Moon attests to the importance of large-scale impact in its early crustal evolution. Previous models of the effects of a massive bombardment on terrestrial crustal evolution have relied on analogies with the Moon, with allowances for the presence of water and a thinner lithosphere [1–3]. It is now apparent that strict lunar-terrestrial analogies are incorrect because of the "differential scaling" of crater dimensions and melt volumes with event size and planetary gravity [4,5].

Impact melt volumes and transient cavity dimensions for specific impacts were modeled according to previous procedures [4,5]. In the terrestrial case, the melt volume (V_m) exceeds that of the transient cavity (V_{tc}) at diameters ≥400 km (see Fig. 1). This condition is reached on the Moon only with transient cavity diameters ≥3000 km, equivalent to whole Moon melting [6]. The melt volumes in these large impact events are minimum estimates, since, at these sizes, the higher temperature of the target rocks at depth will increase melt production.

Using the modification-scaling relation of Croft [7], a transient cavity diameter of ~400 km in the terrestrial environment corresponds to an expected final impact "basin" diameter of ~900 km. Such a "basin" would be comparable in dimensions to the lunar basin Orientale. This 900-km "basin" on the early Earth, however, would not have had the appearance of Orientale. It would have been essentially a melt pool, and, morphologically, would have had more in common with the palimpsests structures on Callisto and Ganymede [8]. With the terrestrial equivalents to the large multiring basins of the Moon being manifested as muted palimpsest-like structures filled with impact melt, it is unlikely they played a role in establishing the freeboard on the early Earth [2,9].

The composition of the massive impact melt sheets (>10^7 km^3) produced in "basin-forming" events on the early Earth would have most likely ranged from basaltic to more mafic for the largest impacts, where the melt volume would have reached well into the mantle. Any contribution from adiabatic melting or shock heating of the asthenosphere would have had similar mafic compositions. The depth of the melt sheets is unknown but would have been in the multikilometer range. Bodies of basaltic melt ≥300 m thick differentiate in the terrestrial environment, with the degree of differentiation being a function of the thickness of the body [10]. We therefore expect that these thick, closed-system melt pools would have differ-

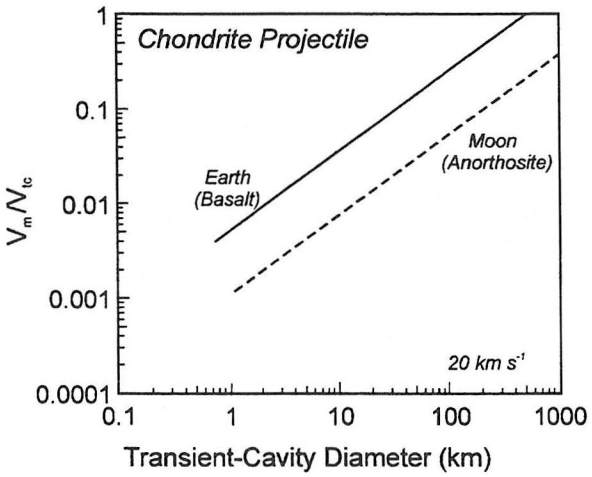

Fig. 1.

entiated into an ultramafic-mafic base and felsic top. If only 10% of the impact melt produced in a single event creating a 400-km diameter transient cavity evolved into felsic differentiates, they would be comparable in volume to the Columbia River basalts. It has been estimated that at least 200 impact events of this size or larger occurred on the early Earth during a period of heavy bombardment. We speculate that these massive differentiated melt sheets may have had a role in the formation of the initial felsic component of the Earth's crust.

References: [1] Green D. H. (1972) *EPSL, 15,* 263–270. [2] Frey H. (1980) *Precambrian Res., 10,* 195–216. [3] Grieve R. A. F. (1980) *Precambrian Res., 10,* 217–247. [4] Cintala M. J. (1992) *JGR, 97,* 947–974. [5] Grieve R. A. F. and Cintala M. J. (1992) *Meteoritics, 27,* 526–538. [6] Tonks W. B. and Melosh H. J. (1993) *JGR, 98,* 5319–5333. [7] Croft S. K. (1985) *Proc. LPSC 15th,* in *JGR, 90,* C828–C842. [8] Croft S. K. (1983) *Proc. LPSC 14th,* in *JGR, 88,* B71–B89. [9] Hargraves R. B. (1976) *Science, 193,* 363–371. [10] Jaupart C. and Tait S. (1995) *JGR, 100,* 17615–17636.

GEOPHYSICAL MODELING OF THE MJØLNIR IMPACT STRUCTURE, BARENTS SEA. S. T. Gudlaugsson, F. Tsikalas, O. Eldholm, and J. I. Faleide, Department of Geology, University of Oslo, P.O. Box 1047, Blindern, N-0316 Oslo, Norway.

Gravity, magnetic, and seismic traveltime anomalies observed at the 40-km-diameter Mjølnir impact structure reveal a distinct spatial correspondence with the radially zoned seismic structure. The gravity anomaly is dominated by a 2.5-mGal, 14-km-wide, centrally located high superimposed on a 45-km-diameter low with minimum values of –1.5 mGal. The magnetic anomaly field exhibits several local, low-amplitude anomalies in the ±100 nT range toward the periphery, while seismic mapping of a prominent, originally planar reflector beneath the structure reveals a central pull-up traveltime anomaly on the order of 80 ms. In terms of impact origin, the integrated geophysical modeling based on the characteristic bowl-shaped seismic disturbance beneath the structure supports the differentiation into a central uplift and peripheral region. Interaction of several impact cratering processes, such as impact-induced porosity increase due to brecciation, mass transport during collapse, and structural uplift, explains the modeled physical properties associated with the disturbance. The modeling further substantiates the interpretation of the Mjølnir Structure as an impact crater and demonstrates the incompatibility of alternative geological origins such as salt or clay diapirism and igneous intrusions. We find that integrated geophysical modeling of this type is a powerful tool for discriminating impact craters from similar features of different origin.

MAGNETIC ANOMALIES OF THE VREDEFORT CENTRAL RISE STRUCTURE. H. Henkel, Department of Geodesy and Photogrammetry, Royal Institute of Technology, S-100 44 Stockholm, Sweden.

The specific magnetization of an impact structure is related to the potential of new coercive mineral phases being created as a result of the impact event and the possibility of these phases becoming thermally overprinted with a new remanence (see discussions in [1, 2]). Such magnetizations will acquire the direction of the then-ambient geomagnetic field. The amount of these remagnetized carrier phases and the volume of their host rocks, together with the direction of the remanence and that of the present geomagnetic field, will determine the amplitude and shape of any associated magnetic anomalies.

The processes that, taken together, create the magnetic patterns are usually complex. Two types of patterns have been found to be common to the several impact craters studied. They are related to impact melt bodies on the one hand and to thermal overprinting of basement structures on the other. In both cases, remanent magnetizations (residing in the highly coercive carrier phases), as well as the always-present induced magnetization (residing in the low coercive carrier phases), might be involved.

Large, strongly magnetic melt bodies are, for example, known from the Mien and Dellen craters [2], while the large melt body of the crater Lappajärvi is low in magnetization [3]. Thermal overprinting is not as well documented. Two aspects of thermal overprinting can be discerned from known cases. One is the hydrothermal change of high-magnetic carrier phases to low-magnetic phases (like the oxidation of magnetite to hematite), which creates a low-magnetic anomaly as seen in craters like Clearwater [1] or Tvären [4]. The other is an additional remagnetization when the remaining thermal energy results in sufficiently high temperatures to imprint a new magnetization onto coercive carrier phases.

The Vredefort central rise region displays the effects of a high-temperature regime that has remagnetized all potentially coercive carrier phases. This occurred after the creation of the rise structure, thereby forming a new, partly discordant magnetic pattern. The extent of this overprinting is related to the temperature distribution cutting through the impact-created geometries of the collapse flow, but is still dependent on the shape of these structures within the thermal region. The extent of the magnetically active thermal region is related to the Curie temperatures of the carrier phases (ranging from 700° to 250°C). This remagnetization is frozen in as remanence, still the dominant magnetization, in a direction opposed to the present local geomagnetic field. The direction of this remanence was determined by Jackson [5] and has, with magnetic data presented by Henkel and Reimold [6], been applied to magnetic modeling. This modeling shows that the observed magnetic anomaly pattern can be reproduced with a 1–4-km-thick, remanent-magnetized layer. The deeper part of this overprinted magnetic structure is to the northwest of the center, shallowing toward the southeast. This is interpreted as a later tilt and, consequently, oblique erosion of the structure, thus exposing a relatively deeper part of the central rise to the northwest.

The issue of the so-called shock magnetization (i.e., remagnetization caused by the shock-wave passage) is illusive, since subsequent chemical and thermal processes totally dominate in potential remagnetizations. The creation of more coercive carrier phases may, however, be directly related to shock metamorphism, thus conditioning the affected rock masses for subsequent magnetic overprinting.

References: [1] Scott et al. (1997) *Meteoritics & Planet. Sci., 32,* 293–308. [2] Henkel H. (1992) *Tectonophysics, 216,* 63–89. [3] Kukkonen I. T. et al. (1992) *Tectonophysics, 216,* 111–122. [4] Ormö J. and Blomquist G. (1996) *Tectonophysics, 262,* 291–300. [5] Jackson M. C. (1982) Unpublished M.S. thesis, Univ. Witwatersrand. [6] Henkel H. and Reimold W. U. (1996) *EGRU Inf. Circ. 299,* Univ. Witwatersrand.

NBCS: THE BALTIC-NORDIC NETWORK FOR IMPACT CRATER STUDIES. H. Henkel, Department of Geodesy and Photogrammetry, Royal Institute of Technology, S-100 44 Stockholm, Sweden.

The Baltic-Nordic Network for Impact Crater Studies, established in 1995, constitutes a cooperation between eight university departments in geosciences in Nordic (Iceland, Denmark, Norway, Sweden, and Finland) and Baltic (Estonia, Latvia, and Lithuania) countries. It is financially supported by NorFa (the Nordic Academy for Advanced Study), a body of the Nordic Council of Ministers.

The network was created to promote impact-crater studies in each of these countries through combined educational and research efforts. There are 16 known and 10 suspected impact structures in the Baltic-Nordic region. The region is accessible for field studies via an extended infrastructure, and detailed geophysical and geological data are available through national geological surveys. The region thus has all the prerequisites for research activity in impact geology.

NorFa supports research students by financing courses, workshops, and symposia. This support includes travel and living costs for participating students. The network's first activity will be a 10-day workshop at the Dellen Crater and will include morning lectures and afternoon field observations. The workshop will focus on impact petrography, geophysics, and stratigraphy. Instructors and scientists have been invited from Stockholm and St. Petersburg. In the next two years, similar workshops will be held at the Gardnos Crater in Norway, with a focus on shock mineralogy, and at the Kaali crater field, with a focus on postglacial craters.

COMBINED GEOPHYSICAL MODELING OF THE VREDEFORT STRUCTURE. H. Henkel[1] and W. U. Reimold[2], [1]Department of Geodesy and Photogrammetry, Royal Institute of Technology, S-100 44 Stockholm, Sweden, [2]Department of Geology, Witwatersrand University, Private Bag 3, P.O. Wits 2050, Johannesburg, South Africa.

Modeling of gravity data for the region of the Vredefort Structure was done by integrating seismic and petrophysic measurements using the principle of mutually complementary and constraining data. The procedure for the integrated modeling is described in detail by Henkel and Reimold [1] and includes six steps: (1) A background crustal model was derived from refraction seismic data from Henkel et al. [2]; (2) a conversion of p-wave velocities to densities using the relations in Durrheim and Green [3] was made for all deep crustal structures; (3) the known surface geology was kept constant in the modeling process; (4) densities of surface rocks derived from Smit and Maree [4] and Stepto [5] were used to calculate formation averages for the supracrustal strata; (5) the northwest basin depth was constrained by reflection seismic data from Durrheim [6]; and (6) the free segments of the subsurface structures were adjusted until the calculated gravity effect equaled the measured effects (within measurement errors).

The resulting gravity models, along northwest-southeast and south-southwest-north-northeast profiles intersecting near the center of the Vredefort Dome, describe the likely present structure of the Vredefort crater. The impact-related basin in the Vredefort Dome area has a diameter of 250 km, preserved in the present south-southwest-north-northeast extension of the structural Witwatersrand basin, and depths ranging from 7 km in the southeast to 12 km in the northwest and north. The remaining structural uplift in the center is 12 km.

Postimpact deformation, as indicated by the asymmetry of the structure, includes tilting (with the southeastern part uptilted), which is responsible for the present asymmetric shape of the central rise (Vredefort Dome), and northwest-southeast shortening of the impact basin by as much as 85 km. This was probably caused by thrusting from the northwest and major flexing in the southeast [7].

The shape of the crystalline central rise structure is hyperbolic in section, with a diameter of 70 km at its base, 35 km at the middle, and 40 km at the present erosion surface. Around its southwestern, western, northwestern, and northern perimeter, the surrounding cover sequences are overturned. This is not the case along the eastern and southeastern perimeter, where the structure is at a deeper erosion level. The upper-lower crustal interface was raised 9 km and occurs now at 16 km depth. The crust-mantle interface was only slightly involved, with a potential rise of about 4 km vaguely indicated by the rise of the deepest seismic reflectors under the northwest basin. The whole crust is, thus, not on edge, as has been previously postulated [8,9], and there is no connection between observed mafic rocks at the surface and the upper mantle as asserted by Hart [10].

References: [1] Henkel H. and Reimold U. W. (1996) *Econ. Geol. Res. Unit. Inf. Circ. No. 299,* Univ. Witwatersrand, 86 pp. [2] Henkel H. et al. (1990) *European Geotraverse: Integrated Studies,* 67–76. [3] Durrheim R. J. and Green R. W. E. (1992) *Geophys. J. Inter., 108,* 812–832. [4] Smit P. J. and Maree B. D. (1966) *Geol. Surv. S. Afr. Bull., 48,* 37. [5] Stepto D. (1979) Unpublished Ph.D. thesis, Univ. Witwatersrand. [6] Durrheim R. J. et al. (1991) *Geodynamics, 22,* 213–224. [7] Friese A. et al. (1995) *Econ. Geol. Res. Unit. Inf. Circ. No. 292,* Univ. Witwatersrand, 67 pp. [8] Slawson W. F. (1976) *GCA, 40,* 117–121. [9] Hart R. J. et al. (1981) *JGR, 86,* 10639–10652. [10] Hart R. J. et al. (1990) *Chem.Geol., 82,* 233–248.

RECONSTRUCTION OF THE VREDEFORT IMPACT CRATER. H. Henkel[1] and W. U. Reimold[2], [1]Department of Geodesy and Photogrammetry, Royal Institute of Technology, S-100 44 Stockholm, Sweden, [2]Department of Geology, Witwatersrand University, Private Bag 3, P.O. WITS 2050, Johannesburg, South Africa.

For the reconstruction of an impact crater, information is needed about crustal structure and conditions at the time of impact and about the properties of the projectile. This information can be deduced from the present deformed and eroded status of impact structures only to a very limited degree. The keys to the crustal structure are provided by regional geology and refraction seismic sections. The present shape of the structure can then be assessed through geophysical modeling using gravity and magnetic data. The central rise feature in large craters will remain even at deep erosion levels and is thus key to determining the position and potential extension of the former crater.

In the Vredefort Structure, the preimpact cover thickness has been estimated to be about 15 km [1], and the gravity model shows a well preserved central rise with remaining stratigraphic uplift of about 12 km [2]. The parameters of the projectile can only be vaguely

assessed by the extent of shock deformation, occurrence of melt bodies, and other shock-induced changes of the crust. The extent of shock deformation in the near range of the explosion is obscured by the subsequent crater collapse. In the far range, the change of rocks from their normal (with respect to composition and position in the crust) rheologic behavior to the shock-induced plastic behavior above their Hugoniot Elastic Limit (HEL) is indicated by the onset of reflection seismic transparency at ~70 km from the explosion center (in those parts of the crater basement that are least deformed by subsequent collapse processes).

Using the estimate of the HEL position, assumptions can be made about the energy of the projectile and thus the potential range of melt volumes [2,3]. Such melt has so far only been identified as dikes in the central rise crystalline core. Its chemical composition indicates an intermediate source, and its position within the low-density crust of the uppermost crystalline basement in the core of the central rise indicates that the shock melting did not occur at deep levels in the basement.

The excavation flow roughly follows a pattern described as the z-model in Melosh [3], implying vertical-downward-directed flow beneath the explosion center injecting and displacing material, and upward-outward-directed flow where ejecta leave the evolving crater at ~45° angles.

It is supposed that this mass-transport pattern conditions the crust for subsequent collapse flow. Whereas the transient crater edge will flow into the crater, the central rise will collapse vertically downward and flow radially outward. The two will collide at some distance from the center, resulting in the final crater, extended by almost a factor of two in diameter and leaving a raised rim, a mega-breccia-filled ring basin, and a central rise overturned in its upper parts.

The energy deposited by the shock wave now resides as heat in the newly formed crater, adding to the elevated temperatures brought in by the central rise from deeper crustal levels. This new temperature regime within a brecciated environment represents a huge potential for hydrothermal processes, leaching, transporting, and precipitating various chemical components.

The remaining topography of the collapsed impact crater will be leveled by erosion and sedimentary infilling. Younger deformation events might reshape the structure. The Vredefort Structure was affected by both tilting (northwest up), faulting or flexing (southeast up), and thrusting (northwest in), so that the present shape of the impact structure is an elongated basin, roughly representing the original extent of the crater only in its southwest-northeast direction. Young cover rocks obscure most of the south and southeast of the structure.

References: [1] Fletcher P. and Reimold W. U. (1989) *S. Afr. J. Geol., 92,* 223–234. [2] Henkel H. and Reimold W. U. (1996) *EGRU Inf. Circ. 299,* Univ. Witwatersrand, 89 pp.; this volume. [3] Melosh H. J. (1989) *Oxford Mono. Geol. Geophys., 11,* 245.

ORIGIN OF CARBONACEOUS MATTER IN ROCKS FROM THE WHITEWATER GROUP OF THE SUDBURY STRUCTURE.

D. Heymann[1] and B. O. Dressler[2], [1]Department of Geology and Geophysics, Rice University, Houston TX 77251-1892, USA, [2]Lunar and Planetary Institute, Houston TX 77058, USA.

It has long been known that heterolithic breccias of the Black member of the Onaping Formation and mudstones of the Onwatin Formation, both formations belonging to the Whitewater Group, contain ~1% carbonaceous matter. Crucial observations show that this large C content is wholly contained within the Sudbury basin and that the C content of the Onaping's Gray member (which, like the Black member, is supposed to be a fallback breccia from the impact) is an order of magnitude smaller. The anthraxolite veins in the Onwatin are thought to consist of the same C that was mobilized. Among the hypotheses that have been set forth for the origin of the C are (1) the reduction of gases during fumarolic activity [1]; (2) C from the impactor [2]; (3) the transformation of CO to CO_2 + C in the cooling atmospheric impact plume [3]; and (4) a biogenetic origin [4]. Each of these hypotheses has its own problems.

Biogenetic processes do not form carbonaceous matter such as is present in the Whitewater Group rocks, but rather produce organic matter with O, N, S, and H still bonded to it. It is generally thought that a metamorphic heating event is required to strip the O, N, S, and H from the organic remains to form carbonaceous matter, and it is known that metamorphic conditions can be deduced from the Raman spectra of the C that is formed [5]. The Raman spectrum of single-crystal graphite has one first-order line at 1580 cm^{-1} (G-line). A forbidden line at 1360 cm^{-1} (D-line) appears in the spectra of disordered graphite. The intensity ratio D/G serves as a rough indicator of grain size or degree of disorder. Carbonaceous matter formed from organic remains during greenschist-facies metamorphism has roughly equally intense G-lines and D-lines [5].

We have obtained Raman spectra for nine Black Onaping (BO) samples and one Onwatin sample and for anthraxolite taken from near the Errington 1 mine. The BO rocks came from High Falls, Chelmsford, Capreol, Nickel Offset Road, and Nelson Lake collection sites. All spectra had nearly equally intense G-lines and D-lines. When these results are combined with C isotopic data ($\delta^{13}C$ of –31.06‰, –30.10‰, and –30.24‰ respectively) for two BO and one Onwatin rocks [4], for an anthraxolite ($\delta^{13}C$ of –31.5‰) from Lot 10, Concession 1, Balfour Township [6], and the presence of algal relics in an Onwatin rock [4], the biogenetic hypothesis for the origin of the carbonaceous matter in the Onaping and Onwatin Formations becomes the leading contender. Its major problem has been one of timing. The Black member is thought to have sedimented rapidly and soon after the deposition of the Gray member. How rapidly and how soon, however, cannot be ascertained with any great precision, and algal blooms, given the extant conditions (warm waters, ample nutrients, and a CO_2-rich atmosphere), could have been super-fast, with the appearance of fresh crops at the surface keeping pace with the burial of older crops beneath the growing thickness of the Onwatin package. The *in situ* biogenetic hypothesis has the additional forte of demanding that the formation of the carbonaceous matter took place entirely within the Sudbury basin.

The impactor- and CO-based hypotheses cannot be totally dismissed, however. The Raman spectra of C in the Allende meteorite are very similar to those obtained for the Onaping and Onwatin rocks, as is the Raman spectrum of a heavily shocked graphite (both obtained in the present study).

References: [1] Burrows A. G. and Rickaby H. C. (1930) *1929 Annual Sudbury Report of Ontario Department of Mines, Vol. 38,* 55 pp. [2] Implied by Becker L. et al. (1994) *Science, 265,* 642–644. [3] Heymann D. et al. (1996) *LPS XXVIII,* 555–556. [4] Avermann M. (1994) *GSA Spec. Paper 293,* 265–274. [5] Pasteris J. D. and Wopenka B. (1991) *Can. Mineral., 29,* 1–9. [6] Mancuso J. J. et al. (1989) *Precambrian Res., 44,* 137–146.

CARBON ISOTOPIC COMPOSITION OF CARBONACEOUS MATTER IN ROCKS FROM THE WHITEWATER GROUP OF THE SUDBURY STRUCTURE. D. Heymann[1], B. O. Dressler[2], R. B. Dunbar[1], and D. A. Mucciarone[1], [1]Department of Geology and Geophysics, Rice University, Houston TX 77251-1892, USA, [2]Lunar and Planetary Institute, 3600 Bay Area Boulevard, Houston TX 77058, USA.

The origin of carbonaceous matter in the heterolithic breccias of the Black member of the Onaping Formation and in mudstones of the Onwatin Formation has long been an enigma [1–4]. Avermann [4] was the first to propose a biogenetic origin, based on the fact that the $^{13}\delta$-values of the carbonaceous matter from two samples of the Black member of the Onaping Formation and one of the Onwatin Formation were all close to –30‰, which is at the lower end of the range of nonmarine plants and animals. Avermann also found relics of algae in an Onwatin slate and concluded that the carbonaceous material had originated from biogenetic material deposited at a slow rate into a local euxinic basin created by the Sudbury event. However, for the biogenetic material to become carbonaceous matter, it had to undergo graphitization associated with the greenschist-facies metamorphic history of the host rocks. Elsewhere in this volume, it is reported that the Raman spectra of the carbonaceous matter are fully consistent with such a metamorphic history [5].

The only other $^{13}\delta$ value (–31.5‰) of carbonaceous matter from the Whitewater group is that of an anthraxolite [6]. Because of the comparatively small number of data available, it seemed useful to do a more comprehensive survey of C isotopic compositions of carbonaceous matter in samples obtained from various geographic locations within the Sudbury Structure. The samples used are listed in Table 1. The powdered rocks were first treated with toluene and then with methanol to remove soluble organic compounds. All powders were treated with HCl to dissolve any carbonate. Sulfides such as pyrrhotite were also dissolved in this step, but some elemental S was formed. Several $^{13}\delta$ measurements were done with such whole-rock samples. A number of samples were demineralized with HF-HCl, and the dried C-enriched residues were used for $^{13}\delta$ measurements. Carbon dioxide for the mass-spectrometric analysis was generated by flash combustion in O_2. In the Carlo-Erba NA-1500 elemental analyzer that was used, N oxides were reduced to N_2 and the separation of CO_2, N_2, H_2O, and SO_2, which were carried along in a stream of He carrier gas, was achieved with a gas-chromatographic column. Typically, 0.2 mg of C was converted to CO_2. The mass spectrometer used in this study was a semi-automated VG 602E. The performance of the instrument was tested with NBS21 and Sulfanilamide CHNS standards. The $^{13}\delta$-values in Table 1 are reported relative to the international PDB standard.

These results strongly support a biogenetic origin for the Sudbury C. However, it is still unknown exactly what organisms were involved and at what rate the Black Onaping Formation accumulated. The observation that the C content of that formation increases from base to top [4] suggests that the sedimentation rate slowed over time.

References: [1] Burrows A. G. and Rickaby H. C. (1930) *1929 Annual Sudbury Report of Ontario Department of Mines, Vol. 38,* 55 pp. [2] Becker L. et al. (1994) *Science, 265,* 642–644. [3] Heymann D. et al. (1996) *LPS XXVIII,* 555–556. [4] Avermann M. (1994) *GSA Spec. Paper, 293,* 265–274. [5] Heymann D. et al., this volume. [6] Mancuso J. J. et al. (1989) *Precambrian Res., 44,* 137–146.

TABLE 1. Isotopic composition of C in carbonaceous matter from Whitewater Group rocks.

Sample	Info	$^{13}\delta$‰	Sample	Info	$^{13}\delta$‰	Sample	Info	$^{13}\delta$‰
SUGJ3	BO/CH	–26.26	SUBF7	BO/HF	–29.55	SUBD5	BO/NC	–31.45
SUGJ5	BO/CH	–29.01	SUGJ1	BO/HF	–31.60	SUBD3	BO/SC	–30.16
SURG1	BO/HF	–34.52	SUGJ2	BO/HF	–31.89	SUGJ6	OW/OF	–31.31
SUBD4	BO/HF	–39.91	SUGJ4	BO/NO	–30.29	ANTHR	"OW"	–31.73
SUBF1	BO/HF	–27.12	SUBF3	BO/EC	–38.17	SUBD1	GO/HF	–39.75
SUBF4	BO/HF	–33.08	SUBF5	BO/EC	–32.77			

BO = Black Onaping; GO = Gray Onaping; OW = Onwatin; HF = High Falls Area; NC = North Capreol; SC = South Capreol; EC = East Capreol; CH = Chelmsford; NO = Nickel Offset Road. ANTHR = Anthraxolite. NBS-21 standard deviation is 0.11‰.

ORIGIN OF NATIVE SULFUR IN ROCKS FROM THE SUDBURY STRUCTURE, ONTARIO, CANADA. D. Heymann[1], B. O. Dressler[2], and M. H. Thiemens[3], [1]Department of Geology and Geophysics, Rice University, Houston TX 77251-1892, USA, [2]Lunar and Planetary Institute, 3600 Bay Area Boulevard, Houston TX 77058, USA, [3]Department of Chemistry and Biochemistry, University of California–San Diego, La Jolla CA 92093-0356, USA.

When native S was discovered in the heterolithic breccias of the Black member of the Onaping Formation, the question of its possible impact origin arose. In addition to the native S (S^o) content, we determined the total C and total S contents in several Whitewater Group rocks (Table 1). We also examined the S^o content associated

TABLE 1. Total C, total S, and native S in Sudbury rocks.

Sample	Info.	C %	S %	S^o ppm	Sample	Info.	C %	S %	S^o ppm
SURG1	BO/HF	0.602	0.596	97	SUBF6	BO/HF	0.739	0.432	4.1
SUBD4	BO/HF	0.300	0.646	230	SUBD2	BO/NL	0.201	0.173	69
SUBF1	BO/HF	0.888	1.172	70	SUBD5	BO/NC	0.782	0.100	7.1
SUBF2	BO/HF	0.947	0.684	15	SUBD3	BO/SC	1.15	0.464	30
SUBF4	BO/HF	0.891	0.822	12	SUBF3	BO/EC	2.43	0.668	0.4
SUBF7	BO/HF	0.731	0.691	13	SUBF5	BO/EC	1.057	0.646	3.5
SUBF8	BO/HF	0.773	1.05	32	SUGJ3	BO/CH	1.91	0.759	11
SUGJ1	BO/HF	1.120	0.315	33	SUGJ5	BO/CH	1.144	0.273	90
SUGJ2	BO/HF	0.625	0.371	28	SUGJ4	BO/NO	1.603	0.586	3.4
SUBD1	GO/HF	0.07	0.05	55	SUGJ6	OW/OF	2.376	0.020	28

BO = Black Onaping; GO = Gray Onaping; O = Onwatin; HF = High Falls Area; NL = Nelson Lake; NC = North Capreol; SC = South Capreol; EC = East Capreol; CH = Chelmsford; NO = Nickel Offset Road. $D33 = \delta^{33}S - 0.5 \times \delta^{34}S$; $D36 = \delta^{36}S - 1.97\ \delta^{34}S$ (for D explanation see [2]).

TABLE 2. Isotopic S compositions.

Sample	$\delta^{33}S$ (‰)	$\delta^{34}S$ (‰)	D33	$\delta^{36}S$ (‰)	D36
Pyrrhotite	2.62	4.75	0.245	8.6	–0.76
So Pyrrhotite	2.93	5.19	0.335	9.7	–0.524
So SUBD4	4.87	9.55	0.095	17.6	–1.21

with pyrrhotite to determine if S^0 is a product of pyrrhotite weathering. In the weathered crust of a block of massive pyrrhotite from the Whistle Mine, S^0 was 29.4 ppm; in pyrrhotite 0–5 mm below this crust, S^0 was 4.4 ppm; and at about 10 cm below the surface, S^0 was undetectably small. The S^0 content of this finely powdered pyrrhotite after exposure to water for 10 days became 1.0%. The S^0 content in a pyrrhotite separate from rock SUBD4 was 1.4%. On the basis of this evidence, it is concluded that the native S in these rocks was formed by the weathering of pyrrhotite and not related to the impact origin of the Sudbury Structure. Furthermore, an impact origin of S^0 is unlikely, because it probably would not have survived the postimpact greenschist facies metamorphism. The isotopic composition of S was determined in three samples, including a pair of pyrrhotite and S extracted from it and a sample of S extracted from rock SUBD4 (Table 2). The $\delta^{34}S$ values of the pyrrhotite/S pair are within the range of data reported by others [1]. For samples with perfect mass-dependent fractionation, both D33 and D36 are zero. Obviously there is a component of mass-independent fractionation present, but its origin is not understood. The isotopic composition of S^0 from SUBD4 strengthens the conclusion that the native S did not come from an extraterrestrial source or a terrestrial biogenetic source.

References: [1] Thode H. G. et al. (1962) *Econ. Geol., 57,* 565–578. [2] Gao X. and Thiemens M. H. (1991) *GCA, 55,* 2671–2679; Colman J. J. et al. (1996) *Science, 273,* 774–776.

THE SEARCH FOR FULLERENES IN ROCKS FROM THE WHITEWATER GROUP OF THE SUDBURY STRUCTURE, ONTARIO, CANADA.

D. Heymann[1], P. R. Buseck[2], J. Knell[2], and B. O. Dressler[3], [1]Department of Geology and Geophysics, Rice University, Houston TX 77251-1892, USA, [2]Departments of Geology and Chemistry, Arizona State University, Tempe AZ 85287, USA, [3]Lunar and Planetary Institute, Houston TX 77058, USA.

The occurrence of fullerenes C_{60} and C_{70} in heterolithic impact breccias of the Black member of the Onaping Formation was reported by Becker et al. [1]. The authors assumed that the fullerenes had formed in the atmospheric impact plume, possibly by the pyrolysis of polycyclic aromatic hydrocarbons (PAHs) of the impactor, but did not explain the high content of carbonaceous matter in these breccias. In 1996, Becker et al. [2] reported the occurrence of fullerenes with isotopically anomalous He trapped inside the C cages and concluded that the impactor must have contained extraterrestrial fullerenes. The C_{60} contents of these rocks were reported as 1–10 ppm [1].

Because of the interesting implications of both findings, it was decided to expand the search for fullerenes in rocks from the Gray and Black members of the Onaping Formation and one C-rich mudstone sample from the Onwatin Formation. The total C and S contents of these 22 rocks are reported in a companion abstract [3]. Fullerenes were searched for by high-performance liquid chromatography [4] in powdered bulk samples of 21 of these rocks (SUB8 was the exception). Typically 100 g of SURG, SUBD, and SUGJ and 10–20 g of SUBF rocks were analyzed [3]. Duplicate measurements were performed in 11 cases and fullerenes were searched for in five HCl-HF demineralized C-rich residues. No fullerenes were detected. A parallel search for fullerenes was conducted in three rocks by mass spectrometry [5]. One of these rocks, SUBF8, had been collected from the same High Falls outcrop as one of the samples of Becker et al. [1]. No fullerenes were found.

If fullerenes occur in the Black member of the Onaping Formation at all, that formation would hardly be "one of the largest natural occurrences of fullerenes found so far on Earth" [1], because the distribution of these molecules is obviously very heterogeneous, with most of the rocks containing no fullerenes. The difficulties inherent in the original hypothesis were spelled out by the authors [1] and hence need not be repeated here. The problems with the extraterrestrial hypothesis [2] are as follows: Because C_{60} and C_{70} are more volatile than Ir and its compounds, and Ir from the analogous Chicxulub event was deposited worldwide [6], one expects the "Sudbury impactor fullerenes" to have become distributed, if not globally, then at least over a much wider area than the Sudbury basin. Unfortunately, because the pre-erosion mass of the C_{60}-bearing rocks at Sudbury is unknown, it is impossible to estimate how much fullerenes the impactor had to contain to account for the known finds [1,2]. However, the C_{60} contents of the rocks that contain it [1,2], normalized to C, are in the range 10^2–10^3 ppm, some 3–4 orders of magnitude larger than reported for a carbonaceous chondrite [7]. Like the suggested terrestrial fullerenes [1], the extraterrestrial fullerenes had to be shielded from destruction in the hot plume, in the hot fallback breccias, and during postimpact greenschist-facies metamorphism. It is unclear how incorporation into sulfides [1] might protect the fullerenes. If a C_{60}-bearing Black member sample were exposed to temperatures of greenschist metamorphism, it would be useful to study the probability of fullerene survival at these temperatures.

Acknowledgments: We would like to thank B. M. French, R. A. F. Grieve, and G. W. Johns for their donations of samples. We also would like to thank R. E. Smalley for allowing us to use his HPLC setup.

References: [1] Becker L. et al. (1994) *Science, 265,* 642–644. [2] Becker L. et al. (1996) *Science, 272,* 249–253. [3] Heymann D. et al., this volume. [4] Heymann D. et al. (1994) *Science, 265,* 645–647. [5] Daly T. K. et al. (1992) *Science, 259,* 1599–1601. [6] Alvarez W. et al. (1994) *LPI Contrib. No. 825,* 3–5. [7] Becker L. et al., *Nature, 372,* 507.

THE STEEN RIVER IMPACT STRUCTURE, ALBERTA, CANADA.

A. R. Hildebrand[1], M. Pilkington[1], R. A. F. Grieve[1], R. R. Stewart[2], M. J. Mazur[2], D. W. Hladiuk[3], and D. Sinnott[3], [1]Geological Survey of Canada, Ottawa, Ontario K1A 0Y3, Canada, [2]Department of Geology and Geophysics, University of Calgary, Calgary, Alberta T2N 1N4, Canada, [3]Gulf Canada Resources Limited, Calgary, Alberta T2P 2H7, Canada.

The ~25-km-diameter Steen River impact structure (59°30'N, 117°38'W) is the remnant of the largest known impact crater in the Western Canadian Sedimentary Basin (WCSB). The eroded crater lies buried under ~200 m of cover with no surface expression, necessitating geophysical and drilling projects for its exploration. In this area, the WCSB is composed of ~1 km-thick, gently southwest-dipping strata. The crater rim hosts seasonal petroleum production of ~600 barrels of oil per day (BOPD) and shut-in gas wells, stimulating continued searches for hydrocarbon reservoirs in the impact structure. Although Steen River was discovered more than 30 years ago with documented evidence of shock metamorphism [e.g., 1,2], little has been published about it.

Hydrocarbon exploration companies have acquired more than

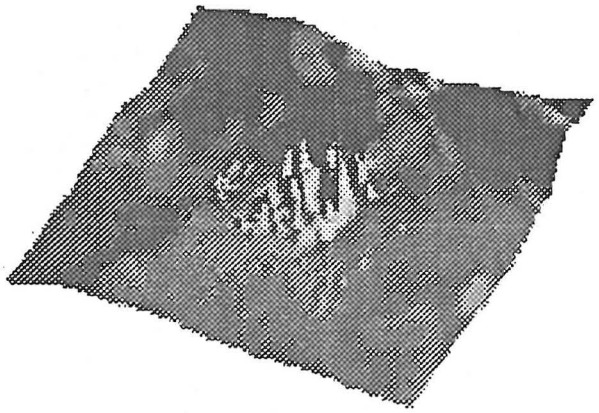

Fig. 1. Total magnetic-field intensity over the Steen River impact structure. Compare short-wavelength crater anomalies to broader regional anomalies.

100 two-dimensional seismic reflection profiles over the impact structure; in addition, one three-dimensional seismic survey was recently executed over part of the crater rim. Approximately 40 wells have been drilled in and near the crater, providing generally good control for the coherent seismic data. The proprietary seismic data outline the rim uplift of the impact structure in some detail, but most profiles record only chaotic reflectors interior to this. Mapping the crater's interior structures has been attempted with magnetic- and gravity-field surveys. An aeromagnetic survey with 0.5-km line spacing has recently been flown across the entire structure (Fig. 1), revealing large-amplitude central and concentric anomalies. A pilot gravity survey revealed associated anomalies with a maximum value of ~3 mGal, slightly smaller than that expected for a crater of this size [3]. Positive anomalies of up to ~0.5 mGal were found associated with the rim uplift. A total of ~1500 gravity stations have now been acquired over the crater. Interpretation of the gravity data is complicated by the high regional gradients (17 mGal decreasing to the northwest across the impact structure), with superimposed regional anomalies of 10–20 km scale.

Rim uplift, down-slumped blocks and central uplift are well to partly delineated. Well 16-19 records the inverted stratigraphy of the overturned flap, lying on the inner down-slumped blocks, and establishes a minimum structural downdrop of ~0.6 km. Only minor relief is indicated on the unconformity developed on the top of the impact lithologies. Rim erosion of ~1 km is indicated by the amount of extra stratigraphy preserved in the slumped blocks in well 16-19 in the crater's interior and by the assumption of a rim-to-crater-floor depth of 0.5 km. This erosion has presumably subdued the crater's gravity expression. Reflection seismic data usually have not detected the down-slumped blocks but occasionally provide vague images, and a slump zone at least 3 km wide is indicated. Wells and seismic profiles reveal an irregular, faulted crater perimeter with rim uplift of up to ~100 m. The central structural uplift has a radius of ~3 km, based on well control and magnetic-field anomalies; substantial asymmetry may occur in the central uplift and slump zone. Well 12-19 penetrated the central structural uplift immediately below the Cretaceous cover at a depth of 184 m, establishing a minimum structural uplift of ~1100 m relative to the surrounding basement surface. Large-amplitude magnetic anomalies are also preserved adjacent to and detached from the central uplift; these may represent remnants of intracrater melt rocks and/or suevitic breccias.

References: [1] Carrigy M. A. and Short N. M. (1968) in *Shock Metamorphism of Natural Materials* (B. M. French and N. M. Short, eds.), pp. 367–378, Mono, Baltimore. [2] Winzer S. R. (1972) *24th Intl. Geol. Cong., Planet.*, Sect. 15, 148–156. [3] Pilkington M. and Grieve R. A. F. (1992) *Rev. Geophys., 30,* 161–181.

MAPPING THE CHICXULUB CRATER STRUCTURE WITH GRAVITY AND SEISMIC REFLECTION DATA. A. R. Hildebrand[1], M. Pilkington[1], J. F. Halpenny[2], R. V. Cooper[2], M. Connors[3], C. Ortiz-Aleman[4], R. E. Chavez[4], J. Urrutia-Fucugauchi[4], E. Graniel-Castro[5], A. Camara-Zi[5], and R. T. Buffler[6], [1]Geological Survey of Canada, Ottawa, Ontario, Canada, [2]Geomatics Canada, Ottawa, Ontario, Canada, [3]Athabasca University, Athabasca, Alberta, Canada, [4]Instituto de Geofisica, Universidad Nacional Autónoma de Mexico, Ciudad Universitaria, Distrito Federal, Mexico, [5]Facultad de Ingeniería, Universidad Autónoma de Yucatán, Mexico, [6]Institute for Geophysics, University of Texas, Austin TX, USA.

The Chicxulub Crater, buried under the Yucatán Platform of Mexico, affords one of the most favorable opportunities on Earth for structural studies of a large complex impact crater, primarily because of its preservation and accessibility. The crater was buried soon after rim erosion in an environment that sustained only minor subsequent tectonic disturbance. In addition, the Chicxulub impact apparently ended the Cretaceous period, and the crater's ejecta blanket is known globally at hundreds of locations. The buried crater is half overlain by a coastal plain and half by a shallow sea, allowing exploration by marine-based, land-based, and hybrid techniques. The radial symmetry of the crater allows data acquired in either terrain to be applied to the entire structure using the common datasets of magnetic- and gravity-field anomalies.

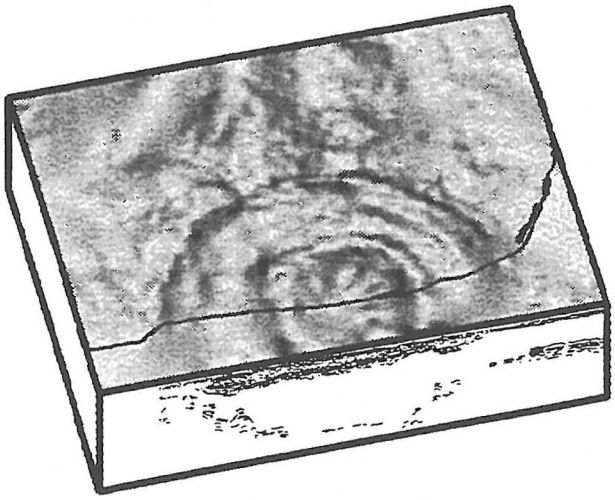

Fig. 1. Perspective view of horizontal gradient of Bouguer gravity anomaly with juxtaposed Chicxulub Crater structure as revealed by nearest offshore seismic reflection profile.

Gravity datasets covering the Yucatán Platform [e.g., 1–2] reveal an ~180-km-diameter low with an internal concentric structure [e.g., 3–4] that is the expression of the Chicxulub Crater impact lithologies and crater fill. The gravity signature is complicated by regional anomalies and early modifications to the crater rim, and the northern half of the crater is not well imaged because of the scarcity and imprecision of marine data. Also, an ~20-km-wide gap in survey coverage (due to shallow water) occurs between the land data and the nearest seismic profile of Camargo and Suarez [5, Fig. 1], which roughly corresponds to the beginning of offshore coverage.

In September–October 1996, a marine gravity survey was successively conducted on 32-m and 10.5-m vessels to survey this gap and offshore seismic lines of the Imperial College/British Institutions Reflection Profiling Syndicate/University of Texas seismic project. Offshore coverage was ~2400 line-km, followed by ~1500 line-km inshore with ~1.3 and ~1.9 mGal unadjusted crossovers, respectively; data precision was strongly influenced by sea conditions.

Preliminary results from the marine surveys confirm the provisional ties of gravity-gradient features to the seismic line. The perimeter fault, crater-fill margin, slump faults, and collapsed transient cavity margin may all be linked to gradient features. Unfortunately, the clearest crater expression in the gravity field is on the east side, where the seismic lines lose resolution at the basin margin. To the west, the strong peripheral gradient splits with one component corresponding to the perimeter slump fault and a larger feature corresponding to the basin margin. This splitting is interpreted as a result of the prompt backwash of crater ejecta into the northwestern part of the crater. Regional gradients also obscure the crater signature to a greater extent to the west. Asymmetry of the central high is indicated, although a weak feature may extend to the northeast; the surrounding sharp low continues until it abuts the regional high to the northwest. Additional land surveys support the correlation of the cenote ring to gravity-gradient features and suggest that a weak high may correlate to the rim uplift in some places.

References: [1] Villagomez A. (1953) *Bol. Asoc. Mex. Geolog.. Petrol., 5,* 77–84. [2] Ness G. E. et al. (1991) *GSA Map & Chart Ser. MCH073.* [3] Pilkington et al. (1994) *JGR, 99,* 13147–13162. [4] Hildebrand A.R. et al. (1995) *Nature, 376,* 415–417. [5] Camargo Zanoguera A. and Suárez Reynoso G. (1994) *Bol. Asoc. Mex. Géofis. Explor., 34,* 1–28.

GEOCHEMICAL CHARACTERISTICS OF IMPACTITES FROM THE POPIGAI IMPACT STRUCTURE, RUSSIA.

Th. Hölker[1], A. Deutsch[1], and V. L. Masaitis[2], [1]Institut für Planetologie, Universität Münster, D-48149 Münster, Germany (holkert@uni-muenster.de), [2]Karpinsky Geological Institute, St. Petersburg 199026, Russia (vsg@sovam.com).

Summary: The 100-km Popigai impact structure, situated on the northeastern slope of the Anbar Shield, Northern Siberia (N71°30', E111°0'), is known for its excellent state of preservation [1,2]. The most precise published age (^{40}Ar-^{39}Ar) of 35.7 ± 5 Ma [3] indicates an origin in the Late Eocene. This crater has been suggested as a possible source of shocked quartz in an Ir-enriched ejecta horizon in the Massignano section, Italy [4,5]. We report Sr and Nd isotope characteristics and rare earth element (REE) distribution patterns of tagamites, impact glasses, and target rocks from Popigai.

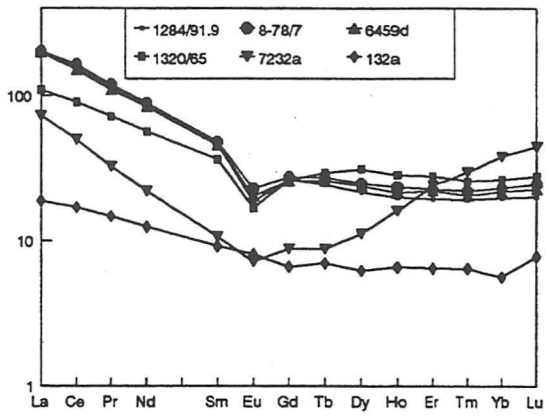

Fig. 1. C1-normalized REE distribution patterns for various lithologies from Popigai. See text for discussion.

These data exclude Popigai as a parent crater of the hitherto-analyzed, Late Eocene distant ejecta horizons.

Samples: We have analyzed whole-rock samples from the Popigai Crater for Nd-Sr isotope signatures and REE concentrations. The samples are (1) variably shocked gneissic target rocks from the ring uplift (garnet gneiss #1320/65), the crater rim (plagiogneiss #132a), and a suevite (garnet-biotite gneiss inclusion #7232a); (2) a tagamite (#1284/91.9); and (3) impact melt glasses, separated from various breccias (specimen #8-78/7, 6459d, 8-616, 4602/88-89, 8-620, 4602/36).

REE Data: The total REE abundance of the tagamite and the melt glasses is high, lying between 216 and 229 ppm. The impact melt lithologies display quite uniform, chondrite-normalized ($_{cn}$) distribution patterns (Fig. 1) with a distinct negative Eu anomaly ($Eu_{cn}/Eu_{cn}^* = 0.54–0.63$) and strong LREE enrichment with La_{cn}/Yb_{cn} between 8.74 and 10.08. The REE distribution patterns of the melt samples differ significantly from those of the gneissic samples from the crater rim and the ring uplift (Fig. 1), whereas gneiss inclusion #7232a has REE abundances similar to the melt lithologies, except for slightly lower LREE.

Strontium, Neodymium Isotope Characteristics: As described in [6], Sr and Nd isotope parameters of the melt lithologies show only minor variations. T^{Sr}_{UR} is 2.07 ± 0.05 Ga, T^{Nd}_{CHUR} is 1.95 ± 0.02 Ga, T^{Nd}_{DM} is 2.21 ± 0.02 Ga ($n = 7 \pm 1_D$; for definition of the parameters, see [7]). The isotopic data and the close range in model ages could help to identify distant ejecta of the Popigai event and to separate such material from ejecta of the Chesapeake Bay impact structure. So far, none of the analyzed 35-Ma tektites and microtektites [7–10] display isotope characteristics such as the Popigai material, confirming the interpretation of Koeberl [11].

References: [1] Masaitis V. L. et al. (1980) *The Geology of Astroblemes,* Nedra, St. Petersburg, Russia, 231 pp. [2] Masaitis V. L. (1994) *GSA Spec. Paper 293,* 153. [3] Bottomley R. J. and York D. (1989) *LPS XX,* 101. [4] Langenhorst F. (1996) *Geology, 24,* 487. [5] Montanari A. et al. (1993) *Palaios, 8,* 420. [6] Hölker Th. et al. (1997) *LPS XXVIII,* 583. [7] Shaw H. F. and Wasserburg G. J. (1982) *EPSL, 60,* 155. [8] Stecher O. et al. (1989) *Meteoritics, 24,* 89–98. [9] Ngo H. H. et al. (1985) *GCA, 49,* 1479–1485. [10] Vonhof H. (1997) personal communication. [11] Koeberl C. et al. (1996) *Science, 271,* 1263.

DIAMONDS IN THE EJECTA AND FIREBALL LAYERS OF THE CRETACEOUS-TERTIARY BOUNDARY IN THE U.S. AND MEXICO. R. M. Hough, I. Gilmour, and C. T. Pillinger, Planetary Sciences Research Institute, The Open University, Walton Hall, Milton Keynes, MK7 6AA, UK (R. M. Hough@open.ac.uk).

Cubic nanodiamonds ranging from 3 to 5 nm were first discovered in the K/T boundary fireball layer in the Knudsens' Farm area, Alberta, Canada [1]. Gilmour et al. [2] subsequently found diamonds measuring up to 6 nm in the fireball layers of the Berwind Canyon, Colorado, and Brownie Butte, Montana, K/T localities in the U.S. We have studied acid-resistant residues of fireball and ejecta layer samples from Berwind Canyon, Raton Pass, and Clear Creek North in the U.S. and also from Arroyo El Mimbral and Arroyo El Peñon in Mexico.

Transmission electron microscope (TEM) observations of the acid-resistant residue from the fireball layer of the Berwind Canyon locality identified a predominance of zircon and rutile, but cubic nanodiamonds up to 10 nm in size were also found. The nature of the acid-demineralization treatment mitigates the survival of less-robust forms of C; therefore, any C released during stepped combustion of the sample represents combustion of either diamond or Si carbide.

Using stepped combustion combined with static mass spectrometry, we have revealed carbonaceous components in both the ejecta and fireball layer samples from the U.S. locations. The acid-resistant residue of the fireball layer from Raton Pass, New Mexico, released 3.3% C in an experiment from 200° to 1200°C, with 77% of this coming from a single release between 425° and 575°C. The C isotopic composition ($\delta^{13}C$) of this release varied between –17‰ and –23‰, indicative of multiple components. The ejecta layer residue from this site yielded 1.5% C in a similar experiment. Of the C released, 83% was in a single pulse from 400° to 550°C. The $\delta^{13}C$ varied from –18‰ to –22‰, again indicating multiple components with values similar to those from the fireball layer. Similar results were obtained using the same experiments on acid-resistant residues from the Clear Creek North and Berwind Canyon localities in Colorado.

Initial TEM observations indicate that the carbonaceous component in the ejecta layers is indeed diamond. The ejecta layer from the Clear Creek North locality revealed diamonds up to 20 nm in size, with d-spacings corresponding to cubic diamond.

In the Mexican localities, the equivalents of the ejecta and fireball layers are the spherule bed and Ir-rich layer. We have studied acid-resistant residues of samples from both of these layers. The Ir-rich layer from Mimbral contained diamond aggregates up to 30 mm in size [3], and the residue of the spherule bed from Peñon contained one grain identified as diamond with the TEM. Although this is preliminary work, the indication is that both the ejecta and fireball layers from K/T localities in the Western interior of the U.S. and the equivalent layers from Mimbral and Peñon in Mexico contain diamonds. These diamonds are presumably impact-produced by shock and/or by condensation from the fireball, in a process similar to chemical vapor deposition. The C isotopic compositions of the diamonds indicate a mixed C source.

References: [1] Carlisle D. B. and Braman D. R. (1991) *Nature, 352,* 709. [2] Gilmour I. et al. (1992) *Science, 258,* 1624–1626. [3] Hough R. M. et al. (1997) *Geology,* in preparation.

SUDBURY IMPACT EVENT: CRATERING MECHANICS AND THERMAL HISTORY. B. A. Ivanov[1] and A. Deutsch[2], [1]Institute for Dynamics of Geospheres, Russian Academy of Sciences, Moscow 117939, Russia (baivanov@glasnet.ru), [2]Institut für Planetologie, Universität Münster, D-48149 Münster, Germany (deutsca@uni-muenster.de).

Summary: The Sudbury Igneous Complex (SIC) is interpreted as the solidified impact melt body of the 1.850-Ga Sudbury impact structure. We present the first results of the numerical modeling of the impact cratering process and the thermal evolution model for this ~250-km multiring structure. To produce the estimated volume (~8000 km^3) of the impact melt, one needs to have a spherical projectile of 14 km in diameter at impact velocity of 20 km s^{-1}. Cooling of the impact melt sheet from the initial temperature of 2000K below liquidus at 1450K lasted about 100 k.y.; below the solidus at 1300K, cooling lasted about 350 k.y.

Impact Modeling: We simulated numerically the vertical impact of a stony (granite) body at the granite target at the impact velocity of 20 km s^{-1}. The SALE hydrocode [1] was modified to handle multimaterial problems with an elastic-plastic description for solids. The projectile diameter varied from 10 to 15 km for a cylinder with a height equal to its radius. To fit the volume of melt (8000 km^3) estimated by Grieve and Cintala [2], one needs to assume a Sudbury projectile of 12.5 km in diameter (or an equivalent spherical projectile of 14 km diameter). Depending on the projectile size, the transient cavity reached a depth of 40–50 km and an excavation radius of 50–60 km. The final crater shape and size would strongly depend on the supposed rheology. With an account to the acoustic fluidization [3], the final diameter is estimated at 200–250 km. The depth of the melting zone is estimated at 35 km, which is less than the present crust-mantle boundary at the Sudbury site (40 km according to Braile et al. [4]). The mantle uplift during the transient crater collapse depends on the assumed rheology and varies from 0 to 25 km. Our simulation allows us to estimate the temperature field beneath the melt layer just at the end of the modification stage.

Thermal Modeling: We made simple estimates (one-dimensional implicit numerical code) to evaluate the cooling history of the SIC body. The geometrical constraints of the model are three flat layers: (1) an overburden material with a thickness of 2.5 km, resting on (2) a 2.5-km-thick melted layer, which in turn is underlain by (3) rocks of the lower crust, uplifted above preimpact level according to the aforementioned numerical simulations. The surface boundary conditions of layer (1) are held constant at a temperature of 300K; temperatures within layer (1) range from 300K ("cold breccia") to 850K ("hot suevite"). The melt layer (2) has an initial temperature of 1800–2000K. For layer (3), a constant temperature of 500–800K was assumed (in accordance with numerical simulations described above) from the interface with the SIC down to the "undisturbed" depth. Thermal constants used in our calculations were the same as those used for thermal modeling of the Manicouagan Crater [5].

We obtained the following results for the impact melt layer of the Sudbury Structure: The time span needed for a decrease of the initial temperature below the liquidus point (assumed at 1450K) is about 100 k.y.; below the solidus point (assumed at 1300K), the time span is about 300 k.y. In contrast, this time span is only 1 k.y. for the 200-m-thick melt sheet of the Manicouagan structure [5].

Our result simply reflects the [length]²/[time] scaling. A factor of 2 is assigned as minimum uncertainty to the solidification time of the SIC, due to uncertainties in thermal properties and boundary conditions. Two-dimensional or three-dimensional thermal modeling and convective heat transfer inside the melted body also can modify the numbers; however, the order of magnitude from our simple estimate will remain unchanged.

Conclusion: The combination of hydrocode simulations together with thermal modeling creates a solid basis for comparisons with observational constraints [6].

References: [1] Amsden A. et al. (1980) *LA-8095,* New Mexico, 101 pp. [2] Grieve R. A. F. and Cintala M. J. (1992) *Meteoritics, 27,* 526–538. [3] Melosh H. J. (1989) *Impact Cratering: A Geologic Process,* Oxford Univ., 245 pp. [4] Braile L. W. et al. (1989) *Mem. GSA, 172,* 655–680. [5] Onorato P. L. K. et al. (1978) *JGR, 83,* 2789–2798. [6] Ostermann M. and Deutsch A., this volume.

ARTIFICIAL OZONE-HOLE GENERATION FOLLOWING A LARGE METEOROID IMPACT INTO AN OCEANIC SITE.

B. A. Klumov[1] and I. I. Korobov[2], [1]Institute of Geosphere Dynamics, Leninsky pr, 38/6, Moscow, Russia, [2]Moscow Institute for Physics and Technology, Institutskii pr, 9, Dolgoprundy, Moscow 141700, Russia.

The impact of a large cosmic body into an oceanic site results in the ejecta of a huge amount of ocean water into the upper atmosphere. We investigated the subsequent evolution of the impact-disturbed region in the atmosphere; in addition, we determined time-spatial characteristics and chemical composition of the region.

The mass of the impact-produced ejecta is calculated using a strong-explosion model. It is believed this mass would be distributed in the disk-shaped region in the stratosphere at altitudes determined by the floating of a water vapor. The spatial distribution of the water vapor is determined using the calculation of ejecta processes.

Subsequent evolution of the region is determined by local atmospheric turbulence and zonal wind distribution. The chemical composition is controlled by photochemical processes.

We used a two-dimensional model of the horizontal baroclinic atmosphere based on the Kadomtsev-Petviashvili equations to evaluate the time-space characteristics of the artificial atmospheric spot. To estimate the chemical impact of the ejected water vapor on the stratosphere, we used the advanced stratospheric photochemistry model.

Our results show that the impact of a 1-km body creates a long-living disturbance of the ozone concentration in the stratosphere, with a diameter of approximately a few thousand kilometers. A significant (~50%) depletion of the ozone concentration occurs in the region; the characteristic lifetime of the disturbance is about a few weeks.

LARGE CHEMICAL VAPOR DEPOSITION DIAMOND-LIKE CARBON FORMED BY MULTI-IMPACT REACTIONS.

H. Kobayashi, Y. Miura, and S. Fukuyama, Department of Chemistry and Earth Sciences, Faculty of Science, Yamaguchi University, Yoshida, Yamaguchi 753, Japan.

Introduction: Large diamond crystal is formed by static high pressure in terrestrial deep-seated crust and in synthetic materials. Microdiamond (known as low-pressure diamond) is formed by high-speed bombardments of electron or ion beams or plasma, a process known as Chemical Vapor Deposition (CVD), in a low-pressure atmosphere, but the microarea of beam bombardment is a dynamic high-pressure-by-impact process [1–3].

The main purpose of this study is to analyze large CVD diamond-like C formed by multireactions of impact at the Barringer meteorite crater, U.S.

Origin of Diamond in the Barringer Crater: High-pressure forms of stishovite and coesite silica minerals were found in the meteorite impact crater of Barringer, Arizona. The same high-pressure C of microdiamond was analyzed as cubic and hexagonal diamond-like C material [3].

There are two types of diamond-like C from the Barringer Crater: (1) Iron meteorite contains a black vein with diamond-like C (as exhibited in the Crater Museum), and (2) a black block of mixed Fe and graphite contains Fe veins with diamond-like C [1]. The second diamond-shaped C type is shocked graphite formed by impact on the crater. This is mainly because the black-graphite block contains the special graphite C (Table 1), including (1) shocked graphite with high density and elements of Si and Ca and (2) main sources of Si and Ca from target rocks of sandstone and limestone on the Earth [1,2,4], not from asteroids [3].

Impact Origin from Mixed Compositions: An impact origin for the graphite block is confirmed by the fact that (1) the Fe-metallic vein contains Si from sandstone and Ca from limestone on the target rock of the crater, and (2) the large graphite block contains fine Fe-metal mixed with Si or Ca (Table 1). These analytical data indicate that the graphite block with CVD diamond-like C formed by impact on the target rocks of the Earth.

Extraction of Cubo-Octahedron of Diamond: The Fe-metallic vein mixed with Si and Ca contains graphite C of hexagonal and cubic-diamond shape, considered to be two types of diamonds [3]. However, the diamond-like C grains were extracted by $6NHNO_3$ as cubo-octahedron [1], previously misinterpreted as two types of diamond shapes [3].

The composition of grains of cubo-octahedron shape was confirmed by high-sensitive energy-dispersive X-ray scanning electron microscopy (ASEM) as C-rich material [1] in this study.

Plasma-Beam Formation of CVD Diamond: Extracted C is considered to be the same shape as CVD diamond formed by electron-, ion-, or plasma-beam bombardments. Plasma conditions are

TABLE 1. AEM analytical data of graphite materials in the Barringer meteorite crater [1,2,4].

Oxides/ element*	Kamacite in meteorite of vein	Iron metals (a) in center	Iron metals (b) in major vein of graphite block	Iron metals (c) in rim
Fe	92.5	81.5	87.7	80.2
Ni	7.5	6.0	6.8	3.4
SiO2	9.5	5.5	14.2	
CaO	2.0	0.0	2.2	

Iron metals (a), (b), and (c) are mixed with iron meteorite and target rocks of ss and ls.

* Atomic or weight percent.

believed to be produced by a meteoritic impact event around the crater. In fact, vapor plumes of large size are formed in the center of impact site as plasma conditions. Similar plasma conditions are confirmed even in a small-size impact [1,2,4].

Multireactions of Graphite Block Formation: A large size of CVD diamond-like C with cubo-octahedron is 50–70 μm in size,which is a few times larger than normal CVD diamond. A source of C is believed to be the limestone target rock [1,2,4]. Conclusions on the large size and source of C require a formation model of multireactions of C within the vapor plume of impact site. The present conclusion of mixed growth as a multireaction within the crater is confirmed in artificial impact crater experiments with an Al metallic target (with ~3-cm-diameter crater and wormy multireacted grains).

References: [1] Miura Y. et al. (1995) *Shock Waves Proc., 19,* 399–404. [2] Miura Y. (1991) *Shock Waves, 1,* 35–41. [3] Brett R. and Higgins G. T. (1967) *Science, 156,* 819–820. [4] Miura Y. (1995) *Shock Wave Proc., 19,* 405–410.

THE JURASSIC-CRETACEOUS BOUNDARY IMPACT EVENT: THE MOROKWENG IMPACT STRUCTURE, SOUTH AFRICA.

C. Koeberl[1], W. U. Reimold[2], and R. A. Armstrong[3], [1]Institute of Geochemistry, University of Vienna, Althanstrasse 14, A-1090 Vienna, Austria, [2]Department of Geology, University of the Witwatersrand, Johannesburg 2050, South Africa, [3]Research School of Earth Sciences, Australian National University, Canberra, ACT 0200, Australia.

Considering that relatively few impact structures are known in Africa, it was of interest when preliminary geophysical, petrological, and geochemical investigations indicated that a large, near-circular magnetic and gravity anomaly in the area around Morokweng, Northwest Province, South Africa (Fig. 1), may represent an impact structure [1,2]. The subsurface structure, centered at 23°32'E, 26°31'S, shows a well-defined circular magnetic anomaly measuring ~70 km in diameter. Refined processing of the gravity and aeromagnetic data indicate the presence of a much larger circular structure with a diameter of ~340 km [3]. Three drill cores were obtained from near the center of the structure [2,4]; these showed the presence of melt rocks with high contents of siderophile elements. We found abundant opaque minerals in the Morokweng melt rock, including various types of magnetite, Cr- and Ni-rich spinel, ilmenite and rutile (often intergrown), monazite, chalcocite, and trevorite. Zircon and baddeleyite (evidence for a high-temperature origin) are also common. Remnants of PDFs are present in various unannealed clasts. The impact melt rock samples are remarkably uniform in composition. High contents of the siderophile elements were measured in the melt rock samples: up to 440 ppm of Cr, 50 ppm of Co, 780 ppm of Ni, and 32 ppb of Ir, with relatively little variation (less than a factor of 2). After correction for the indigenous component, a near-chondritic abundance range remains. PGE contents show a flat, near-chondritic pattern [4], indicating the presence of about 2–5% of a chondritic component. To determine the age of this structure, zircons were extracted from a large melt-rock sample. The zircons were analyzed for their U-Th-Pb isotopic compositions on the ion microprobe SHRIMP I at the Research School of Earth Sciences, Australian National University. Using standard statistical data analysis, a $^{206}Pb/^{238}U$ age of 146.2 ± 1.5 Ma was determined [5]. In addition, an independent $^{208}Pb/^{232}Th$ age of 144.7 ± 1.9 Ma was calculated from this data set [5] (Fig. 2). This age is indistinguishable from the age of the Jurassic-Cretaceous (J/K) boundary, which is placed at the base of the Berriasian Stage at 145 Ma [cf. 5]. This result, which is supported by other recent measurements [6], indicates that large-scale impact events may have influenced the geological and biological evolution of the Earth to a larger degree than was previously assumed.

Fig. 1. The estimated position of the Morokweng impact structure in a schematic paleogeographic map (TME program, Sageware Corp.).

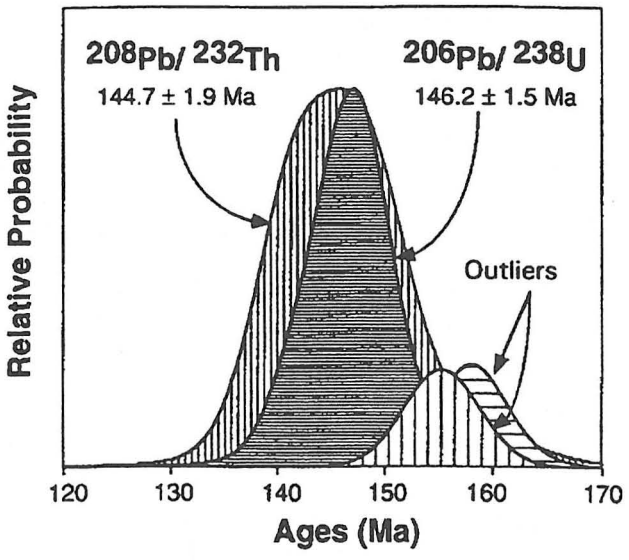

Fig. 2. Relative probability plots of age data for zircons from Morokweng impact melt rock. Errors shown are within a 95% confidence limit.

Acknowledgments: We are grateful to the Council of Geoscience, Pretoria, South Africa, for access to the Morokweng drill cores. Supported by the Austrian Fonds zur Förderung der wissenschaftlichen Forschung (to C.K.) and the Foundation for Research Development, South Africa (to W.U.R.).

References: [1] Corner B. (1994) *Abstr. Proterozoic Crustal and Metallogenic Evolution Conf.*, 9. [2] Andreoli M. A. G. et al. (1995) *Abstr. Centennial Geocongress,* 541. [3] Corner B. et al. (1997) *EPSL, 146,* 351. [4] Koeberl C. et al. (1997) *LPS XXVIII,* 741. [5] Koeberl C. et al. (1997) *Geology, 25,* in press. [6] Hart R. J. et al., *EPSL, 147,* 25.

DEEP ANATOMY, COMPOSITION, AND EVOLUTION OF LARGE METEORITE IMPACTS: SCIENTIFIC DRILLING DATA ON THE PUCHEZH-KATUNKI ASTROBLEME, RUSSIA. A. A. Kremenetsky and N. A. Yushko, Institute of Mineralogy, Geochemistry and Crystal Chemistry of Rare Elements, 15 Veresaeva Street, Moscow 121357, Russia.

The Puchezh-Katunki astrobleme (diameter = 80 km) lies in the eastern part of the Russian Platform. In the center of the astrobleme, a 5354-m-deep scientific borehole has been drilled. A complete sequence of an impact explosive structure is disclosed here. Two structural stages are specified within the sequence: (1) Precambrian basement (550–5354 m) and (2) the so-called Coptogeneous Complex, consisting of allogenic breccia and melt impactites (impact melt rocks) that carry diamonds. In deep parts of the structure (3500–5354 m), the basement rocks are weakly altered. At higher levels (1600–3500 m), the rocks are plasticized by the impact compression and brecciated as a result of relaxation. Higher up (500–1600 m), in the relaxation fissures, thick (up to 30-m) IMR sheets occur. The thickness of the Coptogeneous Complex, which in the studied drillhole occupies an interval of 0–500 m, is smaller in the central rise of the crater (areal extent 40 km^2) and increases in an adjacent trough to 2500 m. From the data obtained from 1650 samples, detailed geological, petrological, and geochemical cross sections of the astrobleme were compiled; peculiarities of mineralogy and chemistry of the preimpact basement rocks and their varieties altered by shock pressure and temperature were established. Besides Pb, K-Ar, and Rb-Sr, isotope studies were conducted with determinations of isotope ratios ($^{87}Sr/^{86}Sr$, $^3He/^4He$, and $^{40}Ar/^{36}Ar$). The following results were obtained: (1) A preimpact age of the basement rocks (2.4 Ga), along with the impact-caused "dating shift" (from 2.4 to 1.6 Ga) and the impact event (0.19 Ga), the latter accompanied by formation of impact melt rocks (IMR), was established; (2) similarity in the I^0_{Sr} ratio in the preimpact basement rocks (0.704 to 0.708) and IMR (0.705 to 0.709) at different levels of the astrobleme sequence proved the *in situ* formation of IMR in an isochemical closed system; and (3) values of I^0_{Sr} ratio in tagamites of the basement (0.707 to 0.709) and in the Coptogeneous Complex (0.711 to 0.713) were significantly different, thus indicating formation of coptogeneous tagamites during the course of the hybride melting of the basement rocks and overlying sediments (I^0_{Sr} from 0.720 to 0.738). The sediments carry the C_{org} required to produce diamonds.

The main features of a new geological and geochemical evolutional model of the impact processes offered for discussion are as follows: (1) *Impact compression*: instanteous duration of hyperpressure prevented melting of the basement rocks and migration of produced fluids; alteration of solid minerals occurred at a relatively isochemical regime, with local diffusional redistribution of K, Na, Fe, Mg, and Al; (2) *shock decompression*: sharply decreased temperature after the shock wave had passed, along with uneven heating of the basement rocks, caused a selective melting of these rocks, with concurrent enrichment of IMR in K, Na, Pb, Fe, Mg, Cr, V, Ni, Sc, Co, Cu, Mn, Ta, and TR. At greater depth, quasi-isochemical melts were formed. Along with decreasing pressure and related overheating, a retrograde boiling had occurred here; this was accompanied by a separation of the gaseous (vapor) fluids rich in K, Na, Li, Rb, Sr, Mo, B, and Hg, whereas the melt had been enriched in Ti, Nb, Zr, and Fe; and (3) *modification* (i.e., relaxation and formation of the central rise): hydrothermal alteration of the basement rocks and the Coptogeneous Complex caused by the gas and vapor fluid attack; whereas the latter produced a smectite-zeolite assemblage in the upper levels of the sequence, an illite-chlorite assemblage was formed in the deep levels; a possibility existed for deposition of potentially productive Mo, Be, Ni, Co, Zn, B, In, and V accumulations.

Acknowledgments: This work was financially supported by RFBR (Project 95-05-14802).

STRUCTURE AND KINEMATICS OF A COMPLEX CRATER: UPHEAVAL DOME, SOUTHEAST UTAH. B. J. Kriens[1], K. E. Herkenhoff[2], and E. M. Shoemaker[3], [1]Department of Earth Sciences, California State University–Dominguez Hills, Carson CA 90747, USA (bkriens@dhvx20.csudh.edu), [2]Mail Stop 183-501, Jet Propulsion Laboratory, Pasadena CA 91109, USA (keh@jplsc8.span.nasa.gov), [3]Branch of Astrogeology, U.S. Geological Survey, Flagstaff AZ 86001, USA (gshoemaker@astrog.span.nasa.gov).

Two vastly different phenomena, extraterrestrial impact and salt diapirism, have been proposed for the origin of Upheaval Dome. Upheaval Dome is a ~2.5-km-diameter structural dome surrounded by a 5-km-diameter ring structural depression, which is in turn flanked by extensive, nearly flat-lying Colorado Plateau strata. Seismic refraction data [1] and geologic mapping indicate that the dome originated by the collapse of a transient cavity formed by impact; data also show that rising salt has had a negligible influence on dome development. Evidence for this includes several factors: (1) a rare lag deposit of impactite is present; (2) fan-tailed fracture surfaces (shatter surfaces) and a few shattercones are present; (3) the top of the underlying salt horizon is at least 500 m below the center of the dome, with no exposures of salt in the dome to support the possibility that a salt diapir has ascended through it; (4) sedimentary strata in the center are significantly imbricated by top-to-the-center thrust faulting and are complexly folded; (5) top-to-the-center low-angle normal faults are found at the perimeter of the structure; and (6) clastic dikes are widespread. The scarcity of melt rocks and shock fabrics is attributed to approximately 0.5 km of erosion; the structures of the dome reflect processes of complex crater development at a depth of about 0.5 km below the crater floor.

Based on mapping and kinematic analysis, we infer that the dome formed mainly by centerward motion of rock units along listric faults. Outcrop-scale folding and upturning of beds, especially common in the center, largely resulted from this motion. In addition, we have

detected some centerward motion of fault-bounded wedges resulting from displacements on subhorizontal faults that conjoin and die out within horizontal bedding in the perimeter of the structure. Collectively, the observed deformation accounts for the creation of both the central uplift and the encircling ring syncline.

References: [1] Louie J. N. et al. (1995) *EOS Trans. AGU, 76,* 337.

CAN IMPACT-GENERATED MELTS HAVE MANTLE CONTRIBUTIONS?: GEOCHEMICAL EVIDENCE FROM THE SUDBURY IGNEOUS COMPLEX. P. C. Lightfoot[1], R. R. Keays[2], and W. Doherty[3], [1]Department of Earth Sciences, Laurentian University, Sudbury, Ontario P3E 2C6, Canada, [2]Mineral Exploration Research Centre, Laurentian University, Sudbury, Ontario P3E 2C6, Canada, [3]Geological Survey of Canada, 501 Booth Street, Ottawa K1A OE8, Canada.

The ~8000-km^3, 1.85-Ga Sudbury Igneous Complex (SIC) and its giant Ni-Cu-PGE sulfide deposits are widely accepted as having been a consequence of the impact of a large meteorite close to the margin of the Superior Province and the Southern Province of the Canadian Shield. Models have variously ascribed the formation of the SIC and its giant Cu-Ni-PGE sulfide deposits to processes ranging from *in situ* melt sheet generation triggered by the impact event to derivation from a highly contaminated mantle-derived melt. We use an extensive new geochemical dataset, including a detailed chemical stratigraphy through the main part of the SIC, to constrain petrological models relating the different rock types that constitute the SIC. We show that the Main Mass Felsic Norite, Transition Zone Quartz Gabbro (TZQG), and Granophyre have similar ratios of highly incompatible trace elements (e.g., La/Sm = 4.5–7, La/Nb = 2.8–4.2, Th/Zr = 0.04–0.05). The fact that the three members of the Main Mass have very similar highly incompatible trace element ratios is regarded as strong evidence that they crystallized from the same or very similar magmas. Variations in major-, minor-, and trace-element chemistry are consistent with the crystallization and differentiation of a similar magma type that was derived largely (>80%) from the upper crust. The geochemical variations also suggest that crystallization of the Main Mass proceeded simultaneously both from its base and top; the TZQG may represent the mixing zone of the two residual magmas. (Cooling of the top of the SIC is believed to have been accelerated by heat loss to convecting fluids from an overlying water cover.)

Although there is no direct evidence for a mantle contribution, a number of features of the SIC require a small (<20%) contribution from a primitive component: (1) 1.85-Ga mafic-ultramafic fragments of olivine melanorite, websterite, wehrlite, and pyroxenite that occur as "xenoliths" in the Sublayer of the SIC; (2) the dominant pyroxene over the lowermost 500 m of the Main Mass that is cumulus orthopyroxene; (3) Fo_{68-87} olivines with 450–3700 ppm Ni and chrome spinels in the matrix and inclusions; and (4) the large inventory of S, Ni, Cu, Co, and Pt group elements (PGE), which, for example, require a parental magma with >250 ppm Cu and >250 ppm. Although Re-Os and Pb-Pb isotope systematics of the sulfide mineralization are consistent with a crustal source for these metals, there is no crustal reservoir around the SIC that has sufficient Ni, Cu, Co, S, or PGE to account for the mineralization. We suggest that this primitive component was provided by picritic magmas that migrated from the mantle through the fracture system generated by the impact shortly after formation of the melt sheet; on entering the melt sheet, the picritic magmas mixed vigorously with the crustal melt to form a hybrid melt, which subsequently underwent solidification and fractionation as described above. Mixing of the picritic melt with the crustal melt prompted formation of magmatic sulfides that sank through the magma column, depleting the melt in Ni, Cu, and PGE due to the marked compositional shift. The "ultramafic" xenoliths may have formed from predominantly picritic melts that had not been as thoroughly mixed with the crustal melt as other mantle-derived picritic melts.

GEOLOGICAL AND GEOCHEMICAL RELATIONSHIPS BETWEEN THE CONTACT SUBLAYER, OFFSETS, AND MAIN MASS OF THE SUDBURY IGNEOUS COMPLEX. P. C. Lightfoot[1], R. R. Keays[2], G. G. Morrison[1], and A. Bite[1], [1]INCO Exploration, Highway 17 West, Engineering Building, Copper Cliff, Ontario P0M 1N0, Canada, [2]Mineral Exploration Research Centre, Laurentian University, Sudbury, Ontario P3E 2C6, Canada.

Many of the giant Ni-Cu-PGE sulfide deposits of the Sudbury Igneous Complex (SIC) are associated with a discontinuous unit at the base of the Main Mass known as the Sublayer; the remainder are associated with Offset (Quartz Diorite) Dikes. The Sublayer consists of two fragment-rich members: (1) a metamorphic-textured Footwall Breccia and (2) an igneous-textured Contact Sublayer. The Contact Sublayer occurs as a thick unit in depressions at the base of the SIC, termed embayments, and contains a range of inclusion types, such as diabase, melanorite, olivine melanorite, pyroxenite, wehrlite, and dunite. The Igneous Textured Sublayer Matrix (ITSM) is geochemically distinct from the Main Mass norites. For example, the ITSM in the Whistle Mine has ratios of La/Sm = 3.8, La/Nb = 5.0, and Th/Zr = 0.02, whereas the Main Mass norites, quartz gabbros, and granophyres have ratios of 4.5–7, 2.8–4.2, and 0.04–0.05 respectively. The homogeneous composition of the ITSM at Whistle Mine can be modeled with small amounts of assimilation of local country rock granitoids (~10%), large degrees of assimilation of diabase inclusions not derived from the local country rocks (~70%), and small contributions from the Main Mass magma type (~20% mafic norite). However, there are significant differences in the composition of ITSM between different embayments that may reflect the degree of digestion of fragments of different composition. The melanorite inclusions in the Sublayer at Whistle Mine and the ITSM have essentially similar ratios of the incompatible trace elements, but they have similar high incompatible-element concentrations (e.g., olivine melanorites have 20–65 ppm Ce in rocks with 15–21 wt% MgO), 1–10% interstitial sulfide, up to 0.5% apatite, 1–15% biotite, and 1.85-Ga zircon and baddeleyite. The mafic-ultramafic inclusions are believed to be the broken-up remnants of an earlier cumulate formed at depth from a Main Mass magma. It is believed that their trace-element geochemistry is controlled by accessory minerals, such as apatite, zircon, and baddeleyite, that formed from late magmatic fluids.

The Offset Dikes occur both radially and concentrically to the SIC. The Offset Dike quartz diorites share many similar geochemical traits to the Main Mass. For example, the Parkin Offset Dike has La/Sm, La/Nb, and Th/Zr ratios of 6.3, 4.5, and 0.05. The Offset

Dikes have compositions intermediate between the felsic norite and the granophyre, and therefore crystallized from the same magma type; arguably, the unmineralized quartz diorites provide the best possible estimate of the original magma from which the SIC crystallized. In detail, there are subtle variations in composition within and between Offset Dikes, with the largest difference being between North and South Range Offsets. North Range Offset Dikes cut Archaean granitoids and gneisses and have low TiO_2 and elevated Sr, La/Yb, La/Sm, and Gd/Yb, whereas South Range Dikes cut Early Proterozoic sediments, mafic volcanics, and intrusions and have high TiO_2 and low Sr, La/Yb, Gd/Yb, La/Sm. These differences may be caused by the assimilation of different country rocks during emplacement of the dike. Interestingly, embayment-related leucocratic norites from the "funnel" of the Whistle Mine embayment, where the Whistle embayment becomes the Whistle Offset, have La/Sm (6.2), La/Nb (5.0), and Th/Zr (0.02) ratios that are similar to the Main Mass and Offset Dikes ratios. Such rocks may represent the link between the ITSM of the sublayers and the quartz diorites of the Offsets.

CRATERING ON TITAN: A PRE-CASSINI PERSPECTIVE.

R. D. Lorenz, Lunar and Planetary Laboratory, University of Arizona, Tucson AZ 85721-0092, USA (rlorenz@lpl.arizona.edu).

The NASA-ESA Cassini mission, comprising a formidably instrumented orbiter and parachute-borne probe to be launched this October, promises to reveal a crater population on Titan that has been heretofore hidden by atmospheric haze. This population on the largest remaining unexplored surface in the solar system will be invaluable in comparative planetological studies, since it introduces evidence of the atmospheric effects of cratering on an icy satellite. Here (and at more length, in *Planetary and Space Science*, in press), I highlight some impact features we may hope to find and could devote some modeling effort toward.

Titan in a Nutshell: Radius = 2575 km. Density = 1880 kgm^{-3}, consistent with rock-ice composition. Surface pressure = 1.5 bar. Surface gravity = 1.35 ms^{-2}. Atmosphere ~94% N_2, 6% CH_4. Surface temperature = 94K. Tropopause temperature = 70K at 40 km alt. Probable liquid hydrocarbon deposits exist on or near the surface.

Titan is comparable to Callisto and Ganymede for strength/gravity, Mars/Earth/Venus for atmospheric interaction, and Hyperion, Rhea, and Iapetus for impactor distribution.

Geographical Distribution: Crater Chains and Clusters: The leading/trailing asymmetry of crater density from heliocentric impactors is expected to be ~5–6, in the absence of resurfacing. Any Saturnocentric impactor population is likely to alter this. In particular the impact disruption of Hyperion is noted; because of the 3:4 orbital resonance with Titan, fragments from the proto-Hyperion breakup would have rapidly accreted onto Titan. Titan's resurfacing history is of course unknown.

The disruption of impactors into fragments that individually create small craters is expected to occur. A crude estimate suggests a maximum separation of about 2 km (compared with 4 km on Venus, or 0.5 km on Earth).

Crater chains are unlikely on Titan, since impactors must pass close enough to Saturn to be tidally disrupted; as a result, they would suffer aerodynamic disruption.

Atmosphere: Shielding, Splotches, and Parabolae: Crater counting on adjacent satellites gives densities of ~200 per $10^6 km^2$ for 20-km-diameter craters. However, the presence of a thick atmosphere leads to atmospheric shielding, depleting the relative abundance of small craters. This has been evaluated by models, and the relative abundance of small craters may be due to a diagnostic atmospheric collapse.

A number of radar-dark "splotches" have been detected on Venus; these have been attributed to the interaction of the surface with the atmospheric shockwave produced by the Tunguska-like explosion of a bolide in the atmosphere. Simple analogy suggests that similar features might occur on Titan, but the shocked mass density (which controls the momentum coupling between the surface and the shockwave) of Titan's cold N_2 atmosphere is ~20× smaller than that of Venus's hot CO_2 atmosphere. Unless ice is much more easily turned to rubble than is rock, such features seem less probable on Titan.

When the energy deposited by an impact forms a fireball with an equilibrate greater than one scale height, the fireball expands upward and can distribute ejecta on ballistic exoatmospheric trajectories. On Venus this process is believed to be responsible for the parabolic features; the interaction of various-sized particles falling through the atmosphere with the zonal wind field winnows the particles to form a parabolic deposit. Although such a process is possible on Titan, the large scale height at higher altitudes would make it more difficult.

Morphology, Ejecta, Crater Lakes, and Hydroblemes: Comparison with craters on other icy satellites suggests that craters on Titan will be fairly shallow (depth/diameter ~0.1) and craters greater than 10 km in diameter will have central peaks or domed bases, perhaps with central pits.

The formation of ejecta blankets may involve the atmosphere in a significant way, both by restraining the expansion of the ejecta cloud and by influencing the thermal history of the ejecta. Compared with Venus, Titan's atmosphere will chill an impact melt somewhat quickly, so the long ejecta flows seen on Venus seem less likely; detailed modeling needs to be performed to determine the impact melt production.

Crater topography on Titan may be highlighted by the influence of liquids forming crater lakes. Craters with central peaks will typically form ring-shaped lakes, although horseshoe-shaped lakes may be common; domed craters with central pits may even form bullseye lakes with islands with central ponds. If liquids have covered a substantial part of Titan's surface for a substantial period, hydroblemes and tsunami deposits may be common.

Acknowledgments: This work is supported by the Cassini project.

ORIGINAL SIZE AND SHAPE OF THE SUDBURY STRUCTURE.

P. D. Lowman Jr., Mail Code 921, Goddard Space Flight Center, Greenbelt MD 20771, USA.

This paper presents new evidence bearing on the original size and shape of the Sudbury impact structure. Current opinion is almost unanimous that the structure is a multiring basin with an original diameter of ~200 km and a circular shape that has since been shortened in a northwest-southeast direction by Penokean deformation. Evidence for this interpretation, collected chiefly from north

of the Sudbury Igneous Complex (SIC), includes supposed outer rings on Landsat imagery, distant occurrences of "Sudbury breccia" (generally defined as pseudotachylite), shatter cone occurrences, and outliers of Huronian sedimentary rock thought to be down-faulted rings [1]. New data from imaging radar and field work north of the SIC, however, contradict this evidence.

Radar imagery shows no sign of the supposed outer rings mapped by earlier workers on Landsat images. The most prominent ring [2] has been found to be a chance alignment of two independent fracture sets. Radar imagery from the CCRS Convair 580, with look direction almost normal to the north rim of the SIC, shows no evidence of rings despite strong look-azimuth highlighting.

Radar imagery [3] has shown many unmapped diabase dikes north of the SIC. Several exposures of supposed Sudbury breccia are associated with these dikes or with Nipissing diabase intrusions, in some cases actually inside the dikes or directly continuous with them. They appear to be igneous intrusion breccias with no relation to impact. Shock-wave interaction at lithologic contacts cannot be invoked for most of these, because they are part of a northwest-trending swarm cutting the SIC in the North Range, and hence too young for an impact origin. Similar diabase-related breccias and pseudotachylite-like veins have been found far outside the Sudbury area between Chapleau and Thessalon.

Shatter cones north of the SIC are few and poorly developed, perhaps due to the coarse-grained Footwall rock, and cannot be considered a continuous zone analogous to their occurrence on the South Range in Huronian rocks. Supposed down-faulted outliers of Huronian rocks north of the SIC show no consistent relation to faulting, and the Huronian/Archean contact is locally erosional [4].

Radar imagery and field-checking confirm Rousell's [5] conclusion that the North Range has undergone little or no Penokean deformation. This implies that the plan view outline of the crater (floor of the SIC) is original. Extrapolation of the North Range as part of a circular arc leads to an impossibly great diameter. It is concluded that although Penokean deformation largely accounts for the structure's shape, the original crater was not circular and was much smaller than 200 km across.

References: [1] Grieve R. A. F. et al. (1991) *JGR, 96,* 22753–22764. [2] Dressler B. O. (1984) in *Ontario Geological Survey Spec. Vol., 1.* [3] Lowman P. D. Jr. (1991) *Can. J. Remote Sensing, 17,* 152–161. [4] Card K. D. and Innes D. G. (1981) *Ontario Geological Survey Rept.,* 206. [5] Rousell D. H. (1984) in *Ontario Geological Survey Spec. Vol., 1.*

THE MYSTERY OF THE 536 A.D. DUST VEIL EVENT: WAS IT A COMETARY OR METEORITIC IMPACT? A. A. Mardon, Antarctic Institute of Canada, #16, 10324-119 Street, Edmonton, Alberta T5K 1Z6, Canada.

Around 536 A.D., famine, frost, and darkness were recorded in Irish and Chinese historical documents. The purpose of this article is to identify a possible cause (i.e., cometary or meteoritic impact) of the dust veil. The cause of the 536 A.D. atmospheric changes can be examined through dendrochronology, Greenland ice cores, and historical records. First, dendrochronology, the study of the growth of tree rings, is useful. By measuring the growth rate, we can deduce the atmospheric environment of a certain period in time. We will concentrate on the tree rings of the Irish oak because of the historical evidence. The dendrochronology of the Irish oak shows that the narrowest rings were made in 540–542 A.D. The stunted growth probably was caused by poor temperature and environment. Second, we will examine the Greenland Dve-3 core to determine whether the poor growth was triggered by volcanic activity. The ice core shows an acid layer of volcanic activity. The acid layer from the volcanos in the Greenland core moved from 540 ± 10 A.D. to 516 ± 4 A.D., indicating that the hypothesis of volcanic activities on Earth that brought about the famine in 536 A.D. is not substantiated. Third, Irish history records that the "dust veil" and "running stars" were shining for 20 days and that there were many earthquakes. Both in China and Byzantium in 530 A.D., it was recorded that Halley's comet continued to shine for 20 days. In both China and Europe, black clouds, earthquakes, crop failures, frost, and dust veils were recorded. In China, it was recorded that "dragons" fought in the ponds and damaged trees. The Chinese thought the comet was connected to the fall of the dynasty; the poor political and economic conditions were more likely caused by power struggles between the states, however, and the poor atmospheric environment compounded the problems. Based on historical documents, it can be concluded that a comet or bolide is a possible cause of the dust veil event. The most plausible hypothesis, up until now, has been that a comet or meteorite hit the Earth. This is because the hypothesis of a volcanic dust veil contradicts the evidence of the acid layer in the ice core. However, if a bolide struck the Earth, it would have brought about reduced sunlight, atmospheric changes, failure of crops, plagues, and earthquakes. Thus, we may have a clue to the cause of the atmospheric changes. If a bolide hit the Earth at this point and caused global effects, the threat might be more than expected.

The explosion of Thera in the 15th century B.C. caused the downfall of several civilizations, and the same result would be expected from a meteoritic impact of the extent hypothesized above.

THREE-DIMENSIONAL MODELING OF IMPACTITE BODIES OF THE POPIGAI IMPACT CRATER, RUSSIA. V. L. Masaitis, M. V. Naumov, and M. S. Mashchak, Karpinsky Geological Institute, Sredny prospekt 74, St. Petersburg 199026, Russia (vsg@sovam.com).

Three-dimensional computer modeling of impactite bodies of the Popigai Crater (diameter = 100 km) was carried out on the basis of (1) geological mapping, (2) core study of more than 500 drilling holes, and (3) study of gravitational anomalies. The geological bodies of monomict and polymict breccia, suevites, and tagamites were traced in detail on the local areas of ~50–100 km^2 and to depths of ~0.5–1.5 km.

Three hierarchical groups of objects were simulated: (1) the inner structure of the multiring impact crater; (2) the principal morphostructural elements; and (3) the large complex bodies of impact melt rocks. The principal structural elements of the crater are (1) central depression, (2) annular uplift surrounded by annular trough, and (3) numerous shallow radial troughs on the outer slope of the last.

Both the relief of the true crater bottom and the entire distribution of molten and fragmented masses are characterized by asymmetry; in particular, centers of masses of impactites are displaced southwestward from the impact point. The true crater bottom is un-

even and made up of megablocks of crystalline rocks (parautochton); relative lifting of blocks reaches up to some hundreds of meters.

Lens-like and sheet-like bodies of impactites and breccia fill annular trough and central depression. Their thickness is irregular, especially in the lower part of the sequence. Sheet-like bodies represent complicated combinations of different impact lithologies, mainly tagamites (impact melt rocks) and suevites. The largest sheets (up to 600-m thick) are located on the outer slope of the circular uplift. Commonly, they occupy concentric depressions and are characterized by radial elements of inner structure. Overlapping is typical with displacements of mass centers of geological bodies and their interdigitations. The upper part of the sequence is made of more flat bodies with a less-expressed inner radial structure. The centers of masses of these bodies relative to the lower ones are located nearer to the center of the crater.

The analysis of columns, distribution of masses of certain complicated bodies, their inner structures, and their interactions show that they were formed by the ejection of jets and currents with distinct trajectories and velocities. Irregular relief of the true bottom originated during a modification stage before sedimentation of the ejected material.

Based on unique geological data, three-dimensional models give a real geological basis for reconstructions of large crater dynamics and mechanisms of transportation of melt and fragments at the time of cratering.

DISCOVERY OF IMPACT DIAMONDS AT THE SUDBURY STRUCTURE. V. L. Masaitis[1], G. I. Shafranovsky[1], R. A. F. Grieve[2], F. Langenhorst[3], W. V. Peredery[4], E. L. Balmasov[1], I. G. Fedorova[1], and A. Therriault[2], [1]Karpinsky Geological Institute, St. Petersburg, Russia, [2]Geological Survey of Canada, Ottawa, Canada, [3]Museum für Naturkunde, Berlin, Germany, [4]Peredery Consultants and Associates, Sudbury, Canada.

Impact diamonds were first discovered at the 100-km Popigai structure in Siberia [1]. Since then impact diamonds have been found at Kara and Puchezh-Katunki, Russia, Boltysh, Ilyinets, Ternovka and Zapadnaja, Ukraine, and Ries, Germany [e.g., 2–4, etc.]. Impact diamonds are generally polycrystalline, usually lonsdaleite-bearing, and are regarded as high-pressure C polymorphs of precursor graphite or coal that has been shocked above 35 GPa [5]. More recently, it has been suggested that some of the impact diamonds at the Ries [6], and possibly at Popigai [7], are the result of chemical vapor deposition.

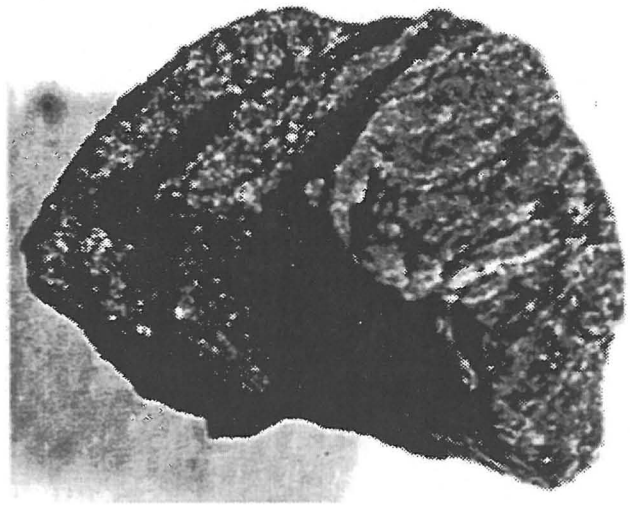

Fig. 1. Black impact diamond aggregate, 0.3 mm in diameter.

As impact diamonds occur most commonly in suevite breccias or rapidly cooled impact melt rocks [5], we concentrated our initial search for impact diamonds at the Sudbury Structure on the Onaping Formation, considered to be a mix of suevite and reworked suevite breccias [8]. Particular attention was paid to the C-bearing Black Onaping, which is also the host of the reported fullerenes at Sudbury [9]. Diamonds were discovered in two of eight samples of the Black Onaping. Other C phases included aggregates and single crystals of graphite, particles of hydrocarbons, and SiC (polytype 6H).

The diamonds are polycrystalline aggregates measuring 0.1–0.6 mm in diameter. They have various colors ranging from white to brown to black. The aggregates are relatively fragile and can be disaggregated by light pressing. The aggregates are relatively amorphous to blocky in morphology (Fig. 1), and their surfaces are corroded and pitted. They contain impurities of graphite, either from incomplete transformation or reversion due to thermal effects during cooling of the 1.8-km-thick Onaping Formation.

X-ray diffraction confirms their polycrystalline nature and indicates the presence of lonsdaleite (up to 20%) in some cases. Transmission electron microscope (TEM) analyses indicate mean grain sizes of individual crystallites in the 50–100-nm range. Selected area electron diffraction patterns reveal preferred orientations of the crystallites, sometimes in 100–200-nm-thick layers, which may reflect the structure of the precursor graphite. Individual diamond crystallites are pervaded by numerous planar defects parallel to {111}, which likely represent stacking faults or microtwins. The microstructural characteristics are equivalent to those of so-called "diamond paramorphs" [5] from other impact structures and indicate a solid-state martensitic transformation of preexisting graphite by shock to form diamond.

The Black Onaping contains 0.06–1.4% C with $\delta^{13}C‰$ –30.2 to –31.1, which suggested to Avermann [8] that the source of C in the Onaping was from biogenetic material deposited into a local euxinic basin created by the Sudbury impact event. While this may be the case for some of the C, the presence of impact diamonds, graphite, SiC, and fullerenes indicate that there was one or more existing sources of C at Sudbury prior to the impact event.

References: [1] Masaitis V. L. et al. (1972) *Zap. Vses. Mineral. Obsh., 101,* 108–112. [2] Gurov E. P. et al. (1985) *Dok. AN Ukrain. SSR, ser. B, 1,* 9–12. [3] Yezersky V. A. (1986) *Zap. Vses. Mineral. Obsh., 115,* 26–33. [4] Rost R. et al. (1978) *Dok. AN USSR, 24,* 695–698. [5] Masaitis V. L. (1995) *Min. Res. Russia,* VSEGEI, 41–43. [6] Hough R. M. et al. (1995) *Nature, 378,* 41–44. [7] Hough et al. (1997) *LPS XXVIII,* 605. [8] Avermann M. (1994) *GSA Spec. Paper 293,* 265–274. [9] Becker L. et al. (1994) *Science, 265,* 642–645.

DIAMONDS ORIGINATED BY METEORITE IMPACT: MAGNETIC AND OTHER PROPERTIES. V. L. Masaitis[1], G. I. Shafranovsky[1], L. J. Pesonen[2], and K.A. Kinnunen[2], [1]Karpinsky

Geological Institute, Sredny Prospect 74, St. Petersburg 199026, Russia (vsg@sovam.com), [2]Geological Survey of Finland, P.O. Box 96, FIN-02151 Espoo, Finland (lauri.pesonen@gsf.fi).

About 25 years ago, the large Popigai impact structure was discovered in the northern part of East Siberia [1]. The structure originated 35 Ma as a result of the collision of an 8-km asteroid with the Earth. The diameter of the complex crater is ~100 km, and it is filled by impactites (melt rocks and strongly shocked target rocks). Small graphite crystals in the metamorphic target rocks (e.g., gneiss) were transformed into diamonds as a result of high pressure exceeding 35 GPa. Such impact diamonds are included in some varieties of the Popigai impactites.

The impact diamonds, because of their microgranular structure, are very tough compared to more fragile kimberlite diamonds and may therefore be used as industrial diamonds. Generally their diameters are approximately <3 mm but may reach 1 cm.

These diamonds inherit the tabular shape and some other pattern of graphite precursors and possess many mineralogical features that are distinct from the single crystal diamonds from kimberlite pipes. The impact diamonds are polycrystalline and are composed of cubic and hexagonal (lonsdaleite) high-pressure phases of C forming structurally arranged microcrystals. The diamonds may be transparent, but more often they are yellow, brown, and black. Some unusual optical features may be observed under the polarizing microscope, including high birefringence and entirely straight extinction. The C isotopic composition of impact diamonds was formed due to polymorphic transition of the precursor.

To further distinguish the impact diamonds from other diamond types (such as kimberlite diamonds, carbonados, other mantle diamonds, and industrial diamonds), we have measured their magnetic properties. The Popigai impact diamonds reveal relatively strong diamagnetic susceptibility ranging from -1000 to -8000×10^{-6} SI. Similar range of susceptibility values are found in kimberlite diamonds. However, one order of magnitude lower value of diamagnetic susceptibility is found in a carbonado sample from Central Africa. In contrast, the industrial diamonds reveal relatively high ferrimagnetic susceptibilities, ranging from 3600 to 5000×10^{-6} SI, because of the common presence of Fe-Ni contaminations in them. Thus, impact diamonds can be distinguished from industrial diamonds (and perhaps from carbonados) on the basis of magnetic susceptibility determinations (the method is rapid and harmless). The Popigai diamonds also reveal measurable Natural Remanent Magnetization (NRM) with an intensity varying from 20 to 260 mAm^{-1}. One specimen showed that the NRM is relatively hard and stable against alternating magnetic field demagnetization treatment. The carriers and origin of this NRM are unknown and will be studied in the future.

At present, impact diamonds of the Popigai type are found in several impact structures in Russia, Ukraine, Germany, and Canada. There are opportunities to find new occurrences of impact diamonds in other impact structures around the world. Good candidates are structures that have diameters greater than ~4 km and in which the target rock contains graphite (or other carbonaceous minerals). Several such structures exist in the Fennoscandian shield, including the Jänisjärvi, the Lappajärvi, the Sääksjärvi, and the Suvasvesi North structures.

References: [1] Masaitis V. L. et al. (1972) *Letters of VMO, 1,* 108–111 (in Russian).

A STUDY OF MINERAL AND ROCK FRAGMENTS AND SHOCK FEATURES IN THE LATE GRANITE BRECCIA AT THE FRASER MINE, NORTH RANGE, SUDBURY STRUCTURE.

K. A. McCormick[1], R. S. James[1], J. S. Fedorowich[2], D. H. Rousell[1], A. M. McDonald[1], and H. L. Gibson[1], [1]Department of Earth Sciences, Laurentian University, Sudbury, Ontario P3E 2C6, Canada, [2]Falconbridge Exploration Limited, P.O. Box 40, Falconbridge, Ontario P0M 1S0, Canada.

The Late Granite Breccia (Footwall Breccia) is a heterolithic breccia, post-Sudbury Breccia in age, that is present in irregularly shaped, discontinuous units, ranging from 0 to ~150 m thick, within the Sudbury Structure [1–3]. It is exposed along the north, west, and east margins of the Sudbury Structure, where it occurs between the footwall Levack Gneiss Complex and the Sudbury Igneous Complex (SIC). The Late Granite Breccia (LGBX) is an important rock unit at Fraser Mine because it is the host for most of the Ni-Cu ores. This breccia is the focus of a detailed Falconbridge-funded study, the object of which is to identify mineralogical and geochemical criteria that indicate proximity to ore zones.

Late Granite Breccia is composed of rock and mineral fragments that vary from <1 mm to tens of meters in size. The mineral fragments are primarily quartz and feldspar, and the bulk chemistry of the breccia matrix varies from dioritic (or tonalitic) to granitic, roughly becoming more granitic toward the contact with the Archean rocks [3]. Rock fragments (derived primarily from the local footwall) consist of felsic, intermediate, and mafic gneisses of the Levack Gneiss complex and fragments from mafic dikes that intrude the Levack complex. Sudbury breccia (pseudotachylite breccia) fragments are generally rare, but can be locally abundant. Ultramafic rock fragments (primarily pyroxenite, but also peridotite) are locally present. Possible sources for the ultramafic fragments include footwall mafic to ultramafic bodies such as those at Strathcona and Fraser Mines, or the "root system" of the Sudbury Igneous Complex. Some pyroxenite fragments may represent migmititic segments of the Levack Gneiss Complex. The percentages of various clast types in the LGBX, determined from one of the drill holes in this study, are 67% gneiss, 9% diabase and gabbro (local dikes), 6.5% pyroxenites, 10% amphibolites, 1.5% Sudbury breccia, and 6% other.

We are also studying the various shock features preserved in quartz, feldspar, pyroxene, biotite, and epidote in the matrix and rock fragments of the LGBX. The shock features we find include (1) as many as three directions of hexagonally or rhombohedrally aligned inclusions in quartz, (2) fractures in feldspar and epidote, (3) bent plagioclase twin lamellae, (4) possible deformation lamellae in feldspar, (5) finely spaced exsolution lamellae in pyroxene, (6) shock decomposition of pyroxene and biotite, and (7) kinked and oxidized biotite. The feldspar and quartz fragments in the LGBX are commonly polygonal in form (inequigranular to seriate) near the footwall. Remnant aligned inclusions in quartz are present in some of the individual polygons. Upward from the footwall, quartz typically becomes porphyrocrystic, and encloses lath-like feldspar. Recrystallization of these phases could have been induced by the overall elevated temperatures of the shocked rocks, the thermal metamorphic effect of the cooling SIC above these breccias, or a regional metamorphic event.

References: [1] Mitchell G. P. and Mutch A. D. (1957) *Sixth Can. Inst. Mining Metal.,* 350–363. [2] Coats C. J. A. and Snajdr P. (1984) *OGS Spec. Vol. 1,* 327–346. [3] Lakomy R. (1990) *Meteoritics, 25,* 195–207.

SLOW IMPACT VAPOR PLUME EXPANSION WITH REALISTIC EQUATIONS OF STATE. H. J. Melosh and E. Pierazzo, Lunar and Planetary Laboratory, University of Arizona, Tucson AZ 85721-0092, USA.

When a meteorite strikes a planetary surface at speeds greater than a few kilometers per second, the kinetic energy of the meteorite is partially converted into heat by irreversible processes. The meteorite and some target material may vaporize after release from high pressure. In the past, a model of vapor-plume expansion based on the expansion of a spherical cloud with a perfect gas equation of state was used to model the expansion of these vaporized gases [1]. A comparison between this model and detailed numerical calculations of the Chicxulub impact [2] shows that the vapor plume in the more realistic numerical model takes far longer than predicted to accelerate out of the crater (more than 30 s, compared to a predicted time of a few seconds). We verified this delayed expansion for an impact of an Al projectile onto an Al target to check that problems of chemical speciation in the vapor plume were not affecting our results. Based on the study of several such computations, we propose that this long delay is due to a combination of the liquid-vapor phase transition in the realistic (ANEOS) equation of state used in this simulation and the nonspherical geometry of the expanding projectile. To examine these effects on plume expansion, we employed a highly simplified equation of state (the Van der Waals equation) that nevertheless exhibits a liquid-vapor phase transition. Using a one-dimensional Lagrangian hydrocode, we investigated the qualitative effect of the phase transition on vapor plume expansion and demonstrated that the expansion is affected by (1) a rapid decompression (compared to a perfect gas) that cools the supercritical rock vapor until it reaches the phase boundary, followed by (2) a very slow phase of acceleration fueled mainly by the latent heat of the two-phase mixture. This slow acceleration occurs mainly because of the extremely low sound speed in the two-phase liquid-vapor system. The final velocity for the realistic equation of state and a perfect gas of the same initial internal energy is nearly the same, but it takes much longer to achieve this velocity with a realistic equation of state. In addition, studies of the expansion of cylinders and planes of hot gas show that the expansion is greatly affected by the geometry of the initial gas cloud. Since an impacting projectile is quickly distorted from its initial spherical shape to a pancake shape lining the growing crater cavity, geometric effects may also strongly affect the expansion rate. Current numerical simulations of impacts do not extend to late enough times to capture correctly the dynamics of this plume expansion; as a result, these simulations greatly underestimate the amount and velocity of ejected debris. This very slow plume expansion may also affect the final phases of melt deposition on top of the crater, leading to a normally graded, apparently air-fall type of deposit consisting of melted rock droplets.

References: [1] Zel'dovich Ya. B. and Raizer Yu. P. (1966) *Physics of Shock Waves and High-Temperature Hydrodynamic Phenomena, Vol. 1,* Academic. [2] Pierazzo E. et al. (1996) *LPS XXVII,* 1029–1030.

INTEGRATED GEOPHYSICAL STUDY OF THE SUDBURY STRUCTURE. B. Milkereit[1] and D. E. Boerner[2], [1]Geophysics, Keil University, 24105 Kiel, Germany (bm@physik.uni-keil.de), [2]Geological Survey of Canada, Ottawa K1A 0Y3, Canada.

The Sudbury Structure is situated at the contact between the Early Proterozoic Huronian supracrustal rocks of the Southern Province and the Archean basement rocks of the Superior Province. Existing evidence strongly supports a meteoritic impact origin. The Sudbury Structure proper contains the Whitewater Group, which infills a central depression, the underlying SIC, and brecciated footwall rocks around the Sudbury Igneous Complex (SIC) [1]. Deducing the original three-dimensional shape of the structure by unraveling the deformation of the southern rim is of critical importance in distinguishing genetic models. The suite of geophysical experiments performed by the Canadian Lithoprobe program in the Sudbury transect area was selected to provide complementary information about the geometrical and lithological properties. Seismic reflection methods were the cornerstone of the transect studies and defined the framework for the geological interpretation of physical rock properties, borehole logging, potential field date, and electromagnetic (EM) data.

Continuous reflections in the relatively pristine North Range data unambiguously delineate lithologies known from surface and drill intersections. The seismic data indicate that the highly reflective footwall complex and mafic units of the North Range continue dipping southward to a depth of ~5 km beneath the center of the basin and ~10 km beneath the Sudbury South Range. The seismic data from the South Range data are dominated by reflections from shear zones, faults, and other tectonized structures in the South Range Shear Zone (SRSZ), a broad zone of pervasive ductile shear [2]. While the overall asymmetry of the Sudbury Structure at depth supports a model of crustal thickening through imbrication [3], important information regarding the collisional style of the Penokean orogeny is preserved in the details of the three-dimensional trace of the SRSZ. Multiple crossings of the highly deformed South Range were conducted to map the shear zone in three dimensions.

Borehole geophysical and laboratory studies confirm significant impedance contrast at contacts between key North Range lithologies. While some local variability is observed, no systematic differences in the acoustic properties exist along strike or between the North Range and South Range. The gravity response of the lithological model derived from interpretation of the North Range seismic data explains fully the observed gravity data and does not require cryptic bodies or footwall topography at depth. Conversely, the magnetic field data from the Sudbury Structure is dominated by small-scale post-tectonic features, such as highly susceptible dikes and alteration zones that are not necessarily apparent in the seismic data. Interpretation of geophysical data in the highly deformed portion of the South Range is difficult since lithological correlations are ambiguous. The electromagnetic survey data, however, indicate the presence of a south-dipping conductive layer, interpreted as the glide plane that mechanically decoupled the South Range deformation from the North Range.

References: Dressler B. O. et al. (1992) *Ontario Geological Survey Guidebook 8,* 33 pp. [2] Shands W. S. and Schwerdtner W. M. (1991) *CJES, 28,* 411–430. [3] Milkereit B. et al. (1992) *Geology, 20,* 807–811.

THE CHICXULUB SEISMIC EXPERIMENT: CRATER MORPHOLOGY. J. Morgan[1] and the Chicxulub Working Group, [1]Department of Geology, Imperial College, London SW7 2BP, UK (j.morgan@ic.ac.uk).

The precise size and morphology of the Chicxulub Crater have been in dispute, with interpretations ranging from a ~170-km-diameter peak-ring crater to a >300-km multiring basin. It has been suggested that this size difference represents an order of magnitude difference in impact energy, with quite different consequences for potential environmental perturbation. The new seismic data indicate why there has been ambiguity in determining the crater's dimensions. The radial extent of the excavated cavity is not much larger than the minimum estimates that have been proposed. However, the outer structure appears to extend further than might be expected on the basis of this small inner cavity, because the crater, at least in the subsurface, appears to possess a multiring basin morphology. Apparently, elements of both models turn out to be substantially correct.

The seismic reflection data presented here reveal a ~155-km-diameter postimpact basin containing a peak ring with a diameter of ~80 km. This is in agreement with previous models suggesting a peak-ring crater with a crater rim at ~180 km. However, outside of this, we observe a major offset in the target stratigraphy at ~195 km diameter; we presume that, immediately after the impact, this fault produced an inward-facing asymmetric scarp. On one line (Chix-C) this outer fault is linked to deep deformation; the fault (or shear zone) offsets the Mesozoic sequence by a few hundred meters in a normal sense, dips at about 35° toward the crater center, cuts through the entire crust, and appears to offset the Moho. The deep deformation, which lies significantly outside the transient cavity and dips subparallel to the inner zone of slumping, may provide the first direct evidence in the deep subsurface for the mechanism of ring formation in a multiring basin.

On one of the reflection profiles, there is a significant offset in the shallow target stratigraphy at ~240 km diameter that appears to be related to the crater. It is a thin-skinned feature, and it is unclear (at this stage of processing) if it is a continuous feature around the crater. The postimpact basin is asymmetric; to the north and northeast of the crater, there is no conspicuous edge to the Tertiary basin, and the Tertiary sequence thickens toward the continental margin. The thick, low-density Tertiary sequence appears to explain the broad gravity low observed in this region.

THE CIRCULAR STRUCTURE AT RAMGARH, INDIA: AN ASTROBLEME(?) V. K. Nayak, Department of Applied Geology, Indian School of Mines, Dhanbad, India.

An isolated, nearly circular structure at Ramgarh (20°20'N, 76°37'30"E), Kota District, Rajasthan, India, is a prominent feature that occurs in sandstone-shale-limestone rocks of the Bhander Group of the Vindhyan Supergroup (mid-upper Proterozoic). The Deccan Basalts of Cretaceous-Eocene age are exposed 50 km south of the Ramgarh structure. The circular structure covers an area of 16 km^2. The outer and inner diameters are 4 km and 2 km respectively; the average radius is about 3 km and the depth-to-diameter ratio is 0.05 [1]. The height of the rim is 200 m, and the highest point is 240 m from the surrounding area. Besides a raised rim, quaquaversal dips, inverted topography, uplifting of rocks in the center, a shatter cone, and shock metamorphic features have been reported, but their true nature has yet to be confirmed.

The circular structure was described in the *Astronaut's Guide to Terrestrial Impact Craters* as an impact crater with a ring of hills and a small central peak from the Landsat image [2]. It is also interesting to note that the shape of the Ramgarh structure is not fully circular but somewhat rectangular and, as such, is analogous to the well-known Meteor Crater in Arizona, U.S.

The origin of this spectacular feature has been a debated subject; from time to time, an overview of various explanations and suggestions is presented. These relate to meteoritic impact, tectonism, volcanic activity, kimberlite and carbonatite intrusions, subsidence, etc. The structure has been suggested to be an impact crater [3–8] and a dome [9–12]. The drilling and geophysical data [13,14] ruled out any possibility of kimberlite, carbonatite, subsidence, and igneous activity as the causative factors in the evolution of the Ramgarh structure. From the evaluation of various explanations, drilling, and geophysical data, it is envisaged that the Ramgarh structure is most likely related to the impact of a meteorite and perhaps impact-induced tectonism.

The origin of this enigmatic structure still remains inconclusive and at present it seems reasonable to consider it as "Ramgarh Astrobleme"(?), until more definitive evidence, such as impact breccia and melt, coesite, stishovite, and other shock-metamorphic characteristics, is recognized and confirmed.

A multidisciplinary approach is proposed to resolve conclusively the origin and age of the Ramgarh astrobleme; in turn, this could lead to further important contributions to the Earth's cratering history.

References: [1] Ahmad N. et al. (1974) Unpublished report, Physical Research Laboratory, Ahmedabad, India. [2] Grieve R. A. F. et al. (1988) *LPI Tech Rpt. 88-03,* 1–89. [3] Crawford A. R. (1972) *Nature, 237,* 96. [4] Balasundaram M. S. and Dube A. (1973) *Nature, 242,* 40. [5] Dietz R. S. and McHone J. (1974) *Meteorites, 2,* 329–333. [6] Rakshit A. M. (1974) Unpublished report, Geol. Surv. India. [7] Khan A. J. (1980) *Geoviews, 7,* 173–179. [8] Nayak V. K. (1984) *Proc. 71st Ind. Sci. Congr.,* 22–23. [9] Sharma J. K. and Singh S. R. (1970) Unpublished report, *Geol. Surv. India.* [10] Gupta S. N. and Prasad B. (1976) *125th Anniversary,* Geol. Surv. India, 11. [11] Ramasamy S. M. (1987) *Rec. Geol. Surv. India, 113(7),* 13–22. [12] Ramasamy S. M. (1988) *Rec. Geol. Surv. India, 114(7–8),* 15–24. [13] Sharma H. S. (1973) *Nature, 242,* 39–40. [14] Vimal K. and Reddy B. V. R. (1984) Unpublished report, Geol. Surv. India.

THE LYCKSELE STRUCTURE, A HUGE RING FORMATION IN NORTHERN SWEDEN: RESULT OF AN IMPACT? D. H. Nisca[1], H. Thunehed[1], L. J. Pesonen[2], and S-Å Elming[1], [1]Division of Applied Geophysics, Luleå University of Technology, S-97187 Luleå, Sweden, [2]Department of Geophysics, Laboratory for Palaeomagnetism, Geological Survey of Finland, P.O. Box 96, FIN-02151 Espoo, Finland.

The current database of impact structures in Fennoscandia reveals 28 proven impact craters of various ages and sizes [1]. Recently, we started to search for large and old impact structures, which may show traces of the impact in their shape or in their rocks and minerals and which can be diagnostically identified through the masking effects of postimpact deformations. Since we are dealing with strongly eroded and often deformed structures, the classical criteria [1] for proving an impact origin are not tenable.

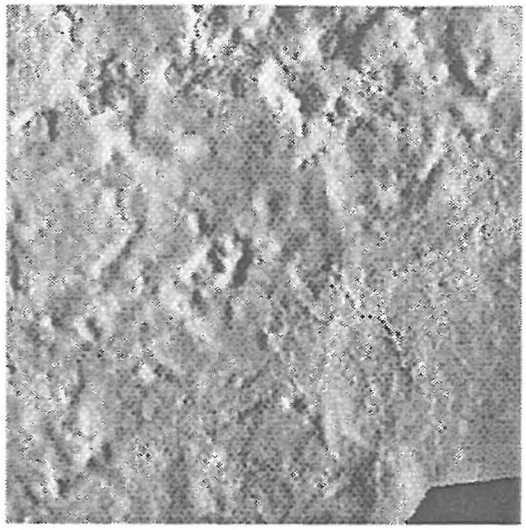

(a)

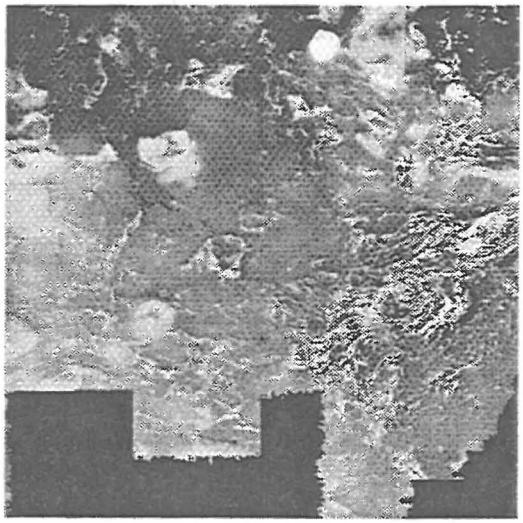

(b)

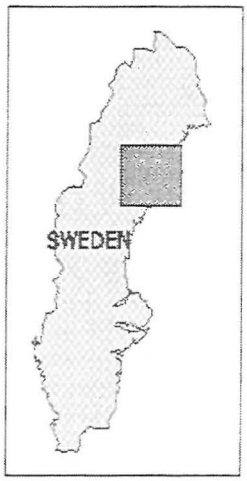

Fig 1. The Lycksele structure seen in **(a)** gravity gradient map and **(b)** in magnetic data.

Through a combined analysis of topography, drainage, gravity, magnetic, and petrophysical data, a circular stru.cture has been identified in northern Sweden (Fig. 1). The structure is characterized by a circular system of faults, arc-shaped contacts between rocks, and a circular distribution of granitic intrusions [2]. The fault zone at the edges is defined from gradients in the gravity data (Fig. 1a), from magnetic data by arc-shaped anomalies (Fig. 1b), and from topographic data by an arc-shaped relief, which is also reflected in the drainage pattern. The zone is characterized by vertical faults that also cut the granitic intrusions at the edge of the formation, and from interpretation of gravity data an uplift of high density rocks (~2850 kgm^{-3}) is indicated in the central part. The age of granites and pegmatites ranges from 1.82 to 1.78 Ga [3]. Therefore, based on age data and on paleomagnetic results of various generations of dikes that cut and are truncated by the structure, the age of the formation lies within 1.80–1.26 Ga. The rocks have not been studied petrologically to see if any traces of shock metamorphism can be found. At present, four models for the origin of the structure are possible: (1) basement doming, (2) meteorite impact, (3) large buried pluton, or (4) fault-bounded block. An impact origin, however, seems most plausible.

References: [1] Pesonen L. J. (1996) *Earth, Moon and Planets, 72,* 377–393. [2] Nisca D. (1996) Ph.D. thesis, Luleå Univ. of Technology. [3] Romer R. and Smeds S.-A. (1994) *Precambrian Res., 67,* 141–158.

CHICXULUB IMPACT EJECTA IN BELIZE. A. Ocampo[1], K. Pope[2], A. Fischer[3], W. Alvarez[4], B. Fouke[4], F. Asaro[5], C. Webster Jr.[6], F. Vega[7], J. Smit[8], A. E. Fritsche[9], P. Claeys[10], M. Rampino[11], and D. King Jr.[12], [1]Mail Stop 183-601, Jet Propulsion Laboratory, California Institute of Technology, 4800 Oak Grove Drive, Pasadena CA 91109, USA, [2]Geo Eco Arc Research, 2222 Foothill Boulevard, Suite E-272, La Canada CA 91011, USA, [3]Department of Earth Sciences, University of Southern California–University Park, Los Angeles CA 90089, USA, [4]Department of Geology and Geophysics, University of California, Berkeley CA 94720, USA, [5]Lawrence Berkeley Laboratory, University of California, Berkeley CA 94720, USA, [6]Geoscience Research Institute, Loma Linda University, Loma Linda CA 92350, USA, [7]Instituto de Geologia, Universita Nacional Autonoma de Mexico, Ciudad Universitaria, Mexico, D.F.; [8]Institute of Earth Sciences, Vrije University, de Boelelaan 1085, 1081 HV Amsterdam, Netherlands, [9]Department of Geological Sciences, California State University, Northridge CA 91330, USA, [10]Museum für Naturkunde, Institut für Mineralogie, D-10115 Berlin, Germany, [11]Department of Earth and Environmental Sciences, New York University, New York NY 10003, USA, [12]Department of Geology, Auburn University, Auburn AL 36849, USA.

Chicxulub ejecta deposits in Belize provide the closest exposures of ejecta to the crater and the only exposures of proximal ejecta deposited in a terrestrial environment. A quarry on Albion Island in northern Belize exposes Late Cretaceous, possibly Maastrichtian, carbonate platform sediments that were folded, eroded, and subaerially weathered prior to the deposition of coarse ejecta from Chicxulub. These ejecta deposits are composed of a basal, ~1-m-thick clay and dolomite Spheroid Bed overlain by a ~15-m-thick coarse Diamictite Bed [1]. Many and perhaps most of the clay spheroids

are altered glass. Many dolomite spheroids have concentric layers and angular cores and are probably of accretionary lapilli origin. A slight Ir concentration (111–152 ppt) was detected in the base of the Spheroid Bed. The Diamictite Bed contains ~10% altered glass, rare shocked quartz, 3–8-m-diameter boulders, and striated and polished cobbles, one with a penetrating rock chip that plastically deformed the cobble. Ejecta deposits extend to the surface at Albion and the maximum thickness in this area is not known.

Ejecta deposits are exposed in several roadside quarries in the Cayo District of central Belize. The Late Cretaceous here is also represented by carbonate platform sediments. The upper surface of the carbonate platform is a highly irregular and extensively recrystallized horizon possibly representing deep karst weathering. Approximately 30 m of diamictite overlies this horizon with a texture similar to the Diamictite Bed at the Albion quarry, but with a more diverse lithology. In three locations the Cayo diamictites contain red clay layers with abundant polished and striated limestone pebbles and cobbles called Pook's Pebbles, several of which have penetrating rock chips and ablated surfaces. We interpret the Albion Spheroid Bed as a deposit from the impact vapor plume and the Albion and Cayo diamictites as the result of a turbulent flow that contained debris derived from the ejecta curtain and local scouring. The polished, striated, and ablated Pook's Pebbles are interpreted as high-altitude ballistic ejecta.

References: [1] Ocampo A. C. et al. (1996) *GSA Spec. Paper 307,* 75–88.

GEOLOGICAL SETTING OF THE MANCHESTER OFFSET DIKE WITHIN THE SOUTH RANGE OF THE SUDBURY IMPACT STRUCTURE. J. P. O'Connor and J. G. Spray, Department of Geology, University of New Brunswick, Fredericton, New Brunswick E3B 5A3, Canada.

The Manchester Offset Dike is located 4–5 km southeast of the Sudbury Igneous Complex (SIC) within the Huronian metasedimentary footwall rocks of the 1.85-Ga Sudbury Impact Structure. The Offset Dike is subconcentric to the SIC and is up to 30 m wide. It strikes discontinuously for at least 10 km, within which occurs a thicker central continuous zone ~5 km in length, and it dips about 60°to the southeast. It is hosted by a zone of Sudbury Breccia (pseudotachylyte) that in part defines the so-called Falcon Fault. The host pseudotachylyte is also discontinuous and up to 350 m thick. Contacts between the pseudotachylyte and the dike are generally sharp. The dike is chilled against the breccia and typically comprises the assemblage quartz + plagioclase + alkali feldspar + amphibole + biotite. Granophyric and myrmekitic intergrowths are particularly common. Clinopyroxene relicts also occur. The dike is a quartz diorite and, although clearly genetically related to the SIC, is more siliceous than many of the other offsets of the Sudbury Structure. This may reflect the effects of assimilating the quartzo-feldspathic wall rocks.

Critical to this study is the original mode of connection between the Manchester Offset and the SIC, since there is no apparent physical attachment between the two at present exposure levels. Field studies indicate that the Offset Dike may have been emplaced from below, via listric faulting initiated during the collapse of the transient cavity sometime after hypervelocity impact.

THE MIDDLE ORDOVICIAN LOCKNE CRATER AS A SMALL-SCALE MODEL FOR IMPACTS AT SEA. J. Ormo, M. Lindstrom, E. Sturkell, and R. Tornberg, Department of Geology and Geochemistry, Stockholm University, S-10691 Stockholm, Sweden (jens.ormo@geo.su.se).

The Lockne Crater is situated in the county of Jamtland in central Sweden. It is one of six known craters from Baltoscandia and North America formed at different water depths in the Middle Ordovician sea. The structure was soon covered by Caledonian overthrusting and was protected from erosion until the Cenozoic. The morphology and lithology of the crater is therefore well preserved.

The water depth at the time of impact was at least 200 m. The target rocks consisted of approximately 80 m of sedimentary rocks covering the crystalline basement. The water and the sediments served as a weak upper layer. The structure is phenomenologically a nested crater. The 7.5-km-wide inner crater is developed in the crystalline basement and surrounded by a shallow, 3-km-wide, outer crater developed in the sedimentary strata and the topmost part of the crystalline rocks [1]. No clear rim has been observed. This was most likely partly developed in the water mass and collapsed moments after the impact. The resurging water was heavily loaded with debris, and the resulting high-density flows eroded deep gullies through the outer crater. The resurge material filled most of the inner crater with a mixed breccia.

Because water and wet sediments more easily form a melt than crystalline rocks, more energy is available for the excavation. This results in craters with 20–50% larger diameters than those that would result from a single crystalline target [2]. Although sediments are more easily melted, melt sheets are seldom found in craters with sedimentary targets. The water and carbonates form volatiles that disperse the melt [2]. In the Lockne structure, no melt sheet or suevite layer has been found through extensive search, both with drillings and with geophysics [3].

References: [1] Lindström M. et al. (1996) *GFF, 118,* 193–206. [2] Kieffer S. U. and Simonds C. H. (1980) *Rev. Geophys. Space Phys., 18,* 143–181. [3] Sturkell E. and Ormo J., in preparation.

THE SUDBURY IGNEOUS COMPLEX (SIC) AS IMPACT MELT LAYER: GEOCHEMICAL EVIDENCE FOR *IN SITU* DIFFERENTIATION. M. Ostermann and A. Deutsch, Institut für Planetologie, Universität Münster, D-48149 Münster, Germany (ostermm@uni-muenster.de).

Summary: The 1.85-Ga Sudbury Igneous Complex (SIC) of the Sudbury multiring impact structure [1], together with the coeval clast-rich impact melt breccias, the Sublayer, and the Offset Dikes, is herein interpreted as the product of an *in situ* differentiation of a homogeneous impact melt. The origin of the SIC by impact melting of crustal lithologies has already been demonstrated [e.g., 1], yet the genetic relationships between the SIC lithologies, i.e., norite, quartz-gabbro, and granophyre, have remained controversial (see [2] for discussion). New major-, minor-, and trace-element data, as well as Sr-Nd isotope characteristics for the continuously sampled drillcore 70011 (INCO Ltd., North Range, Wisner Township), indicate for the first time that these lithologies are linked by *in situ* differentiation, without the need for additional assimilation of crustal

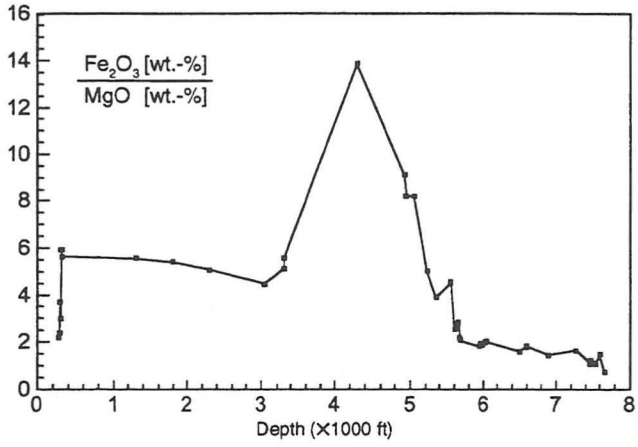

Fig. 1. Variation of the Fe_2O_3/MgO-ratio (wt%) in samples of the drill core 70011. The maximum value is not correlated to a lithological boundary (granophyre ≈ 400–5000 ft; quartz-gabbro ≈ 5000–6000 ft; norite ≈ 6000–7500 ft; Sublayer ≈ 7500–8000 ft).

rocks or contributions from the contemporaneous subcontinental mantle.

Drill Core 70011 Geochemistry: The concentrations of most elements change continously over the 2.5-km-thick SIC. The norite/quartz-gabbro transition, however, is characterized by a relatively sharp increase in TiO_2, P_2O_5, V, Sc, and Zr, as well as a sudden drop in SiO_2. This seemingly distinct boundary is not a discontinuity; rather, it reflects cooling of the SIC liquid below a thermal boundary, corresponding to the upper stability of Fe-Ti-oxides, apatite, and sphene. The quartz-gabbro, therefore, compares well with Fe-Ti-oxide (apatite-rich transition zones at true magmatic "layered intrusions"). The Fe_2O_3/MgO ratio varies smoothly over the SIC, reaching a maximum in the lower third of the granophyre (Fig. 1). All these features are well known from differentiated endogenic magmatic bodies of a homogeneous starting composition. Except for the silica-rich initial composition, and the origin by impact melting of the crust, the evolution of the SIC as delineated by elemental concentration profiles in the drill core 70011 matches that of, for example, the Skaergaard Intrusion [3]. The hypothesis that the felsic (granophyre) and the mafic (quartz-gabbro, norite) units of the SIC have been produced by different processes [4] can clearly be rejected on the basis of our geochemical results.

Typical features of a gravitational differentiation (for example, cumulate layers) are missing in the case of the SIC. *In situ* differentiation, therefore, is assumed to be the mechanism for the chemical evolution of the impact melt pool.

The Offset Dikes, discussed as "separate magmatic pulse," unambiguously belong to the impact melt system as exemplified by our investigation of the Foy Offset [5]. Total absence of inherited zircons demonstrates that the melt in the dikes was superheated; Sr-Nd isotope parameters as well as geochemical data reveal again crustal precursor material and a composition close to the norites in the North Range of the SIC. Therefore, the Offset Dikes must have been formed in a late stage of cratering when differentiation of the SIC had begun. Numerical modeling of the cooling history of the SIC indicates that emplacement of the Offset Dikes occurred not later than 0.25 m.y. after the impact event [6,7].

References: [1] Deutsch A. et al. (1995) *Geol. Rundsch., 84,* 697–709. [2] Ostermann M. (1997) Ph.D. thesis, Univ. Münster. [3] Ostermann M. and Deutsch A. (1997) *LPS XXVIII,* 1049. [4] Chai G. and Eckstrand O. R. (1994) *Chem. Geol., 113,* 221. [5] Ostermann M. et al. (1996) *Meteoritics & Planet. Sci., 31,* 494. [6] Ivanov B. A. et al. (1997) *LPS XXVIII,* 633. [7] Ivanov B. A. and Deutsch A., this volume.

THE KARIKKOSELKÄ IMPACT STRUCTURE, CENTRAL FINLAND: NEW GEOPHYSICAL AND PETROGRAPHIC RESULTS.

L. J. Pesonen[1], S. Elo[1], R. Puranen[1], T. Jokinen[1], M. Lehtinen[2], L. Kivekäs[1], and I. Suppala[1], [1]Geological Survey of Finland, P.O. Box 96, FIN-02151 Espoo, Finland (lauri.pesonen@gsf.fi), [2]Geological Museum, Finnish Museum of Natural History, FIN-00014 Helsinki, Finland.

Karikkoselkä, the seventh recognized impact structure in Finland, was discovered in 1995 because of the strikingly circular shape and unusual bathymetry of the lake [1]. This partly preserved simple impact structure with an estimated diameter of 1.2–1.4 km lies in a Palaeoproterozoic porphyritic granite. A comprehensive geophysical and petrographic study of the structure was carried out in 1996. Here we report new results providing a model for the structure and an estimate of its age.

Samples of porphyritic granite from the lake shore outcrops show marks of shatter cones and shock metamorphism. One boulder sample is an impact breccia consisting of rock and mineral clasts of various grain sizes cemented by rock powder. Most of the quartz clasts (diameter ~1 mm) contain planar deformation features (PDFs); in addition, feldspars show mosaicism and incipient vesiculation, and biotite flakes are strongly kinked. The closely spaced, partially decorated PDFs usually occur in three to four sets of orientations.

Low-altitude (25–45 m), two-frequency (3125 and 14368 Hz), aeroelectromagnetic (AEM), SAMPO wideband (2–20000 Hz), electromagnetic (EM), and detailed gravity profiles all show anomalies related to the structure. The amplitude of the residual gravity anomaly is –4 mGal, and the density of the unaffected bedrock is estimated to be 2650 kgm^{-3}. The gravity data define the locations and dips of the contacts of the whole structure. Based on gravity modeling, the crater fill is about 140 m thick if a typical density contrast of 225 kgm^{-3} is assumed. The gravity data also indicate a slight decrease of density in the bedrock surrounding the crater proper. This effect increases the diameter of the anomalous structure to 2.1–2.4 km.

The AEM and EM results delineate the horizontal layer structure with estimates of typical resistivities. The in-phase AEM anomaly is distinctly higher than the corresponding anomalies of typical Finnish lakes, which might serve as a diagnostic criteria in the search for impact structures. Based on geophysical data, the structure can be described by a bowl-shaped model of four layers and slightly altered bedrock around and below the crater. The first layer consists of water (20 m) with a (winter) resistivity of 400 m and a density of 1000 kgm^{-3}. Below this is a triplet layer with a ~5 m veneer of Quaternary mud on top (density 1050–1910 kgm^{-3}, resistivity 30–60 m). The middle part is a 45-m-thick layer with a resistivity of 65 m, and the bottom part is a 20-m-thick low-resistivity (20 m) layer. The triplet layer, lying on highly resistive granite

(>5000 m), is interpreted to be either postimpact sedimentary rocks or allochtonous suevite and impact breccia.

Preliminary palaeomagnetic data reveal three remanence directions. Samples far away from the lake show a Svecofennian (1880 Ma) magnetization (=unshocked). A very stable magnetization of reversed polarity characterizes the southeast and northwest sites of the lake. This direction corresponds to a magnetization of either Triassic (~230 Ma), or, if alternative polarity interperetation is adopted, Cambrian (~530 Ma) age, when interpolated from the Phanerozoic APWP-curve of the Fennoscandian Shield. The origin and nature of this probably impact-related, remanent magnetization is as yet unknown. A drilling of the structure is planned for winter 1998.

References: Lehtinen et al. (1996) *LPS XXVII,* 739–740.

HYDROCODE SIMULATIONS OF CHICXULUB AS AN OBLIQUE IMPACT EVENT.

E. Pierazzo[1] and D. A. Crawford[2], [1]Lunar and Planetary Laboratory, University of Arizona, Tucson AZ 85721, USA, [2]Computational Physics and Mechanics Department, Sandia National Laboratories, P.O. Box 5800, Albuquerque NM 87185, USA.

Since the confirmation that the buried Chicxulub structure is the Cretaceous-Tertiary boundary crater long searched for, numerous efforts have been devoted to modeling the impact event and trying to estimate the amount of target material that underwent melting and vaporization. Several two-dimensional hydrocodes have been used to simulate vertical impacts on targets that resemble the target lithology at Chicxulub [1–4]. It is clear, however, that real impact events are rarely vertical, and the most probable angle of impact of a randomly incident projectile is 45° [5]. Consequently, any conclusion based on two-dimensional models is severely affected by this simplification, and fundamental details of the impact event cannot be reproduced. Schultz and D'Hondt [6] have recently noted how the impact angle could be responsible for possible asymmetries in the K/T boundary record of extinctions. We present the first three-dimensional simulation of the Chicxulub event as an oblique impact. A preliminary estimate for the amount of sediments and crust material melted and/or vaporized in the impact has been calculated and compared to previous two-dimensional results.

The simulation, carried out using the shock-physics computational hydrocode CTH developed at Sandia National Laboratories [7], consists of a spherical, 10-km-diameter projectile impacting the target at 45° from the normal with an impact velocity of 20 km/s. The target layout is similar to previous two-dimensional simulations [4]. A 30-km granitic crust on top of the mantle is overlain by a sedimentary layer 2.9 km thick. A shallow sea (100 m deep) completes the target. The materials used for this simulation are dunite for the mantle and projectile, granite for the crust, calcite/limestone for the sedimentary layer, and water for the sea. The introduction of an atmosphere allows a better representation of the plume evolution for terrestrial impacts.

One thousand tracer particles have been distributed regularly in both the target and the projectile. Through a method successfully used for two-dimensional simulations [8], the maximum shock pressure experienced by each tracer has been used to reconstruct and evaluate the amount of target material that underwent melting or degassing.

Most of the melting and degassing occurs downrange from the impact point. We estimate that around 930 km^3 of the sedimentary layer is shocked at pressures >100 GPa, and about 4400 km^3 of sediments is shocked at pressures >20 GPa. A pressure of 100 GPa is generally used as the threshold pressure for the degassing of anhydrite [3], which represents one of the main sources of S in the target, while we use 20 GPa as the threshold pressure for the degassing of porous calcite. In comparison, the corresponding two-dimensional simulation carried out with CSQ produced about 450 km^3 of sedimentary layer shocked above 100 GPa and 1990 km^3 of sediments shocked above 20 GPa. The two calculations differ by about a factor of 2. On the other hand, the amount of crust shocked above 56 GPa, the pressure corresponding to complete melting of granite, is only about 9000 km^3 for the three-dimensional calculation, vs. an estimate of about 14,000 km^3 in the two-dimensional case. Recent experimental work on oblique impacts [9] indicates an increase of vaporization of the surface layers of the target (in particular, experiments where the surface layer was made of carbonates were carried out) as the impact angle (measured from the normal to the surface) increases. One of the results of the experiments is a weakening of the shock wave as function of the impact angle. In this case the lower amount of melting of the crust is a logical result of a weaker shock propagating in the target. Further work, in particular at different impact angles, is needed to verify the consistency of this result.

References: [1] O'Keefe J. D. and Ahrens T. J. (1989) *Nature, 338,* 247–249. [2] Takata T. and Ahrens T. J. (1994) *LPI Contrib. No. 825,* 125–126. [3] Ivanov B. A. et al. (1996) *GSA Spec. Paper 307,* 125–139. [4] Pierazzo E. et al. (1996) *LPS XXVII,* 1029–1030. [5] Melosh H. J. (1989) *Impact Cratering,* Oxford Univ. [6] Schultz P. H. and D'Hondt S. (1996) *Geology, 24,* 963–967. [7] McGlaun J. M. et al. (1990) *Intl. J. Impact Eng. 10,* 351. [8] Pierazzo et al. (1997) *Icarus,* in press. [9] Schultz P. H. (1996) *JGR, 101,* 21117–21136.

ESTIMATES OF CLIMATICALLY IMPORTANT GASES RELEASED IN THE CHICXULUB IMPACT EVENT.

E. Pierazzo, H. J. Melosh, and D. A. Kring, Lunar and Planetary Laboratory, University of Arizona, Tucson AZ 85721, USA.

The size and the location of the Chicxulub structure, on the Yucatán Peninsula in Mexico and produced by an impact event that occurred ~65 Ma, have driven many speculations that an impact-related abrupt climate change, with catastrophic effects on the biota, resulted in the dramatic extinction event that marks the Cretaceous-Tertiary boundary. We carried out hydrocode calculations of the Chicxulub event using newly developed equations of state of the materials that are believed to play a crucial role in the impact-related extinction hypothesis, namely carbonates (calcite) and evaporites (anhydrite). The outcomes of the simulations rule out CO_2 as the major cause for climate changes, as was previously suggested [1,2], and indicate that the S-bearing gases and water vapor are the most dangerous impact-related agents for climate change.

Impact simulations were carried out using Sandia's two-dimensional hydrocode CSQIII [3] coupled with the semianalytical equation of state ANEOS [4]. The simulations consist of spherical dunite projectiles (5–10 km in radius) impacting vertically at a speed of 20 km/s. Simulations with 0% and 50% porous projectiles were carried out for each projectile size. According to the scaling law of

Schmidt and Housen [5], the simulations correspond to transient crater diameters ranging from about 60 to 135 km. Actual estimates of the size of the Chicxulub structure vary between 180 and 300 km [6–10], corresponding to transient crater sizes in the range of 90–180 km. The target consists of a dunite mantle and an overlying 30-km layer of granitic crust. The local sedimentary sequence of carbonates and evaporites, 2–3 km thick, is modeled by alternating layers of calcite and anhydrite, and the shallow sea that covered the site at the time of the impact is modeled with a 100-m-thick layer of water. ANEOS equations of state for dunite, granite, and water had been previously developed, while ANEOS equations of state for calcite and anhydrite were developed for this work. Finally, the atmosphere is modeled by the ANEOS air equation of state with the terrestrial temperature profile.

For each run, the amount of melt and vapor produced in the projectile and various target materials has been calculated. We assumed an average porosity of 20% for the carbonate layer, in agreement with published values between 14% and 26% [11], and complete saturation with water.

We estimated the amount of climatically important species produced in the impact simulations (CO_2, S, and water vapor). The estimates, increasing linearly with transient crater size, vary from about 360 to 1700 Gt for CO_2, from 300 to 700 Gt for water vapor, and from 60 to 300 Gt for S. A small amount of additional S and water vapor may have been produced from the projectile as well [12].

The CO_2 production from our simulations are one to two orders of magnitude lower than previous two-dimensional experiments [1,2]; the atmospheric injection of such an amount would have produced, at most, an increase of 30% in the atmospheric CO_2 inventory at the end of the Cretaceous (about 4× present values [13]). Because of the lack of an equation of state for S-rich materials like anhydrite and gypsum, very little work has been done until now to model the amount of S-bearing gases that would be produced by a Chicxulub-sized event. Ivanov et al. give a possible estimate of the amount of S-bearing sediments degassed by the impact [14]. Our simulations produced results not too far from that estimate but consistently higher. Our estimates of the amount of S released in the impact are several orders of magnitude higher than any known volcanic eruption (e.g., Mt. Pinatubo: 0.01 Gt; Toba: 1 Gt), clearly able to perturb the global climate over timescales of years.

References: [1] O'Keefe J. D. and Ahrens T. J. (1989) *Nature, 338,* 247–249. [2] Takata T. and Ahrens T. J. (1994) *LPI Contrib. No. 825,* 125–126. [3] Thompson S. L. (1979) *SAND77-1339,* Sandia Natl. Lab. [4] Thompson S. L. and Lauson H. S. (1972) *SC-RR-710714,* Sandia Natl. Lab. [5] Schmidt R. M. and Housen K. R. (1987) *Int. J. Imp. Eng., 5,* 543–560. [6] Hildebrand A. R. et al. (1991) *Geology, 19,* 867–870. [7] Espindola J. M. et al. (1995) *Phys. Earth Planet. Inter., 92,* 271–278. [8] Sharpton V. L. et al. (1993) *Science, 261,* 1564–1567. [9] Pope K. O. et al. (1996) *Geology, 24,* 527–530. [10] Kring D. A. (1995) *JGR, 100,* 16979–16986. [11] Viniegra O. F. (1981) *J. Petrol. Geol., 3,* 247–278. [12] Kring D. A. et al. (1996) *EPSL, 140,* 201–202. [13] Berner R. A. (1994) *Am. J. Sci., 294,* 56–91. [14] Ivanov B. A. et al. (1996) *GSA Spec. Paper 307,* 125–139.

GEOPHYSICAL SIGNATURES OF LARGE IMPACT STRUCTURES. M. Pilkington, R. A. F. Grieve, and A. R. Hildebrand, Geological Survey of Canada, Ottawa, Ontario, Canada.

Geophysical data are being used increasingly in the identification and characterization of possible and known impact structures [e.g., 1–3], particularly buried structures. Based on the current database of geophysical data over known impact structures, several characteristics of the signature of impact are apparent [4–6]. The most notable is a circular negative gravity anomaly extending out to the crater rim. This effect is primarily caused by the reduction in the density of the target rocks through fracturing and brecciation. Magnetic anomalies associated with terrestrial impact structures are generally more variable than gravity effects, reflecting the greater variation possible in the magnetic properties of rocks. The dominant effect over structures is a magnetic low or subdued zone [4–6]. The cause of these lows is not clear. Recent studies of several Canadian structures indicate that all impact lithologies show a reduction in both induced and remanent magnetization levels that is not sufficient to account for the observed magnetic lows [7]. The fractured target rocks also show diminished magnetization levels at depths well below the crater floor, suggesting that the transient stress wave is the likely cause.

The primary geophysical signature of impact, consisting of a gravity and magnetic low, can be modified by secondary effects caused by both the preimpact geological structure and postimpact processes such as erosion, burial, and tectonism. At larger complex craters, the gravity low may be modified by the presence of a central gravity high, which is caused by deeper denser crustal material being brought closer to the surface (e.g., Manicouagan, Chicxulub). The magnetic low can be modified by the presence of shorter wavelength, large-amplitude, localized anomalies, which usually occur at or near the center of the structure. Several different sources produce these central magnetic anomalies: magnetic basement rocks may be exposed in the central uplift (e.g., Vredefort, Carswell) and anomalies may correspond to alteration zones within the central uplift area (e.g., Saint Martin), magnetic impact melt rocks, or suevite/breccias (e.g., Chicxulub, Ries). Erosional effects are most prominent when the structure has been eroded to levels below the original crater floor [5]. In these cases, both gravity and magnetic lows may be removed, and only central anomalies caused by the central uplift remain. Burial will also reduce anomaly amplitudes, possibly to regional anomaly levels, thus obscuring the impact-related signature. Tectonic processes are likely important only for older structures. Deformation may destroy the circularity of the anomalies, while folding and faulting may complicate the preexisting signature (e.g., Sudbury). Regional metamorphism also tends to reduce gravity anomalies by annealing impact-induced porosities. The effect on magnetic anomalies is more difficult to predict because of the greater influence of target-rock composition on magnetic properties [8].

The high level of geological activity on Earth can drastically modify the primary geophysical signature of impact, resulting in geophysical anomalies associated with impact structures having widely varying characteristics. Consequently, the interpretation of geophysical data over a possible structure cannot be done in isolation; rather, it needs to be done in conjunction with the known database and with the consideration of the local geological environment.

References: [1] Henkel H. and Pesonen L. J. (1992) *Tectonophys., 216,* 31–40. [2] Shoemaker E. M. and Shoemaker C. S. (1997) *LPS XXVIII,* 1309–1310. [3] Corner B. et al. (1997) *EPSL, 146,* 351–364. [4] Dabizha A. I. and Fedynsky V. V. (1977) *Meteoritika, 36,* 113–120. [5] Pilkington M. and Grieve R. A. F. (1992) *Rev. Geophys., 30,* 161–181. [6] Henkel H. (1992)

Tectonophys., 216, 63–90. [7] Scott R. G. et al. (1997) *Meteoritics & Planet. Sci., 32,* 293–308. [8] Grant F. S. (1984/1985) *Geoexpl., 23,* 303–333.

GRAVITY AND MAGNETIC MODELING OF A COMPLEX IMPACT STRUCTURE: EFFECT OF DEFORMATION AND EROSION. J. Plado[1], L. J. Pesonen[2], and V. Puura[1], [1]Institute of Geology, University of Tartu, Vanemuise 46, EE2400 Tartu, Estonia (jplado@math.ut.ee), [2]Laboratory for Paleomagnetism, Geological Survey of Finland, P.O.Box 96, FIN-02151 Espoo, Finland (lauri.pesonen@gsf.fi).

The relatively small number (~155) of verified meteorite impact structures on Earth is mainly due to tectonic activity and terrestrial erosion, both of which may partially or totally erase the geological signatures of old impact structures. Terrestrial geological processes such as deformation, postimpact sedimentation, and subsequent erosion also play a role in the changes of the geophysical anomalies of terrestrial impact structures. Although there have been numerous attempts to model the geophysical anomalies of impact structures, little effort has been made to model the changes in the geophysical anomalies as a function of deformation and erosion.

To this end, we present two case histories. In the first case, we have calculated geophysical anomalies related to the 4-km-diameter, 0.5-km-deep Kärdla impact structure for the hypothetical cases of further burial (0.1-km-thick cover) and erosion (removal of the 0.1–0.3-km-thick uppermost layer) [4]. It was discovered that the influence of burial on the detection of ring structures by gravity and magnetic data is not as destructive as erosion. In the second case, we have tried to carry out gravity and magnetic modeling as applied to a complex hypothetical impact structure (1.2 km in depth, 30 km in diameter) whose schemes were published by Rondot [5] and Melosh [2]. The target on the model approximately simulates the Precambrian geology of the Baltic Shield in southwestern Finland. The modeling was done using 16 simulated radial profiles across the center of the structure. In the modeling, we looked at the progressive changes in the geophysical anomalies of this structure at six successive geological situations: (1) preimpact, (2) impact, (3) deformation, and (4–6) three erosional levels. We have used 2.5-dimensional modeling where the geological units are defined as homogeneous polygonal prisms with different strikes. Each unit has specified petrophysical characteristics (density, magnetic susceptibility, and natural remanent magnetization, the latter two as vector properties). The calculated gravity and magnetic anomalies at the various stages are presented as contour maps and profiles to demonstrate the effect of deformation and erosion on geophysical signatures.

The 2.5-dimensional modeling approach produces two problems. First, the software [3] does not allow gravity and magnetic data to be calculated for profiles outside the model structure. Second, data on top of the model are slightly incorrect because of a failure to take into account the three-dimensional effects. Using three-dimensional *gravity* software [1], we are able to demonstrate that the 2.5-dimensional program produces errors up to 15% for off-structure calculation points. These errors are not randomly located, and, therefore, the geophysical anomaly patterns show "butterfly"-type features that are purely artifacts of the model. Despite these drawbacks, the signature of the impact in geophysical data is clearly visible as circular anomaly patterns.

Our impact model shows a slightly distorted circular gravity anomaly, with a –18 mGal amplitude, as well as a circular negative relief on a magnetic map. We found that simple tectonic deformation (such as faulting) and erosion of 2 km below the target level (1/15 of the crater diameter) does not destroy the circular gravity and magnetic anomalies of the structure. Even with 4 km of erosion (1/7.5 of the crater diameter), we can still see traces of the gravity and magnetic impact anomalies.

References: [1] Elo S. (1986) *Program GRAV3DC,* Geological Survey of Finland. [2] Melosh H. J. (1989) *Impact Cratering: A Geologic Process,* Oxford Univ., 245 pp. [3] Pedley R. C. (1991) *GRAVMAG-User Manual,* Interactive 2.5-D Gravity and Magnetic Modelling Program, British Geological Survey (unpublished). [4] Plado J. and Puura V. (1995) *Ann. Geophys., 13,* suppl. III, C741. [5] Rondot J. (1993) *Earth Sci. Rev.,* 331–365.

THE CHESAPEAKE BAY STRUCTURE: EARTH'S LARGEST SUBMARINE PEAK-RING IMPACT CRATER. C. W. Poag, U.S. Geological Survey, Woods Hole MA 02543-1598, USA.

More than 1200 km of seismic reflection profiles, four cores of impact breccia, and a bull's-eye negative gravity anomaly document the buried Chesapeake Bay impact crater. Its structure and morphology indicate that the feature is a complex peak-ring crater that also exhibits a small central peak. The 90-km-wide crater was excavated from mixed-target lithologies comprising 300–1000 m of sedimentary strata overlying crystalline basement rocks (granitic and metasedimentary rocks of the Appalachian orogen). Biochronologic and paleoenvironmental analyses indicate that the bolide struck the late Eocene inner continental shelf (200–500 m water depth) ~35 Ma. The impact took place within a 0.8-m.y. interval in which the upper part of planktonic foraminiferal biochronozone P15 overlaps the

TABLE 1.

Name and (Type)	Location	Age (m.y.)	Diameter (km)	Depth (km)	Burial Depth (m)	Water Depth (m)	Breccia Thickness (km)	Target Rocks
Chicxulub (multiring)	Yucatán, Mexico	~65	180–300	>1.0	~1000	0–60	>0.6	Mixed
Chesapeake Bay (peak ring)	Southeastern Virginia, U.S.	~35	90	1.5 (?)	300–500	0–20	1.3 (?)	Mixed
Montagnais (central peak)	Scotian Shelf, Canada	~51	45	2.7	500	113	>0.6	Mixed
Mjølnir (central peak)	Barents Sea, Norway	~145	40	0.2–0.3	400	375	1.0–1.3	Sediment
Toms Canyon (unknown)	New Jersey Shelf, U.S.	~35	20	0.5	1000	100	0.5	Sediment

lower part of calcareous nannoplankton biochronozone NP19–20. Due to its submarine location, marine sedimentation resumed immediately following the impact and buried the crater under 300–500 m of mostly marine, shallow-water deposits. Because of its submarine origin, immediate burial, and location on a passive continental margin, the structure has undergone virtually no erosion or tectonic alteration, and is therefore unusually well preserved.

Only three other well-documented impact craters (and an additional *possible* impact crater) are currently known to be partly or entirely buried beneath marine waters. Their principal characteristics can be compared to the Chesapeake Bay crater as shown in Table 1.

The Chesapeake Bay structure is currently the largest, and perhaps the only, submarine peak-ring crater identified on Earth (there is some question regarding the structure and morphology of Mjølnir). Its shallow burial and easy accessibility to geophysical surveys and coring provide a good opportunity to study the detailed structural, morphological, erosional, and depositional consequences of bolide impacts into mixed target rocks under shallow seas.

THE PUBLIC INTEREST IN IMPACT CRATERING: THE RIES CRATER MUSEUM, NÖRDLINGEN, GERMANY.

G. Poesges and M. Schieber, Rieskrater–Museum, Nördlingen, Germany.

Introduction: After five years of preparation, the Rieskrater-Museum was opened in May 1990 [1]. The museum is dedicated to the presentation of the Ries impact, its planetary roots, its importance for a better understanding of cosmic interactions, the geology of the Jura mountains, and the development of the landscape after the impact. To this day the museum has been visited by approximately 350,000 visitors. More than 1500 tours of the museum and some 60 field excursions have been arranged.

The Museum: The museum, which includes 800 m² of floor space, is subdivided into six rooms for the presentation of the following topics: (1) *Room A:* geomorphology and geographical position of the Ries Crater; (2) *Room B:* our planetary system, including types of impact craters, meteorite systematics, distribution of impact craters on the planet Earth, a video about the origin of our planetary system, and the meaning and importance of impacts; (3) *Room C:* preimpact geology of the Ries, with displays on the impact point, crater mechanics, NASA experiments, and progressive shock wave metamorphism; (4) *Room D:* formation of the Ries impact structure, including information on the types of impact rocks, a geological cross section of the crater, drill cores, and a slide show of the crater formation; (5) *Room E:* Ries lake deposits and fossils, landscape development, exploitation of postimpact rocks, land utilization; and (6) *Room F:* Ries Crater research history, lunar samples, and an Apollo 16 mission video.

Visitors: The average number of visitors per year (see Fig.1) indicates a great interest of the public in impact processes and impact hazards on our globe, especially after the Shoemaker-Levy event in 1994 and encounters with Comet Hyakutake in 1996 and Comet Hale-Bopp in 1997. The great number of tours of the museum, as well as field excursions, is also due to the conception of a modern museum in one of the best-known craters on Earth. Among the numerous annual visitors are schoolchildren, students, and members of scientific societies; many revisit the museum at regular intervals.

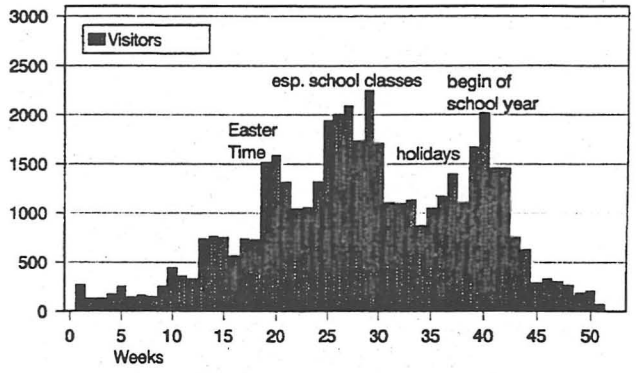

Fig. 1. The number of weekly visitors to the Ries Crater Museum, Nördlingen, Germany, for 1996.

The Museum as Transmitter: The staff in the museum make it their business to act as a transmitter in conveying science and research results to the public. They participate in scientific congresses and have established contacts with planetary scientists, museums, NASA, and other research institutions.

To this day, three scientific societies have held meetings in the museum: the European Science Foundation (1993), the Meteoritical Society (1994), and Gesellschaft für Geowisssenschaften (1995). Separate exhibits present the research results of these meetings and other events.

References: [1] Poesges G. and Schieber M. (1994) *Das Rieskrater Museum Nördlingen,* Museumsführer, Verlag Pfeil, München (English edition available).

MORPHOLOGY OF DIAMONDS FROM IMPACTITES AND METAMORPHIC ROCKS.

T. V. Posukhova[1] and E. D. Nadezhdina[2], [1]Moscow State University, Geological Department, Moscow 119899, Russia, [2]TSNIGRI, Geological Survey of Russia, Moscow, Russia.

The main sources of diamond crystals (kimberlites, lamproites, etc.) are well known. The morphology of diamonds from impactites and metamorphic rocks, however, is uncommon and not as well known.

Metamorphic diamonds are known from Kazakhstan, China, and Norway [1–4]. They are very small (0.01–0.01 mm) and have a yellow color and anomaly refraction. Their mineral companions are garnet, zircon, graphite, mica, rutile, titanite, and kyanite. The concentration of N and REE impurities in these diamonds is high [2]. They have very weak yellow-green luminescence and unusual forms, with no dodecahedra and very few octahedra. Several crystal forms can be seen in these rocks: skeletal and sphere, faced (antiskeletal) and edge rays, boxy and tabular forms, and unusual aggregate-skeletal cubic crystals formed by coarse-layered blocks. We investigated different crystals and proposed their morphological classification [5]. The comparison of the metamorphic and synthetic diamonds warrants application of the growth theory to explain the specific morphology of the metamorphic diamond. The diamonds crystallized very quickly by fibrous mechanism of growth, during a short time at nonequilibrium conditions with low temperature and

pressure from the supersaturated solutions that were rich in impurities. A fast saturation of mineral solution caused the formation of a great number of crystal embryos. This explains very small sizes of metamorphic diamonds and the frequent occurrence of twins. The impurities increase the speed of growth and make the diamond defective. The diamonds acquired unhomogeneous sector and zone structure, which is characteristic of metamorphic diamonds.

Typomorphic features of diamonds from impactites are the same as paramorphozes by graphite. Their mineral satellites are quartz, pyrite, ilmenite, hematite, graphite, and glass. They are commonly gray and black and have an uncommon isotopic composition (13.2–18.8‰ $\delta^{13}C$) and impurities (lonsdeilite and much REE). They have an anisotropy refraction and weak yellow and red-orange luminescence. They consist of hexagonal, plate, and xenomorphic aggregates of small crystallites (grains = 0.1–10 × 10^{-4}–10^{-2} mm). Their surfaces are plain, hatching, shading, gofer, flexure, cellular, and cavernous. Their structure is polycrystalline, strongly textured, stratified, and strained. Comparisons with experimental data give us a foundation to speculate on the origin of impact diamonds, believed to be the recrystallization of graphite at high temperature, pressure, and velocity of growth. Such conditions may be realized during the meteoritic fall, which would account for anomalous stresses and temperatures.

References: [1] Dobrzhinetskaya L. et al. (1993) *Terra Nova Abstract Supplement, Proc. Fourth International Eclogite Conf., 5,* 9. [2] Martovitsky V. Yu. et al. (1987) *Mineral. J., 9,* 26–27 (in Russian). [3] Sobolev N. V. and Shatsky V. S. (1990) *Nature, 343,* 742–745. [4] Xu S. et al. (1992) *Science, 256,* 80–82. [5] Nadezhdina E. D. and Posukhova T. V. (1990) *Mineral. J., 12,* 3–15 (in Russian).

POSTMAGMATIC ZIRCON GROWTH OR EXOTIC EARLY MAGMATIC PHASES ASSOCIATED WITH THE EMPLACEMENT OF THE SUDBURY IGNEOUS COMPLEX: SAMARIUM-NEODYMIUM ISOTOPIC, GEOCHEMICAL, AND PETROGRAPHIC EVIDENCE. S. A. Prevec[1], F. Corfu[2], M. L. Moore[3], P. C. Lightfoot[4], and R. R. Keays[1], [1]Department of Earth Sciences, Laurentian University, Sudbury, Ontario P3E 2C6, Canada, [2]Department of Geology, Royal Ontario Museum, Toronto, Ontario M5S 2C6, Canada, [3]Geoservices Centre, Ramsey Lake Road, Sudbury, Ontario P3E 6B5, Canada, [4]INCO Limited, Highway 17 W., Copper Cliff, Ontario P0M 1N0, Canada.

The timing of both the crystallization of the Sudbury Igneous Complex (SIC) and the shock deformation of the country rocks within the contact aureole has been reliably established using a variety of isotopic techniques, including U-Pb in zircon and baddeleyite [e.g., 1,2], Rb-Sr in whole rocks, and Re-Os in ores. The physical evidence of shock metamorphism in affected rocks and mineral grains has been well characterized. However, in a number of cases, ca. 1850-Ma ages have been produced from zircons in a variety of Footwall breccia-hosted rocks where petrologic and geochemical arguments strongly suggest that the true crystallization age predates the zircon age.

Samples from a plagioclase-phyric basaltic to diabasic raft at Whistle mine, an ultramafic intrusion in the North Range Footwall at Fraser mine, and a metaleucogabbro-noritic sill in Drury Township have been studied during the course of various studies of SIC and Huronian magmatism. All these bodies lie within the immediate Footwall rocks adjacent to the basal Main Mass or Sublayer norite and well within the contact metamorphic aureole of the SIC. These units are characterized by suites of magmatic-textured zircons with U-Pb ages within error of 1850 Ma. The zircon populations vary in habit, color, and U content between units and are consistent with igneous magmatic origins, although they are different in character from similarly aged SIC zircons. However, all these units are characterized by Sm-Nd isotopic and trace element geochemical signatures that clearly distinguish them from SIC magmatic material. ε_{Nd}^{1850} values range from –2.2 to –5.8, in contrast to SIC values of –6.8 to –9.1. Trace-element abundances are significantly lower and show flatter mantle-normalized profiles than do SIC samples. Petrographic evidence from the plag-phyric and ultramafic bodies is indicative of deformation of preexisting magmatic textures, distinguishable from later regional upper greenschist grade metamorphic overprinting. Finally, older correlative rocks present in adjacent country rock show geochemistry and isotopic signatures comparable to the bodies in question.

The variation in morphologies and chemistry of the 1850-Ma zircons in these bodies, plus the morphologies themselves, would appear to be inconsistent with crystallization from pervasive, SIC-induced hydrothermal fluids. The evidence therefore requires either the growth of magmatic-looking zircons in existing rocks, where the geochemistry of the host rock or at least the immediate environment plays a role in the mineral growth, or alternatively, the emplacement of exotic magma batches (possibly remelted Footwall or lower crustal rocks) in the early stages of formation of the SIC followed by subsequent deformation and local incorporation into the noritic Sublayer magmas.

References: [1] Krogh T. E. et al. (1984) *Ontario Geol. Surv. Spec. Vol., 1,* 431–446. [2] Corfu F. and Lightfoot P. C. (1996) *Econ. Geol., 91,* 1263–1269.

ORIGIN OF THE SUBLAYER OF THE SUDBURY IGNEOUS COMPLEX: SAMARIUM-NEODYMIUM ISOTOPIC, GEOCHEMICAL, AND PETROGRAPHIC EVIDENCE FOR INCOMPLETE CRUSTAL HOMOGENIZATION. S. A. Prevec[1], R. R. Keays[1], P. C. Lightfoot[2], and Q. Xie[1], [1]Department of Earth Sciences, Laurentian University, Sudbury, Ontario P3E 2C6, Canada, [2]INCO Limited, Highway 17 West, Copper Cliff, Ontario P0M 1N0, Canada.

The major repository of Ni sulfides in the 1850-Ma Sudbury Igneous Complex (SIC) is the discontinuous marginal zone known as the Sublayer. The Sublayer is characterized by the presence of large amounts of sulfide and a variety of inclusions, ranging from xenocrysts to decameter-sized blocks. The inclusions can be broadly subdivided into five groups: (1) felsic or granitic (*sensu lato*) xenoliths attributable to proximal country rock; (2) ultramafic inclusions, including peridotite (generally rare), olivine melanorite, and pyroxenite; (3) plagioclase-phyric, recrystallized "anhedral porphyries"; (4) gabbroic and anorthositic fragments; and (5) centimeter-scale felsic or anorthositic blebs.

The anhedral porphyries are distinguished from the other SIC rocks and inclusions therein in that they display relatively flat chondrite-normalized REE profiles [e.g., $(Ce/Yb)_N = 3$, as compared to

values around 8–9 for the Main Mass and >20 for North Range country rock] and have a very limited, relatively depleted range of ε_{Nd}^{1850} values, from –2.2 to –5.4, in contrast to values of –6.8 to –9.1 for the Main Mass and Offset Dikes. The Sublayer displays isotopic and trace element geochemical characteristics consistent with derivation from materials represented by its inclusion population, among which the anhedral porphyries are prominent. Sublayer ε_{Nd}^{1850} values range between –5.5 and –7.5, and REE abundances and ratios are intermediate between those of the porphyries and those of the country rocks.

A comparison of the Sm-Nd isotopic and geochemical signature of the anhedral porphyries with those of Early Proterozoic (ca. 2470 Ma) mafic volcanics of the basal Huronian Supergroup and the associated plutons (i.e., "East Bull Lake-type") and dikes (i.e., Matachewan) indicates strong similarities to these populations, particularly with the Huronian tholeiitic basalts and the Matachewan dikes. Geochemical variation diagrams show a prominent influence from this Huronian component as a mixing end member for SIC magmas, particularly to the Sublayer. Sublayer magmas can be described, at least qualitatively, in terms of mixtures between this Huronian component and Archean basement (in particular the Levack Gneiss Complex thought to underlie the SIC), with additional variation induced by mineralogical control, in particular by orthopyroxene, and incompatible-element-enriched accessory minerals (e.g., apatite).

The association of mineralization in the Sublayer and offsets with the presence of anhedral porphyry inclusions can be used to infer that the source of the metalliferous sulfides in the SIC may have been the Early Proterozoic mafic suite. Much of this suite is well mineralized with Cu, Ni, and PGE (in particular Nipissing and East Bull Lake-type intrusives). Impact-induced melting and variable assimilation of Huronian country rock could have induced variable segregation and reconsolidation of the preexisting sulfides and subsequent redeposition into "traps" such as the Sublayer troughs. The major inconsistency with this premise is that the Cu/Ni ratio of Huronian mineralization is on average generally much higher than that observed in the SIC. The alternative, a contribution from juvenile mantle, is not supported by any direct evidence. However, the addition of a relatively small (i.e., <10%), well-homogenized picritic contribution (such as from the lithospheric mantle), which could provide an alternate source for the metals, cannot be ruled out.

GEOCHEMICAL AND SAMARIUM-NEODYMIUM ISOTOPIC EVIDENCE REGARDING THE ORIGIN OF OFFSET DIKES OF THE SUDBURY IGNEOUS COMPLEX, ONTARIO. S. A. Prevec[1], Q. Xie[1], R. R. Keays[1], and P. C. Lightfoot[2], [1]Department of Earth Sciences, Laurentian University, Sudbury, Ontario P3E 2C6, Canada, [2]INCO Limited, Highway 17, Copper Cliff, Ontario P0M 1N0, Canada.

One of the magmatic features that distinguishes the Sudbury Igneous Complex (SIC) from potentially comparable igneous layered mafic intrusions is the presence of relatively leucocratic linear vertical dikes extending into the country rock. These bodies, known as Offset Dikes, may be divided into two categories on the basis of their geometric relationship to the SIC and are described as radial and concentric dikes. While the majority of the identified offsets project radially outward into the footwall rocks from the base of the SIC at the Sublayer, a smaller number have been identified that run subparallel to the SIC contact and may be found between 4 km (Manchester Offset) and 12 km from the SIC (in Hess Township). In addition, within individual offsets, a marginal, relatively inclusion- and sulfide-poor facies and a central, inclusion- and sulfide-rich facies have been identified. Although early workers grouped Offset and Sublayer magmas as subtypes of the same phase of the SIC, recent geochemical work [1] has indicated both relatively homogeneous and relatively incompatible-element-enriched geochemistry in offsets, more comparable to Main Mass Norites than to Sublayer.

Samarium-neodymium isotopic data from Parkin Offset in the North Range indicate a homogeneous signature consistent with a large crustal component. The ε_{Nd}^{1850} values for the offsets vary around –8.0, comparable to new and exisiting data from the main mass. Incompatible-trace-element geochemical variation within a given offset is relatively small, and average compositions of offsets from the North and South ranges display variations consistent with strong influence from the local country rock. Offsets emplaced within the North Range Archean gneisses and granitoids display trace-element abundances that are similar to one another and slightly enriched relative to average main-mass felsic norite. In contrast, offsets emplaced into South and East Range Proterozoic metavolcanic and metasedimentary rocks display trace-element abundance profiles that differ from one another and from the North Range Offset signature. Although inclusions within the central facies of the offsets have quite distinctive isotopic and geochemical signatures, the host quartz noritic to quartz dioritic offset rocks show minimal variation either along or across strike within an offset, as profiled in examples from the Foy and Hess offsets in the North Range and the Worthington Offset in the South Range. The marginal offset facies may show geochemical evidence for local footwall assimilation. In addition, there is no systematic geochemical distinction between the radial Foy Offset and the longitudinal Hess Offset.

Given that the offset magmas were emplaced into shock-induced and/or existing crustal fractures, a mechanism is required whereby the relatively leuconoritic melts pooled at the base of the melt sheet and assimilated and homogenized local footwall material. Sulfide mineralization (as a fractionating sulfide liquid and then solid solution) and the prominent mafic and ultramafic inclusion population associated with the Sublayer and the offsets were then introduced. The offset magmas were either released into the fractures as homogenous dike-like bodies carrying the inclusions and sulfides entrained within or were emplaced prior to Sublayer development and acquired inclusions and sulfides that settled out of the Sublayer.

References: [1] Lightfoot et al. (1997) *Ontario Geol. Surv. Open File Report 5959,* 231 pp.

POSTIMPACT IMPACTITE PHASE. J. Raitala, Department of Geosciences and Astronomy, University of Oulu, Oulu, Finland (jouko.raitala@oulu.fi).

Shock-related changes in feldspar composition were found by Feldman [1]. The diaplectic mineral zone fracturing was substituted by concentric and radial fractures across crystal boundaries in the amorphous zone when the pressure exceeded 30 GPa. With pressures >60 GPa, the high-shocked metamorphic phase consisted of

impact melt. Significantly, the feldspar composition remained unaltered until 25 GPa, but after that there was increased cation migration by increasing pressure. The exchange of K and Na was found between albite and K-feldspar as well as a cation outflow from feldspars. The authors suggested that this cation exchange zone width could be used as a shock-metamorphic geobarometer. This idea, as well as the processes that allow the cation exchange in impactites, should be studied in detail.

Impactite mineral changes may derive from the two main impact-related events: the high-to-vibrating pressure impact event and/or an extended thermal postimpact time. Both of these events may result in the cation exchange between the heated and crushed/melted matrix phase and surviving/new crystals. An extremely fast cation exchange or depletion may occur during the high-pressurized vibration phase immediately following the impact and mechanical crushing of the rock. Another possibility is a high-temperature postimpact environment that results in an extended cation diffusion between remaining crystals and the milled and/or melted matrix material, where new crystals are formed if the duration of the thermal phase is long enough. It may be difficult to distinguish between the two processes. The vibrational pressure phase may be most effective if two or three active mineral phases are present in the rock. The hot low-pressure phase that follows may favor additional cation exchange between the remaining crystals and the melted matrix. Both effects may be limited to edge zones of remaining crystal phases where the diffusive distance is the shortest. Cation migration paths through the whole crystal lattice are slower and more difficult and may take place in the case of the largest impacts where melt is abundantly present and the cooling time is long enough to allow reactions between crystal and melt phases. A long cooling time and high-temperature and concentration gradient increase the cation migration.

The two alternative metamorphoses (impact event shock-metamorphosis and thermal postimpact metamorphosis) have to be reconsidered according to the ideas of Feldman [1]. These more straightforward impact-induced changes need to be contrasted against previous suggestions of the effects of the late high-temperature environment in diffusional cation exchange between garnet crystals and the surrounding matrix during the extended thermal postimpact period [2]. High and low pressure may favor different outflow and inflow at the crystal's edge zones. The high temperature and concentration gradient also increase diffusion coefficient and cation migration [3,4]. The shock-wave effects may be favored if most of the cation migration is limited to crystal edge zones where the diffusive distance is shortest. Longer cation migration paths through the crystal lattice and a possible equilibrium between the crystals and/or the matrix materials may support the effects of the extended thermal phase.

Even if the impact and postimpact phases produce qualitatively similar changes, the heated low-pressure postimpact phase may provide a more balanced outcome of the crystal-matrix cation diffusion. This is especially evident in the case where a reasonable amount of melt is present. Samples collected from deep levels or from large craters should show more signs of the thermal phase. There is more time for controlled diffusion in the thermal phase than the shock-vibration phase.

References: [1] Feldman V. I. et al. (1996) *Vernadsky-Brown Microsymposium 24,* 25–26. [2] Raitala J. and Halkoaho T. (1995) *LPS XXVI,* 1151. [3] Loomis T. P. (1983) in *Kinetics and Equilibrium in Mineral Reactions* (S. K. Saxena, ed.), pp. 1–60, Springer-Verlag. [4] Lasaga A. C. (1984) *JGR, 89,* 4009–4025.

IMPACT CRISES, MASS EXTINCTIONS, AND GALACTIC DYNAMICS: A UNIFIED THEORY. M. R. Rampino, NASA Goddard Institute for Space Studies, 2880 Broadway, New York NY 10025, Earth and Environmental Science Program, New York University, 26 Stuyvesant Street, New York NY 10003, USA.

A general hypothesis linking mass extinctions of life with impacts of large asteroids and comets is based on astronomical data, impact dynamics, and geological information [1,2]. The waiting times of large-body impacts on the Earth, derived from the flux of Earth-crossing asteroids and comets, and the estimated size of impacts capable of causing large-scale environmental disasters predict that impacts of objects ^{3}5 km in diameter (^{3}10^7 Mt TNT equivalent) could be sufficient to explain the record of ~25 extinction pulses in the last 540 m.y., with the five recorded major mass extinctions related to the impacts of the largest objects of ^{3}10 km in diameter (^{3}10^8 Mt events). Smaller impacts (~10^6–10^7 Mt), with significant regional and even global environmental effects, could be responsible for the lesser boundaries in the geologic record.

Tests of the "kill curve" relationship for impact-induced extinctions based on new data on extinction intensities and several well-dated large impact craters suggest that major mass extinctions require large impacts, and that a step in the kill curve may exist at impacts that produce craters of ~100 km diameter, with smaller impacts capable of only relatively weak extinction pulses. Single impact craters <~60 km in diameter should not be associated with global extinction pulses detectable in the Sepkoski database (although they may explain stage and zone boundaries marked by lesser faunal turnover), but multiple impacts in that size range may produce significant stepped extinction pulses.

Statistical tests of the last occurrences of species at mass-extinction boundaries are generally consistent with predictions for abrupt or stepped extinctions, and several boundaries are known to show "catastrophic" signatures of environmental disasters and biomass crash, impoverished postextinction fauna and flora dominated by stress-tolerant and opportunistic species, and gradual ecological recovery and radiation of new taxa. Isotopic and other geochemical signatures are also generally consistent with the expected after-effects of catastrophic impacts. Seven of the recognized extinction pulses are associated with concurrent (in some cases multiple) stratigraphic impact markers (e.g., layers with high Ir, shocked minerals, microtektites), and/or large, dated impact craters. Other less-well-studied crisis intervals show elevated Ir, still well below that of the K/T spike, which might be explained by low-Ir impactors, ejecta blowoff, or the sedimentary reworking and dilution of impact signatures.

The best explanation for a possible periodic component of ~30 m.y. in mass extinctions and clusters of impacts is the modulation of the comet flux associated with the solar system's periodic passage through the plane of the Milky Way Galaxy [3,4]. The quantitative agreement among paleontological, geological, and astronomical data suggests an important underlying unification of the processes involved.

References: [1] Rampino M. R. and Haggerty B. M. (1996)

Earth, Moon & Planets, 72, 441–460. [2] Rampino M. R. et al. (1997) *N. Y. Acad. Sci. Ann.,* 9616. [3] Rampino M. R. and Stothers R. B. (1984) *Nature, 308,* 709–712. [4] Matese J. J. et al. (1995) *Icarus, 116,* 255–268.

STRIATIONS, POLISH, AND RELATED FEATURES FROM CLASTS IN IMPACT-EJECTA DEPOSITS AND THE "TILLITE PROBLEM." M. R. Rampino[1], K. Ernstson[2], F. Anguita[3], and F. Claudín[4], [1]New York University, New York NY 10003 and NASA Goddard Institute for Space Studies, 2880 Broadway, New York NY 10025, [2]Facultät für Geowissenschaften, Leistenstrasse 62, Universität Würzburg, D-97082, Würzburg, Germany, [3]Departamento de Petrologia y Geoquimica, Facultad de Ciencias Geológicas, Universidad, Complutense de Madrid, 28040 Madrid, Spain, [4]Museu de Geologia, Parc de la Ciutadella, 08003 Barcelona, Spain.

Proximal ejecta deposits related to three large terrestrial impacts, the 14.8-Ma Ries impact structure in Germany (the Bunte Breccia) [1], the 65-Ma Chicxulub impact structure in the Yucatán (the Albion and Pook's Hill Diamictites in Belize) [2,3] and the mid-Tertiary Azuara impact structure in Spain (the Pelarda Fm.) [3,4] occur in the form of widespread debris-flow deposits most likely originating from ballistic processes. These impact-related diamictites typically are poorly sorted, containing grain sizes from clay to large boulders and blocks, and commonly display evidence of mass flow, including preferred orientation of long axes of clasts, clast imbrication, flow noses, plugs and pods of coarse debris, and internal shear planes [5]. Clasts of various lithologies show faceting, various degrees of rounding, striations (including nailhead striae), crescentic chattermarks, mirror-like polish, percussion marks, pitting, and penetration features.

Considering the impact history of the Earth, it is surprising that so few ballistic ejecta deposits have been discovered, unless the preservation potential is extremely low, or such materials exist but have been overlooked or misidentified as other types of geologic deposits [5,6]. Debris-flow diamictites of various kinds have been reported in the geologic record, but these are commonly attributed to glaciation based on the coarse and poorly sorted nature of the deposits and, in many cases, on the presence of clasts showing features considered diagnostic of glacial action, including striations of various kinds, polish, and pitting. These diamictites are the primary evidence for ancient ice ages [7].

We present evidence of the surface features on clasts from known proximal ejecta debris-flow deposits and compare these features with those reported in diamictites interpreted as ancient glacial deposits (tillites). Our purpose is to document the types of features seen on clasts in diamictites of ejecta origin in order to help in the interpretation of the origin of ancient diamictites. The recognition of characteristic features in clast populations in ancient diamictites may allow identification and discrimination of debris-flow deposits of various origins (e.g., impact, glacial, tectonic) and may shed light on some climatic paradoxes, such as inferred Proterozoic glaciations at low paleolatitudes [8].

References: [1] Chao E. C. T. (1977) *Geol. Jahrb. 43,* 3–81. [2] Ocampo A. et al. (1996) *GSA Spec. Paper, 307,* 75–88. [3] Rampino M. R. et al. (1996) *GSA Abstr. with Progr., 28,* A-182. [4] Ernstson K. and Claudin F. (1990) *N. Jb. Geol. Palaont. Mh., 10,* 581–599. [5] Hambrey M. J. and Harland W. B. (1981) *Earth's Pre-Pleistocene Glacial Record,* 14–27, Cambridge Univ. Press. [6] Rampino M. R. (1994) *J. Geol., 102,* 439–456. [7] Oberbeck V. R. et al. (1993) *J. Geol., 101,* 1–19. [8] Evans D. A. et al. (1997) *Nature, 386,* 262–266.

VREDEFORT 1997: A CONTROVERSY RESOLVED—STILL A CHALLENGE FOR THE FUTURE. W. U. Reimold, Department of Geology, University of the Witwatersrand, Private Bag 3, P.O. Wits 2050, Johannesburg, South Africa (065wur@cosmos.wits.ac.za).

At Sudbury '92, a rather confusing image of the Vredefort Structure in South Africa was presented [1]. No definite shock-metamorphic evidence had been obtained, and a major stumbling block on the way toward universal acceptance of an impact origin for this structure was the alleged existence of multiple generations of "pseudotachylites." The critical reception this presentation met with led to the continuation of multidisciplinary studies in South Africa and kindled the interest of some overseas workers. The following years brought a wealth of new information bearing on the origin of the Vredefort Structure and its relationship to the surrounding Witwatersrand Basin [2]. Milestone results included (1) the confirmation that most pseudotachylitic breccia was formed at ca. 2 Ga, (2) the recognition of bona fide shock-metamorphic effects in quartz and zircon, (3) U-Pb single zircon dating of pseudotachylitic breccia at 2023 ± 4 Ma, providing the first well-constrained age for the impact event, and (4) the identification of a trace meteoritic component in Vredefort Granophyre. Scaling of deformation effects and integrated geophysical modeling resulted in estimates for the original size of the Vredefort impact structure of ~300 km.

The impact origin of the Vredefort Structure, as well as the fact that it represents one of the three largest impact structures known on Earth, has now been resolved convincingly. The Vredefort Dome was recognized as the root zone of the central uplift structure of a much larger, Witwatersrand Basin-wide, impact structure. Vredefort provides, in comparison to the less deeply eroded Sudbury and Chicxulub structures, a window into the deep-level structure of a very large impact structure. However, recent work casts doubt on the validity of several earlier conclusions, including the stratigraphy of the basement core, previously believed to represent an extension of the upturned collar strata ("crust-on-edge" model), and the alleged presence of a Vredefort Discontinuity between Outer Granite Gneiss and Inlandsee Leucogranofels. The nature of the general deformation styles exposed in the basement core is less than well understood, and the role of various possible heat sources that could have contributed to the regional thermal metamorphism is still debated. Another aspect of vital importance to the understanding of large impact structures and for future exploitation of the economic resources of the Witwatersrand Basin is the nature of the macrodeformation throughout the basin and which aspects of it are of pre-, syn-, and postimpact age.

These and other remaining problems must be addressed through detailed mapping and geophysical study. In addition, the vast Witwatersrand drill-core repository and structural information pertaining to the whole basin need to be reexamined from an impact-geological view.

References: [1] Reimold W. U. (1992) *LPI Contrib. No. 790,* 59–60. [2] Reimold W. U. and Gibson R. L. (1996) *J. Afr. Earth Sci., 23,* 125–162.

PALEOPROTEROZOIC TECTONISM IN THE EASTERN PENOKEAN OROGEN AND ITS SIGNIFICANCE FOR THE ORIGIN OF THE NORITE OF THE SUDBURY IGNEOUS COMPLEX. U. Riller[1] and W. M. Schwerdtner[2], [1]Institut für Geologie, Universität Würzburg, Pleicherwall 1, 97070 Würzburg, Germany (uriller@geologie.uni-wuerzburg.de), [2]Department of Geology, University of Toronto, 22 Russell Street, Toronto, Ontario M5S 3B1, Canada.

Lower Huronian supracrustal rocks host the 2.3-Ga granitoid Creighton and Murray plutons and form the southern footwall of the 1.85-Ga synformal Sudbury Igneous Complex (SIC). Understanding the history and style of Paleoproterozoic deformation of these rocks is necessary to constrain the primary geometry and origin of the SIC. An interpretation of the SIC as a thick impact-melt sheet that differentiated *in situ* into a granophyre, gabbro, and norite layer has recently gained popularity, but this intepretation requires geometric modification of the horizontal melt sheet by noncylindrical folding. Alternatively, models in which the SIC is regarded as a discordant funnel-shaped intrusion or as a combination of an intrusive component (the norite) and an impact melt (the granophyre) are open to discussion.

Because of their proximity to the SIC, the preservation of synformal Huronian outliers in Archean granitoids, high-grade metamorphic rocks of the Levack gneiss complex, and overturned Huronian strata in the southern footwall have often been linked to impact cratering. We attribute these effects to crustal doming (noncylindrical buckling) during the Blezardian tectonic pulse, ca. 2.4–2.2 Ga. This led to the formation of broad antiforms cored by Archean basement and tight synformal keels of Huronian cover rocks in the eastern Penokean Orogen. Synkinematic emplacement of the Creighton and Murray granitoid sheets into the hinge zone of a south-verging dome, larger than the SIC at the present erosion level, constrains the age of doming in the Sudbury area. Furthermore, structures attributed to steepening of Huronian strata in the southern footwall of the SIC are cut by unstrained norite. Large amounts of shear-related tilting of Huronian strata after emplacement of the norite are therefore implausible.

Although buckle folding was a major deformation process during the Penokean tectonic pulse (ca. 1.9–1.75 Ga), shortening of the SIC appears to have been accomplished mostly by northwestward translation of the South Range along thrust surfaces of the South Range Shear Zone. Strain fabrics of this shear zone are continuous with, and kinematically related to, granitoid and quartzite mylonite at the basement-cover interface southwest of the SIC and are most likely linked to the Murray Fault. The paucity of ductile strain fabrics in the southwestern nose of the norite sheet and in its thermal aureole suggest that the norite nose is not due to high-amplitude buckling after its solidification. Furthermore, uniform northwest-southeast-directed contraction indicated by small-scale brittle discontinuities is incompatible with noncylindrical folding of the SIC at a late stage of Penokean deformation. In summary, new structural data and insights do not support an origin of the norite with a simple horizontal sheet geometry (i.e., impact melting). Therefore, we favor an intrusive origin of the norite whereby its emplacement and deformation were strongly controlled by preexisting curved lithotectonic interfaces.

CHARLEVOIX AND SUDBURY AS SIMPLE READJUSTED CRATERS. J. Rondot, Astrobléme Exploration, 1111 d'Amiens, Sainte-Foy, Quebec G1W 4C8, Canada.

The geomorphometry of the Charlevoix astrobleme (Quebec) is easy to measure because of slipping out of allothonous breccia in the Saint-Laurent depression, which has left a hollow in the Precambrian shield. Here we can observe the crater rim (D), an annular graben between –0.64 D + 13% and 0.64 D – 13%, a crown of small hills in the inner plateau, a small inner depression at 0.32 D ± 13%, which is also the lowest part of the crater with impactite and the limit of the central uplift, and finally, for Charlevoix, Manicouagan, etc., a central peak at 0.13 D, not always in the center (Fig. 1). The modification stage of the original crater at 0.5 D has been made by slipping of great masses of terrain along listric surfaces, which are faults with a special type of breccia (mylolisthenite) [1]. In Charlevoix, mylolisthenite dikes have a mostly cataclastic matrix with 10% to >60% of fragments of former breccia. These dikes are concentrated around the central uplift, near the inner depression, in the graben, and at the rim. There are also injected impactite dikes in the floor of the excavated crater and filling of transient crevices by allochthonous debris to the rim in the open listric fault.

Geomorphometry of the Ries (Germany) will help to compare Charlevoix with Sudbury. Features include a rim (D) at 26 km [2], a ring of subsidence of the sedimentary cover at 0.64 D, and a basin at 0.4 D, with the deepest part at 0.32 D, which is 0.030 D below the old surface (measurements are based on a schematic cross section determined by geophysical methods) [3]. The inside crater suevite is about 0.015-D thick [4].

Geomorphometry of the Sudbury Structure (Ontario) is similar to that of the Ries, with a central basin and a crown of down-faulted Huronian outliers. Since the time of the discovery of the structrue as an astrobleme by Dietz [5], the estimated diameter of the structure has grown (100–120 km [6], 140 km [7], 190–200 km [8], 175–

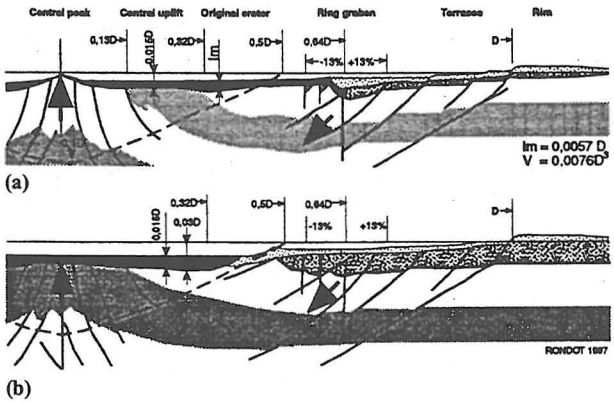

Fig. 1. Schematic cross section of two types of astroblemes modified from Rondot [1]. Im = inside crater breccia and impactite. V = excavated volume; for Sudbury = 6×10^4 km³; **(a)** well-readjusted crater; **(b)** partly readjusted crater.

245 km [9], and 200–280 km [10]). The center of the Sudbury Structure before deformation can be placed at the southwestern end of Lake Kelly, based on the deposition of the Huronian outliers in an arc. They begin 49 km from that point. At 0.48 D, as it is for the beginning of Ordovician beds in the Siljan graben [11], the diameter is given as 200 km. Peredery and Morrison found dike breccia at the northwestern arm of Lake Temagami, 99 km from the center or 200 km from the final diameter [8]. That diameter would give the thickness of the SIB 0.015 D as 3 km, measured in Deutsch et al. [10]. Sudbury is a simple readjusted crater as Charlevoix but with a central uplift proportionately 15% less important in volume. The Creighton granite was uplifted at least 14 km before Penokean deformation.

References: [1] Rondot (1994) *Earth Sci. Rev., 35,* 331–365. [2] Hüttner et al. (1980) *Geol. Jahrb. Reihe E., 19,* 95–117. [3] Pohl et al. (1997) in *Impact and Explosion Cratering,* pp. 343–404, Pergamon. [4] von Engelhardt and Graup (1984) *Geol. Rundsch., 732,* 447–481. [5] Dietz (1964) *J. Geol., 72,* 412–434. [6] French (1970) *Bull. Volcanol., 34,* 466–517. [7] Grieve and Robertson (1979) *Icarus, 38,* 211–229. [8] Pederery and Morrisson (1984) in *Ontario Geol. Surv. Spec. Vol., 1,* pp. 491–511. [9] Lakomy (1990) *Meteoritics, 25,* 195–207. [10] Deutsch et al. (1995) *Geol. Rundsch., 84,* 697–709. [11] Rondot (1975) *Bull. Geol. Inst. Univ. Upps.,* N.S. 6 Uppsala.

DO OUTLIERS OF THE HURONIAN SUPERGROUP MARK THE DOWNFAULTED RIM OF THE SUDBURY CRATER? D. H. Rousell and D. G. F. Long, Department of Earth Sciences, Laurentian University, Sudbury, Ontario P3E 2C6, Canada.

A series of outliers of the Paleoproterozoic Huronian Supergroup is preserved in a 20-km-wide arcuate belt northwest of the Sudbury Igneous Complex. Forty years ago it was suggested that these outliers represented the remnants of a discontinuous syncline. Ten years later it was proposed that they were preserved in grabens formed as a result of collapse of a multiring impact crater associated with emplacement of the Sudbury Igneous Complex. This interpretation has been accepted by most subsequent investigators without question, to the extent that the position of the outliers has been used to estimate the size of the supposed crater. Our observations indicate that Huronian strata in the outliers were deposited in a series of paleo-valleys on a terrane with considerable topographic relief. The asymmetric nature of the fill in some of the outliers suggests deposition may have taken place in half-grabens. The outliers are preserved in synclines developed during an early phase of the Penokean Orogeny, prior to 1850 Ma. These were cut by later transverse, oblique, and longitudinal faults. The geometry of the outliers, combined with the character and directional attributes of the sedimentary fill, indicates that the outliers are not related to the Sudbury event.

SERENITATIS: THE OLDEST, LARGEST IMPACT BASIN SAMPLED IN THE SOLAR SYSTEM. G. Ryder, Lunar and Planetary Institute, 3600 Bay Area Boulevard, Houston TX 77058-1113, USA (zryder@lpi.jsc.nasa.gov).

The Serenitatis Basin was recognized in the early 1960s as a multiring impact basin [see 1]. Poikilitic impact melt breccias collected on the Apollo 17 mission, generally inferred to be Serenitatis impact melt, precisely define its age as 3.893 ± 0.009 Ga [2]. On the topographic map produced from Clementine data, the basin has a well-defined, circular structure corresponding closely with mare fill [3]. In the review by Spudis [1], this circular structure has a diameter of 620 km (Taurus ring). The main rim is deemed to have a diameter of 920 km (Vitruvius ring). Thus Serenitatis is both the oldest and the largest basin in the solar system to which we can confidently assign samples.

The central flooded part of the Serenitatis Basin displays a mascon gravity anomaly. Gravity and topographic studies by Neumann [3], correcting for the mascon, indicate that the crust was thinned to ~30 km compared to a surrounding thickness of ~55 km. The rim has a slightly thickened crust.

The Apollo 17 landing site lies between the Taurus and the Vitruvius rings. Remote studies show that the Taurus highlands differ in chemical composition from those around the Crisium and Nectaris Basins. They are consistently lower in alumina and higher in Fe and radioactive elements: the highlands are the noritic, rather than the anorthosite, stereotype of the ancient highlands. Tracks show that many of the poikilitic impact melt breccias rolled from high in the massifs, possibly from ledges. They vary in grain size and texture. Larger boulders display sharp contacts between texturally different units, which differ slightly but significantly in composition [4]. They have about 18% Al_2O_3 and incompatible elements of ~100× chondrites.

The breccias contain lithic clasts. Feldspathic granulitic breccias are the most common, but these do not form any significant component of the melt composition itself [5]. Other lithic components are mainly plutonic igneous rocks such as norite and troctolite. Ferroan anorthosites and mare basalts are absent. Mineral fragments suggest similar but more diverse mafic lithologies [6].

The evidence from rocks, remote sensing, and geophysics suggests that the target for the Serenitatis impact was a noritic one and consisted largely of pristine igneous mafic rocks rather than a megabreccia. As the melt moved out, it first picked up heavily comminuted mineral fragments similar to the target and later picked up larger fragments of such material. Finally, it picked up feldspathic granulitic breccias when the melt was too cool to dissolve them significantly into the melt. The melt finally came to rest in a location that, following slumping, formed the Taurus highlands.

References: [1] Spudis P. D. (1993) *The Geology of Multi-Ring Impact Basins,* Cambridge Univ. [2] Dalrymple G. B. and Ryder G. (1996) *JGR, 101,* 26069. [3] Neumann G. A. et al. (1996) *JGR, 101,* 16841. [4] Stockstill K. R. and Ryder G. (1995) *GCA Abstr. with Progr., 27,* A-290. [5] Ryder G. (1997) *LPS XXVIII,* 1227. [6] Ryder G. et al. (1997) *GCA,* 1083.

IMPACT-INDUCED MELTING OF GRANITIC ROCK SAMPLES IN SHOCK EXPERIMENTS. C. Schrand and A. Deutsch, Institut für Planetologie, Universität Münster, Wilhelm-Klemm-Strasse 10, D-48149 Münster, Germany (schrchr@uni-muenster.de).

For the simulation of impact-induced melting phenomena on Earth, a granitic whole-rock sample has been shocked at 85 GPa using a high-explosive reverberation technique [1] modified according to Hornemann [2]. Peak shock temperatures reached in reverberation experiments are significantly lower than those reached in

natural impact processes [e.g., 3]. To compensate for this effect, the device was preheated at 935 K to force whole-rock melting [2,4]. Peak pressure duration in the experiment amounted to ~1 μs. After the shock, the sample container was quenched; sample recovery was close to 100%. The thin section was investigated using optical microscopy, REM, and electron microprobe techniques.

The experiment was performed with a both-sides-polished, cylindrical disk (diameter = 15 mm, thickness = 0.5 mm) of granite from St. Blasien, Black Forest (Germany). This rock with a mean grain size of 0.1–0.3 mm is composed of 31.6 vol.% quartz, 32% plagioclase (An_{8-38}), 20.3% K-feldspar, 14.3% biotite, and 1.8% apatite and zircon.

The main characteristic of the shocked granite is the total loss of the original texture. The recovered sample displays diaplectic as well as shock-fused melt glass with textural and compositional heterogeneities on the micrometer scale. Most parts of plagioclase and K-feldspar are transformed to melt glasses with a high density of vesicles. Biotite is transformed to vesicular melt glass with flow structures pervading large parts of the sample. For the first time in experimentally shocked rocks, we have observed tiny spinels (magnesio-spinel-hercynite solid solution with minor ulvöspinel, magnetite, and chromite components) and biotite crystals, newly crystallized from the shock-induced biotite melt [5]. Evidence for the total melting of quartz grains is lacking; the cores of individual grains consist of diaplectic glass with a high density of bubbles. Their alignment along roughly parallel planes indicates that these bubbles are remnants of fluid inclusions in the quartz of the unshocked reference rock. Quartz fragments <50 μm incorporated in mobile vesicular melts show a 2-μm-thick glass rim reflecting the incipient dissolution and mixing with the surrounding melt. Still smaller fragments are transformed to droplets of shock-fused quartz glass.

The original grain boundaries between K-feldspar, biotite and plagioclase are in part lined with impact-melt glasses containing schlieren with a high degree of compositional heterogeneity on the micrometer scale. The presence of such melt glasses establishes that the threshold for shock melting was reached in the experiment, despite the short peak pressure pulse.

In its overall characteristics, the experimentally shocked granite sample resembles highly shocked gneiss clasts reported from the allochtonous breccia lens at the Haughton impact structure in Canada [4].

References: [1] Müller W. F. and Hornemann U. (1969) *EPSL, 7,* 251. [2] Hornemann U. (1994) *Workshop Nördlingen, Vol.* 9. [3] Martinez I. et al. (1995) *JGR, 100,* 15465. [4] Langenhorst F. and Deutsch A. (1994) *EPSL, 125,* 407. [5] Schrand C. and Deutsch A. (1996) *Meteoritics & Planet. Sci., 31,* A124. [4] Martinez I. et al. (1993) *EPSL, 119,* 207.

CONSTRAINTS ON THE NATURE AND DISTRIBUTION OF IRIDIUM HOST PHASES AT THE CRETACEOUS-TERTIARY BOUNDARY: IMPLICATIONS FOR PROJECTILE IDENTITY AND DISPERSAL ON IMPACT.

B. C. Schuraytz[1], D. J. Lindstrom[1], and V. L. Sharpton[2], [1]Planetary Science Branch, Mail Code SN4, NASA Johnson Space Center, Houston TX 77058, USA, [2]Lunar and Planetary Institute, 3600 Bay Area Boulevard, Houston TX 77058, USA.

Among Cretaceous-Tertiary boundary sites worldwide, variations in the concentrations and ratios of elements commonly enriched in meteorites complicate traditional geochemical attempts at impactor identification. Yet they may provide constraints on the physical and chemical processes associated with large-body disruption and dispersal, as well as with diagenesis of projectile components. To this end, we continue our efforts to identify the mineral host-phases of projectile-derived elements, particularly for Ir, and to document their partitioning between crater deposits and ejecta resulting from the Chicxulub basin-forming impact.

Building on earlier work [1], we used INAA to measure Ir concentrations in successively smaller splits of finely powdered impact melt breccia from the Chicxulub Crater in Mexico (sample Y6-N19-R(b); Table 1 in [2]), and K/T boundary fish clay from Stevns Klint, Denmark (sample FC-1, split from 40 kg of homogenized material intended as an analytical standard [3]). Results (see Fig.1) for the Chicxulub sample show a heterogeneous Ir distribution and document that at least five discrete Ir-bearing host phases were isolated in subsequent splits (filled symbols), having Ir masses equivalent to pure Ir spheres from ~0.8 to ~3.5 mm in diameter. Three of these are within a sufficiently reduced mass of powder to warrant searching for them using backscattered electron microscopy.

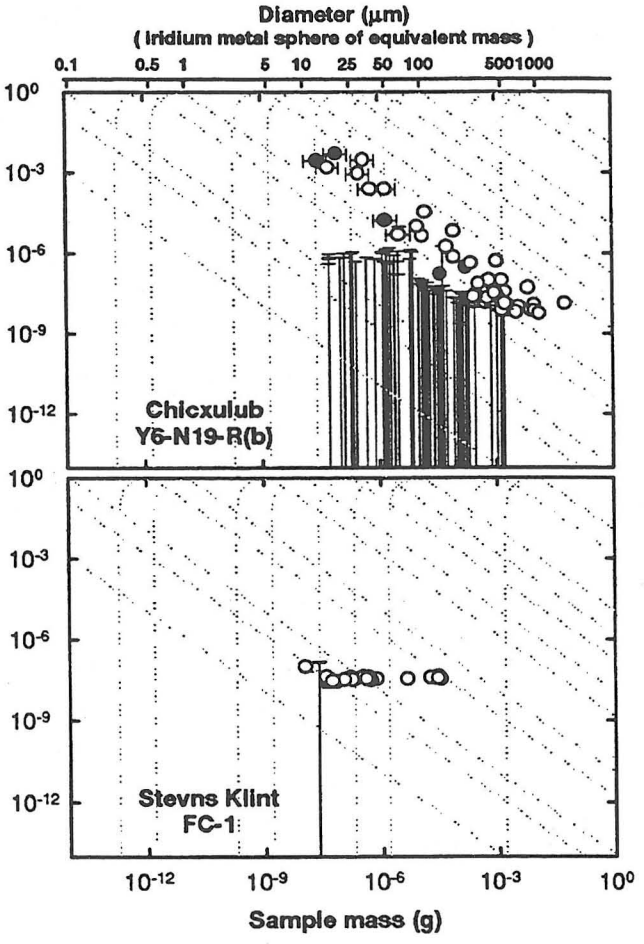

Fig. 1.

In contrast, successively smaller splits of the Stevns Klint fish clay show no statistically significant deviation from the reported value of 32 ± 2 ng/g Ir [3], suggesting a uniform Ir host-phase distribution. For the smallest split obtained thus far (100 ± 40 ng/g Ir), a pure Ir sphere of equivalent Ir mass would be <0.05 mm in diameter. (*n.b.* Although homogenizing and sieving of FC-1 to <75 mm obviously obscured variations in stratigraphic distribution, it is unlikely to have affected the size-frequency distribution of Ir host phases.)

We previously identified micrometer-scale Ir host phases by electron microscopy in melt-rock samples from two widely separated drill holes at the Chicxulub Basin [1], including a replicate split of Y6-N19-R. One is an aggregate of subhedral Ir metal grains enclosed in silicate, in which no other Pt group elements (PGE) were detected. A second particle with twice the mass as the first, concentrated predominantly in a single grain, is associated with minor concentrations of Os, Ru, and Pt, and with adhering particles of corundum and perovskite. A third Ir-rich particle, with a greater apparent Os concentration, was identified before being lost as a result of charging under the electron beam.

In addition to demonstrating the preservation of projectile components within the Chicxulub Crater, analogous phase associations in Ca- and Al-rich inclusions (CAI) from C2 and C3 chondrites [4,5] suggest to us that these melt-rock Ir host phases are relics from a carbonaceous chondrite K/T boundary impactor. Although the obviously low Ru/Ir ratios of the Chicxulub Ir host phases are qualitatively consistent with suggested PGE fractionation with distance during condensation in an ejecta cloud [6], it seems difficult to explain the accumulation of the ~3 × 10^{11} Ir atoms required to form a ~10^{-10} g nugget of pure Ir metal within a jet of vaporized projectile expanding at 1–4 km/s [6], or to effectively exclude or remove commonly alloyed PGE and siderophile elements by fractionation processes resulting from condensation, oxidation, sulfidization, exsolution, or autometamorphism during cooling of the melt. We do not dismiss the importance of these processes entirely; on the contrary, other geochemical and mineralogical aspects of the melt rocks require them, and condensation from the expanding ejecta cloud appears to best explain the primary Ir host-phase distribution in the fish clay, as well as the high Ir concentrations associated with spinel-bearing spheroids at the K/T boundary in the Pacific Ocean [7,8]. If the "relict" hypothesis is correct, micronuggets of other PGEs and alloys, not detected by our INAA screening, should also occur in the melt rocks. Possibly, the discrete host phases with lesser Ir masses (see Fig. 1) are such alloys with subordinate Ir, rather than simply smaller, predominantly Ir-bearing particles. A CAI source for the relics would be consistent with either a comet or an asteroid K/T impact at Chicxulub.

References: [1] Schuraytz B. C. et al. (1996) *Science, 271,* 1573–1576. [2] Schuraytz B. C. et al. (1994) *Geology, 22,* 868–872. [3] Gwozdz et al., unpublished report. [4] El Goresy A. et al. (1978) *Proc. LPSC 9th,* 1279–1303. [5] Greshake A. et al. (1996) *Science, 272,* 1316–1318. [6] Evans N. J. et al. (1995) *EPSL, 134,* 141–153. [7] Robin E. et al. (1993) *Nature, 363,* 615–617. [8] Kyte F. T. et al. (1996) *GSA Spec. Paper 307,* 389–401.

CHARACTERISTICS OF THE FROOD-STOBIE PSEUDOTACHYLYTE BELT, SUDBURY IMPACT STRUCTURE, CANADA. R. G. Scott and J. G. Spray, Department of Geology, University of New Brunswick, Fredericton, New Brunswick E3B 5A3, Canada (h1jaw@unb.ca; jgs@unb.ca).

The Frood-Stobie breccia belt is a subconcentric arc of pseudotachylyte, ranging from 0.1 to 0.5 km in width and 45 km in length, to the Sudbury Igneous Complex (SIC) in the South Range basement rocks of the 1.85-Ga Sudbury impact structure. The belt is best exposed to the east of the Copper Cliff radial offset, which intersects it. To the west, the belt is poorly exposed but is well expressed in regional aeromagnetic data as a 120 nT high.

The belt consists of rounded, elongated breccia clasts and blocks of 2.0-Ga Huronian Supergroup metasedimentary and metavolcanic basement rocks [1], ranging in size from several millimeters to tens of meters. The pseudotachylyte matrix is a dark, fine-grained recrystallized frictional melt consisting of quartz, biotite, plagioclase, potassic feldspar, and ilmenite, along with minor pyrite and pyrrhotite. The biotites typically contain Cl, which, with other halogen-bearing minerals, is particularly evident in association with the ore deposits. Numerous inclusions of biotite and apatite are found within the quartz and feldspar grains. Zircons are ubiquitous in association with the biotite grains and provide an avenue for future U-Pb dating of the pseudotachylyte. The matrix appears annealed, with no melt glasses remaining. The pseudotachylyte is locally massive but is usually strongly foliated. This biotite foliation may represent a primary flow structure or a metamorphic foliation formed during Penokean (1.85 Ga) and/or Grenvillian (1.0 Ga) compression from the southeast [2,3].

The belt hosts one of the world's richest deposits of Ni-Cu-PGE ore, the Frood-Stobie mine complex, which has been in production for more than 100 years. Additionally, deposits at the Kirkwood mine at the eastern contact with the SIC, and at the Victoria mine at the western contact with the SIC, contribute to the considerable economic significance of the pseudotachylyte belt.

These Ni-Cu deposits are associated with quartz diorite bodies that are typically hosted by the pseudotachylyte, both of which may have been injected into the pseudotachylyte from the lower levels of the SIC at an early stage of its differentiation. The ores are primarily composed of massive to disseminated chalcopyrite, pyrrhotite, and pentlandite. Unusual Pd-bearing minerals such as michenerite (PdBiTe) and froodite ($PdBi_2$) have been found in ore samples from the Frood mine [4].

The Frood-Stobie belt is thought to be derived from high strain-rate (>1 m s^{-1}) frictional comminution and melting of the country lithologies during collapse of the transient cavity and subsequent slumping of the crater walls [5]. Structural studies of Penokean and Grenvillian thrusting from the southeast indicate that the exposed rocks of the belt have been uplifted 5–6 km and subsequently eroded [2,3]. This contrasts with pseudotachylyte belts in the North Range, which are considerably thinner in width and less tectonically deformed [6], but are nevertheless indicative of multiring basinal formation by high-speed slip along concentric fault surfaces [5].

References: [1] Card K. D. et al. (1977) *Geoscience Study 16,* Ontario Div. Mines. [2] Deutsch A. et al. (1995) *Geol. Rundsch., 84,* 697–709. [3] Hirt A. M. et al. (1993) *Tectonophysics, 225,* 231–254. [4] Cabri L. J. et al. (1973) *Can. Mineral., 11,* 903–912. [5] Spray J. G. and Thompson L. M. (1995) *Nature, 373,* 130–132. [6] Thompson L. M. and Spray J. G., *Contrib. Mineral. Petrol., 125,* 359–374.

ASSESSING IMPACT TRAJECTORY IN THE GEOLOGIC RECORD. P. H. Schultz, Department of Geological Sciences,

Brown University, Providence RI 12912, USA (peter_schultz@brown.edu).

A paradigm exists that impact craters must be largely circular due to the overall symmetry of the intense, expanding shock at large distances from the point of impact. This paradigm is reinforced by a cursory examination of impact craters on other planets, by terrestrial field experience, and by laboratory impact experiments in particulate targets. With this paradigm, most observed asymmetries are attributed to either differential erosion or overprinting by the regional structure. Only the lowest-angle impacts producing obviously elongated shapes, therefore, are easily recognized [1,2]. Here it is proposed that impact angles as high as 50° from the horizontal can produce diagnostic asymmetries in primary patterns of deformation and modification that hold clues for impact trajectory.

Trajectory Indicators: Most terrestrial impacts are heavily eroded; hence, correlations between asymmetries in ejecta deposits and crater structure are rarely possible. Consequently, the planetary impact record and laboratory experiments provide the best clues for recognizing trajectory effects. These clues include the following features for complex craters and basins: uprange offset of the central uplift (peak, peak-ring, or gravity anomaly) related to the maximum transient depth; breached or elongated central peak or ring reflecting the compression stage; greater central peak diameter ring relative to crater diameter (for a given diameter); pear-shaped crater outline; deep rim faults uprange (shallow downrange); maximum structural rim uplift perpendicular to the trajectory; maximum shock effects at depth perpendicular to the trajectory; minimal shock effects uprange; reduced shock at depth downrange; faults and fractures at depth parallel to trajectory downrange; enhanced shear deformation at depth downrange; and enhanced impactor signature in downrange melts. These general signatures of trajectory apply for impact angles between 15° and 30°, but some elements persist to higher angles. They also become more evident with increasing crater size due to reduced cratering efficiency at large scales [3]. All signatures, however, can be clearly documented for craters from 15 to >1000 km diameter on the Moon, Mars, and Venus, where the preserved distribution of ejecta allows corroborating evidence [4,5]. Moreover, all signatures can be documented in much smaller-scale hypervelocity laboratory experiments under controlled conditions that trace the distribution of peak pressures.

Because many terrestrial impact structures have been extensively eroded below the crater rim and well into the central peak, asymmetries in crater outline comparable to preserved analogs on planetary surfaces are lost. The outer limits of impact-induced failure near the surface are not the same as at depth. Near-surface failure is controlled by tensile strength following passage of the shock. Tensile strength is not only weaker than compressive strength but also depends on strain rate. Consequently, near-surface failure should extend well beyond the excavation rim and should increase with crater size beyond expectations for constant strength versus gravity scaling [5]. This strain-rate dependence complicates derivation of impactor size from crater diameter and contributes to the apparent shallowing of craters with scale. Because the central uplift reflects the conditions of impactor penetration, it provides a more reliable indicator of impactor size [4,6]. Such processes contribute to the overall symmetry of the outer boundary of most craters, but asymmetry of the central structure preserves the fingerprint of the trajectory.

Possible Terrestrial Examples: The Chicxulub impact is believed to exhibit evidence for an impact trajectory from the southeast at 20°–30° [7]. It is suggested, however, that the Sierra Madera, Clearwater east-west lakes, and Vredefort impact structures also exhibit evidence for impact angles <45°. The Sierra Madera (Texas) structure is a heavily eroded structure (~13 km diameter) [8] that exhibits four key signatures: an elongated central uplift indicative of a northwest-southeast impact; maximum shock effects perpendicular to the elongated uplift (expressed by the outer limit of shatter cones); offset placement of the uplift to the northwest in this zone; and breccia dikes parallel to the uplift trend.

The Vredefort Structure also exhibits structural, gravitational, and magnetic asymmetries [9,10] that are often attributed to preexisting or postimpact faulting. Nevertheless, the striking similarity with other, even larger oblique impact structures on the Moon should at least raise the possibility that its pear-shaped outline is an expression of trajectory. Such a proposal may help explain its enigmatic shock record [11].

References: [1] Gault D. E. and Wedekind J. (1978) *Proc. LPSC 9th,* 3843–3875. [2] Schultz P. H. and Gault D. E. (1990) *GSA Spec. Paper 247,* 239–261. [3] Schultz P. H. and Anderson R. A. (1996) *GSA Spec. Paper 302,* 397–417. [4] Schultz P. H. (1992) *JGR, 97,* 16183–16248. [5] Schultz P. H. (1996) *LPS XXVII,* 1147–1148. [6] Schultz P. H. and Gault D. E. (1993) *LPS XXIV,* 1257–1258. [7] Schultz P. H. and D'Hondt S. (1996) *Geology, 24,* 963–967. [8] Wilshire H. G. et al. (1972) *Geol. Surv. Prof. Paper 599-H.* [9] Corner et al. (1990) *Tectonophysics, 171,* 49–61. [10] Hart R. J. et al. (1995) *Geology,* 277–280. [11] Grieve R. et al. (1990) *Tectonophysics, 171,* 185–200.

SHOCK ATTENUATION AND BRECCIA FORMATION AT A COMPLEX IMPACT STRUCTURE: SLATE ISLANDS, NORTHERN LAKE SUPERIOR, CANADA.

V. L. Sharpton and B. O. Dressler, Lunar and Planetary Institute, 3600 Bay Area Boulevard, Houston TX 77058, USA (sharpton@lpi.jsc.nasa.gov; dressler@lpi.jsc.nasa.gov).

The Slate Islands archipelago, located ~10 km south of Terrace Bay, Ontario, represents a 7–8 km diameter central uplift of a 30–32 km complex impact structure [1]. Recent ^{40}Ar-^{39}Ar analyses indicate that the structure is ~450 m.y. old [2]. Archean and Proterozoic felsic and mafic intrusive and extrusive rocks and metasediments constitute the target assemblage [3]. Shatter cones, strong brecciation, and shock-metamorphic mineral deformation demonstrate that the structure was formed as the result of a comet or asteroid impact.

Impact-generated breccias account for ~15–25% of the islands [4]: (1) *pseudotachylites*: These fine-grained-to-aphanitic, inclusion-poor veinlets have sharp host-rock contacts and dendritic apophyses; field relationships indicate that these breccias are some of the earliest formed, probably during the compressional stage of the impact process, and they appear to be relatively scarce; (2) *polymict, clastic matrix breccias*: these occur as dikes and irregularly shaped bodies, a few centimeters to >10 m wide; they have sharp contacts with the host rocks and were formed during the decompression stage of the impact process, somewhat later than the pseudotachylites; they cut across pseudotachylite veins and contain inclusions of them; this is the most common type of Slate Islands breccia; (3) *monomict, autoclastic breccias*: these have a shattered appearance but retain

the basic target stratigraphy and structural elements; these breccias have transitional host-rock contacts and appear to be confined primarily to exposures on the outlying islands of the archipelago; fragments of polymictic clastic matrix breccia dikes found within some autoclastic breccias indicate that generation of these deposits extended into the later stages of the impact process; and (4) *allogenic breccia deposits*: these consist of vestiges of extensive polymict clastic matrix breccia overlying the shocked parautochthonous basement. Some deposits are suevitic and show evidence of having once contained glass as well as highly shocked rock fragments; others, however, showing no conspicuous evidence of altered glass, may be more akin to bunte breccia. These deposits constrain the level of erosion to only a few hundred meters at most [5], considerably less than previous estimates [e.g., 1].

Shatter cones occur on all islands of the archipelago, indicating that all target rocks on the islands experienced minimum shock pressures of 4 ± 2 GPa. Other shock metamorphic features are kink bands in micas, planar microstructures in quartz and feldspar, minor maskelynite, and impact glass. Based on the petrography of more than 100 thin sections of quartz-bearing target rocks and the correlation of the frequency of low-index planar deformation features in quartz with results from shock recovery experiments, the peak shock pressures experienced by individual samples were estimated. In general there is a decrease in shock pressure from ~20 to 25 GPa near east-central Patterson Island, the largest and central island of the archipelago, to about 5–10 GPa at the eastern shore of this island. The shock attenuation gradient is ~4.5 GPa/km across the island group. The shock level distribution, however, has a roughly circular plan only over the western part of the archipelago, consistent with the recently revised placement of the crater center [5]. A relatively large area of southeastern Patterson Island is characterized by shock levels below those needed to produce planar deformation features. These results are not consistent with the conventional view that shock levels across the uplifted basement near the center of a complex crater accurately preserve the systematic radial attenuation of the shock wave from a point source. Instead, differential movement of large target blocks during the uplift has imparted a decidely irregular and fragmented pattern to the recorded shock pressures across the exposed central portion of this crater.

The orientation of planar deformation features in quartz was studied in one oriented chert sample, and it appears to be independent of the shock-wave direction, suggesting that the crystal structure exerts the primary control on planar microstructure development.

References: [1] Halls H. C. and Grieve R. A. F. (1976) *Can. J. Earth Sci., 13,* 1301–1309. [2] Sharpton et al. (1997) *LPS XXVIII,* 1287–1288. [3] Sage R. (1991) *Ont. Geol. Surv. Rpt. 264.* [4] Dressler B. O. and Sharpton V. L. (in press) *Tectonophysics.* [5] Sharpton et al. (1996) *Geology.*

IMPACT DEPOSITS FROM THE SOUTHERN INNER FLANK OF THE CHICXULUB IMPACT BASIN. V. L. Sharpton[1], L. E. Marín[2], C. M. Corrigan[3], and B. O. Dressler[1], [1]Lunar and Planetary Institute, 3600 Bay Area Boulevard, Houston TX 77058, USA (sharpton@lpi.jsc.nasa.gov), [2]Instituto de Geofisica, Universidad Nacional Autónoma de Mexico, Ciudad Universitaria, Mexico City 04510, Mexico, [3]Michigan State University, E. Lansing MI, USA.

The Chicxulub impact basin formed in a mixed target sequence consisting of 2–3 km of interbedded carbonates and evaporites of Cretaceous age overlying Pan-African granites and gneisses with minor sands and shales [1]. During an UNAM-led campaign of shallow drilling along the southern flank of the buried basin, ~1000 m of impact breccia and melt-rock samples were extracted from three wells located 110–150 km from the center. Figure 1 shows the basic crater stratigraphy in these three wells.

The U5 well (~110 km) intercepted an apparently complete impact sequence at a depth of ~330 m. This sequence consists of a 30–40-m-thick altered melt-rock unit overlying crater suevite. Within the melt-rock unit are infrequent pebble-to-cobble-sized clasts of highly shocked and partially melted basement, as well as weakly shocked platform rocks. Major-element chemistry of the matrix materials [2] within the suevite indicates that this unit is strongly enriched in silicate basement protolith. The contribution from the overlying platform sediments, either as a primary component or a local component added during emplacement, is constrained to be <30% of the total mass [2]. Centimeter-scale clasts of partially altered to unaltered melt rock and decimeter-to-meter-scale highly shocked basement clasts are found throughout the cored interval. Melt clasts are the most abundant clast type near the top of the suevite. Coring was terminated (T.D. = 503 m) in suevite.

The U7 well (~125 km; 702 m T.D.) penetrated a thick sequence of suevite, but no melt rock was recovered. Instead, an unconformity separates the truncated upper part of the suevite deposit from the overlying post-crater sediments. Core inspections and major-element chemistry indicate that a major change in the breccia characteristics occurs at a depth of 375–578 m. Breccia samples below this boundary have considerably fewer and smaller crystalline rock clasts, virtually no melt clasts, and a matrix dominated by protolith derived from the platform sequence [2]. In these ways, this lower breccia is analogous to bunte breccia from the Ries Crater. Below ~375 m, the breccia sequence is interrupted by 10–50 m thick zones of tilted and disrupted Cretaceous limestone and dolomite. The jumbled nature of these blocks indicates that they represent large clasts incorpo-

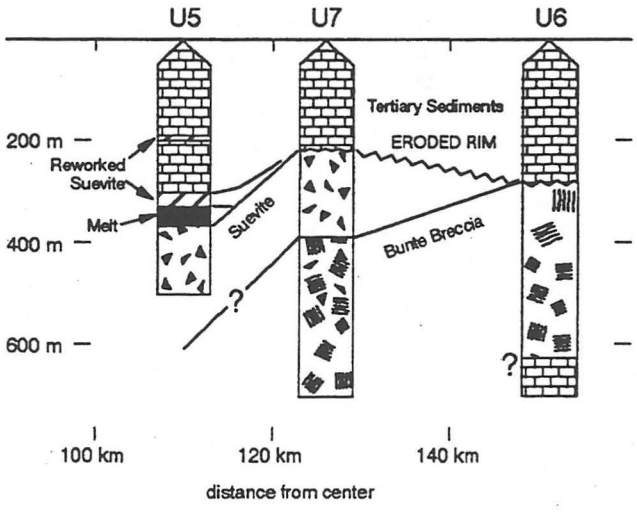

Fig. 1. Stratigraphy of drill-core sites UNAM5, UNAM6, and UNAM7. Vertical axis is depth from surface and horizontal axis shows distance from basin center.

rated within the breccia-like deposits, either as spall from the excavation cavity or as large local blocks disrupted and mobilized during ejecta emplacement. Drill core U6 (~150 km; 700 m T.D.) revealed even more severe indications of erosion: The suevite unit is completely absent and the uppermost impact unit is an anhydrite-dolomite bunte breccia similar to that observed at similar distances in Pemex wells [1].

Prior to impact, the region was covered by a shallow sea probably no deeper than ~50 m [1], and the rim and ejecta units were subjected to subaerial erosion and reworking. Well stratigraphy suggests that, immediately after the impact event, there was over 400 m of total stratigraphic relief from U5 to U6, with the top of the U5 impact sequence ~150 m below the K/T sea level (approximated by the unconformity) and the preerosional top of the U6 sequence ~350 m above sea level. This paleobathymetry accounts for the preservation of an apparently complete sequence of impact units at U5 but not in wells located at greater distances. Furthermore, the zones of reworked suevite above the impact units at U5 indicate that erosion of more distal rim deposits continued well into the Eocene. All these observations affirm that, prior to its erosion, the topographic rim crest of the Chicxulub impact basin was outside U7, and not inside U5 as would be the case if Chicxulub were <200 km in diameter.

References: [1] Sharpton V. L. et al. (1996) *GSA Spec. Paper 307,* 55–74. [2] Corrigan C. M. et al., this volume.

DISTORTION INDEXES AND OTHER STRUCTURAL PARAMETERS AS A MEASURE OF DEGREE OF SHOCK METAMORPHISM IN QUARTZ. R. Skála, Czech Geological Survey, Klárov 3/131, CZ-11821 Praha, Czech Republic (skala@cgu.cz).

As the most important rock-forming mineral and an important material in technology, quartz has been subjected to many studies in mineralogy and material science. Existing studies of quartz properties and behavior cover almost every aspect concerning this phase.

Since quartz is one of the really ubiquitous minerals on Earth, and there are only a small number of terrestrial impact structures where this phase is not present, it is understandable why quartz was selected as an indicator of shock metamorphism in rocks. Many methods were used to study quartz grains to reveal fingerprints of shock comminution. Recently, transmission electron microscopy (TEM) and NMR spectroscopy have been the most popular examination methods. Research using TEM in some cases has even indicated that previous optical studies describing PDFs had found a kind of optical discontinuity, which, however, had nothing to do with impact metamorphism (structures Sevetin, Susice, and Azuara). Powerful X-ray diffraction methods were often forgotten in these studies although they could have provided valuable data on a relatively limited amount of material, mainly in the lower-pressure range where the lattice defects are not so pronounced. A number of papers have dealt with static compression studies of quartz using single-crystal X-ray diffraction methods. The aim of this abstract is to show how Rietveld crystal structure refinements of naturally shocked quartz corresponds to observations of statically compressed material.

For the study, quartz from the world-renowned Barringer (or Meteor) Crater in Arizona, U.S., was selected. Two samples expected to undergo different pressure histories were studied for mutual comparison. A weakly shocked specimen was collected at the crater rim, whereas the second specimen, corresponding to heavily shocked Coconino sandstone, was taken from the bottom of the crater and contained hyperbaric silica phases (coesite and stishovite) at low concentration. Both samples were crushed and ground in agate mortar in alcohol. The resulting powder was then placed on a Si wafer as the flat sample holder for diffractometric studies.

TABLE 1. Comparison of distortion indexes, tilt angle, bond angle variance, bond length variance, and tetrahedral volume for quartz form rim and center of the Meteor Crater.

	Rim	Center
Tilt angle, ϕ (°)	21.917	21.292
DI(TO)	0.058	0.034
DI(OTO)	3.018	3.066
DI(OO)	0.044	0.048
V_T(Å^3)	2.273	2.249
σ^2(OTO)	20.180	19.132
Δ(TO)	12.527	4.255

Powder patterns for Rietveld crystal structure refinement were collected using Philips X'Pert PW3710-MPD system with PW1830 X-ray generator and PW3020 goniometer in Bragg-Brentano reflecting arrangement with Cu-sealed tube and secondary graphite monochromator. High voltage was set to 40 kV and current was set to 40 mA. Step-scanned data were collected in the range 18–140°2θ with 0.01°2θ step and 10-s exposure per step.

The Rietveld program FullProf [1] was used to fit selected general (scale factor, half-width parameters, background coefficients, PSF shape factor, and asymmetry) and crystal structure parameters (unit-cell dimensions and fraction coordinates of Si and O). The space group used for refinement was $P3_121$, and starting unit-cell parameters were adopted from Glinnemann et al. [2] for quartz at ambient pressure.

The structural data were then processed by program BONDSTR to calculate bond lengths and angles. These values were then used for the computation of distortion indices as defined in Glinnemann et al. [2], tetrahedral tilt as in Grimm [3], quadratic elongation, and bond average variance as defined in Robinson et al. [4] (see Table 1). All these parameters were found to be dependent on static pressure during relevant experiments [2,5]. I had expected that natural shock load, as in the case of samples collected at the Meteor Crater, would have the same influence on these parameters as static compression. However, this was not the case. Dynamically compressed quartz does not follow trends observed for a statically compressed phase in values c/a ratio, tilt angle, absolute values of Si-O-Si angle, O-to-O distance between tetrahedra, and tetrahedral Si-O distances. On the contrary, the same trend was observed for distortion indices DI(OTO) and DI(OO), but the values of indices were significantly higher than those in static compression experiments. Values of DI(TO) cannot be used because there is no apparent correlation between pressure and DI(TO) (see controversial results in [2] and [5]). Results of this study show interesting behavior of quartz crystal structure on shock loading and should be repeated with a larger number of samples experiencing different impact histories to allow correlation between individual parameters and the expected pressure load. The calibration on experimentally shocked recovered material using single-crystal

data would significantly contribute to the discussion of this topic and could provide the necessary calibration. When properly tested, the method described here could provide important insight into the compression process and how material like quartz can accommodate the changes induced by shock by distortion of their lattice.

Acknowledgments: This research was undertaken as a comparative study to the project 205/95/0980 of the Grant Agency of the Czech Republic, which studies shock-induced effects in carbonate minerals to test applicability of this approach to carbonate phases on the phase with best-known behavior upon shock load.

References: [1] Rodriguez-Carvajal J. (1997) *FullProf v.3.2* (computer program). [2] Glinnemann J. et al. (1992) *Z. Kristal., 198,* 177–212. [3] Grimm H. and Dorner B. (1975) *J. Phys. Chem. Solids, 36,* 407–413. [4] Robinson K. et al. (1971) *Science, 172,* 567–570. [5] Levien L. et al. (1980) *Am. Mineral., 65,* 920–930.

X-RAY DIFFRACTION STUDY OF THREE CALCITE-RICH SAMPLES FROM THE KARA STRUCTURE.

R. Skála, Czech Geological Survey, Klárov 3/131, CZ-11821 Praha, Czech Republic (skala@cgu.cz).

The Kara Crater is located on the Kara River, near the shore of the Kara Sea on the slopes of the Pai-Khoi Ridge. The crater is developed in rocks of Proterozoic to Paleozoic age (shales, limestones, diabases, etc.) and was formed ~67 Ma [1,2]. The diameter of the crater was recently given as 120 km [2].

Eight samples from drill cores located within the Kara impact crater were studied. They came from suevites (six) and from shocked basement (two). All specimens were very fine grained, so optical microscopy appeared to be of limited use. Therefore, I examined all samples using powder X-ray diffraction. Five of the eight specimens revealed significant admixtures of quartz, feldspars, and clay minerals, so they were rejected from further XRD research. Nevertheless, clasts from suevite (drill cores KA1 and SA1) and the sample from shocked basement (KH0) contained small or no quartz admixture and were subjected to detailed study. Powder samples were prepared and placed on Si wafers. Step-scanned diffraction data were collected using a Philips PW3710-MPD diffractometer with Cu-sealed tube in the range 15–145°2θ with step width 0.02°2θ and step duration of 8–12 s.

Individual profile fitting has provided angular positions of reflections and their breadths and intensities. Profile breadths expressed as FWHM (in °2θ) plotted against diffraction angle differentiate data sets very well. As expected, clasts from suevite where the shock degree is variable revealed different values of peak widths.

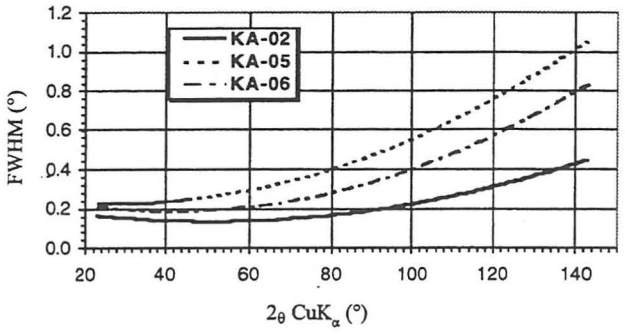

Fig. 1. Peak breadth vs. diffraction angle. Curves fitted on measured data using polynoms of second order.

TABLE 1. Unit cell parameters and integral intensities of reflections 012, 024, and 006 for studied carbonates.

	KA-02	KA-05	KA-06
a (Å)	4.9849(1)	4.9829(7)	4.9858(4)
c (Å)	17.0451(6)	17.040(4)	17.048(2)
V (Å³)	366.81(2)	366.4(1)	367.02(7)
c/a	3.4193	3.4197	3.4193
I(012)	16.5	14.8	17.2
I(024)	14.5	12.6	12.9
I(006)	21.0	14.4	7.6

TABLE 2. Oxygen fraction coordinate *x*, and bond lengths Ca-O and C-O for the calcite samples studied.

	KA-02	KA-05	KA-06
x	0.2721(6)	0.2731(5)	0.2723(5)
Ca-O	2.3204(7)	2.3191(6)	2.3194(5)
C-O	1.3538(13)	1.3559(11)	1.3577(10)

Peak widths measured from material coming from heavily shocked crater basement were higher than those of one of the suevite clasts (KA-02) but lower than those observed for the other suevite material (KA-05). Therefore, it can be expected that samples KA-05 and KA-06 underwent a shock event of a higher degree than did sample KA-02. In Fig.1, KA-02 stands for sample KA1, KA-05 is taken from specimen SA1 (both corresponding to suevite clasts), and KA-06 is identical with specimen KH0 and comes from the crater basement.

Another aspect revealed from individual profile fitting was change of unit-cell parameters and volume. Unit-cell volumes follow generally accepted trends: the higher degree of impact metamorphism, the higher the cell volume, though volume calculated for KA-05 does not agree with expected degree of shock inferred from other parameters. Details are given in Table 1.

Intensities of peaks (see Table 1) also change, the largest being a difference in intensity of 006 reflection. This large intensity is probably due to overlaps of 006 with 014, which is the highest peak at the diffraction pattern. In this case, the lower the 006 intensity, the higher expected impact-induced comminution.

Rietveld analysis of the whole diffraction patterns provided crystal structure information. Oxygen fractional coordinate *x* (the only variable parameter in the calcite crystal structure) remains almost essentially the same. Small differences were met only in bond lengths Ca-O and C-O within the crystal structure. For details see Table 2. The trend observed indicates shortening of Ca-O bond length with increasing expected shock load while the length of C-O bond becomes higher.

Based on all observed parameters, it can be concluded that the most intense impact metamorphism is recorded in samples KA-05 (clast from suevite) and KA-06 (crater basement).

Acknowledgments: The author would like to thank the Grant Agency of the Czech Republic for support of this project under contract No. 205/95/0980 and M. A. Nazarov, who provided samples from the Kara structure.

References: [1] Marakushev A. A. (1981) *Impaktiti.* [2] Nazarov M. A. et al. (1993) *Bull. Mosc. Izdat. Prirody, Otd. Geol., 68(3),* 13–32.

SHOCK-INDUCED EFFECTS IN MALMIAN LIMESTONES FROM THE STEINHEIM CRATER REVEALED BY X-RAY POWDER DIFFRACTION STUDY.

R. Skála[1] and P. Jakeš[2], [1]Department of Mineralogy and Petrology, National Museum, CZ-11579 Praha 1, Czech Republic (ais@nm.anet.cz), [2]Institute of Geochemistry, Faculty of Science, Charles University, Albertov 6, CZ-12843 Praha 2, Czech Republic (jakes@prfdec.natur.cuni.cz).

The goal of the study was to show the effects of impact metamorphism on carbonate sedimentary rocks of the Steinheim Crater as revealed in X-ray powder diffraction data.

The Steinheim Crater in Southern Germany lies in carbonate sedimentary lithologies of the Swabian Alb. Detailed data on the history and geology of the basin are given in Reiff [1]. The diameter of the structure varies between 3.1 and 3.8 km. The central feature of the crater is ~900 m in diameter and roughly 50 m high. Rocks occurring in the crater vicinity are Upper Malmian limestones and marls. Limestones and marls of Lower Malm and clays, limestones, and sandstones of Dogger are found in the central hill.

Limestones found both within and outside the crater are generally very fine grained. The use of optical microscopy thus does not allow for the indisputable recognition of impact-induced features in calcite grains. On the other hand, powder diffraction patterns can clearly record both dynamic and static pressure-induced defects in many types of target material (as described in [2]).

We have chosen unshocked Upper Malmian limestone from Heidenheim (about 6 km east of the crater center) as a reference material (ST-02), and country rocks from crater rim at Burgstall (ST-03, ST-12, ST-13), limestone breccia (ST-10), and samples containing shatter cones found near Steinheim on the slopes of the crater central feature (ST-05) as typical representatives of shocked lithology.

Our attention was focused on profile shapes that are generally sensitive to any change in size of crystallites and/or lattice strain. Unit-cell parameters as a measure of shift of position of individual reflections were also refined by ZDS software.

Rock samples were prepared in a routine way for the powder diffraction study. Diffraction data were collected using a Philips PW3710-MPD powder diffractometer in Bragg-Brentano reflecting geometry equipped with a proportional counter and graphite secondary monochromator. Copper radiation was utilized (PW1830 high-voltage generator operated at 40 kV and 40 mA). The range of step-scanning was 15–145°2θ with step size 0.02°2θ and exposure between 7 and 12 s per step for individual samples.

The most apparent feature of all collected powder patterns was increasing deformation of reflections shape with more violent expected pressure comminution. Generally, the higher expected shock metamorphism, the lower and broader reflections were observed. Another effect easily observable in the patterns was the progressive disappearance of reflection 006 at about 31.5°2θ CuKα due to its overlapping by tails of 104 reflection corresponding to the most intense peak in diffraction patterns and significant decrease of possibility to distinguish reflection 024 in clusters of three reflections roughly between 47 and 49°2θ CuKα. Mutual intensity ratios thus dramatically change, but this striking difference cannot be used uncritically because of the possible variation in chemistry that must be taken into account before any serious conclusions can be made.

There is a strong tendency for increase of absolute FWHM value for particular reflections in certain powder patterns with higher expected shock load (see Fig. 1). This tendency is fully compatible with observations for quartz published by Skála [3].

Unit-cell volumes follow trends found in, e.g., shocked quartz (i.e., they become higher with more severe expected impact treatment of the sample). Nevertheless, overall differences are not so pronounced as in the case of FWHM's.

X-ray powder diffraction study thus has proved its usefulness for research of this type of target material, and the study of reflection broadening has clearly indicated the way strong shock-induced effects can be found in calcite-bearing material.

Acknowledgments: The authors would like to express their thanks to the Grant Agency of the Czech Republic for supporting the study of the effects of shock metamorphism in carbonates with its grant No. 205/95/0980. We are also indebted to Winfried Reiff for providing samples for the study.

References: [1] Reiff W. (1977) in *Impact and Explosion Cratering* (Roddy et al. eds.), pp. 309–320, Pergamon. [2] Klug H. P. and Alexander L. E. (1974) *X-ray Diffraction Procedures,* Wiley, 966 pp. [3] Skála R. (1996) *Meteoritics & Planet. Sci., 31,* A130–A131.

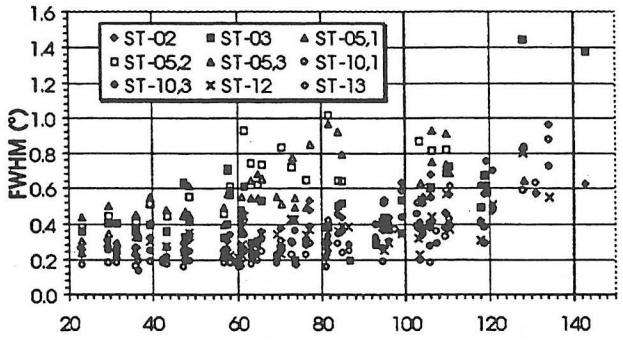

Fig. 1. Graph showing dependency of peak breadth (FWHM) on the diffraction angle.

CHARACTERIZATION OF TERRESTRIAL IMPACT STRUCTURES BY RADARSAT.

S. K. Smith, R. A. F. Grieve, J. Harris, and M. Lamontagne, Geological Survey of Canada, Ottawa, Canada.

We have used synoptic RADARSAT synthetic aperture radar (SAR) to aid in the basic characterization of a select number of terrestrial impact structures as part of RADARSAT ADRO Project 122. In addition to RADARSAT, we have employed other SAR (ERS-1, airborne), digital topographic (1:50,000, 1:250,000), and other data (including LANDSAT) where possible to compensate for look-direction bias in an individual SAR image and provide maximum enhancement of structural features.

RADARSAT data delineate lithological units in only a few cases. For example, the principal outcrops of the massive impact melt rocks

(tagamites) are evident at Popigai [1], as is the outcrop of the impact melt sheet at Manicouagan [2]. The expression of these lithological units is much less or not at all evident in satellite data of optical wavelengths such as LANDSAT.

In terms of structural analysis and based on past experience with ERS-1 data, we have focused on structures that have been subject to glaciation, since RADARSAT tends to accentuate regional and impact-related fracture patterns. A general characteristic in the RADARSAT data is the modification of regional fracture trends by the impact structure. For example, at the Clearwater Lake structures, the dominating east-west regional fracture pattern [3] is modified to more concentric and radial patterns as the structures are approached. These are exterior to existing estimates of the original rim diameters.

At more deeply eroded structures, e.g., Mistasin and Charlevoix, such an exterior fracture halo and modification to the regional structure is less obvious. What is apparent, however, is the essentially complete cessation of regional fracture patterns within the estimated original rim, with the radar texture within the estimated rim area being distinct from that in the exterior. This is most likely due to impact-induced fracturing in the original crater floor being isotropic with respect to direction and overwhelming any preexisting regional fracture pattern.

Charlevoix is the most seismically active area of the St. Lawrence Rift system [4], and we have used slope analysis from a 1:50,000 DEM to identify subtle topographic and drainage features. The interpreted features are being correlated with lineament analysis from SAR imagery and classified according to their nature as (active) faults, possible faults, and fractures to assess the contribution of impact-related structural features to local seismic activity.

At the tectonically deformed Sudbury Structure [5], the imagery is complicated by 1.85 Ga of postimpact geological history. Features such as the Onaping Fault Swarm are clearly evident, as are post-impact diabase dikes [6]. There does, however, appear to be a reduction in the expression of regional fracturing, which is believed to be related to the impact structure, north and west of the Sudbury Igneous Complex. Concentric (ring?) fractures defined from LANDSAT imagery [6] are not apparent in the SAR imagery. Exterior concentric fracturing, such as that observed at the Clearwater Lake structures, is highly evident in the SAR imagery at the younger and smaller (D = 7.5 km) Wanapitei structure [7], which is superimposed on the Sudbury Structure.

References: [1] Masaitis V. L. (1994) *GSA Spec. Paper 293,* 153–162. [2] Currie K. L. (1972) *GSC Bull. 198.* [3] Hische R. (1994) Ph.D. thesis, Univ. Münster. [4] Lamontange M. and Ranalli G. (1997) *Seis. Res. Lett., 68,* 337–352. [5] Stöffler D. et al (1994) *GSA Spec. Paper 293,* 303–318. [6] Butler H. R. (1994) *GSA Spec. Paper 293,* 319–329. [7] Dence M. R. and Popelar J. (1972) *GAC Spec. Paper 10,* 117–124.

CRUSTAL-SCALE STRUCTURAL GEOMETRIES OF THE CHICXULUB IMPACT FROM BRITISH INSTITUTIONS REFLECTION PROFILING SYNDICATE SEISMIC REFLECTION PROFILES. D. B. Snyder[1], R. W. Hobbs[1], and the Chicxulub Working Group, [1]British Institutions Reflection Profiling Syndicate, University of Cambridge, Madingley Road, Bambridge CB3 0EZ, UK (synder@esc.cam.ac.uk).

The deep seismic reflection profiles acquired during the British Institutions Reflection Profiling Syndicate (BIRPS) survey off the north coast of Yucatán in September–October 1996 have clarified the geometries of several major features of the Chicxulub impact structure. The most prominent reflector observed on each of the four 150–200-km-long radial profiles are related to a Jurassic-Cretaceous stratum at 2–3 km depths and to the Moho at 30–35 km depths. The Mesozoic reflector appears relatively undisturbed throughout most of the Yucatán continental shelf, but becomes gently domed at about 120–130 km radial distance from the hypothesized "ground zero" of the Chicxulub impact. At a distance of 75–90 km, this reflector is strongly folded, contorted, or faulted. At 70–90 km it is downdropped 4 km, and at 40–45 km, it disappears completely. If the downdropped sections are crudely restored to the regional and shallower level, a semicircular hole in this early Cretaceous anhydrite-carbonate stratigraphic section with a diameter of just less than 100 km is revealed. Impact-related structures appear at much greater radial distances (100–150 km) at shallower stratigraphic levels within the Mesozoic section. A layer with more chaotic reflectivity, interpreted as impact breccia that includes significant amounts of melt throughout, separates the Cretaceous and Tertiary sedimentary sequences out to radial distances of 100–125 km. In parts of the central region of the impact structure, this more chaotic seismic layer is at least 5 km thick. Near its upper boundary it contains several secondary impactors with diameters of several kilometers and Tertiary sedimentary units draped over their top surfaces.

The lower crust is generally very reflective throughout the survey area at depths greater than 20 km. The base of prominent reflectivity occurs at 30 km, except beneath the impact structure, where it deepens to 32–35 km levels. The reflective lower crust is thus generally thicker beneath the impact structure. Individual reflections of bands of reflectivity are continuous for several to tens of kilometers, and these deepen or shallow gradually, suggestive of folding or flow rather than of brittle faulting.

The upper crust is generally less reflective except for a few prominent reflectors that dip at ~30° toward the center of the impact structure. One of these reflectors projects to the surface at a radial distance of ~96 km and offsets the Mesozoic strata by ~250 m with a normal sense of offset. Another reflector projects to the surface at 130 km where the doming of the Mesozoic strata described above suggests a reverse "blind thrust" sense of displacement. A third set of dipping reflectors occurs beneath the interior of the impact structure and these project up from 25 km depth toward the downdropped blocks of the Mesozoic strata. These dipping reflectors within the crystalline basement probably represent shear zones with their reflectivity possibly enhanced by intrusions. If these shears were active during the impact or during the collapse phase, these intrusions could be related to melts generated deep in the crust by the impact.

NEW TYPES OF FAULT BEHAVIOR ASSOCIATED WITH HYPERVELOCITY IMPACT. J. G. Spray, Department of Geology, University of New Brunswick, Fredericton, New Brunswick E3B 5A3, Canada (jgs@unb.ca).

The investigation of selected terrestrial impact structures reveals that two distinct varieties of large displacement faults can develop in response to hypervelocity impact.

The first type is characterized by large displacement, unidirec-

tional slip (maximal offset) occurring during a single slip event at seismogenic velocity (>1 m s^{-1}). This is referred to as a superfault [1]. Superfaults can facilitate transient cavity collapse and the general modification of impact structures. This can lead to the formation of terraces as well as the development of more distal ring features [2]. These are essentially gravity-driven faults that undergo unconstrained (free surface) dip-slip or reverse-slip movement. Considerable disruption of stratigraphic sequences can occur due to the large offsets realized.

The second type of fault is characterized by large displacement, oscillatory slip (minimal offset) occurring during a single event at seismogenic velocity (>1 m s^{-1}). This is referred to as a "vibrafault." The unusual feature of a vibrafault is the virtual lack of offset. However, the total effective displacement can be significant depending on the frequency and duration of oscillation. Vibrafaults are probably activated during shock-wave propagation and acoustic dissipation. Additive interference of shock and/or sound waves may lead to the development of discrete zones of oscillatory slip. Vibrafaults therefore predate superfaults, though the latter may evolve from vibrafaults in time.

Both fault types result in total displacements estimated to range from 10^2 to 10^4 m per single event, with the potential for massive energy release at the moving interface. Field evidence and calculation indicate that the bulk of the energy is converted to heat through frictional processes. Typically, this leads to the generation of giant friction melt bodies (pseudotachylyte), as can be observed at Sudbury and Vredefort.

These new fault types offer explanations for the development of certain unusual features in impact structures. For example, superfaults can facilitate the penetration of impact melt deep into footwall rocks, as is the case for the economically important Offset Dikes at Sudbury. Vibrafaults can account for the development of thick pseudotachylyte bodies despite the lack of offset documented across such zones [3,4].

References: [1] Spray J. G. (1997) *Geology, 25,* in press. [2] Spray J. G. and Thompson L. M. (1995) *Nature, 373,* 130–132. [3] Fairbairn H. W. and Robson G. M. (1942) *J. Geol., 50,* 1–33. [4] Speers E. C. (1957) *J. Geol., 65,* 497–514.

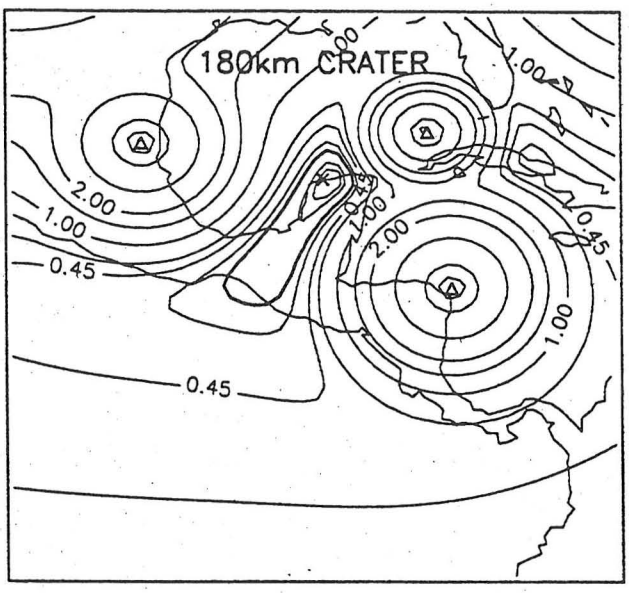

Fig. 1.

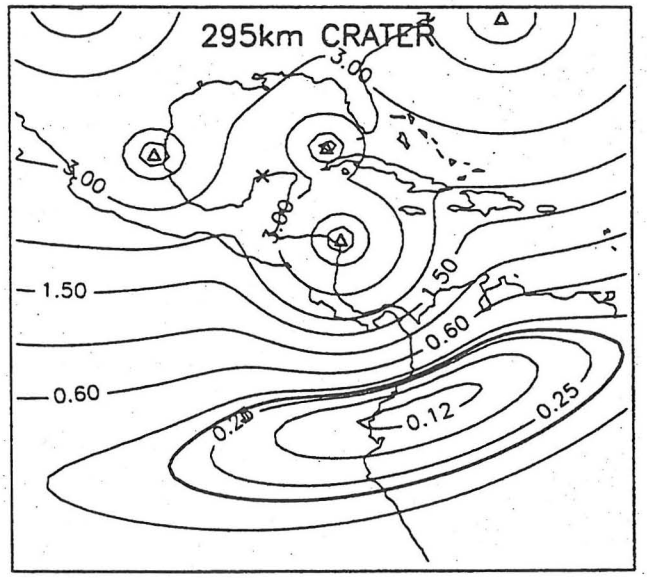

Fig. 2.

CRETACEOUS-TERTIARY EJECTA LAYER: A CASE STUDY FOR LOCATING SOURCE CRATERS AND IMPLICATIONS FOR EJECTA SCALING.

J. A. Stansberry[1], A. R. Hildebrand[2], and P. A. Collins[3], [1]Lowell Observatory, Flagstaff AZ 86001, USA (stansber@lowell.edu), [2]Geological Survey of Canada, Ottawa, Ontario K1A 0Y3, Canada, [3]Massachusetts Institute of Technology, Cambridge MA 02139, USA.

We used measurements of the thickness of the K/T ejecta blanket in the Caribbean, Central American, and North American regions to determine statistically the size and location of the K/T source crater. While the source of the K/T deposit is perhaps less controversial now than it has been in the past, the ejecta blanket provides a good opportunity to test ejecta scaling relations and explore the possibility of using other ejecta blankets as a means of "remotely sensing" undiscovered terrestrial source craters.

Our method of analysis is based solely on a set of measurements of ejecta-blanket thickness and the selection of a relationship between ejecta thickness, crater size, and distance to the crater [1,2]. Given these, it is straightforward to calculate the χ^2 statistic for any given hypothetical location and size of the source crater. A measure of goodness-of-fit between a dataset and a model for that dataset is $\chi^2 = 1/N,\Sigma\ (t_i - m_i)^2/\sigma_i$ (where N is the number of thickness measurements, t_i is the measured thickness at the i^{th} location, m_i is the model value for the thickness at the i^{th} location, determined from the scaling relation and the guess for the crater location and size, and σ_i is the uncertainty in the thickness measurement). For a model that describes the data well, χ^2 approaches a value of unity. Models that do not fit as well result in larger values of χ^2.

We established a geographic grid of hypothetical source-crater locations and computed model thickness values for craters at each location on the grid. These model thicknesses were then compared with the measured thicknesses in order to compute χ^2, resulting in a map of χ^2 vs. crater location. We also varied our guess for the crater

size at each location, so that we ended up with a family of χ^2 maps consisting of one map for each crater size we used.

Figures 1 and 2 show two contour maps of $\log_{10}(\chi^2)$ vs. latitude and longitude for a region around the Caribbean. The χ^2 values are based on thickness data (triangular symbols) for the K/T ejecta blanket (for proximal sites at Beloc, Haiti, DSDP 540, Yucatán Channel, and Mimbral, Mexico, plus distal sites located to the northwest and northeast) and two estimates, 180 km and 295 km, for the diameter of the K/T source crater. The map based on the 180-km crater size has an χ^2 minimum (with a value of 0.99) that coincides almost exactly with the location of Chicxulub. The heavy contour line shows the region where there is a 90% likelihood, statistically speaking, of finding the source crater for the dataset, if the source crater has a diameter of 180 km. The size of the 90% likelihood region, which is bounded by the heavy contour at $\chi^2 = 1.65$, is related to the size of the uncertainty in the thickness measurements, which we chose to be 50% of the measured value based on the observed thickness variability in outcrop. The map based on an assumed 295 km diameter for the source crater has a χ^2 minimum of 1.3, located over northwest South America. The 90% likelihood region is bounded by the dashed contour at $\chi^2 = 1.9$ and encompasses a huge region of northern South America extending westward into the Pacific Basin. Using additional ejecta localities reduces the regions of high probabilities, particularly if additional localities are well separated from previously incorporated data and lie in radial directions previously unconstrained.

With a view toward using our method for finding source craters, we will present results evaluating its sensitivity to sampling effects and to uncertainties and biases in thickness measurements.

References: [1] McGetchin T. R. et al. (1973) *EPSL, 20,* 226–236. [2] Hildebrand A. R. and Stansberry J. A. (1992) *LPS XXIII,* 537.

SEISMIC ANALYSIS OF THE MJØLNIR IMPACT STRUCTURE, BARENTS SEA. F. Tsikalas, S. T. Gudlaugsson, and J. I. Faleide, Department of Geology, University of Oslo, P.O. Box 1047 Blindern, N-0316 Oslo, Norway.

A dense grid of high-resolution single-channel, shallow multichannel, and conventional multichannel seismic-reflection profiles defines in detail the structural and stratigraphic framework of the impact-induced disturbance and postimpact evolution of the Mjølnir Structure. Excellent seismic images of the well-preserved, 40-km-diameter structure reveal that the primary impact-induced deformation is bounded on top by a discernible structural relief. At this level, the structure exhibits a distinct radial zonation pattern comprising a 12-km-wide complex outer zone, including a marginal fault zone and a modest peak ring, a 4-km-wide annular depression, and an 8-km-diameter uplifted central high. Furthermore, we show that the key features of the Mjølnir Structure are similar to those found at the majority of large terrestrial complex craters. Such features include sharp rim faults with a cumulative throw of ~150 m that separate highly deformed strata within the crater from intact platform strata, and a 45–180-m-thick seismic unit, formed during impact, characterized by disturbed and incoherent reflectivity patterns and confined by prominent fault-blocks and the postimpact strata. The seismic data also provide evidence of crater-influenced sedimentation, as well as extensive secondary postimpact deformation expressed by structural reactivation and differential subsidence. Reconstruction of the original crater relief brings out an initially subtle structure with only ~30–40 m average residual depth, demonstrating substantial enhancement of structural features by the post-impact burial and deformation. A large degree of gravitational collapse explains much of the shallow depth of the Mjølnir Structure. However, volume balance analysis shows that additional infilling by other processes is required to fully explain the present relief. The extensive postimpact deformation is closely related to lateral changes in physical properties, such as porosity and compactibility, within the impact-affected rock volume, triggered by prograding postimpact sediments.

ON FORMATION MECHANISM OF FLATTENED SUBSURFACE FRACTURE ZONE IN METEORITE CRATERS: RESULTS OF HIGH-EXPLOSIVE LABORATORY EXPERIMENTS. V. M. Tsvetkov and Y. V. Zenchenko, Institute for Dynamics of Geospheres, 38 Leninsky Prospect, Building 6, Russian Academy of Sciences, Moscow 117979, Russia.

The study of well-preserved craters on the Earth's surface (e. g., Kaali, Estonia [1], and Meteor Crater, U.S. [2]) demonstrates a presence of an approximately hemispherical fractured zone under the crater floor. In addition, there is a flattened subsurface fractured zone under the rim, with a depth that decreases from the crater center. In the geophysical model of the meteorite crater offered in Dabizha and Ivanov [3], the radius of the subsurface fracture zone is assumed to be equal to two crater radii vs. one crater radius of the hemispherical part of the fracture zone. Such a fracture-zone configuration contradicts the picture of shock pressure isobars; those are approximately hemispherical in all the half-space, except for a thin region near the free surface. In Dabizha and Ivanov [3], it was suggested that fracture-zone geometry is the result of secondary fragmentation during crater excavation, enhanced by cratering flow peculiarities. This suggestion has a serious drawback because secondary fragmentation takes place in the inner part of the fracture zone rather than at its periphery [4].

High-explosive laboratory modeling of the cratering process allowed us to observe all features of the fracturing process, including subsurface fracture-zone formation. We used a pine rosin as a model material. Rosin is a brittle material having the following

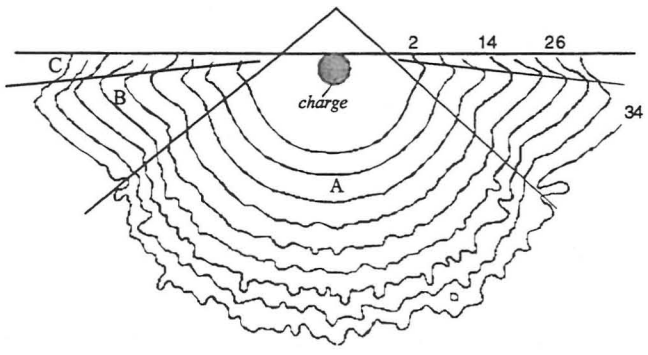

Fig. 1. Successive positions of fracture front. Numbers express time after detonation in milliseconds.

properties: density, 1.08 g/cm^3, longitudinal wave velocity, 2470 m/s, and unconfined compressive strength, 20 MPa. The fracturing process was registered by optical technique due to the relative transparency of rosin. Spherical charges of PETN with R = 4 mm and mass = 0.38 g were used as the explosive. Successive positions of the fracture front are shown in Fig. 1. In region A, the fracture front is approximately spherical. Its velocity equals 1200 m/s at distances less than 10R and 960 m/s in the range of 10–15R. At larger distances, the fracture front decays. In region B, the fracture front represents a conical surface with a constant angle between its element and free surface. The velocity of the conical front is 960 m/s in the entire region B. Its elements terminate under the free surface. Immediately adjacent to the surface, zone C fragmentation is due to spall phenomena. It was shown [4] that value 960 m/s is the maximum velocity of tension fractures propagation; the conical front propagates with maximum tension-cracks velocity. It is obvious that the conical fracture-front appearance is the result of stress-wave-free boundary interaction. In general, the final fracture zone form that is visible in the experimental sample section repeats the fracture-front configuration. Its horizontal radius equals four crater radii, while its depth equals two radii.

Thus, experimental results show that both subsurface and hemispherical fracture-zones formation take place simultaneously and precede crater formation. The horizontal-to-vertical dimensions of the fracture-zone ratio are the same as that of Earth's craters. A discrepancy between laboratory and natural fracture-zone dimensions with respect to crater diameter may be caused by the relatively low strength of rosin vs. rocks on one hand and by rock properties alteration due to geological processes on the other.

References: [1] Aaloe A. et al. (1976) *Geology, 25,* 1, 58. [2] Ackermann H. D. et al. (1975) *JGR, 80,* 765. [3] Dabizha A. I. and Ivanov B. A. (1978) *Meteoritika, 37,* 160. [4] Tsvetkov V. M. et al. (1977) *Impact and Explosion Cratering,* p. 669.

NUMERICAL MODELING OF THE FORMATION OF MULTIRING BASINS. E. P. Turtle and H. J. Melosh, Lunar and Planetary Laboratory, University of Arizona, Tucson AZ 85721-0092, USA.

Among the different morphological types of impact structures are multiring basins, very large craters surrounded by one or more concentric rings with asymmetric topographic profiles. Recently it has been suggested that three terrestrial impact structures are possible multiring basins: Vredefort [1], Chicxulub [2], and Sudbury [3]. While the morphology of multiring basins has been studied in some detail, the processes that lead to their formation are still relatively poorly understood, and a number of theories have been advanced to explain their formation. We are using finite-element modeling to investigate the collapse and relaxation stage of impact crater formation with the specific intention of determining the mechanisms necessary to form concentric scarps external to the crater cavity.

Starting with a uniform mesh, we form a transient crater using Maxwell's Z-model [4] to predict which material will be ejected and the displacements of the unejected material due to excavation flow. For this research we have been using a transient crater 50 km in radius and 30 km deep; using scaling relations, this corresponds to a final crater comparable in size to the estimates that have been made for Sudbury, Chicxulub, and Vredefort. To model the collapse and modification of the transient crater, we are using the finite element code Tekton [5]. Our model incorporates realistic power-law rheologies for the upper crustal rocks in the vicinity of the Vredefort structure in South Africa above a granitic lower crust that extends down to the Moho at a depth of 45.5 km.

We included a low-viscosity layer of variable thickness and depth to investigate the theory Melosh and McKinnon [6] developed to explain the formation of multiring basins. So, in essence, the mesh has two rheologies: the relatively low-viscosity Newtonian rheology of the low-viscosity layer and the stiffer power-law rheology of the surrounding material. We have run simulations for low-viscosity layers with thicknesses ranging from 14 to 42 km and depths (of the top of the layer) ranging from 7 to 49 km. For each simulation, we followed the evolution of the surface stress field external to the transient crater. For a shallow layer (top of layer at 7 km depth) of any thickness within our range, we found that the radial stresses are typically extensional and are sufficiently large (peak extensional stresses >1–3 kbar) to induce normal faulting in a thin layer. While the value of the maximum radial stress achieved is dependent on the thickness of the low-viscosity layer, its radius is insensitive to the thickness of the layer and does not shift significantly with time. Moreover, the maximum extensional stresses occur at a radius of roughly 100 km, which is consistent with the $\sqrt{2}$ spacing that has been observed for rings around numerous craters [e.g., 7].

For deeper low-viscosity layers (top of layer below 14 km depth) the stresses near the final crater rim become compressive as the thicker upper layer is flexed upward. A region of extensional radial stress lies just outside the region of compressive stress. Progressively deeper low-viscosity layers result in a decrease in magnitude of the extensional stresses and a slight outward migration of the location of the peak stress.

Our results indicate that the presence of a low-viscosity layer is consistent with the formation of at least one external ring. For a shallow (top of layer at <14 km depth) low-viscosity layer of any thickness up to 42 km and a transient crater 50 km in radius, the peak extensional stress occurs at a radius of ~100 km. We will present these model results. We also plan to investigate how the addition of a fault or faults in the stiff upper layer affects the subsequent evolution of the stress field to explore conditions under which more than one ring could form. The significance of plastic and power-law rheologies will also be studied.

References: [1] Martini J. E. J. (1992) *J. Metamorphic Geol., 10,* 517–527. [2] Sharpton V. I. et al. (1993) *Science, 261,* 1564–1567. [3] Spray J. G. and Thompson L. M. (1995) *Nature, 373,* 130–132. [4] Maxwell D. E. (1977) in *Impact and Explosion Cratering* (D. J. Roddy et al., eds.), pp. 1003–1008, Pergamon. [5] Melosh H. J. and Raefsky A. (1980) *Geophys. J. R. Astr. Soc., 60,* 333–354. [6] Melosh H. J. and McKinnon W. (1978) *GRL, 5,* 985–988. [7] Melosh H. J. (1989) *Impact Cratering,* Oxford Univ.

MINERALOGICAL, GEOCHEMICAL, AND GEOLOGICAL DATA FOR THE INTERPRETATION OF THE CRATER BASE STRUCTURE OF THE COMPLEX TERNY ASTROBLEME, KRIVOY ROG, UKRAINE. A. A. Valter, Malyshko Stra., 3, Apt. 449, Kiev, Ukraine.

The deeply eroded (H ≥ 0.8 km) Terny astrobleme was formed in the rocks of the Krivoy Rog Fe formation and related banded Lower Proterozoic metamorphic rocks and granitoids [1–4].

The present-day diameter of the structure is estimated to be 8 km, but the original diameter might have been twice as large. The diameter of the eroded central uplift is ~2.5 km. In the exploration and production of ores, the sinking of quarries (to 350 m deep), mines (to 1 km deep), and boreholes was performed within the astrobleme.

The K-Ar age determination of glass impactites gave 280 ± 10 Ma.

Observations in the mines show that the monoclinal-occurrence rocks were crushed into blocks and overturned "to be pulled up" into the uplift area. As the depth exceeds 1 km, the occurrence approaches the normal value.

Numerous bodies of fine fragmented breccia that separate large blocks of rocks have a preferred orientation that corresponds to the tectonic plan of the region. This gives evidence of breccia zones formation along the weakest and strained planes of the massif.

The ferroginous glassy impactites near the center of the uplift are formed by the melting of ferroginous quartzites, shists, and Fe ores. Most of the impactide bodies are of complicated origin, formed by shock metamorphism, rock crushing, mixing of fragments varying in shock alteration, and, finally, secondary heating by gaseous fluids. In these impactites the condensation of the Fe-Cr-Ni phase with a composition approaching the eutectic one was found. The geochemical traces of the "meteorite explosion cloud" were observed down to the deepest level of the glassy impactite occurrence (850 m): 2.4 ppb of Ir (× 60 enrichment), 86 ppm of Ni (× 40 enrichment), and ratios Ni/Co = 12 and Ir/Au = 2.

The veins of alkaline silicate impactites in the western part of the uplift occur in the microgneisses shists of similar composition. These impactites exhibited no significant meteorite material contamination. The presence of impact diamond grains found in these veins shows that the impulse pressure is sufficient for silicate melting in the shock wave or rarefaction wave.

The models of impactite formation and mass dynamics in the crater base are proposed.

Because of its good exposure and the specific composition of the target rocks, the Terny astrobleme can be used as a standard in studies of large meteorite crater bases.

References: [1] Nikolsky A. P. (1979) *Dokl. Akad. Nauk USSR, 249,* 436. [2] Masaitis V. L. et al. (1981) *LPS XII,* 655. [3] Eremenko G. K. and Yakovlev V. M. (1980) *Dokl. Akad. Nauk USSR, 253,* 449. [4] Valter A. A. et al. (1981) *Dokl. Akad. Nauk Ukr. SSR, N2,* 3.

ON THE WATER REGIME OF IMPACTITES IN LARGE ASTROBLEMES. S. A. Vishnevsky, Institute of Mineralogy and Petrography, Novosibirsk-90, Russia.

Due to scarce data and limited sample selection (tektites or glasses from small craters in arid regions), terrestrial impact melt rocks are usually characterized as extremely dry (on average <0.05 wt% H_2O) in what is considered a typical feature of impact glasses [1,2]. However, imposing H_2O contents are found (from data on petrology, gas chromatography, fluid inclusions, etc.) in impactites of the 100-km Popigai Crater localized in AR gneisses + PR-MZ sedimentary cover.

A large (~2000 km³) body of Popigai impact melt rocks consists of two petrographic groups (T1 and T2 tagamites and their suevitic equivalents, fragments of G1 and G2 glasses): very fine-/non-crystallized T1/G1 glasses, respectively, vs. "coarse"/well-crystallized T2/G2 glasses. Such a distinction in melt crystallization is due to a different water content ("dry" T1-G1 rocks vs. "wet" T2-G2 rocks, with H_2O wt% of 0.73 and 2.23 respectively) inherited by melt from target gneisses [3].

Impact anatexis of gneisses is found in some water-rich T2 tagamites [4]. Anatectic glass here (globules in rock matrix, borders and interstitial films in residual gneiss fragments) originated by shock-induced separation of Si, K, and H_2O from source rocks at pressures 27–50 GPa and residual temperatures 700°–1700°C; Al and Ti were indifferent, but Fe, Ca, Mg, and Na were essentially lost in this process. As a result, an "asid" (up to 77 wt% SiO_2), K-rich (up to 6 wt% K_2O), and "wet" (4.2–6.9 wt% H_2O in fresh glasses) anatectic melt was formed prior to tagamite crystallization, possibly due to an extremely high rate of element diffusion in strongly excited rocks. Microsized (down to 0.1 mm) globules in the tagamite matrix may indicate their mixing up and, consequently, fast origin still in shock-load state (× <1 s). Fresh leshatelierite and high-silica (87–95 wt% SiO_2) glasses in Popigai impactites often contain various fluid inclusions, including gas, gas-liquid, and entirely liquid. The liquid phase is a water. Dense water inclusions (ρ = 0.7–1.0 g/cm³ at 20°C) in the suevite glasses indicate a high confining pressure (1.4–3.3 GPa) during quenching of the melt from 1900°C to subsolidus state [5], which is explained by water buffer action providing relatively slow pressure release of shocked "wet" rocks. Coesite growth from hot shock-disordered quartz should be stimulated by slow unloading.

Postshock residual temperatures in target rocks (with liquid water content from 1.8–2.6 wt% in AR gneisses to 8–10 wt% in sedimentary cover and dislocation zones) should provide high pressures of water fluid. Estimates range from 2.7 to 1.4 GPa for initial pressures of the fluid at 1400°–660°C in shocked target rocks at postcratering depths of 6–10 km beneath the surface at Popigai. This high-pressure, up-directed superheated fluid flow might help in the origin of central uplift (by expansion and local explosions), and could provide intensive pneumatolysis and chemical mass transport in crater formations. In particular, K-enrichment of impactites in some craters might be caused by this process.

Given examples show that the water fluid was an important agent in large-scale cratering, shock metamorphism, and postimpact evolution of the crater rocks. "Dry" regimes may be common only for some highly dispersed/condensed impact glasses (tektites, microspherules, etc.).

References: [1] Koeberl (1992, 1994). [2] Beran and Koeberl (1997). [3] Vishnevsky (1996). [4] Vishnevsky and Pospelova (1986). [5] Vishnevsky and Pospelova (1988).

CHICXULUB SEISMIC EXPERIMENT: OVERVIEW AND SIZE OF THE TRANSIENT CAVITY. M. Warner[1] and the Chicxulub Working Group, [1]Department of Geology, Imperial College, London SW7 2BP, UK (m.warner@ic.ac.uk).

The Chicxulub seismic experiment was designed to image the subsurface reflectivity and seismic velocity structure of the Chicxulub impact from the base of the Tertiary section to the Moho and below. Our scientific objectives were to use these data, together with con-

straints provided by existing boreholes and potential field observations, to determine (1) the radial extent and morphology of the impact structure, (2) the diameter and depth of the transient and excavation cavities, (3) the position, depth, and geometry of slumped blocks on the flanks of the structure, and the style of associated faulting and deep deformation, (4) the amount, style, and extent of structural uplift at the center of the crater, (5) the variation in thickness of the crust across the crater, (6) the extent of the melt sheet, and (7) the degree of radial asymmetry of the major structural and morphological elements within the crater.

Our broader objectives were to improve our understanding of the cratering process for large impact events and to constrain the environmental effects of the impact. The quality of the data are such that we expect to meet all these objectives. Outside the central region of the crater, we image the preimpact Mesozoic stratigraphy as a sequence of bright, subhorizontal, layered reflectors at depths of ~1–4 km. These marker horizons enable us to map a series of large slumped blocks within the interior of the crater and hence delineate the inner edge of the collapsed transient cavity. This has an average diameter of ~85 km. We have restored these slumped blocks to their preimpact position, and have used the z-model with a value of z ~2.7 to determine the diameter of the transient cavity. This lies in the range 105–120 km when defined by the position of the transient rim uplift excluding any overlying ejecta. The diameter of the transient cavity, restored to original ground level, lies between 90 and 105 km and corresponds closely to the diameter of the excavated cavity. This is the value required to calculate volumes of material ejected or volatilized by the impact and hence has the most relevance to questions about environmental perturbation at the K/T boundary.

The size of the transient cavity is toward the lower end of the range of values that have been previously suggested, and it is clear that some previously published estimates of the volumes of SO_2 and CO_2 released by the impact have been significantly too large.

LARGE METEORITIC IMPACTS AND LUNAR DIFFERENTIATION. P. H. Warren, Institute of Geophysics and Planetary Physics, University of California, Los Angeles, Los Angeles CA 90095-1567, USA.

The Moon is a body where meteoritic impacts have played an even more important evolutionary role than on Earth. A key issue is the role of impact as a cause of melting on a large enough scale to engender igneous differentiation. What fraction of Apollo rock samples generally viewed as "pristine" products of early endogenous magmatism are actually products of impact melt?

Cold clastic debris has a strong chilling effect on impact melt [1]. Consequently, the melting displacement ratio m/d is probably the paramount influence on the potential for an impact-generated magma to undergo internal igneous differentiation (fractional crystallization) [2]. For calibration of the relationship between m/d and the potential for impact magma igneous differentiation (IMID), we must look to large terrestrial structures with well-exposed melt sheets. IMID was evidently vastly greater at Sudbury (m/d ≈ 0.46) than at the two next largest such structures, Popigai and Manicouagan (both m/d ≈ 0.24). The Sudbury IMID may have been enhanced by endogenous melting potential (deep-crustal heat) in the Penokean Sudbury region. Considering that at Manicouagan and Popigai the melt sheets did not differentiate even slightly, it seems likely that a robust IMID requires m/d > 0.3.

On the Moon m/d is much smaller for a given crater size than on Earth. Of the known (young enough to be seen) large basins, only a few formed with m/d > 0.3 (Table 1; basin size data from [3], m/d calculated à la Melosh [4]). Any differentiated lunar melt sheet is probably capped by a clastic debris-rich, heterogeneous but nondifferentiated Onaping analog. Igneous differentiates (cumulates) making their way into an Apollo rock collection would require a later large crater to excavate from several km in depth, with sufficient lateral transport (anticorrelated with depth of excavation in any single event) to bring the rock into the small Apollo sampling region. Except by starting from Procellarum (or some other basin not currently visible), this series of events appears unlikely (Table 1). A strong objection to the hypothesis that a single basin (Procellarum) is the source of the apparent pristine rocks is the correlation among these samples between trace-element compositions and Apollo sampling locations [5].

The distinction between impact melt and endogenous, mantle-derived melt begins to blur when extremely large events are considered. In big lunar events, impact melt that avoids immediate dissemination (ejection) is of mainly mantle derivation (Table 1; numbers in parentheses indicate results from hemispheric-spherical melt zone shapes). For Sudbury, the same approach predicts crust/(mantle + crust) is not <100% and could well be 1. On the early Moon, big impacts probably influenced the times and places where magmas intruded the crust, but except for basins too young to have yielded samples, the heat for the magmatism was probably mainly endogenous.

References: [1] Simonds C. H. et al. (1976) *Proc. LSC 7th.* [2] Warren et al. (1996) *GSA Spec. Paper 307.* [3] Wilhelms D. E.

TABLE 1. Lunar basins as potential sources of Apollo samples from Sudbury-like differentiated melt "sheets."

Basin	Diameter (km)	Melting/ Displacement	Crust/(mantle + crust) in unejected impact melt	Likelihood of "sheet" pieces (excavated by younger craters) among Apollo samples
Procellarum?	3200	77 vol%	0.1 vol%	*If* Procellarum is real, excellent (via Imbrium)
South Pole Aitken	2500	65 vol%	0.3 vol%	Well excavated, but too far from Apollo sites
Imbrium	1160	37 vol%	7 (5–10) vol%	Younger excavating craters too small and distant
Crisium	1060	35 vol%	11 (7–16) vol%	Extremely insignificant (no excavation)
Fecunditatis	990	33 vol%	14 (9–21) vol%	Insignificant (distant, poorly excavated)
Orientale	930	32 vol%	19 (12–28) vol%	Extremely insignificant (no excavation)
Australe	880	31 vol%	23 (13–34) vol%	Extremely insignificant (too distant)
Nectaris	860	30 vol%	25 (15–37) vol%	Insignificant (distant, poorly excavated)

(1987) *USGS Prof. Paper 1348.* [4] Melosh H. J. (1989) *Impact Cratering.* [5] Warren P. H. and Taylor G. J. (1981) in *Multi-Ring Basins.*

EXAMINATION OF THE EFFECTS OF FIREBALL RADIATION ON MATERIAL OF THE EJECTA CURTAIN. T. J. Wdowiak[1], K. M. Arnoult[1], and B. G. R. Coltress[1,2], [1]Astro and Solar System Physics Program, Department of Physics, University of Alabama at Birmingham, Birmingham AL 35294-1700, USA (wdowiak@phy.uab.edu), [2]Ramsay Alternative School, Birmingham AL 35205, USA.

Although the radiation emitted by the ascending fireball would be intercepted by material of the ejecta curtain, examination of the consequences of this occurring seems to have escaped the attention of those who study impacts. For the terrestrial situation, the effects could include dessication of ejecta while above the atmosphere, annealing of shock-induced features of crystals such as quartz, which are considered to be indicators of an impact event, and perhaps even tektite formation through fusion of ejecta material in ballistic flight above the atmosphere. The luminosity history of the fireball, on the basis of preliminary calculations, appears to be the most significant factor in evaluating the role of radiation in the impact event.

If radiation heating of ejecta is to be significant, it would be expected that the process would be relatively insensitive to variation of parameters, and even simple models for the luminosity history should be useful in the assessment of radiant heating. It is also obvious that the duration of the period of high luminosity of the fireball would have the greatest effect.

Prior to the Comet Shoemaker-Levy 9 impact with Jupiter, Zahnle and MacLow [1] attempted to predict the fireball luminosity history for a bolide impacting a thick H atmosphere. The situation for a terrestrial impact would be a different one because high opacity sources would not only arise from the impactor but also from the more abundant target rock. In addition, there is a likelihood that condensation of solids would slow the expansion of the fireball [2].

We have generated a family of fireball luminosity histories and used this information to estimate the temperatures of in-flight test particles at the inner surface of the ejecta curtain. The results have been applied to the questions of annealing of shock-induced distortions in grains and fusion of clumps into tektites. The results of these calculations will be presented. In addition, an apparatus for radiant heating in a vacuum of test samples, including tektite material, has been constructed. The apparatus has the capability of an irradiance of 10,000 suns, which is a level of interest, as indicated by our preliminary calculations. The results of experiments carried out with the apparatus will be discussed.

References: [1] Zahnle K. and MacLow M. (1994) *Icarus, 108,* 1–17. [2] Melosh H. J. and Pierazzo E. (1997) *LPS XXVIII,* 935–936.

THE STRUCTURE OF LUNAR BASINS: IMPLICATIONS FOR THE BASIN-FORMING PROCESS. M. A. Wieczorek and R J. Phillips, Department of Earth and Planetary Sciences, Washington University, 1 Brookings Drive, Box 1169, St. Louis MO 63130 (markw@wurtzite.wustl.edu).

Introduction: Using lunar gravity and topography data obtained from the Clementine mission, a global crustal thickness map was recently generated [1]. This model had a two-layered crust; gravity anomalies were assumed to be due primarily to upper crustal thickness variations, and a spherical analog of Parker's algorithm [2] was used in computing the potential anomalies due to finite amplitude relief along the surface, intracrustal interface, and Moho.

This dual-layered model of lunar crustal structure has several important properties:

1. The upper crust (~30 km thick) was entirely removed during the formation of the major nearside basins. This is consistent with the fact that the ejecta for these basins shows a considerable noritic component, which presumably was derived from the lower crust [3].

2. The large South-Pole Aitken Basin also had its entire upper crust removed, but has a 30-km-thick lower crust present. This basin apparently did not excavate into the lunar mantle, which is consistent with spectral reflectance studies of the regolith in this basin [4].

3. Surrounding most basins is an annulus of thickened crust [see also 5]. This is a result of a low "gravity moat" that surrounds most multiring basins.

4. The crust below the Crisium Basin is extremely thin (~5 km). By adjusting the parameters of the above gravity model, it is possible to get a zero total crustal thickness beneath this basin. Thus, based on gravity studies, Crisium is the only basin that could possibly have excavated mantle material.

In this study we use the above crustal thickness model, as well as the lunar gravity field, to study several aspects of the basin-forming process: (1) What was the size of the excavation cavity? (2) How much lower crustal material was excavated? (3) Is the gravity moat surrounding the basins due to crustal thickness variations, low-density ejecta deposits, or brecciated bedrock (i.e., the "strength crater" [6])? and (4) Were the basins in isostatic equilibrium before or after the emplacement of mare basalts?

Excavation Cavity Reconstruction: Radially averaged crustal thickness profiles for the major basins all show that the upper crust is significantly thinned and that the Moho is substantially uplifted

TABLE 1.

Basin	D_{cx} (km)	h_{cx} (km)	V_{cx} (10^6 km^3)
Orientale	417	49	3.3
Imbrium	636	30	7.0
Serenitatis	627	43	9.7
Crisium	508	54	7.9
Hertzsprung	335	20	0.87
Humboldtianum	456	16	1.3
Humorum	341	40	2.7
Mendeleev	302	17	0.60
Korolev	314	18	0.69
Mendel-Rydburg	365	19	0.99
Moscoviense	356	30	1.5
Nectaris	413	45	4.3
Grimaldi	190	17	0.24
Freundlich-Sharonov	335	27	1.2
Smythii	463	46	5.7
Coulomb-Sarton	324	21	0.86
Fecunditatis	334	7	0.31

beneath these basins. We use a relatively simple technique to reconstruct the size of the excavation cavity. Within the annulus of thickened crust, the Moho is "restored" to its average value outside of the basin. It is assumed that the resulting cavity is a good approximation of the excavation cavity (that portion of the preimpact crust that is ballistically ejected from the transient crater). Although this method does not take into account any basin modification effects such as slumping, nor does it restore the uplifted crater rim material to its original location, given the uncertainty in the lunar gravity field and the assumptions that went into the gravity modeling, we will assume that the excavation cavity is adequately described to the first order by this method.

Table 1 shows the diameter of the excavation cavity, D_{cx} (which is equivalent to the diameter of the transient cavity), the depth of excavation, h_{cx}, and the volume of material that was excavated, V_{cx}. A best fit between h_{cx} and D_{cx} yields $h_{cx} = 0.07\ D_{cx}$. Although this correlation is not great (R = 0.54), the excavation depth always lies between 0.12 and 0.02 of the excavation cavity diameter, which is consistent with most previous estimates.

A good correlation (R = 0.82) is found between the transient cavity diameter and the most prominent ring diameter, D, for the multiring basins, given by $D_t = 0.41D + 134$ (most prominent ring diameter taken from [7]). This correlation is very similar to that given by Spudis [7].

In Progress: We are currently in the process of determining the pre- and postmare isostatic state of the nearside mascon basins. These results should give an indication of the variability in strength of the lunar lithosphere with time. Additionally, the origin of the gravity moats that surround most basins is being investigated. Particularly, we are attempting to discern whether these gravity lows are caused by (1) thickened crust due to the excavation flow during crater formation, (2) low-density ejecta, or (3) brecciated *in situ* bedrock. If it can be shown that either (2) or (3) is the most likely cause, estimates of the ejecta thickness or "strength crater" diameter may be able to be obtained.

References: [1] Wieczorek M. A. and Phillips R. J. (1997) *LPS XXVIII.* [2] Parker R. L. (1972) *Geophys. J. R. Astron. Soc.,* 447. [3] Spudis P. B. et al., (1984) *Proc. LPSC 15th,* in *JGR, 89,* C197. [4] Pieters C. M. et al. (1997) *LPS XXVIII.* [5] Neumann G. et al. (1996) *JGR, 101,* 16841. [6] Croft S. K. (1981) *Proc. LPS 12A,* 227. [7] Spudis P. (1993) *The Geology of Multi-Ring Impact Basins,* Cambridge.

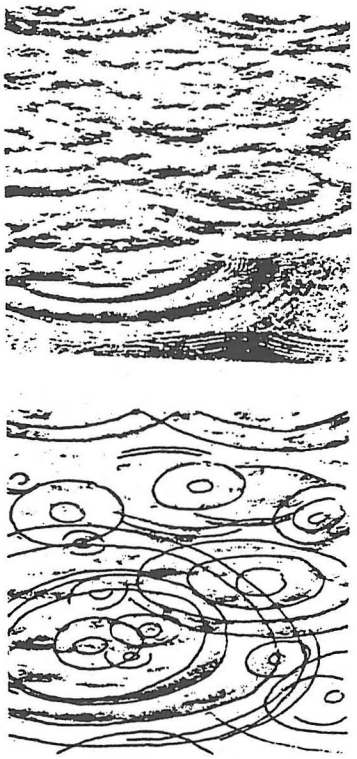

Fig. 1. Multiring impact overprint in water, showing cancellation and reinforcement wave patterns.

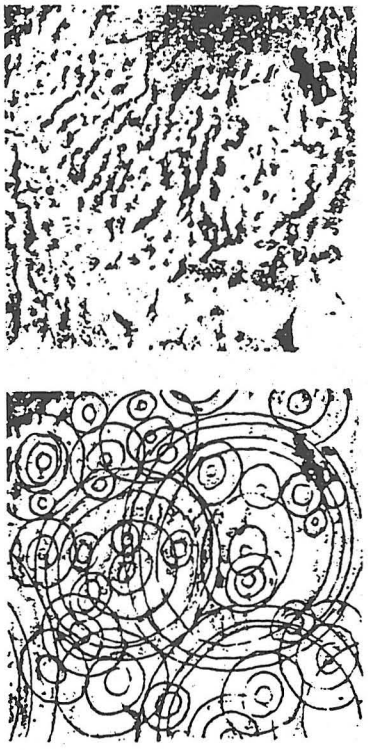

Fig. 2. Multiring cryptobleme overprint in U.S. basin range (Great Salt Lake in upper right corner), showing cancellation and reinforcement wave patterns.

CRYPTOBLEMES: A NEW DISCOVERY WITH MAJOR ECONOMIC IMPLICATIONS AND PROFOUND CHANGES TO THE GEOLOGIC PARADIGM.

J. Windolph Jr.[1] and J. Sutton[2], [1]U.S. Geological Survey (retired), Boyds MD 20841, USA, [2]National Aeronautics and Space Administration.

Cryptoblemes [1] are subtle impact shock signatures imprinted by cosmic debris on the crustal surfaces of lunar planetary bodies. These signatures constitute a complex cumulative overprinting of topographic, structural geophysical, and tectonic patterns that have a conspicuous radial centric, multiringed symmetry. The geometry and distribution of cryptoblemes on Earth is comparable to the size and density of impact features on lunar planetary surfaces. Analysis of satellite imagery, sea-floor sonar, side-looking radar, and aerial

photographs of specific sites reveals new criteria for the identification and confirmation of impact-shock signatures. These criteria include joint and foliation patterns with asbestiform minerals, ribbon-quartz, spheroidal weathering, domal exfoliation, pencil shale, and shock spheres, which may originate from hydrocavitation of water-saturated sedimentary rocks. Cryptoblemes may also be associated with breccia pipes, sinkholes, buttes, mesas, and bogs, high-Rn anomalies, nodular Mn concentrations, and earthquake epicenters.

Major implications of cryptobleme identification include exploratory targeting of hydrocarbon and mineral deposits and the explanation of their origin. Analysis of known mineral deposits, structural traps, and sedimentary basins shows a direct correlation with cryptobleme patterns. Significant geologic paradigm shifts related to cryptoblemes include mountain building processes, structural orogenies, induced volcanism, earthquake origins, hydrocarbon diagenesis, formation of mineral deposits, continental rifting and plate movements, magnetic overprinting, and local, regional, and global biologic extinction and speciation patterns.

Figures 1 and 2 provide a comparison between a multiring impact overprint in water and a multiring cryptobleme overprint in the U.S. basin range.

References: [1] Windolph J. (1993) *Comptes Rendus XII ICC-P, 1,* 455–466.

EMPLACEMENT OF THE HESS OFFSET IN THE NORTH RANGE OF THE SUDBURY IMPACT STRUCTURE. C. R. Wood[1], J. G. Spray[1], and M. Napoli[2], [1]Department of Geology, University of New Brunswick, Bailey Drive, Fredericton, New Brunswick E3B 5A3, Canada (K474S@unb.ca), [2]INCO Limited, Highway 17 West, Copper Cliff, Ontario P0M 1N0, Canada.

The Hess Offset dike is subconcentric to the Sudbury Igneous Complex (SIC) between 13 and 15 km to the north of it. The offset extends from at least as far west as Clear Lake, and as far east as the Foy Offset, for a total distance of ~23 km. The dike is up to 30 m wide and intermediate in composition. It appears to be vertical but may dip steeply to the south. The 1.85-Ga Sudbury Structure is superimposed on the Archean basements rock in the North Range to the north of the SIC and the Proterozoic supracrustal rocks (Huronian Supergroup) in the South Range to the south of the SIC. The high-grade Levack gneisses are exposed near the contact of the SIC in the North Range. North of the Hess Offset occur erosional remnants of the Huronian Supergroup. These outliers form a ringlike zone subconcentric to the SIC. In the Hess and Foy Offset area, these Huronian remnants lie ~12–17 km north of the SIC. To the east of the North Range in the Whistle-Parkin Offset area, the remnants lie only 3–4 km northeast of the SIC. These Huronian Outliers are considered to be a down-faulted ring graben, whereas the Levack Gneisses proximal to the SIC represent uplift. The Foy Offset is apparently displaced to the east, where it intersects the Hess Offset and changes in strike.

The common association of the Hess Offset with Sudbury Breccia (pseudotachylyte) indicates that the Hess Offset delineates a subconcentric fault system that defines part of the collapsed and modified northern margin of the transient cavity of the Sudbury Impact Structure. Pseudotachylyte occurs as discrete veins (up to 0.5 m wide and as mm to microscopic veinlets), which form a border zone of more cataclastic deformation that may or may not contain pseudotachylyte. The larger veins of pseudotachylyte are typically subparallel to the Hess Offset, whereas the finer veinlets of pseudotachylyte are more anastomosing and ubiquitous. Granite clasts containing pseudotachylyte veinlets have been found within larger pseudotachylyte veins, implying at least two phases of brecciation/slip.

The contacts with the host rocks display varying degrees of brecciation. These range from relatively undeformed or relatively unaltered granitoids, gradational with discrete veins of pseudotachylyte along the margin, to more cataclastically deformed granite, with varying degrees of chilled margin against the contacts.

Major, trace, and REE chemistry of selected Hess samples clearly indicates an affinity with the SIC. The primary mineralogy is quartz + plagioclase + pyroxene + hornblende + biotite; opaque phases include pyrite, pyrrhotite, pentlandite, and chalcopyrite, with minor amounts of argentiferous pentlandite, michenerite, and hessite. The pyroxenes have been extensively altered to actinolite. Other secondary minerals include sphene, chlorite, biotite, and epidote.

ORIGIN OF THE SUDBURY IGNEOUS COMPLEX AND SULFIDE MINERALIZATION: EVIDENCE FROM PLATINUM GROUP ELEMENTS. Q. Xie[1], R. R. Keays[1], S. A. Prevec[1], and P. C. Lightfoot[2], [1]MERC, Laurentian University, Sudbury, Ontario P3E 2C6, Canada, [2]INCO Limited, Highway 17 W., Copper Cliff, Ontario P0M 1N0, Canada.

Despite intensive studies, some fundamental questions remain concerning the origin of the SIC and associated sulfide mineralization. Two questions are of primary importance: (1) Was the SIC formed by crustal melting resulting from a meteorite impact, or was it generated in an explosive intrusion of mantle-derived mafic magma? and (2) Where did all the metals (Ni, Cu, PGE, and S) come from? New geochemical data, including major and trace elements and PGE, have provided further constraints on these questions.

Four drill cores that intersect the main mass felsic and mafic norite and the Sublayer were sampled. In all four drill cores, there is no simple trend of major and trace elements, nor of PGE, with increasing depth from felsic norite through mafic norite to the Sublayer, as would be expected if the SIC represented a simple differentiated melt sheet. Rather, there is a major compositional gap between the main mass and the Sublayer. Chemically, the Sublayer is highly heterogeneous due to a highly variable inclusion content in both type and abundance.

Compared with mantle-derived mafic and ultramafic magmas, the SIC is relatively depleted in PGE, with Ni/Pd (30,000–300,000) and Cu/Ir (60,000–7,000,000) ratios that closely resemble those of average continental crust. Sulfur/selenium ratios in the SIC range from 500 to 25,000, far exceeding those in mantle-derived magmas (3000–5000). Modeling of sulfide-silicate melt immiscible separation and fractional crystallization of monosulfide solid solution (mss) indicates that PGE data for the SIC may be best described by melting of continental crust with silicate/sulfide mass ratios (R factor) between 500 and 5000. The above evidence supports the hypothesis that the SIC was formed by crustal melting resulting from meteorite impact, and that metals (Ni, Cu, and PGE) came from preexisting crustal rocks, such as Early Proterozoic Nipissing diabase and East Bull Lake-type intrusions. Mass balance calculations for Ni, Cu,

and PGE, the presence of ultramafic xenoliths in the Sublayer, and the orthopyroxene-rich nature of the felsic norite, however, suggest a contribution from a mantle-derived, high-MgO magma, possibly a picrite. While the addition of up to 20% picritic magma to the crustal melt sheet would not alter its composition significantly, it would provide the Ni, Cu, and PGE required to form the ore deposits as well as, by turbulent mixing with the crustal melt sheet, the mechanism by which sulfide saturation could be achieved.

New PGE data further indicate that there is a large variation in ratios between PPGE (Pd-Pt-Rh) and IPGE (Ir-Os-Ru). In particular, Pd/Ir ratios vary from 2 to 600 in the Sublayer and Offset. Although the range of Pd/Ir ratios in the Sublayer and Offset may be largely explained by fractional crystallization of mss, and imperfect separation of mss and residual sulfide liquid, other processes, such as late-stage metasomatism, may have contributed to the large variation in PPGE/IPGE ratios.